Interactions of Proximate Amino Acid Residues in Polyaza Macrocycles

Sally Elisabeth Plush, B. Sc (Hons)

A thesis submitted for the degree of
Doctor of Philosophy
In

The University of Adelaide

Department of Chemistry

August 2004

THE UNIVERSITY
OF ADELAIDE
AUSTRALIA

Table of Contents

Abstract

This thesis describes the synthesis and complexation characteristics of a series of pendant arm polyaza macrocycles, designed to test the practicality of attaching amino acids to tri and tetra amino cyclic aliphatic amines and their adaptation as fluorescent sensors for metal ions. The ligands designed were based on 1,4,7-triaazacyclononane (tacn) and 1,4,7,10-tetrazacyclododecane (cyclen) with chiral amino acid pendant arms. The fluorescent sensors were based on the Fluorophore-Spacer-Receptor model and consisted of a 9-substituted anthracene fluorophore, an ethylamine spacer and a cyclen receptor, in which a variety of pendant arms varying in substitution pattern, were attached.

The acid dissociation constants and metal complex ion stability constants for all ligands were determined in a methanol/water (80:20; v/v) solvent system (I = 0.1 mol dm^{-3} (NEt_4ClO_4)) by potentiometric titration. The complexation behaviour of the ligands in this study was found to be very similar to that of other pendant arm ligands based on *N*-substituted tacn and cyclen macrocycles. The anthracene substituted ligands were found to exhibit a high affinity towards the metal ions, making them potential metal ion fluorescent sensors. The use of chiral amino acid pendant arms allows for the formation of two possible diastereomers for each metal complex, however, NMR spectral studies suggested that only one diastereomer exists.

The photophysical nature of the anthracene substituted ligands was also investigated by UV-visible absorption spectroscopy and fluorescence spectroscopy. Spectrofluorimetric titration of the anthracene substituted ligands indicated that protonation of the ethylamine nitrogen adjacent to the anthracene occurred at a pK_a of around 4.5. Minimal changes to the UV-visible absorption spectra were observed. The three anthracene substituted ligands investigated exhibited very different fluorescence behaviour on metal ion complexation.

Declaration

This work contains no material which has been accepted for the award of any other degree or diploma in any university of other tertiary institution and, to the best of my knowledge and belief, contains no material previously published or written by another person, expect where due reference has been made in the text.

I give consent to this copy of my thesis, when deposited in the University Library, being available for loan and photocopying.

Sally Plush

Acknowledgements

I would like to sincerely thank both Prof. Stephen Lincoln and Assoc. Prof. Kevin Wainwright for all their time, support and advice throughout my PhD, and for giving me this fantastic opportunity.

A big thankyou to Dr Jason Geue, for without him, I can safely say that I would never have achieved as much as I have. His advice, scientifically and socially in the roles of both mentor and friend (even though it may not have appeared as though I listened and absorbed any of it), have been invaluable. And no quantity of food, beer or wine could repay the debt I owe him.

I also wish to thank Dr Bruce May for his part, as a sounding board, interpreter, and for all his helpful suggestions. Special thanks go to the dark side (lab 12), and to those people who realised early on, that a lab all on my own far, far away, without exposure to light and in sub-arctic conditions was the best thing for all concerned.

Special thanks to Mark and Julia for their friendship and for sharing this once in a lifetime experience with me (because lets face it who in their right mind would do this twice?). I loved our long lunch breaks (and the fact we didn't always return), the sharing of anecdotes and the communal drowning of sorrows, for without this I would have been committed (to the funny farm) early on in my first year.

Thanks must go to everyone else I have had the joy of sharing a lab with, and those who have helped me along this long and treacherous road, Mark Smith and Steve Inglis (thanks for the beer), Oska Wyness (thankyou), Huy Tien Ngo and Jacquie Cawthray (I am sorry). Thanks also to the rest of the Lincoln group (Jo).

I also need to thank my support crew outside of uni, Nicole, Shelly, Anna, Prue, Cathie-Anne, Kara and Megan. Thanks.

And last but not least, my family, Mum, Dad and David. Thankyou from the bottom of my heart for supporting me in every endeavour I put my mind to (including all the crazy ones like doing a PhD). I do really appreciate everything you have ever done for me.

Abbreviations

Å	Ångstrom (10^{-10} m)
β	Overall stability constant
bp	Boiling point
calcd.	Calculated
conc.	Concentrated
cyclen	1,4,7,10-tetraazacyclododecane
X^2	Chi squared
[ ]	Concentration
δ	Chemical shift
d	Doublet
DMF	*N*,*N*-dimethylformamide
DMSO	Dimethyl sulphoxide
E	Observed electrode potential (mV)
E_o	Standard electrode potential (mV)
ε	Molar extinction coefficient / Molar absorptivity
EI	Electron impact
I	Ionic strength
IR	Infra red
J	Coupling constant
K	Apparent stability constant
K_a	Acid dissociation constant
Khphthalate	Potassium hydrogen phthalate
L	Unspecified ligand
LCQ	
lit.	literature
log	Logarithm (base 10)
υ_{max}	Maximum infrared absorbance (cm^{-1})
λ_{ex}	Fluorescence excitation wavelength
λ_{max}	Maximum wavelength
m	Multiplet
M^+	Univalent metal ion
M^{2+}	Divalent metal ion
M^{n+}	Unspecified metal ion

m/z	Mass to charge ratio
MHz	Megahertz (10^6 s^{-1})
mp	Melting point
NEt_3	Triethylamine
NMR	Nuclear magnetic resonance (spectroscopy)
PET	Photoinduced electron transfer
pH	$-\log_{10}[H^+]$
pK_a	$-\log_{10}[K_a]$
pK_w	$-\log_{10}[K_w]$
ppm	Parts per million
q	Quartet
s	Singlet
t	Triplet
tacn	1,4,7-triazacyclononane
TLC	Thin layer chromatography
UV	Ultraviolet
NEt_4Br	Tetraethylammonium bromide
NEt_4ClO_4	Tetraethylammonium perchlorate
$HClO_4$	Perchloric Acid

Chapter 1. Introduction

1.1 Introduction

The field of macrocyclic complex chemistry has undergone a rapid expansion over recent years, especially in the area of bioinorganic chemistry. Macrocyclic systems with the ability to complex metal ions have been synthesised to act as luminescent sensors,[1-5] MRI relaxation agents[6-9] and chiral receptor systems.[10-14] Many trace metal ions such as Na^+, K^+, Ca^{2+}, Fe^{2+}, Co^{2+}, Cu^{2+} and Zn^{2+} are essential to living cells and although they constitute only about 3% of the human body weight they are vital to many processes. The transport of energy and metabolites relies on the chemistry of Na^+, K^+ and Ca^{2+} and their involvement in the ion pump mechanism.[15] Transition metal ions such as Zn^{2+} and Co^{2+} are found in a variety of metalloenzymes where they coordinate with amino acids and enhance catalysis reactions at active sites.[16] The electronic nature of Fe^{2+} and Cu^{2+} allows for their involvement in the transport of electrons through porphyrin-type groups.[17] Due to the importance of metal ions in biological systems, the development of metal binding chelates is important not only to gain an understanding of the role they play in these systems, but also in the development of receptors and sensors. There is a plethora of molecules, which have been shown to coordinate metal ions in a range of environments. These include those based on coronands, cryptands and polyaza macrocycles.

1.2 Chiral receptors

Many biological processes rely on the selectivity endowed by chiral centres for their unique properties. There are numerous examples in which only one enantiomer is active; for example phenylalanine, when acting as a receptor, is only active in its L form, and not in its D form.[18] Similar selectivity is observed in many synthetic drugs, and in some cases the opposite enantiomer of the active drug can in fact have detrimental effects. Recently, there has been significant interest shown in the development of chiral coordination complexes. This has arisen from the role that chiral metal complex ions play in asymmetric synthesis, as well, as in the advances into both the fields of bioinorganic chemistry and metallosupramolecular chemistry.[19-21]

Chiral coordination species can generally be divided into two classes: (1) metal complex ions, in which chirality only appears on metal ion coordination, and (2) metal complex ions in which the ligand possesses one or more chiral centres.[22] There are numerous examples of both types of chiral complexes.

1.2.1 Examples of chiral receptors

A simple ligand designed as a chiral receptor is 1,4,7,10-tetrakis(2-hydroxyethyl)-1,4,7,10-tetraazacyclododecane (**1**), based on the polyaza macrocycle 1,4,7,10-tetraazacyclododecane (cyclen). Ligand (**1**) was found to complex a variety of alkali metal ions, including Li^+ ($\log K/dm^3\ mol^{-1}$ = 8.07) and Na^+ ($\log K/dm^3\ mol^{-1}$ = 6.66), in acetonitrile.[23,24] The stability of the complex was found to be highly solvent dependent. The free ligand is achiral; however, on metal ion coordination ligand (**1**) was found to adopt a chiral conformation, producing two enantiomers (**Figure 1.1**). The enantiomers are formed by ring inversion around the amine nitrogens involving the release and recapture of the metal ion, leading to the exchange of the macrocyclic ring carbons between environments a and b. Overall, ligand (**1**) was found to form eight-coordinate Δ and Λ complexes around the metal ion.[25] In the Δ enantiomer the pendant arms twist in a clockwise direction, while in the Λ enantiomer the pendant arms twist in an anti-clockwise direction.

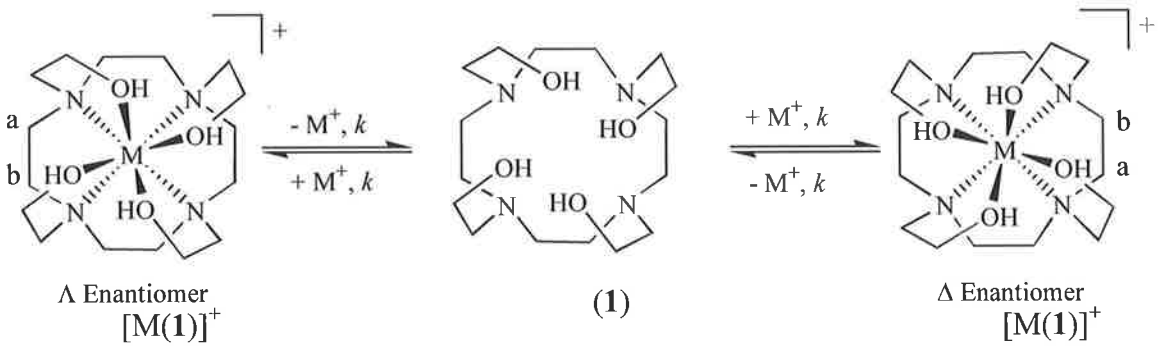

Figure 1.1. Schematic representation of the two possible enantiomers of Δ and Λ $[M(\mathbf{1})]^+$, where a and b represent the macrocyclic ring carbons.

Lincoln *et al* also carried out further work in the area of chiral receptors based on polyaza macrocycles with pre-existing chirality. The metal ion receptor 1,4,7,10-tetrakis((*S*)-2-hydroxyethylpropyl)-1,4,7,10-tetraazacyclododecane (**2**) was developed using cyclen with (*S*)-2-hydroxypropyl pendant arms. The receptor was found to

coordinate Li^+ ($\log K/dm^3\ mol^{-1}$ = 3.24) and Na^+ ($\log K/dm^3\ mol^{-1}$ = 3.76) in dimethylformamide.[26] The incorporation of chiral pendant arms is known to result in the formation of diastereomers and induces homochirality in the system (**Figure 1.2**). It was observed that there is a thermodynamic preference for one of the diastereomers and its complexes of ligand (**2**). Ab initio geometry optimisation in the gas phase of the free ligand (**2**) showed that the Δ diastereomer has the lowest energy conformation. However, it was found that the geometry of ligand (**2**) changed on coordination of an alkali metal ion; the Λ diastereomer of ligand (**2**) was then found to have the lowest energy state. This was consistent with X-ray crystallography structure determination.[27] The steric effects of the pendant arm and the nature of the metal ion are believed to be the cause of the differentiation.

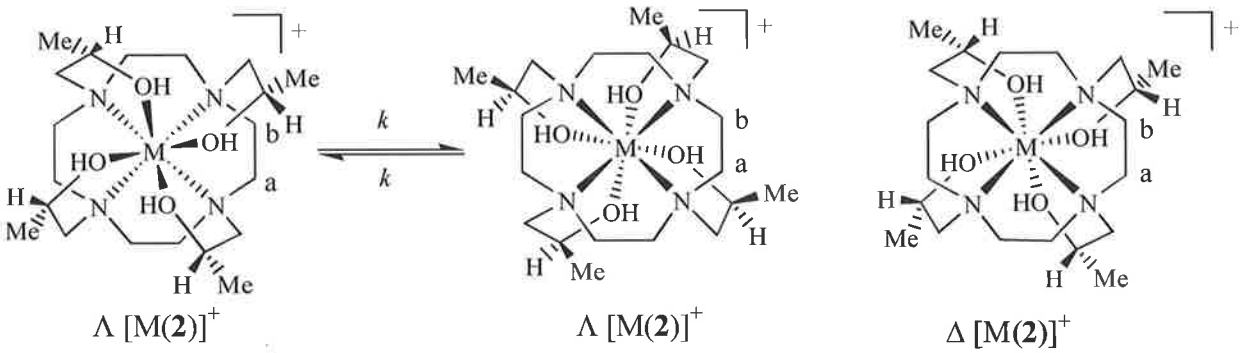

Figure 1.2. Schematic representation of the two possible diastereomers of Λ[M(**2**)]$^+$, and the undetected Δ [M(**2**)]$^+$, where a and b indicate the macrocyclic ring carbons which exchange their environments in Λ[M(**2**)]$^+$.

There are numerous other ligands that exhibit this induced chirality in their secondary structure on incorporation of chiral pendant arms; cyclodextrins (CD) are one such example. Cyclodextrins are cyclic oligomers made up of repeating glucose units comprising of a hydrophobic cavity. Tabushi reported the first example of a chiral receptor involving a functionalised CD (6^A-amino-6^B-carboxy-β-CD) (**3**).[28] The receptor was designed as a tryptophan selector through charge interactions between the zwitterionic amino acid and the functional groups of the CD. Unfortunately, the effect of the interaction with the amino acid was very similar for both enantiomers; the observed thermodynamic enantioselectivity was very small ($\Delta\Delta G$ = 0.7 kJ mol^{-1}).[28]

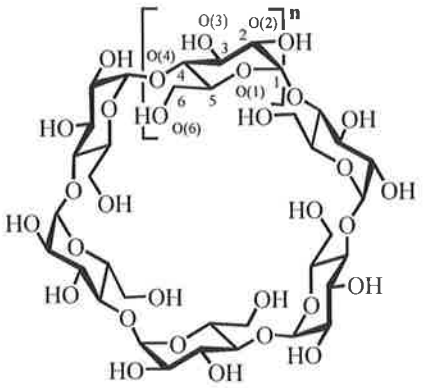

β-Cyclodextrin, β-(CD)

where **n** = 2

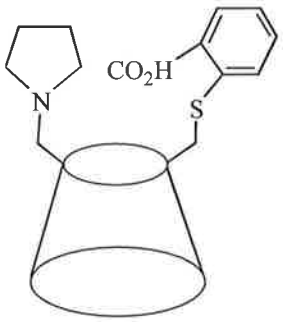

(**3**)

The incorporation of metal ions into functionalised CDs has improved the enantiomeric selectivity of some receptors.[29] One example is the Cu^{2+} complex of 6^A-deoxy-6^A-histamine-β-CD (**4**), which can be used to resolve racemic mixtures of amino acids in ligand exchange (HPLC).[30-32] A good chromatographic separation factor and thermodynamic enantioselectivity can be achieved for tryptophan ($\alpha_{L/D}$ = 1.23 and $\Delta\Delta G$ = 2.0 kJ mol^{-1}, respectively). The metal complex ion exhibited very interesting enthalpy and entropy characteristics for amino acid coordination. It was found that the complexes of the D-enantiomers were significantly more stable than the L-enantiomers for amino acids containing aromatic residues[31] The D-enantiomer was found to assume a preferred *cis*-geometry allowing for an interaction between the aromatic group and the hydrophobic cavity of the CD (**Figure 1.3**). The overall result is that in HPLC the D-enantiomers are eluted first.[33]

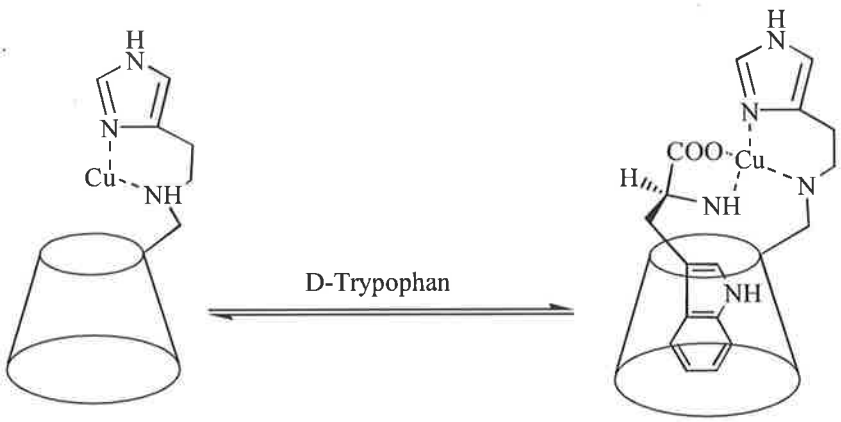

(**4**) (**4**)-*D*-tryp

Figure 1.3. Schematic representation of the tertiary complexes of the CD (**4**) and its diastereomeric complex with D-tryptophan

Calixarenes have also been used in the development of chiral receptors. The chiral calixarene (**5**) was developed from a bridged calix[4]arene, with C_2 symmetry, incorporating substituents on its hydroxy moieties. The ability of the calixarene (**5**) to act as a chiral receptor was evaluated by investigating its interactions with chiral amines, it was shown to form a strong 1:1 complex with the chiral *R*-(+)-α-phenylethylammonium picrate.[34] Okada and co-workers investigated a wide variety of similar calixarenes, differing in substitution patterns. They found that receptors of a similar structure to calixarene (**5**) preferred to form host-guest complexes with guests of opposite chirality.[34]

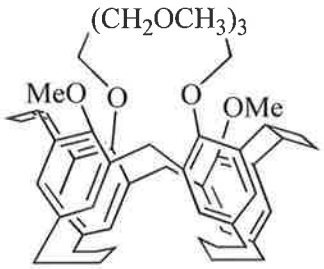

(**5**)

1.2.2 Designing chiral receptors

There are many ways in which a chiral receptor can be altered to improve selectivity towards target compounds, be they cations, anions or molecular analytes. The addition of pendant arms, with different properties, is one change that allows for the preparation of a large range of possible receptor systems with a variety of targets. Pendant arms incorporating aromatic residues have the ability to create substantial hydrophobic cavities.[25] The presence of such a cavity in ligands containing aromatic residues may lead to the formation of a wide range of chiral receptors with the ability to complex, and target, a variety of biologically important analytes.[35] When targeting guest molecules containing aromatic residues, aromatic pendant arms may also help to stabilise host-guest complexation through π-π interactions. These interactions may play a significant role in chiral discrimination in some inclusion complexes.[36] Another important type of pendant arm that would be advantageous in the design of chiral receptors is one that aids water solubility. The problem associated with many receptors synthesised to date is low water solubility, which is a hindrance to their application in biological systems. This can sometimes also be overcome by the incorporation of metal ions, which aid water solubility. The introduction of different pendant arms into a receptor molecule may allow for the fine-

tuning of complex properties by enhancing the selectivity of the ligand for a given guest molecule.[37]

The use of the hydrophobic cavity in CDs sometimes has a large affect on the separation of amino acid enantiomers; therefore altering the size of the CD may also affect its molecular recognition properties. The same principle can be applied to all macrocycles; the size, and hence binding properties, of all polyaza macrocycles, cryptands and crown ethers can be altered to target different analytes.

1.2.3 Determination of chirality

For a ligand to be used in molecular recognition and host-guest complex studies, its structure and conformation must be known. A wide range of analytical tools may be used, including NMR spectroscopy, chiral HPLC, X-ray crystallography, gas phase optimisations and circular dichroism experiments.

Chiral HPLC allows for the separation of enantiomers, which can lead to the subsequent determination of the specific rotation [α_D] for individual enantiomers. Separation is achieved through the use of a chiral stationary phase; most phases have specific structural requirements limiting the range of detectable compounds.[38,39] Using solid-state structures to determine the diastereomeric preference for the receptor also has numerous benefits since only small quantities of material are generally required and structures can be obtained with a high degree of accuracy. Studies involving circular dichroism provide information about the effect that metal ion coordination has on a ligand's secondary structure. Circular dichroism is based on the difference between the absorption of a right circularly polarized beam, compared with its left counterpart. The optical rotation of any ligand can be affected by pH, temperature and time.[40]

Gas phase optimisations by means of computational chemistry can provide an invaluable supplement to experimental chemistry through simulations of chemical structures. It allows for the prediction of the minimum energy conformations of macrocyclic ligands alone and as metal complex ions. NMR spectroscopy studies are an effective and simple device, used widely in the determination of diastereomeric conformation. NMR spectroscopy cannot differentiate between enantiomers without prior transformation into diastereomers. This is achieved by the use of chiral reagents; either a

chiral solvent which induces a chemical shift difference between enantiomers, or a shift reagent such as an optically active lanthanide. The formation of metal complex ions for NMR spectroscopy studies is also used. Enantiomerization of the free ligand is often too fast for observation on the NMR time scale. Complexation of a ligand with a metal ion is known to slow the exchange process between conformations. This can be detected within the NMR time scale as indicated for $\Lambda[M(\mathbf{2})]^{+}$ (**Figure 1.2**).

1.3 Detection of metal ions by fluorescence

There are many different analytical methods used for the detection of metal ions in solution, such as atomic absorption spectroscopy,[41] ion selective electrodes[42] and fluorescence spectroscopy.[43] The detection of metal ions through fluorescence is a relatively cheap, convenient and sensitive technique with many desirable properties.[44,45] The results can be obtained in real time, as solutions, or at interfaces, and at low concentrations. The concentrations at which measurements can be recorded are similar to that of UV-visible absorption spectroscopy. Sensors designed for detection by UV-visible absorption spectroscopy however, are not ideal for biological applications, as exposure to UV-radiation often leads to cell and tissue damage. The fluorescent signal is easily altered by increases or decreases at a single wavelength, intensity-ratio measurements (ratiometry), or changes to fluorescent life times.[46] Through the use of fluorescence imaging spectroscopy, signal measurements can also be localised.[47] Many of the other analytical techniques, which exist for the detection of metal ions in solution, do not allow for such types of measurements. These techniques often require pre-treatment of the sample by separation or concentration, and most significantly, are often very expensive.

1.3.1 Design of fluorescent metal ion sensors

Luminescence sensors, including fluorescence, phosphorescence and metal luminescence, use light signals to transmit information about recognition events in chemistry and biology. A sensor is defined as a two-component system, in which an intended substrate receptor is connected to a subunit, capable of signalling the occurrence of the receptor-substrate interaction.[48] The ease with which the signalling event can be monitored determines the method of detection. The development of fluorescent sensors is of significance due to the ease with which fluorescence can be monitored.[44,45]

Most fluorescent sensors are based on a design that incorporates a receptor and a fluorophore connected by a spacer unit.[49] Such sensors rely on the reversible binding of analytes such as protons, metal ions or anions which can act as both ON and OFF signals. The receptor must therefore be able to specifically bind the guest of interest out of a mixture of possible analytes. The selectivity depends on the nature of the coordinating analyte (ionic radius, charge, coordination number, hardness, etc), the solvent, pH and ionic strength.[50] The signal, which results from the receptor-substrate interaction, must be significantly different from the emission of the fluorophore prior to guest molecule complexation. The final component in the design of a fluorescent sensor is the spacer unit. There are no restrictions on the spatial relationship between the fluorophore and the receptor unit.[51]

The usefulness of a fluorescent sensor is dependent on the efficiency with which the recognition event is transmitted to the fluorophore component. There exist a number of mechanisms by which the emission of the fluorophore can be altered. These include the incorporation of such processes as proton, energy or electron-transfer, or the inclusion of heavy metal ions. Changes to electron density and to the stability of the non-emissive $n\pi^*$ excited state also affect fluorescence emission.[52] In the design of a fluorescent sensor, the stability constant of the complex determines the concentration range at which detection is possible. In general, a higher stability constant for a complex allows a lower detection limit, a highly desirable property in a sensor.

Many of the fluorescent sensors designed to date have focused on the recognition of group I and II cations, and are becoming more readily available commercially.[53,54] One problem associated with fluorescent sensors is water solubility, which is often related to the hydrophobic nature of the fluorophore group. There is a great interest in the development of fluorophore sensors, which are water soluble, exhibit greater diversification in both the receptor and fluorophore unit, and which target specific analytes, including metal ions.

1.4 Photoinduced electron transfer (PET) based fluorescent sensors

There are many ways in which the recognition event, controlled by the receptor, can be expressed by the fluorophore. Photoinduced electron transfer (PET) is one such method. A PET type sensor is founded on the Fluorophore-Spacer-Receptor model, which allows for the transfer of electrons from the receptor to the fluorophore (or vice versa) (**Figure 1.4**).[55]

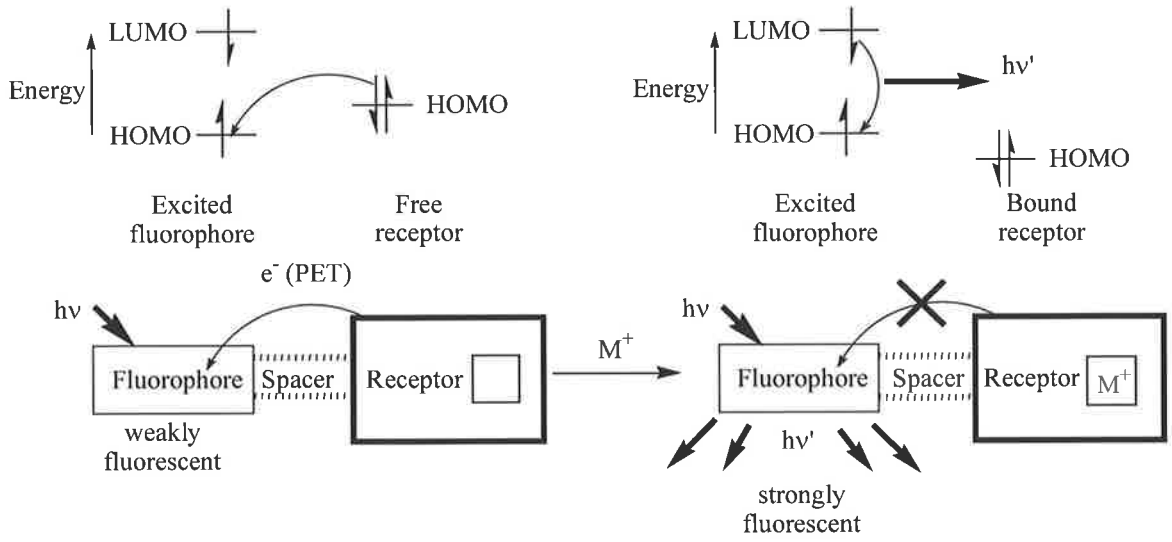

Figure 1.4. Schematic representation of a photoinduced electron transfer (PET) process in a Fluorophore-Spacer-Receptor signalling system.

When a fluorophore group undergoes excitation, an electron in the highest occupied molecular orbital (HOMO) is promoted to the lowest unoccupied molecular orbital (LUMO). This then allows for PET from the HOMO of the receptor (donor) to that of the fluorophore (acceptor), which then quenches the fluorescence of the fluorophore unit. This process only occurs when the receptor is in the unbound form.

The coordination of the receptor to an analyte, either a metal ion or a proton, raises the redox potential of the donor. This causes the relevant HOMO of the donor to have a lower energy than that of the acceptor. The PET process is thus hindered, and the fluorescence of the fluorophore is accordingly restored.[50] In general, it can be taken that the fluorescence of a ligand, in which a PET based signalling pathway is present, will be

enhanced by metal ion complexation or protonation. Many of the PET type fluorophores developed to date, utilise macrocyclic amines, either aliphatic or aromatic, as their nucleophilic nature aids complexation. Receptors based on all-oxygen type molecules, even though they too can exhibit strong complexation and a degree of discrimination between cations, are not ideal fluorescent sensors.[56,57]

There are many advantages to be gained from incorporating a PET based signalling pathway into a sensor. One is the large change in fluorescence intensity usually observed upon metal ion complexation. The term OFF/ON or ON/OFF in relation to fluorescent sensors is generally employed to describe the change in emission intensity.[58] An ON/OFF switch is one in which the intensity of the fluorescence signal decreases on coordination of a guest molecule. The guest triggers PET either to or away from the fluorophore, depending on its redox potential, which results in fluorescence quenching. An advantage of an OFF/ON switch is that the large enhancement of fluorescence on complexation causes the appearance of a signal from a dark background, lowering the detection limit.[59]

There are many different examples of PET sensors available, which vary in both receptor and fluorophore. Most have been designed to act as metal ion sensors. However, there are a limited few that do respond to other analytes. The following is a brief description of a few examples of PET type sensors.

1.4.1 Crown containing PET sensors

One of the first PET sensors was based on the azacrown ether (**6**), a monoaza-18-crown-6 with a simple aryl fluorophore, anthracene, and a methylene spacer.[56] Anthracene is a well-known fluorophore, the properties of which have been extensively studied, making it a good basis for PET sensors. Monoazacrowns are known to selectively complex a variety of metal ions; thus making them suitable receptors for sensors incorporating a PET pathway. The intensity of the fluorescence emission of sensor (**6**) increases on coordination with Na^+ and K^+. The quantum yield (Φ_F) increased from 0.003 to 0.14 on the binding of K^+ in methanol.[56] This is an example of an OFF/ON PET type sensor, in which metal ion complexation restores the fluorescence of the fluorophore.

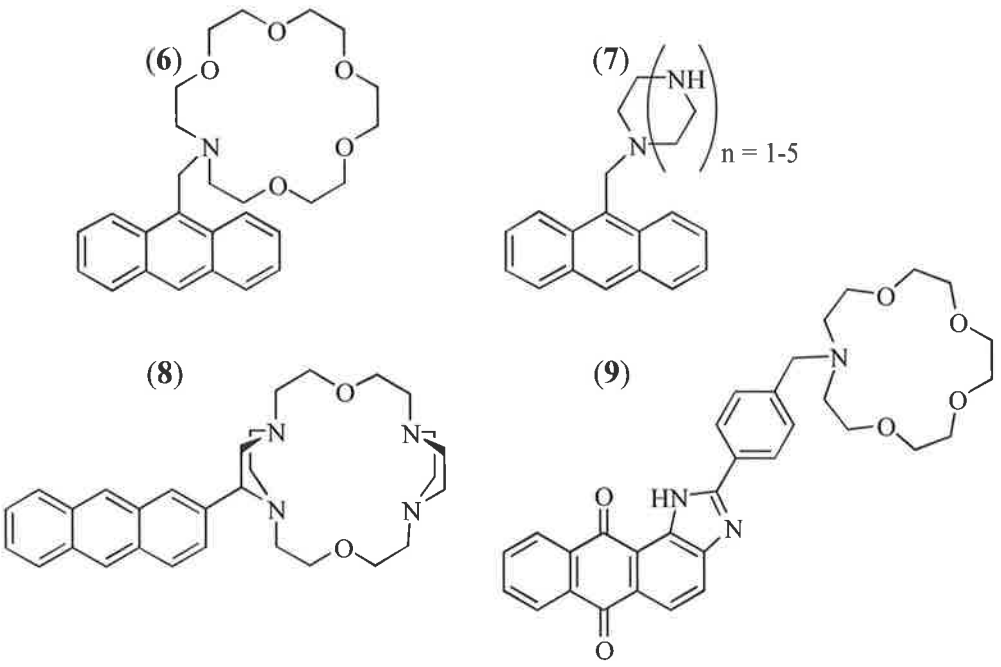

Another example of an early PET type fluorophore was one developed by Czarnik and co-workers, in which a polyaza macrocycle, namely cyclen, was appended to anthracene by a methylene spacer unit, to give ligand (**7**) where n = 3.[60] The sensor was designed to recognise Zn^{2+} and Cd^{2+}. The anthrylaza macrocyclic ligand (**7**), exhibited a large change in the intensity of its fluorescence emission on binding of a transition metal ion. A 14-fold enhancement for Zn^{2+} and a 9-fold enhancement for Cd^{2+} were observed in buffered pH 10.0 aqueous solution. The observed fluorescence for ligand (**7**) was shown to have a high dependence on pH. The free ligand exhibited a maximum fluorescence at pH 2-3; at higher pH values the fluorescence decreased. Protonation of the amine group, involved in the PET process, hindered the transfer of electrons and resulted in restoration of the ligands fluorescence.[60]

Czarnik and co-workers also investigated the effect of changing the substitution on the anthracene fluorophore from the 9-position to the 2-position in the anthryl cryptand ligand (**8**).[61] It was shown that fluorescence quenching by the amine at the anthracene 2-position was not as efficient as at the 9-position. An increase of only 3.5-fold in the fluorescence intensity was observed for ligand (**8**), whereas a 20-fold enhancement had been observed for ligand (**7**) on amine protonation.[61]

Anthracene is not the only fluorophore to have been exploited in the development of novel PET sensors. Another common example is phenylimidazoanthraquinone. Sensor (**9**) contains both, a phenylimidazoanthraquinone fluorophore, and a monoaza-15-crown-5

group as the receptor. Sensor (**9**) was found to form a stable Ca^{2+} complex in acetonitrile ($K = 3.24 \times 10^6$ dm^3 mol^{-1}).[62] However, complexation of the PET type sensor (**9**) with Ca^{2+} did not have a large effect on the sensor's fluorescence emission. A low quantum yield was observed.[62]

In the search for novel sensors and signalling systems, metal ion based fluorophores have also been successfully employed. The Re(I) complex (**10**) selectively binds Pb^{+} over Hg^{2+} and Ba^{2+} in methanolic environments.[63] Formation of the complex, (**10**)-Pb leads to a 3-fold increase in emission intensity, coupled with a 20 nm bathochromic shift to the emission spectrum.[63] In the absence of heavy metal ions, ligand (**10**) exhibits some background luminescence. On coordination of a heavy metal ion, a binding-induced inversion of the lowest and second lowest energy electronic excited states occurs, which results in the observed luminescence enhancement.[64]

(**10**)

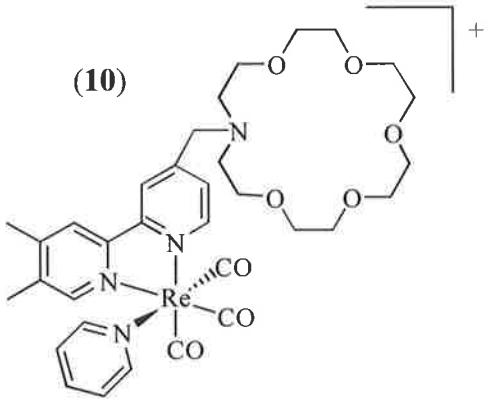

1.4.2 Cryptand-based PET sensors

Cryptands generally offer better selectivity towards alkali cations than other commonly used macrocyclic structures. The anthracenyl cryptand derivative (**11**) was designed to bind K^{+} with a high degree of selectivity. A 7.5-fold increase in the fluorescence quantum yield, with little change to the UV-visible absorption spectra, was observed on complexation.[65] For sensors designed to incorporate PET, the lack of change in the UV-visible absorption spectrum on metal ion complexation is of little consequence, as fluorescence quenching only affects the excited state.[58] Sensor (**11**) was also capable of undergoing intensity-ratio measurements due to the formation of exciplex species.

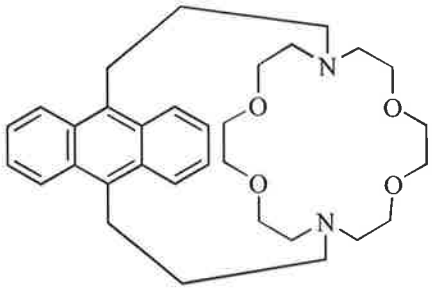

(11)

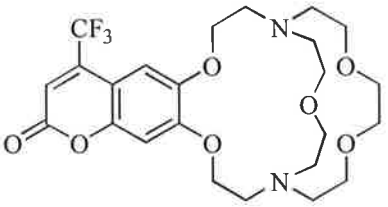

(12)

The incorporation of a coumarin fluorophore into a cryptand sensor has led to successful PET type sensors, as exemplified by the trifluromethylcoumarin ligand (**12**). Ligand (**12**) can selectively bind Na^+ over K^+. Unfortunately, ligand (**12**) is very sensitive to protonation of its nitrogen atoms, and requires strict pH control for its use. Full protonation of ligand (**12**) results in a highly luminescent state (Φ_F = 0.60). Mono-deprotonation of the species leads to a 10-fold reduction of the quantum yield. Upon complete deprotonation, a further but smaller reduction to the observed quantum yield results.[66] This result indicates that the presence, and hence participation of a single amine nitrogen, in a PET mechanism, is sufficient to quench the fluorescence of ligand (**12**).

1.4.3 Simple PET sensors

All of the previously discussed PET sensors are quite complicated. This need not apply for those incorporating podand-like fluorophores. Podand-based PET sensors can be very simple molecules; for example ligand (**13**) is an efficient transition metal ion sensor.[67]

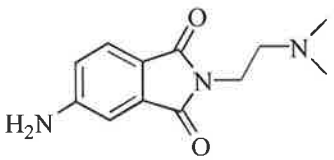

(13)

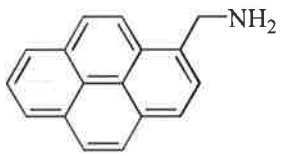

(14)

When designing efficient fluorescent sensors, the manner in which the metal ion complexation signal is transmitted is very important. It is vital that the metal ion-fluorophore communication be less than the metal ion-receptor interaction. This is achieved by the use of an electron deficient fluorophore, which minimises the redox interaction between the fluorophore and the metal ion.[67] Using fluorophores of this nature can minimise the quenching properties of some metal ions. It also enhances the PET

quenching in the unbound state. This concept has been incorporated into numerous sensors; ligand (**13**) is an example. Its fluorescence was found to undergo enhancement on coordination with Cu^{2+}(41-fold), a transition metal ion normally associated with fluorescence quenching.[67]

The pyrene based sensor, 1-aminomethylpyrene (**14**), is another good example of a simple photophysical device. Sensor (**14**) is capable of monitoring CO_2 levels by reversible covalent binding. Coordination of a CO_2 molecule with the amine nitrogen in the sensor results in the formation of a carbamic acid. On formation of the carbamic acid the fluorescence emission of sensor (**14**) is resolved, because the lone pair of the nitrogen is no longer able to participate in the PET mechanism.[68] The pyrene unit has several features, which make it ideal as a fluorescent sensor. It exhibits fluorescence emission with a high quantum yield, a long excited state lifetime, and it has the added possibility of forming dimers and exciplexes.[69]

1.4.4 Other examples of PET sensors

A sensor based on PET does not necessarily require the incorporation of an amine nitrogen to fluorophore transfer of electrons. There are a wide variety of sensors, which exploit alternate pathways for PET. An example of one such sensor is ligand (**15**), incorporating the open-chain counterpart of dioxocyclam as the receptor.[70] Dioxocyclam is a powerful ligand capable of binding divalent metal ions of the late 3*d* series.[71]

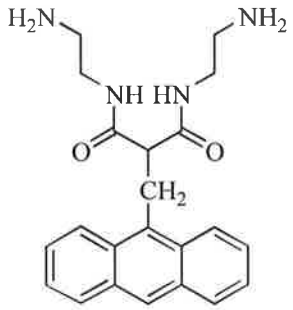

(**15**)

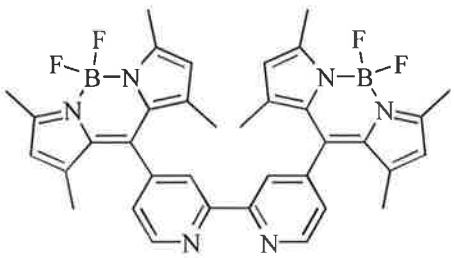

(**16**)

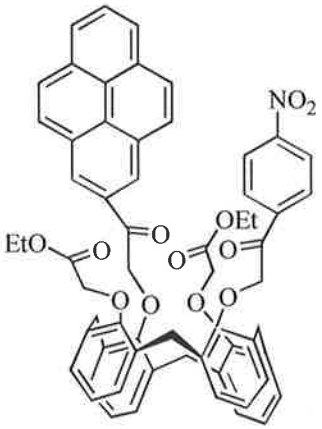

(**17**)

The fluorescence emission of sensor (**15**) was observed to undergo quenching on complexation with Cu^{2+} or Ni^{2+} in an acetonitrile/water (4:1) solution. The complexation mechanism involved the deprotonation of the two amide groups by the metal ion. This resulted in the PET mechanism occurring from the metal centred state.[52] It was shown through studies in frozen glass solution that the quenching did not occur by a Dexter type energy-transfer mechanism (simultaneous double electron exchange)[71] because the fluorescence emission was not restored upon cooling of a solution of ligand (**15**) with Cu^{2+} to 77 K.[70] Investigation into a similar compound, in which the amide groups were replaced by amines, found quenching occurred exclusively through an energy transfer mechanism.[70] In the case of the dioxyclam ligand (**15**), the amide groups have the affect of altering the oxidation potentials, allowing for the creation of the Cu^{3+} state and PET from the metal to the fluorophore.[70]

PET can take place in two directions, from donor to excited state fluorophore (reductive PET), or from an excited state fluorophore to a receptor (oxidative PET). The former is the mechanism generally employed in PET type sensors. An example of a sensor capable of oxidative PET is the boradiazaindacene ligand (**16**).[72] A large stability constant is found for the complexation of ligand (**16**) with Zn^{2+} (K = 1.1 x 10^7 cm^3 mol^{-1}), accompanied by a significant quenching of the fluorescence emission in acteonitrile.[72] The quenching is caused by the favourable energetics of the electron transfer to the LUMO of the bipyridyl-metal complex because metal ion complexation lowers both the HOMO and LUMO energy levels of ligand (**16**).[72]

It has also been shown that PET can be controlled by alterations to the proximity of the donor to the acceptor. Shinakai and co-workers successfully designed one such sensor, ligand (**17**), using a calixarene scaffold, with nitrobenzene as the electron acceptor and pyrene as the electron donor.[73] Complexation of ligand (**17**) with Na^+ (K = 2.0 x 10^4 dm^3 mol^{-1}) resulted in a 6-fold increase to the fluorescence emission; however, a low quantum yield was still observed (Φ_F = 0.016). In the free ligand (**17**), quenching of the pyrene's native fluorescence was observed due to PET from the excited state of the donor to the nitrobenzene acceptor. The complexation of the Na^+ ion into the calixarene placed a conformational restriction on the arms. This resulted in the separation of the nitrobenzene group from the electronically excited pyrene as well as restoration of the pyrene's fluorescence emission.[73]

1.4.5 Dual PET input sensors

The incorporation of two PET active receptors offers a new range of luminescent devices with the ability to recognise more than one anion. This has led to switching phenomena more reminiscent of information technology.[74]

(18)

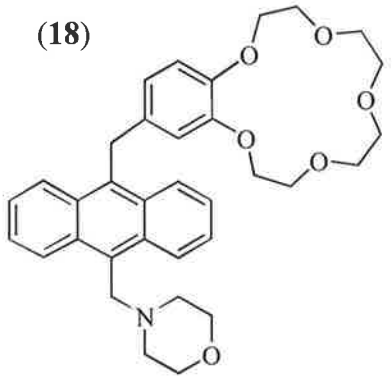

An example of one such sensor is the anthracenyl benzo-15-crown-ether derivative (**18**), which exhibits the $Receptor_1$-$Spacer_1$-Fluorophore-$Spacer_2$-$Receptor_2$ design.[75] The amine group in the free ligand efficiently quenches the fluorescence emission of the anthracene at high pH. Protonation of the amine group stops the PET process. The protonated aminomethyl moiety then behaves as an electron-withdrawing group, away from the anthracene fluorophore. This permits rapid PET from the benzocrown ether moiety to the fluorophore.[75] The quenching of the anthracene's fluorescence is still observed. It is not until the second PET pathway is interrupted that the fluorescence of the fluorophore is restored. This is achieved through the selective coordination of Na^+. A resultant 92-fold enhancement to the fluorescence intensity of the free ligand (**18**) was observed on complexation.[75] A problem associated with many sensors incorporating dual PET responses is that the second ionic input cannot be recognised by the system without prior entry by the first input. Sensor (**18**) does not require such a pathway because the recognition of either ionic input is independent of the other.

Another example of a dual PET sensor is ligand (**19**), which has the ability to target zwitterionic species through both cation and anion recognition.[76] The sensor was designed to target γ-aminobutyric acid (GABA), which is an important neurotransmitter in the brain.[77,78] Ligand (**19**) incorporates a crown ether receptor for the ammonium terminal of GABA and a guanidinium unit for the carboxylate end. Ammonium ion binding and

carboxylate ion binding restrict the PET process from the azacrown to the anthracene, and from the guanidinium to the anthracene, respectively. Fluorescence is restored when both receptors are involved in GABA recognition. The guanidinium moiety is very sensitive to protonation; therefore the binding studies were carried out at pH 9.5 to minimise the interference by protons, whilst maintaining the zwitterion form.[76]

(19)

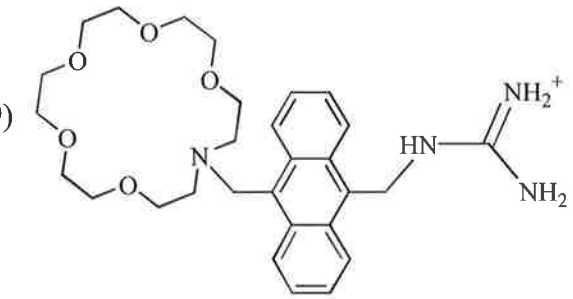

1.4.6 PET sensors for anions and molecular analytes

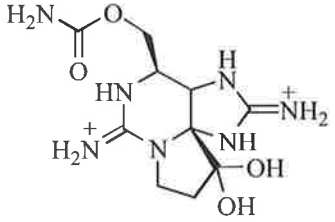

Saxitoxin

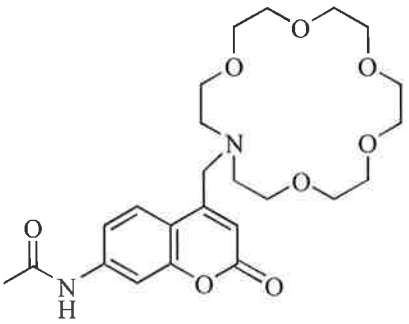

(20)

PET type sensors are not limited to the detection of metal ions. The recognition of anions and molecular analytes by fluorescent sensors through PET is of interest both biologically and industrially.[79,80] Sensor (**19**) is an example of a dual PET sensor designed to recognise biological analytes (see section **1.4.5**). It was observed to selectively bind GABA in preference to similar neurotransmitters like guanidine, by the use of an anion and a cation receptor.[81] Another sensor, the courmaryl-aza-crown derivative (**20**), incorporating only a single PET sensor, was designed by Leblanc and co-workers to recognise saxitoxin.[82] Saxitoxin is a dangerous marine toxin produced by dinoflagellates and some blue green algae species.[83,84] It can cause respiratory paralysis when eaten and this is generally referred to as paralytic shellfish poisoning (PSP).[45] Sensor (**20**) is based on a coumarin fluorophore attached to an aza crown receptor, and is found to bind saxitoxin (K = 1.35 x 10^5 dm^3 mol^{-1}) in water.[82] This sensor is an example of an OFF/ON device, in

which fluorescence is switched on as the aza crown ether becomes involved in saxitoxin recognition.

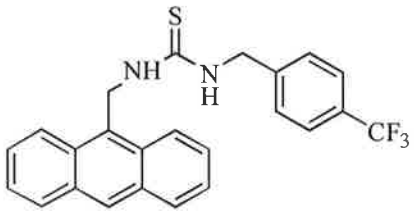

(21)

There exist only limited examples of PET type anion fluorescent sensors.[85] The methyl isothiocyanate substituted aminomethylanthracene ligand (**21**) is one such sensor, designed to bind acetate ($K = 2.24 \times 10^3$ dm^3 mol^{-1}) in dimethyl sulphoxide solution.[86] The binding of the acetate allows for PET to occur from the thiourea-acetate complex to the excited state of the fluorophore, resulting in quenching of the anthracene's fluorescence.[87] Anions, as targets, present a problem since they exist in a variety of structures and conformations, and are highly pH sensitive and hygroscopic.

1.5 Photoinduced charge transfer (PCT) based fluorescent sensors

There are many ways, apart from PET, in which the fluorescence of a sensor can be modulated. A different method is that of photoinduced charge transfer (PCT). A PCT sensor involves a fluorophore directly attached to a receptor molecule with no spacer unit. Without the spacer moiety, the fluorophore and receptor share the same π–system and therefore are in direct electronic conjugation. There are two types of PCT sensors frequently employed; those in which the cation interacts with either an electron donating group, or an electron withdrawing group.

Upon excitation with light, a system in which a metal ion interacts with an electron-donating group undergoes intramolecular charge transfer from the donor (the electron donating group, often an amine) to the acceptor (electron withdrawing group). The resultant change in dipole moment causes the emission band to shift to a lower wavelength relative to the absorption band. This is often referred to as a Stokes shift, and is dependent on the environment in which the fluorophore exists (**Figure 1.5**).

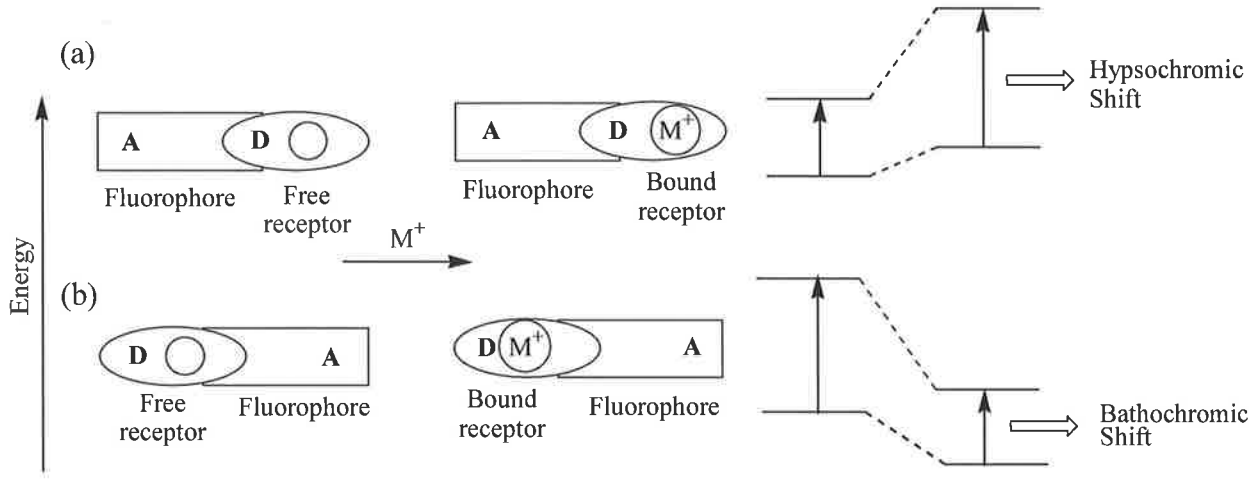

Figure 1.5. Schematic representation of the spectral changes in a photoinduced charge transfer process upon metal ion complexation within (a) a Donor(**D**)-Acceptor(**A**) fluorescent sensor, in which the metal ion interacts with an electron donating group or (b) an Acceptor(**A**)-Donor(**D**) fluorescent sensor, in which the metal ion interacts with an electron withdrawing group.

The complexation of a metal ion by a donor or an acceptor group affects the intramolecular charge transfer process, PCT, and thus alters the photophysical properties of the fluorophore.[88-90] The electron donating character of the donor group is reduced on interaction with a metal ion.[50,91] This results in a reduction to conjugation, resulting in hypsochromic shifts in the absorption spectra and a decrease in molar absorption coefficients. Hypsochromic shifts are observed when the centres of the emission, or absorption bands, are shifted to shorter wavelength. This is sometimes referred to as a blue shift. Conversely when a metal ion interacts with an acceptor group, the absorption spectra undergo bathochromic shifts, and an increase to molar absorption coefficients are observed. Bathochromic shifts are observed when the centres of the emission or absorption bands are shifted to longer wavelength. This is commonly referred to as a red shift.[50] The fluorescence emission spectra undergo a similar shift in the same direction as the absorption spectra.[50,91]

Charge dipole interactions can also be used to describe the photophysical changes that occur upon cation binding. In the case where the dipole moment in the excited state is larger than in the ground state, metal ion interactions strongly destabilise the former over the latter. Hypsochromic shifts to the absorption and emission spectra are thus observed. The converse will occur when a metal ion interacts with an acceptor group because the

excited state will be stabilised by the coordination, and bathochromic shifts to both absorption and emission spectra are observed.[50]

In PCT type sensors, smaller wavelength shifts are often observed in the fluorescence spectra than in the absorption spectra. The charge transfer from the nitrogen atom results in a decrease to its electron density and positive polarisation. The nitrogen atom then, in effect, becomes a non-coordinating atom. Excitation causes the destabilisation of the donor-metal interaction, with the overall effect that, in the excited state, the metal ion moves away from the donor nitrogen group.[92] The fluorescence spectra are thus only slightly affected, because a large proportion of the fluorescence is emitted from species in which the interaction between the metal ion and the fluorophore is weak, or does not exist.[50] Due to the limited changes that occur to fluorescence intensity emissions, PCT sensors are generally used as wavelength-ratiometric sensors.

1.5.1 Examples of PCT Sensors

An example of a PCT sensor in which the bound cation interacts with a donor group is ligand (**22**), which has an azacrown functionality containing a nitrogen group as the cation receptor, conjugated to the electron withdrawing group.

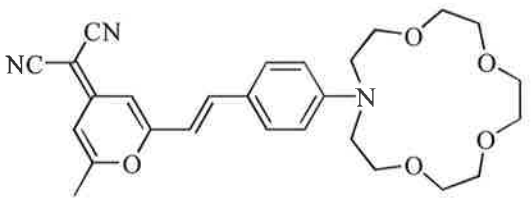

(**22**)

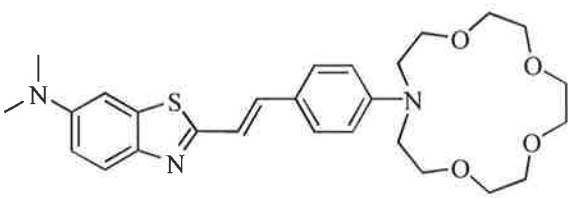

(**23**)

Complexation of sensor (**22**) with alkali and alkaline earth metal ions in acetronitrile results in fluorescence quenching, with hypsochromic shifts to both the emission and absorption spectra observed. The extent to which fluorescence quenching is observed is dependent on the metal ion. In the absence of a metal ion the ligand is fluorescent (Φ_F = 0.73). In the presence of Li^+ (K = 3.16 x 10^2 dm^3 mol^{-1}) a slight quenching is observed (Φ_F = 0.57), while in the presence of Ca^{2+} (K = 5.25 x 10^3 dm^3 mol^{-1}) a significant decrease to fluorescence intensity is observed (Φ_F = 0.27).[93] The metal

ion has the ability to hinder the charge transfer; halting the usual fluorescence decay pathway and thus resulting in quantum yield decreases. This is most evident with Ca^{2+}, which has a much larger ionic radius than Li^{+}, and so has a larger effect on the charge transfer process. Calcium(II) complexation results in a large hypsochromic shift to the absorption spectrum, and a decrease in molar absorptivity.[93]

A more complex example of a PCT sensor can be found in ligand (**23**), incorporating two donor groups, a dimethylamino moiety as well as the nitrogen atom in the azacrown. This is a $Donor_1$-Acceptor-$Donor_2$ (D_1-A_1-D_2) type sensor. Upon metal ion complexation, the fluorescence emission of ligand (**23**) undergoes a bathochromic shift with an increase in emission intensity. Calcium(II) complexation ($K = 3.31 \times 10^4$ dm^3 mol^{-1}) results in a 32-fold increase to the emission intensity.[94] The interesting phenomenon exhibited by this type of sensor is the conversion from the D_1-A-D_2 system in the free ligand, to a D_1-A-A_2 system on metal ion complexation. Complexation converts the D_2 group into an acceptor group A_2, which extends the emissive π–system and allows PCT to occur from the dimethylamino moiety.

There are numerous examples in which a cation interacts with a donor group, but only a limited number of systems in which interactions between a cation and an electron-withdrawing group generate a PCT mechanism. One such example is ligand (**24**), in which a diaza-18-crown ether links two courmarin groups.

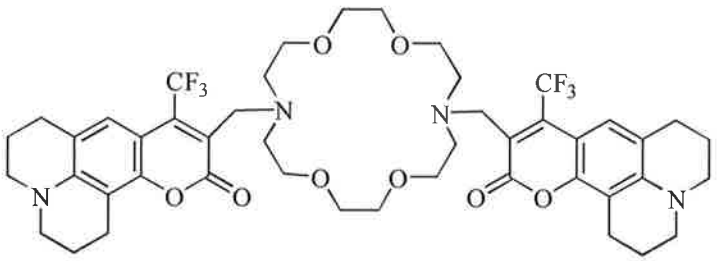

(**24**)

It is well known that a cation can interact with the carbonyl group of a courmarin, increasing the stability of the complex.[95-98] Complexation of ligand (**24**) with Ca^{2+} ($K = 6.3 \times 10^7$ dm^3 mol^{-1}) in acetonitrile causes a bathochromic shift to both the absorption and emission spectra, as a direct result of the increase to the courmarin's electron withdrawing nature.[96] The dipole moment of the aminocourmarin ligand (**24**) is larger in the excited state than in the ground state. This is due to the PCT occurring between the nitrogen atom and the carbonyl group.[50] The free ligand exhibits self-quenching and a low quantum yield. This is due to the flexibility of the azacrown, which allows the two fluorophores to exist in

close proximity to one another. In complexes with metal ions such as K^+ and Ba^+, the process of self-quenching is hindered, because the courmarin groups exist on opposite sides with respect to the metal ion. This is true only for metal ions which exhibit a good fit for the crown receptor.[96]

1.6 Excimer based fluorescent sensors

An excimer is an excited dimer, and is the result of two excited molecules (of the same identity) existing in close proximity to one another during the lifetimes of the excited states. It should be noted that an exciplex is an excited complex, which is formed when a molecule, in its ground state, interacts with another of a different chemical identity. Excimer formation is characterised by dual fluorescence, with an observed monomer band and a structureless broad band at longer wavelength.[99,100] The structureless band arises because the ground state is dissociative (i.e. it does not exist), resulting from repulsion of the ground state molecules.[71]

The distinct advantage in designing fluorescent sensors capable of excimer formation is that they allow for ratiometric detection. Ratiometric measurements involve the ratio of two fluorescence peaks instead of the absolute intensity of one peak.[101] Ratiometry allows for the determination of cation concentrations independently of various parameters such as sensor concentration, incident-light intensity, sample thickness and photobleaching.[102,103]

There are several fluorophores that can form excimers; anthracene and pyrene are common examples. The bis-(9,10-anthracenediyl)coronand (**25**) exhibits a fluorescence spectrum with both a monomer and excimer band.[104] Gradual titration of Na^+ with ligand (**25**) in methanol results in an increase to the intensity of the excimer band, and consequently a decrease to the monomer band. Complexation of the metal ion brings both anthracene functionalities closer together, favouring excimer formation. A 1:2 complex with Na^+ was observed to form by a cooperative effect (**Figure 1.6**).[105] When the larger metal ion K^+ was investigated for excimer formation, only a 1:1 complex was observed to form, the larger ionic radius of K^+ not allowing the metal ion to fit within the coronand cavities.[50]

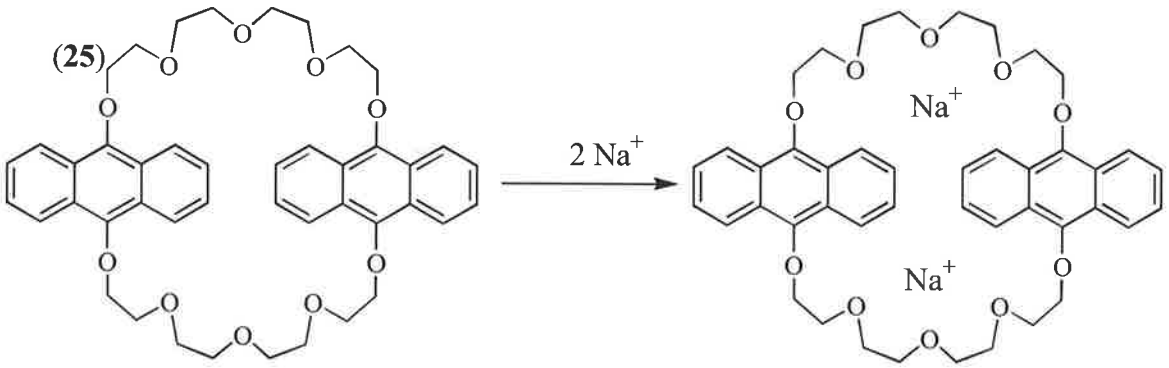

Figure 1.6. Schematic representation of the encapsulation of two molecules of Na^+, in ligand (**25**), an excimer based fluorescent sensor.

The types of sensors described so far are by no means the full extent to which the design of fluorescent sensors can be altered. Conformational geometric rearrangement on metal ion complexation can be used as a signal,[106-109] or, conversely, a simple geometric restriction of rotation in extended π–systems has also been shown to efficiently modulate signalling pathways.[110] There exist fluorescent sensors based on peptides which exhibit high selectivity for metal ions in water,[103] as well as those that utilise π,π-stacking to monitor fluorescence.[111] The fluorophore group of a fluorescent sensor does not even necessarily need to be covalently linked to the receptor. This technique is used in antibody immunoassays and involves the displacement of a fluorescent receptor group by an analyte, altering the photophysical properties of the fluorophore.[112,113]

1.7 Suitability of polyaza macrocycles as metal ion receptors

Since their first synthesis, polyaza macrocycles have played important roles in the area of metal ion complexation. They have the ability to complex metal ions with a much higher thermodynamic and kinetic stability than their non-cyclic counterparts.[114,115] The enhanced stability of the cyclized macrocyclic complexes in comparison with that of their open chain analogues is referred to as the "macrocycle effect".[116] There are two components to this effect; enthalpy and entropy.[117] The complexation of the macrocycle is favoured entropically due to its pre-ordered and more rigid structure, as it already exists in a favoured geometric arrangement for metal ion complexation.[118,119] This is in contrast to the open chain form, which must undergo significant rearrangement, and becomes more ordered on complexation, thus decreasing the entropy of the system. The geometric structure of cyclized macrocycle also plays an important part in the decrease to the measured enthalpy. The open chain form must expend more energy to orientate itself around the metal ion, than the ring, which is already in a favoured form for metal ion coordination. Thus the open chain form has a higher observed enthalpy.

It is important, when designing macrocycles as metal ion chelates, that the complexing properties are understood. The strain energy of a complex directly affects its stability. The strain energy is calculated as the sum of the bond length, bond angle and torsional distortions of the molecule as well as all the non-bonded interactions.[120] It is said that a ligand is sterically efficient when, on complexation with a metal ion, it has a low steric strain. Therefore, when a ligand is sterically efficient for a specific metal ion, it is said to have an increased selectivity for that metal ion. An important concept in ligand design is that increasing chelate ring size leads to a greater complex destabilisation for larger metal ions compared with smaller metal ions.[120,121] The rationale behind this is related to coordination numbers, and ligand-metal-ligand bond angles in larger metal ions.

The attachment of pendant arms has led to a large and diverse group of macrocyclic ligands with many varied applications. The range of donor atoms incorporated into pendant arms used in the investigation of polyaza macrocycles is quite broad; they include alcohol (**26**)[122,123] phosphate (**27**),[25] ester (**28**),[25] amine (**29**),[124] carboxylate[125] and sulfur[126] derivatives. Hancock *et al* have shown that the addition of pendant arms containing neutral donor atoms increases the selectivity of a ligand for large metal ions over that of small metal ions.[120] It has been shown that pendant arms containing carbonyl oxygens, when

compared with alcoholic oxygen groups, increase stability to a greater extent. This is thought to be due to the difference in strain energy between the two groups; the attached hydrogen atom sterically hinders the alcoholic oxygen as opposed to the carbonyl oxygen.[127]

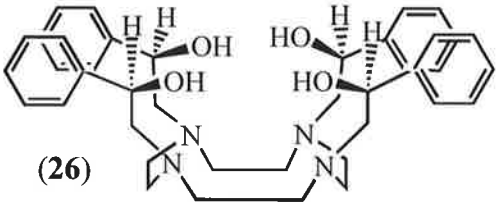

(26)

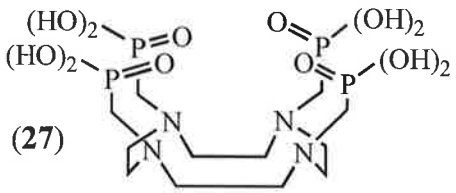

(27)

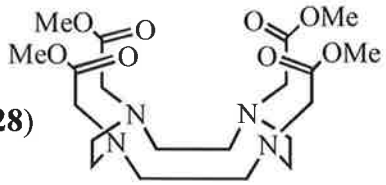

(28)

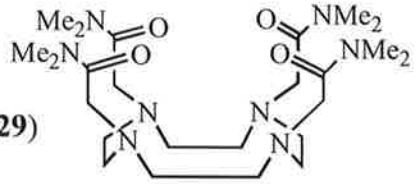

(29)

An important facet of pendant arm macrocycles is their ability to aid metal ion complexation. An example of this type is 1,4,7-triazacyclononane-*N,N,N*-triacetate (**30**). Ligand (**30**), has the ability to bind metal ions through both nitrogen and oxygen donor atoms. The metal ion complexes the ligand in a bifacial arrangement, giving the ligand a "sandwich" type effect, with the amine nitrogens on one side of the metal ion, and the donor oxygen atoms on the other. This coordination can be seen to form a "cage-like" geometry around the metal ion (**Figure 1.7**).

(30)

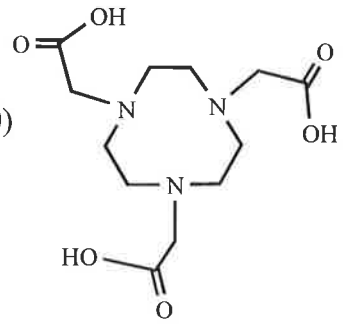

(a)

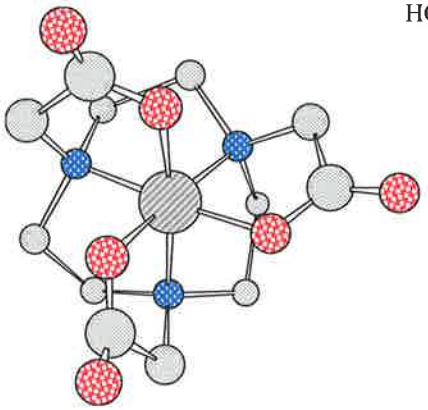

(b)

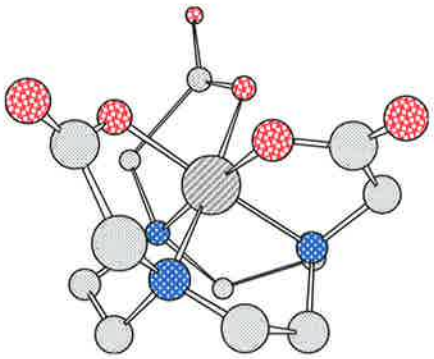

Figure 1.7. Molecular models of a metal ion complex of ligand (**30**); (a) stereoview and (b) perpendicular view to C_3 axis.

1.8 Work described in this thesis

This study is based on a series of pendant arm substituted polyaza macrocycles, 1,4,7-triazacyclononane (tacn) and 1,4,7,10-tetraazacyclododecane (cyclen), designed as either metal ion receptors or PET type fluorescent sensors.

The initial target ligands were designed as chiral receptors, capable of selectively complexing a variety of transition metal ions with high stability. Previous research in this field by Farilie *et al* has shown that it is feasible to functionalise tacn with three amino acids, as in ligand (**31**).[128] This involved the synthesis of an *N*-functionalised macrocycle with L-phenylalanine, and the investigation of its metal complex ions in the solid-state.

(31)

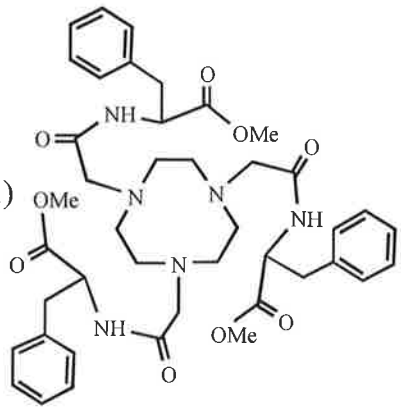

The solid-state structure of the metal complex ion of ligand (**31**) revealed the first coordination sphere to have distorted octahedral geometry. The metal ion was shown to coordinate to the three amine nitrogen atoms as well as the three amide oxygen atoms. It is known that this type of metal complex ion results in diastereomeric six coordinate Λ and Δ complexes, which often exhibit a preference for one of the diastereomeric forms. The induced chirality of these molecules is important in chiral recognition studies, such as those involving molecular recognition of host guest complexes.

The supramolecular chiral receptors discussed in this study are based on polyaza macrocycles appended with amino acid arms (**Figure 1.8**). Amino acids play a vital role in many processes. The incorporation of these into the macrocycle may lead to improved metal ion coordination and aid water solubility. Using amino acids with aromatic residues will provide a site for small molecule reception. This, coupled with the macrocyclic base for metal ion coordination, may allow for the generation of complexes with possible applications as metal ion receptors in biological fields. An acetyl linker, used to attach the amino acid pendant arms to the macrocycle, may improve the metal ion complexing ability of the system. Two types of amino acids were chosen for study, L-phenylalanine and L-tryptophan; both contain an aromatic moiety. Details of the synthesis of these ligands are presented in **Chapter 2**. The incorporation of chiral amino acids into macrocyclic ligands is important because these types of compounds are the building blocks of biological molecules[129] and because they may influence the stereoselective binding of the receptor. Important information into the use of ligands as chiral receptors will be gained through the determination of protonation constants, and stability constants, from potentiometric titrations. NMR spectral analysis will also be carried out in an effort to gain insight into the induced chirality of the synthesised receptors.

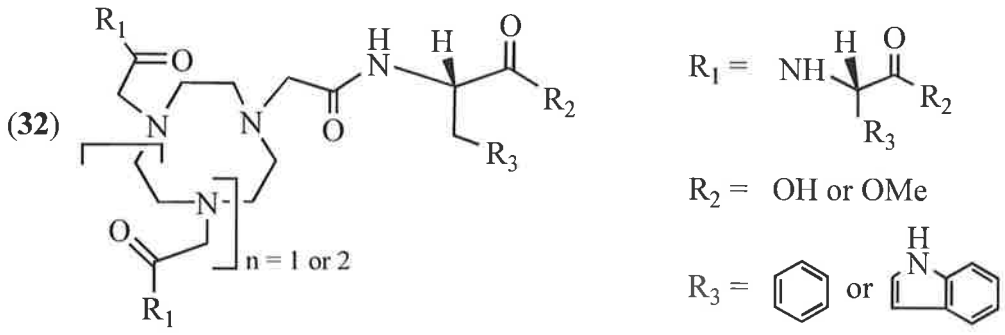

Figure 1.8. Proposed synthetic structures for chiral molecular receptors.

Polyaza macrocycles will also be modified to act as fluorescent sensors, based on the mechanism of photoinduced electron transfer (PET).[130] Polyaza macrocycles provide a unique opportunity to gain a better understanding into the mechanism of PET. They are active over a wide pH range, and many coordinate metal ions in both acidic and basic media. This is important because the ON/OFF or OFF/ON signal, so vital in the PET process, can be affected by protonation of the electron donor atom.

Anthracene has been shown to be a valuable fluorescent sensor; it can be mono-[49] or di-substituted,[131] and shows good photochemical stability.[132] The use and benefits of anthracene in similar types of molecules has been extensively studied.[58,133,134] Previous work has shown that when an anthracenyl residue is attached, via an amido bond, to a metal ion receptor, the PET process can be controlled at physiological pH 7-8, and, most importantly, it is selective for metal ions of importance.[1]

With the aim of harnessing the metal ion complexing properties of polyaza macrocycles, the incorporation of an anthracene group, through a spacer unit, should act as a highly selective fluorescent probe (**Figure 1.9**). Previous studies have shown that the cyclen molecule provides a suitable base for metal ion complexation.[135] This, coupled with an anthracene unit linked directly to the ring,[136] or through an ethylamine spacer,[5] has produced several selective fluorescent probes. The problem associated with many fluorophore systems is their lack of water solubility, due to the highly conjugated chromophore. The addition of hydroxyethyl arms to these systems should provide for a highly water-soluble derivative, which is also metal ion selective in its PET mechanism. The incorporation of chiral amino acid arms into this system may also provide a wealth of information. The introduction of chirality into the binding site may result in the sensor being capable of enantioselective recognition of chiral organic molecules.[137] Not only would the molecule have the important fluorescent moiety as well as the metal ion receptor, but it may also be able to target other molecules through its amino acid residues. This ability could prove to be of promise in the design of anti-cancer targets, metal ion sensing and drug discovery. All PET type systems will undergo both potentiometric titration and photophysical studies in order to gain insight into their behaviour in solution as well as their relevant sensing mechanisms.

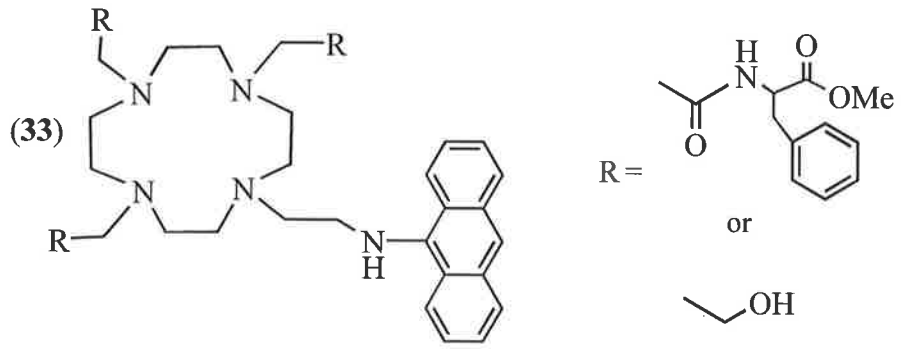

Figure 1.9. Proposed synthetic targets for the anthracene substituted ligands incorporating a PET pathway.

The aim of the study is to gain an increased understanding into the design of metal ion receptors, and fluorescent sensors incorporating PET, through the use of polyaza macrocycles with a variety of attached pendant arms.

1.9 References

(1) Fabbrizzi, L.; Licchelli, M.; Pallavicini, P.; Parodi, L. *Angew. Chem. Int. Ed. Eng.* **1998**, *37*, 800-802.

(2) Kimura, E.; Koike, T. *Chem. Soc. Rev.* **1998**, *27*, 179-184.

(3) Parker, D.; Senanayake, K.; Williams, J. A. G. *J. Chem. Soc., Perkin Trans. 2* **1998**, 2129-2140.

(4) Gunnlaugsson, T.; MacDonail, D. A.; Parker, D. *J. Chem. Soc., Chem. Commun.* **2000**, 93-94.

(5) Aoki, S.; Kaido, S.; Fujioka, H.; Kimura, E. *Inorg. Chem.* **2003**, *42*, 1023-1030.

(6) Aime, S.; Botta, M.; Fasano, M.; Terrano, E. *Chem. Soc. Rev.* **1998**, *27*, 19-29.

(7) Caravan, P.; Ellison, J. J.; McMurry, T. J.; Lauffer, R. B. *Chem. Rev.* **1999**, *99*, 2293-2352.

(8) Comblin, V.; Gilsoul, D.; Hermann, M.; Humblet, V.; Jacques, V.; Mesbahi, M.; Sauvage, C.; Desreux, J. F. *Coord. Chem. Rev.* **1999**, *185-186*, 451-470.

(9) Clarkson, I. M.; Beeby, A.; Bruce, J. I.; Govenlock, L. J.; Lowe, M. P.; Mathieu, C. E.; Parker, D.; Senanayake, K. *New J. Chem.* **2000**, *24*, 377-386.

(10) Smith, C. B.; Wallwork, K. S.; Weeks, J. M.; Buntine, M. A.; Lincoln, S. F.; Taylor, M. R.; Wainwright, K. P. *Inorg. Chem.* **1999**, *38*, 4986-4992.

(11) Davies, P. J.; Wainwright, K. P. *Inorg. Chim. Acta* **1999**, *294*, 103-108.

(12) Smith, C. B.; Lincoln, S. F.; Wainwright, K. P. *Inorg. Chim. Acta* **2001**, *317*, 21-26.

(13) Smith, C. B.; Stephens, A. K.; Wallwork, K. S.; Lincoln, S. F.; Taylor, M. R.; Wainwright, K. P. *Inorg. Chem.* **2002**, *41*, 1093-1100.

(14) Smith, C. B.; Buntine, M. A.; Lincoln, S. F.; Wainwright, K. P. *J. Chem. Soc., Dalton Trans.* **2003**, 3028-3033.

(15) Joergensen, P. L. *Biochimica et Biophysica Acta* **1982**, *694*, 27-68.

(16) Berg, J. M.; Shi, Y. *Science* **1996**, *271*, 1081-1085.

(17) Feiters, M. C. *Metal Ions in Biological Systems* **2001**, *38*, 461-655.

(18) Koukal, J.; Conn, E. E. *J. Biol. Chem.* **1961**, *236*, 2692-2698.

(19) Knof, U.; Von Zelewsky, A. *Angew. Chem. Int. Ed. Eng.* **1999**, *38*, 303-322.

(20) Provent, C.; Williams, A. F. *Transition Metals in Supramolecular Chemistry*; John Wiley and Sons: Chichester, 1999.

(21) Von Zelewsky, A. *Stereochemistry of Coordination Compounds*; John Wiley and Sons: Chichester, 2000.

(22) Mamula, O.; Von Zelewsky, A. *Coord. Chem. Rev.* **2003**, *242*, 87-95.

(23) Turonek, M. L.; Clarke, P.; Laurence, G. S.; Lincoln, S. F.; Pittet, P.; Politis, S.; Wainwright, K. P. *Inorg. Chem.* **1993**, *32*, 2195-2198.

(24) Whitbread, S. L.; Politis, S.; Stephens, A. K.; Lucas, J. B.; Dhillion, R. S.; Lincoln, S. F.; Wainwright, K. P. *J. Chem. Soc., Dalton Trans.* **1996**, 1379-1384.

(25) Wainwright, K. P. In *Advances in Inorganic Chemistry*; Academic Press, 2001; Vol. 52, pp 293-334.

(26) Dhillion, R. S.; Madback, S. E.; Ciccone, F. G.; Buntine, M. A.; Lincoln, S. F.; Wainwright, K. P. *J. Am. Chem. Soc.* **1997**, *119*, 6126-6134.

(27) Saghatelian, A.; Yokobayashi, Y.; Soltani, K.; Gahdiri, M. R. *Nature* **2001**, *409*, 797-801.

(28) Tabushi, I.; Kuroda, Y.; Mizutani, T. *J. Am. Chem. Soc.* **1986**, *108*, 4514-4518.

(29) Brown, S. E.; Coates, J. H.; Duckworth, P.; Lincoln, S. F.; Easton, C. J.; May, B. *J. Chem. Soc., Faraday Trans. 2.* **1993**, 1035-1040.

(30) Impellizzeri, G.; Maccarrone, G.; Rizzarelii, E.; Vecchio, G.; Corradini, R.; Marchelli, M. *Angew. Chem. Int. Ed. Eng.* **1991**, *30*, 1348-1349.

(31) Corradini, R.; Impellizzeri, G.; Maccarrone, G.; Marchelli, M.; Rizzarelii, E.; Vecchio, G. In *Chemistry and Properties of Biomedical Systems*; Rizzarelii, E., Theophanides, T., Eds.; Kluwer: Dordrecht, 1991.

(32) Corradini, R.; Impellizzeri, G.; Maccarrone, G.; Marchelli, M.; Rizzarelii, E.; Sartor, G.; Vecchio, G. *J. Am. Chem. Soc.* **1994**, *116*, 10267-10274.

(33) Rizzarelii, E.; Vecchio, G. *Coord. Chem. Rev.* **1999**, *188*, 343-364.

(34) Okada, Y.; Mizutani, T.; Ishii, F.; Nishimura, J. *Tet. Lett.* **1997**, *38*, 9013-9016.

(35) Damil de Namor, A. F.; Velarde, S. F. J.; Cabaleiro, M. C. *J. Chem. Soc., Faraday Trans.* **1996**, *92*, 1731-1737.

(36) Kim, S.-G.; Kim, K.-H.; Jung, J.; Shin, S. K.; Ahn, K. H. *J. Am. Chem. Soc.* **2002**, *124*, 591-596.

(37) Denat, F.; Brandes, s.; Guilard, R. *Synlett* **2000**, *5*, 561-574.

(38) Stevenson, D.; Williams, G. A.; Stevenson, D., Wilsion, I., Eds.; Plenum Press: New York, 1987, pp 1-9.

(39) Lam, S.; Lough, W. J., Ed.; Blackie: New York, 1989, pp 85-101.

(40) Crabbe, P. *Optical Rotatory Dispersion and Circular Dichrosim in Organic Chemistry*; Holden-Day: San Francisco, 1965.

(41) Bernhard, W. *Atomic absorption spectroscopy*; Verlag Chemie: Weinheim, 1976.

(42) Koryta, J. *Ion-selective electrodes*; 2nd ed. Cambridge, 1983; Vol. Cambridge University Press.

(43) Willard, H. H.; Merrit, L. L., Jr; Merrit, L. L.; Dean, J. A. *Instrumental Methods of Analysis*; 6th Ed ed.; Wadsworth Publishing Co: Belmont, 1981.

(44) Kawai, H.; Nagamura, T.; Mori, T.; Yoshida, K. *J. Phys. Chem. A* **1999**, *103*, 660-663.

(45) Wang, S.; Zhang, Q.; Datta, P. K.; Gawley, R. E.; Leblanc, R. M. *Langmuir* **2000**, *16*, 4607-4612.

(46) Baeyens, W. R. G.; Keukeleire, D.; Korkidis, K., Eds. *Luminescence Techniques in Chemical and Biochemical Analysis*; Marcel Dekker: New York, 1991.

(47) Mason, W. T., Ed. *Fluorescent and Luminescent Probes for Biological Acitivity*; Academic Press: London, 1993.

(48) Quici, S.; Manfredi, A.; Buttafava, M. *J. Org. Chem.* **1996**, *61*, 3870-3873.

(49) Fabbrizzi, L.; Licchelli, M.; Parodi, L.; Poggi, A.; Taglietti, A. *Eur. J. Inorg. Chem.* **1999**, 35-39.

(50) Valeur, B.; Leray, I. *Coord. Chem. Rev.* **2000**, *205*, 3-40.

(51) de Silva, A. P.; Gunaratne, H. Q. N.; Gunnlaugsson, T.; Huxley, A. J. M.; Rademacher, J. T.; Rice, T. E.; Desvergne, J.-P., Czarnik, A. W., Eds.; Kluwer Academic Publishers: Netherlands, 1997, pp 143-157.

(52) Prodi, L.; Bolletta, F.; Montalti, M.; Zaccheroni, N. *Coord. Chem. Rev.* **2000**, *205*, 59-83.

(53) Haugland, R. P., Ed. *Handbook of Fluorescent Probes and Reasearch Products*; 9th ed.; Molecular Probes, Inc: Eugene, 2002.

(54) Slavik, J. *Fluorescent Probes in Cellular and Molecular Biology*; CRC Press: Boca Raton, 1994.

(55) de Silva, A. P.; Fox, D. B.; Huxley, A. J. M.; Moody, T. S. *Coord. Chem. Rev.* **2000**, *205*, 41-57.

(56) de Silva, A. P.; de Silva, S. A. *J. Chem. Soc., Chem. Commun* **1986**, 1709-1710.

(57) Bissell, R. A.; de Silva, A. P.; Gunaratne, H. Q. N.; Lynch, P. L. M.; Maguire, G. E. M.; McCoy, C. P.; Sandanayake, K. R. A. S. *Top. Curr. Chem.* **1993**, *168*, 223-264.

(58) de Silva, A. P.; Gunaratne, H. Q. N.; Gunnlaugsson, T.; Huxley, A. J. M.; McCoy, C. P.; Rademacher, J. T.; Rice, T. E. *Chem. Rev.* **1997**, *97*, 1515-1566.

(59) Kollmannsberger, M.; Rurack, K.; Resch-Genger, U.; Daub, J. *J. Phys. Chem. A* **1998**, *102*, 10211-10220.

(60) Akkaya, E. U.; Huston, M. E.; Czarnik, A. W. *J. Am. Chem. Soc.* **1990**, *112*, 3590-3593.

(61) Chae, M.-Y.; Cherian, X. M.; Czarnik, A. W. *J. Org. Chem.* **1993**, *58*, 5797-5801.

(62) Yoshida, K.; Mori, T.; Watanabe, S.; Kawai, H.; Nagamura, T. *J. Chem. Soc., Perkin Trans. 2* **1999**, 393-397.

(63) Shen, Y.; Sullivan, B. P. *Inorg. Chem.* **1995**, *34*, 6235-6236.

(64) Keefe, M. H.; Benkstein, K. D.; Hupp, J. T. *Coord. Chem. Rev.* **2000**, *205*, 201-228.

(65) Fages, F.; Desvergne, J.-P.; Boaus-Laurent, H.; Marsau, P.; Lehn, J.-M.; Kotzyba-Hubert, F.; Albrecht-Gary, A.-M.; Al-Joubbeh, M. *J. Am. Chem. Soc.* **1989**, *111*.

(66) Buet, P.; Kastenholz, F.; Grell, E.; Kaeb, G.; Hafner, A.; Schnieder, F. W. *J. Phys. Chem. A* **1999**, *103*, 5871-5881.

(67) Ramachandram, B.; Samanta, A. *Chem. Commun.* **1997**, 1037-1038.

(68) Hampe, E. M.; Rudkevich, D. M. *Chem. Commun.* **2002**, 1450-1451.

(69) Prodi, L.; Ballardini, R.; Gandolfi, M. T.; Roversi, R. *J. Photochem. Photobiol. A* **2000**, *136*, 49-52.

(70) Fabbrizzi, L.; Licchelli, M.; Pallavicini, P.; Perotti, A.; Taglietti, A.; Sacchi, D. *Chem. Eur. J.* **1996**, *2*, 75-82.

(71) Suppan, P. *Chemistry and Light*; Royal Society of Chemistry: London, 1994.

(72) Turfan, B.; Akkaya, E. U. *Org. Lett.* **2002**, *4*, 2857-2859.

(73) Aoki, L.; Sakaki, T.; Shinkai, S. *J. Chem. Soc., Chem. Commun.* **1992**, 730-732.

(74) de Silva, A. P.; McCoy, C. P. *Chem. Ind.* **1994**, 992.

(75) de Silva, A. P.; Gunaratne, H. Q. N.; McCoy, C. P. *J. Am. Chem. Soc.* **1997**, *119*, 7891-7892.

(76) de Silva, A. P.; Gunaratne, H. Q. N.; McVeigh, C.; Maguire, G. E. M.; Maxwell, P. R. S.; O'Hanlon, E. *Chem. Commun.* **1996**, 2191-2192.

(77) Kruck, Z. L.; Pycock, C. J. *Neurotransmitters and Drugs*; Chapman and Hall: London, 1990.

(78) Nicoll, R. A.; Malenka, R. C.; Kauer, J. A. *Physiol. Rev.* **1990**, *70*, 513-565.

(79) Gunnlaugsson, T.; Davies, P. J.; Hussey, G. M.; Tierney, J.; Glynn, M. *Org. Biomol. Chem.* **2004**, *2*, 1856-1863.

(80) Kubo, Y.; Kato, M.; Misawa, Y.; Tokita, S. *Tet. Lett.* **2004**, *45*, 3769-3773.

(81) de Silva, A. P.; Gunaratne, H. Q. N.; McCoy, C. P. *Chem. Commun.* **1996**, 2399-2400.

(82) Kele, P.; Orbulescu, J.; Calhoun, T. L.; Gawley, R. E.; Leblanc, R. M. *Tet. Lett.* **2002**, *43*, 4413-4416.

(83) Falconer, I. R., Ed. *Algal Toxins in Seafood and Drinking Water*; Academic Press: London, 1993.

(84) Hall, S.; Strichartz, G.; Moczydlowski, E.; Ravindran, A.; Reichardt, P. B. *Marine Toxins. Origin, Structure and Molecular Pharamcology*; American Chemical Society: Washington DC, 1990; Vol. 418.

(85) Miyaji, H.; Sessler, J. L. *Angew. Chem. Int. Ed. Eng.* **2001**, *40*, 154-157.

(86) Lee, D. H.; Lee, K. H.; Hong, J. *Org. Lett.* **2001**, *3*, 5-8.

(87) Gunnlaugsson, T.; Davis, A. P.; Glynn, M. *Chem. Commun.* **2001**, 2556-2557.

(88) Valeur, B.; Badaoui, F.; Bardez, E.; Bourson, J.; Boutin, P.; Chatelin, A.; Devol, I.; Larrey, B.; Lefevre, J. P.; Soulet, A. In *Chemosensors of Ion and Molecule Recognition*; Desvergne, J.-P., Czarnik, A. W., Eds.; Kluwer: Dordrecht, 1997.

(89) Rettig, W.; Lapouyade, R. In *Topics in Fluorescence Spectroscopy*; Lakowicz, J. R., Ed.; Plenum: New York, 1994.

(90) Valeur, B.; Bourson, J.; Pouget, J. *Fluorescent Chemosensors for Ion and Molecule Recognition*; American Chemical Society: Washington Dc, 1993.

(91) Rurack, K. *Spectrochim. Acta, Part A* **2001**, *57*, 2161-2195.

(92) Martin, M. M.; Plaza, P.; Dai Hung, N.; Meyer, Y. H.; Bourson, J.; Valeur, B. *Chem. Phys. Lett* **1993**, *202*, 425-430.

(93) Bourson, J.; Valeur, B. *J. Phys. Chem.* **1989**, *93*, 3871-3876.

(94) Rurack, K.; Rettig, W.; Resch-Genger, U. *Chem. Commun.* **2000**, 407-408.

(95) Bourson, J.; Borrel, M.-N.; Valeur, B. *Anal. Chim. Acta* **1992**, *257*, 189.

(96) Bourson, J.; Pouget, J.; Valeur, B. *J. Phys. Chem.* **1993**, *97*, 4552-4557.

(97) Bourson, J.; Badaoui, F.; Valeur, B. *Fluoresc* **1994**, *4*, 275.

(98) Habib-Jiwan, J.-L.; Branger, C.; Soumillion, J.-P.; Valeur, B. *J. Photochem. Photobiol. A* **1998**, *116*, 127-133.

(99) Bhattacharyya, K.; Chowdhury, M. *Chem. Rev.* **1993**, *93*, 507-535.

(100) Katoh, R.; Katoh, E.; Nakashima, N.; Yuuki, M.; Kotani, M. *J. Phys. Chem. A* **1997**, *101*, 7725-7728.

(101) King, M.; Kopelman, R. *Sensors and Actuators B* **2003**, *90*, 76-81.

(102) Leray, I.; Lefevre, J. P.; Delouis, J.-F.; Delaire, J.; Valeur, B. *Chem. Eur. J.* **2001**, *7*, 4590-4598.

(103) Deo, S.; Godwin, H. A. *J. Am. Chem. soc.* **2000**, *122*, 174-175.

(104) Marquis, D.; Desvergne, J.-P.; Bouas-Laurent, H. *J. Org. Chem.* **1995**, *60*, 7984-7996.

(105) Marquis, D.; Desvergne, J.-P. *Chem. Phys. Lett.* **1994**, *230*, 131-136.

(106) Krauss, R.; Weinig, H.-G.; Seydack, M.; Bendig, J.; Koert, U. *Angew. Chem. Int. Ed.* **2000**, *39*, 1835-1837.

(107) Glass, T. E. *J. Am. Chem. Soc.* **2000**, *122*, 4522-4523.

(108) Raker, J.; Glass, T. E. *J. Org. Chem.* **2001**, *66*, 6505-6512.

(109) Raker, J.; Glass, T. E. *Tetrahedron* **2001**, *57*, 10233-10240.

(110) Hendrickson, K. M.; Rodopoulos, T.; Pittet, P.-A.; Mahadevan, I.; Lincoln, S. F.; Ward, A. D.; Kuruscew, T.; Duckworth, P. A.; Forbes, I. J.; Zalewski, P. D.; Betts, W. H. *J. Chem. Soc., Dalton Trans.* **1997**, 3879-3882.

(111) Fenniri, H.; Hosseini, M. W.; Lehn, J.-M. *Helv. Chim. Acta* **1997**, *80*, 786-803.

(112) Wiskur, S. L.; Ait-Haddou, H.; Lavigne, J. J.; Anslyn, E. V. *Acc. Chem. Res.* **2001**, *34*, 963-972.

(113) Fabbrizzi, L.; Leone, A.; Taglietti, A. *Angew. Chem. Int. Ed. Eng.* **2001**, *40*, 3066-3069.

(114) Kodama, M.; Kimura, E. *J. Chem. Soc., Chem. Commun.* **1975**, 326-327.

(115) Thom, V. J.; Boeyens, J. C. A.; McDougall, G. J.; Hancock, R. D. *J. Am. Chem. Soc.* **1984**, *106*, 3198-3207.

(116) Cabbiness, D. K.; Margerum, D. W. *J. Am. Chem. Soc.* **1969**, *91*, 6540-6541.

(117) Munro, D. *Chem. In Britain* **1997**, *13*, 100-105.

(118) Izatt, R. I.; Pawlak, K.; Bradshaw, J. S. *Chem. Rev.* **1991**, *91*, 1721-2085.

(119) Comba *Coord. Chem. Rev.* **1999**, *182*, 343-371.

(120) Hancock, R. D.; Martell, A. E. *Chem. Rev.* **1989**, *89*, 1875-1914.

(121) Hancock, R. D.; Bhavan, R.; Wagner, C. A.; Hosken, G. D. *S. Afr. J. Chem.* **1986**, *39*, 238-242.

(122) Whitbread, S. L.; Valente, P. V.; Buntine, M. A.; Clements, P.; Lincoln, S. F.; Wainwright, K. P. *J. Am. Chem. Soc.* **1998**, *120*, 2862-2869.

(123) Whitbread, S. L.; Valente, P. V.; Buntine, M. A.; Clements, P.; Lincoln, S. F.; Wainwright, K. P. *J. Am. Chem. Soc.* **1998**, *120*, 11212.

(124) Hancock, R. D.; Reibenspies, J. H.; Maumela, H. *Inorg. Chem.* **2004**, *43*, 2981-2987.

(125) Hambley, T.; Lawrance, g.; Maeder, M.; Wilkes, E. N. *Inorg. Chim. Acta* **1996**, *246*, 65-71.

(126) Bazzicalupi, C.; Bencini, A.; Bianchi, A.; Fedi, V.; Giorgi, C.; Paoletti, P.; Tei, L.; Valtancoli, B. *Inorg. chim. Acta* **2000**, *300-302*, 653-660.

(127) Hancock, R. D. *Pure Appl. Chem.* **1993**, *65*, 941-946.

(128) Watson, A. A.; Willis, A. C.; Fairlie, D. P. *Inorg. Chem.* **1997**, *36*, 752-753.

(129) Zhao, H.; Hua, W. *J. Org. Chem.* **2000**, *65*, 2933-2938.

(130) Piotrowiak, P. *Chem. Soc. Rev.* **1999**, *28*, 143-150.

(131) Czarnik, A. W. *Acc. Chem. Res.* **1994**, *27*, 302-308.

(132) Becker, H. D. *Chem. Rev.* **1993**, *93*, 145-172.

(133) de Silva, S. A.; Amorelli, B.; Isidor, D. C.; Loo, K. C.; Crooker, K. E.; Pena, Y. E. *Chem. Commun.* **2002**, 1360-1361.

(134) De Santis, G.; Fabbrizzi, L.; Faravelli, I.; Licchelli, M.; Poggi, A.; Taglietti, A. *Angew. Chem. Int. Ed.* **1996**, *35*, 202-204.

(135) Aoki, S.; Iwaida, K.; Hanamoto, N.; Shiro, M.; Kimura, E. *J. Am. Chem. Soc.* **2002**, *124*, 5256-5257.

(136) Czarnik, A. W. *Acc. Chem. Res.* **1994**, *27*, 302-308.

(137) Pu, L. *Chem. Rev.* **2004**, *104*, 1687-1716.

Chapter 2. Synthesis

2.1 Synthesis of 1,4,7 triazacyclononane (tacn)

The size of the macrocyclic ring has been shown to confer selectivity for both metal ions and other analytes. Therefore, in an effort to develop chiral receptors capable of targeting a variety of species, two different sized macrocyclic rings have been incorporated into the receptor design; 1,4,7-triazacyclononane (tacn) and 1,4,7,10-tetraazacyclododecane (cyclen). Recent developments in macrocyclic synthesis have meant that cyclen is both readily available and cheap to purchase. A high yielding preparative method by Richman and Atkins[1] has allowed a facile synthesis of tacn. However, the process remains lengthy and involves numerous steps, **Scheme 1**.

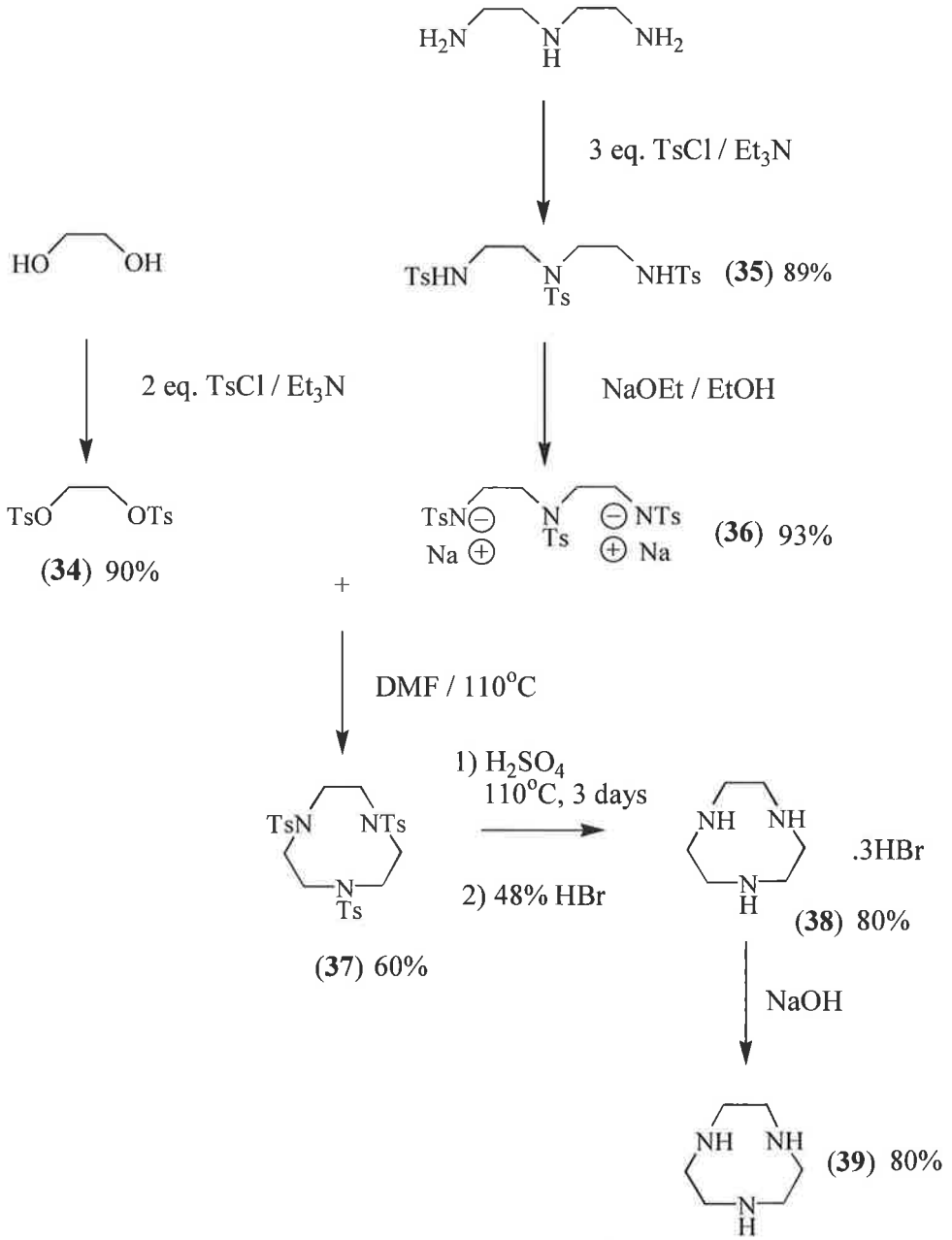

Scheme 1

The initial steps toward the synthesis of tacn involved the functionalisation of two linear starting materials; the tosylated derivatives of ethylene glycol and diethylenetriamine. The di-tosylated ethane species (**34**) was prepared by the addition of two equivalents of *p*-toluenesulfonyl chloride to ethylene glycol, in the presence of triethylamine, to yield white crystals in 90% yield. The functionalisation of diethylenetriamine was performed under similar reaction conditions, to yield the tri-tosylated diethylenetriamine (**35**) in 89% yield. ^{1}H and ^{13}C NMR spectra of both compounds showed characteristic aromatic resonances consistent with the presence of the incorporated tosyl groups. The sharp melting point observed for each compound corresponded to literature values.[2,3]

Prior to cyclisation of the two linear starting materials, the tri-tosylated diethylene triamine was converted to a sodium salt in order to facilitate the condensation reaction. Compound (**35**) was dissolved in ethanol, 2.8 equivalents of sodium metal were added slowly, and the reaction mixture was left overnight. This resulted in the formation of a white precipitate, which was dried under high vacuum to yield the tri-tosylated sodium salt (**36**) as a powder in 93% yield. Due to the insolubility of the sodium salt (**36**) in common deuterated solvents, a melting point analysis was the only viable option to confirm the identity of the product. The melting point of the sodium salt (**36**) (293-294°C) was consistent with literature values.[2]

The cyclisation of the di-tosylated ethane derivative (**34**), with the di-sodium salt of diethylenetriamine (**36**), was achieved by the drop-wise addition of compound (**36**) into a solution of (**34**) in dry DMF. The reaction mixture was left to stir overnight. The DMF was subsequently removed by means of high vacuum distillation. Recrystallisation from acetone/water yielded the tri-tosylated macrocycle (**37**) as a white crystalline product in 60% yield. Compound (**37**) was characterised by means of ^{1}H and ^{13}C NMR spectroscopy. A ^{1}H NMR single methylene resonance at δ 3.42 ppm, and a single ^{13}C NMR resonance at δ 51.9 ppm, confirmed the symmetrical nature of the ring. The characteristic tosyl group ^{1}H NMR resonances were also identifiable. Electrospray mass spectrometry (LCQ) detected a molecular ion at *m/z* 592.

The next step in the synthetic pathway was the removal of the *N*-tosyl groups attached to each of the three amine groups in the macrocyclic ring. This was achieved by heating the tri-tosylated macrocycle (**37**) in concentrated sulfuric acid for 3 days under nitrogen at 110°C. This gave a grey precipitate of the sulfonic acid salt of tacn. The salt is unstable. To improve stability, it was converted to the stable tri-hyrdrobromide tacn salt (**38**), by the drop-wise addition of 48% hydrobromic acid, to a solution of the sulfonic acid salt in hot water.[3] This yielded the tri-hydrobromide tacn salt (**38**) as a pale grey solid. The final step was the liberation of the free amine (**39**), which was achieved by adjusting the pH of an aqueous solution of the tri-hydrobromide salt (**38**) with aqueous sodium hydroxide to pH 9, upon which the solution turned brown.[4] Water was removed by means of azeotropic distillation with a Dean-Stark apparatus, to afford tacn (**39**) as a white amorphous solid in 80% yield. A single ^{13}C NMR resonance and a melting point over the range of 43-44°C was measured, consistent with literature values for tacn.[1]

2.2 Synthesis of the chiral amino acid pendant arm ligands

A series of *N*-functionalised polyaza macrocycles, incorporating chiral amino acid pendant arms, have been developed with the potential to act as chiral receptors, utilising the tacn and cyclen rings as backbones. Two different amino acids were incorporated to observe the influence each had on metal ion complexation, L-phenylalanine and L-tryptophan. Both amino acids have aromatic residues, which may possibly act as receptors for small molecules. It has been shown that in similar molecules, the inclusion of a carbonyl group β to the macrocyclic ring amine, aids metal ion complexation.[5] Thus both amino acids have been similarly functionalised. The initial amino acid chosen for investigation was the L-phenylalanine residue.

2.2.1 Tacn series, L-phenylalanine

The synthetic pathway involves the acylation of a protected amino acid with bromoacetyl bromide, followed by alkylation to the macrocycle, **Scheme 2**.[6]

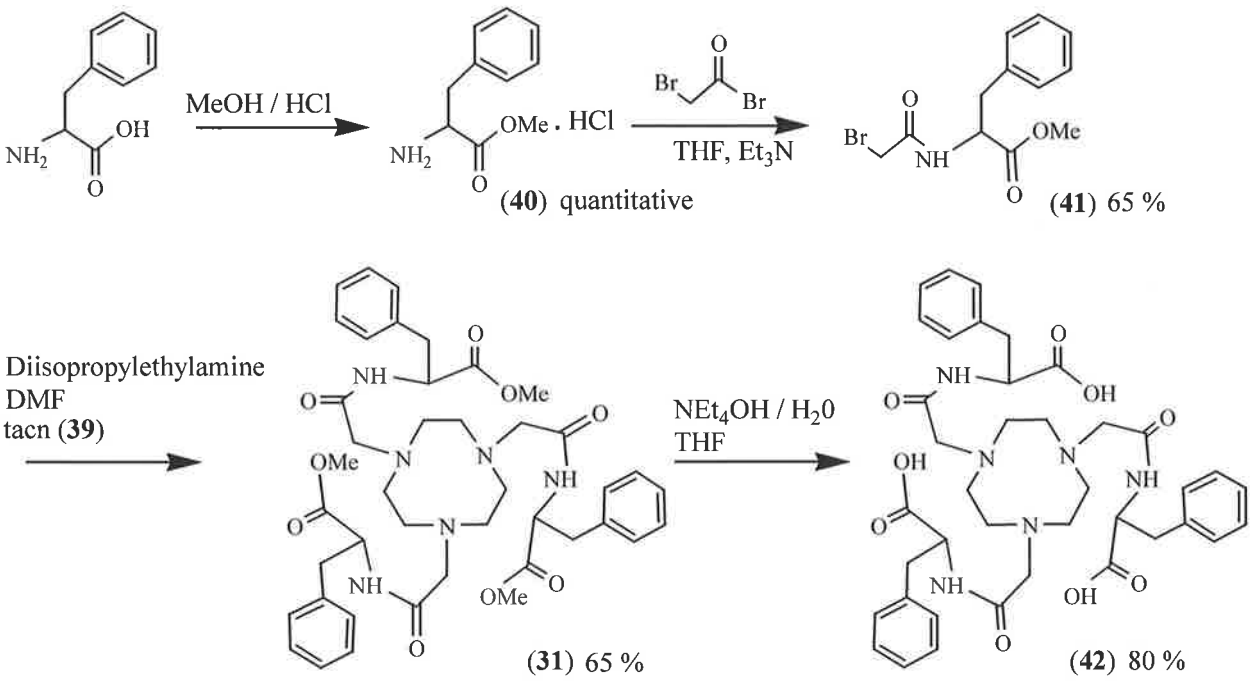

Scheme 2

The first step in the synthetic pathway involved the protection of the carboxylic acid group of L-phenylalanine, ensuring that further reactions occurred at the amine nitrogen. The conversion of the acid group to the methyl ester was achieved by acid catalysed esterification. This yielded the L-phenylalanine methyl ester hydrochloride salt (**40**) in quantitative yield. The disappearance in the ^{1}H NMR spectrum of a broad singlet at δ 4.33 ppm and the appearance of a sharp singlet at δ 3.68 ppm, were used to monitor the reaction. All other physical and spectral data was consistent with literature values.[7,8]

Once protected, the *N*-terminus of the L-phenylalanine methyl ester (**40**) was acylated by a reaction involving bromoacetyl bromide under anhydrous conditions. The amino acid derivative (**40**) was dissolved in a solution of dry THF and triethylamine, which was cooled to 0°C. A solution of bromoacetyl bromide in dry THF was then added, drop-wise by a syringe, over a period of 20 minutes. Following this addition, the reaction mixture was left to warm to room temperature over a period of 1 hour. After an acidic

workup the resultant brown oil was dried under high vacuum to yield the product (**41**) as a crystalline solid in 65% yield. The product (**41**) was used without further purification in the following reactions. ^{1}H and ^{13}C NMR spectroscopy and mass spectrometry confirmed the identity of product (**41**). The presence of the two carbonyl groups in the amino acid derivative was seen in the ^{13}C NMR spectrum, with two resonances appearing above δ 160 ppm; one at δ 165.0 ppm for the acetyl carbonyl and one at δ 171.2 ppm for the methyl ester. The molecular ion at *m/z* 300 was also consistent with literature values.[6] It was found that an improved yield resulted if the reaction temperature was kept below 10°C at all times during the addition of bromoacetyl bromide. The major by-product, formed in the reaction of the amino acid derivative (**40**) with bromoacetyl bromide, was a dimer of the L-phenylalanine methyl ester (**43**). ^{1}H and ^{13}C NMR spectroscopy and mass spectrometry confirmed the formation. The by-product (**43**) was found to form only above the 10°C threshold see **Scheme 3**.

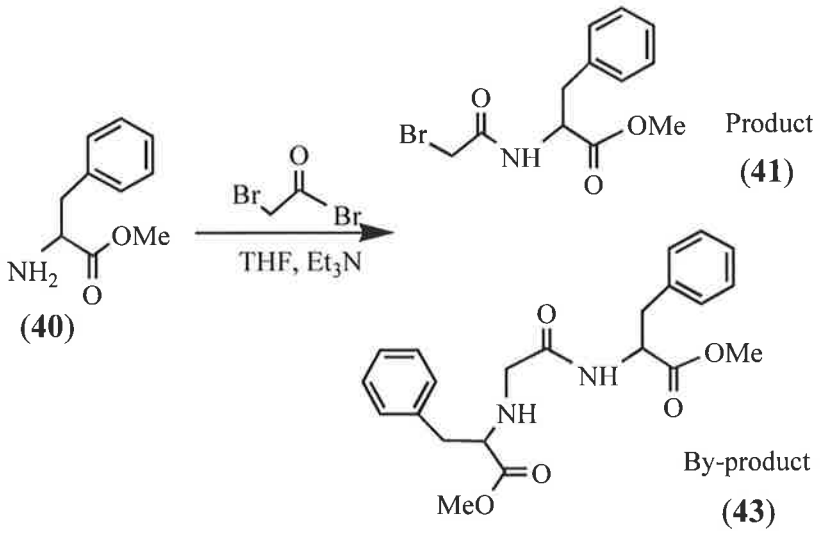

Scheme 3

The next step in the synthetic pathway was the alkylation of the macrocycle by the bromoacetylated amino acid (**41**). The reaction was carried out under nitrogen at 0°C in a solution of dry DMF, *N*,*N*-diisopropylethylamine and 3.5 equivalents of the amino acid derivative (**41**). Solid tacn was then added, and the reaction mixture left to stir overnight. An extensive workup and purification procedure followed, to yield the *N*-functionalised macrocycle (**31**) as a white fluffy solid in 65 % yield. The methylene signals in the macrocyclic ring were clearly observable in both the ^{1}H NMR spectrum, as an AA'BB' multiplet at δ 2.45 ppm, as well as in the ^{13}C NMR spectrum as a broad singlet at δ 56.5 ppm, in a solution of $CDCl_3$.

The macrocycle (**31**) was observed to decompose into a yellow sticky gum over a period of time. Analysis of the resulting product revealed that fragmentation of the macrocycle had occurred, by means of hydrolysis at the amide group in the pendant arm, to give the methyl ester of L-phenylalanine (**40**). Confirmation of this was gained by NMR spectroscopy. The instability of the compound was overcome by storage under vacuum over the drying agent, P_4O_{10}.

Ligand (**31**) was found to be soluble only in partially aqueous solvents systems, consequently leading to the final product in this pathway, ligand (**42**). Ligand (**31**) was dissolved in a solution of THF and 0.1 mol dm^{-3} aqueous tetraethylammonium hydroxide (NEt_4OH). The reaction mixture was left to stir at room temperature under nitrogen for 4 days, after which the solvent was removed under reduced pressure, and excess NEt_4OH removed by trituration with acetone. Ligand (**42**) was isolated as a tetraethylammonium (NEt_4) salt, $C_{39}H_{45}O_9N_6.3NEt_4$, in 80% yield. The ^1H NMR spectrum confirmed the hydrolysis of the ester group by the disappearance of the signal at δ 3.72 ppm, and this was corroborated by the ^{13}C NMR spectrum, by the loss of the signal at δ 52.3 ppm. The number of NEt_4^+ ions, incorporated per molecule of ligand (**42**), was confirmed by ^1H NMR integration and electrospray mass spectrometry (LCQ). The ligand was found to be very hygroscopic, rapidly forming an oil on exposure to air. Isolation of ligand (**42**) as a zinc triflate salt (**44**) allowed for identification by microanalysis. Ligand (**42**) was found to be water soluble at neutral pH 7.

2.2.2 Cyclen series, L-phenylalanine

The next ligands to be synthesised were the tetraaza macrocycles, utilising cyclen. The same amino acid, L-phenylalanine, was incorporated as the pendant arm. Both the ester and the acid derivatives were synthesised, to allow for a direct comparison of the physical and spectral characteristics of the receptors based on the two macrocycles, tacn and cyclen. The synthetic pathway for this series was analogous to that of the tacn based ligands (**31**) and (**42**), **Scheme 4**.

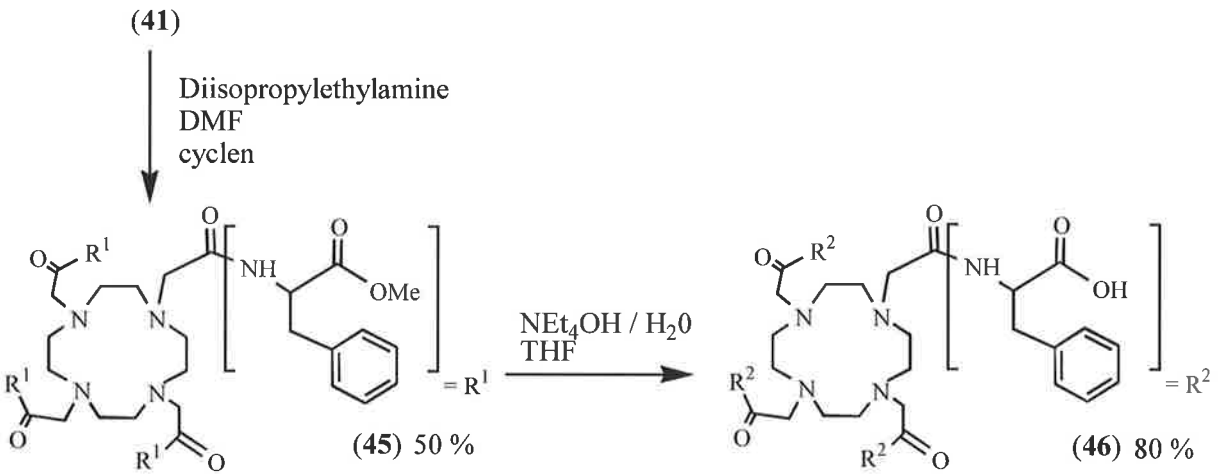

Scheme 4

N-Bromoacetyl-L-phenylalanine methyl ester (**41**) in the appropriate molar ratio, was dissolved in dry DMF and *N,N*-diisopropylethylamine under nitrogen, and cooled to 0°C. Solid cyclen was then added, and the reaction mixture left to stir overnight. This was followed by the same purification technique used in the synthesis of ligand (**31**), to produce a white solid, ligand (**45**) in 50% yield. Ligand (**45**) was characterised by ^{1}H NMR spectroscopy and microanalysis. A ^{1}H NMR resonance at δ 3.68 ppm with an integration of 12H, due to the hydrogens in the methyl ester group, confirmed the addition of all four pendant arms to the tetraaza macrocycle. An AA'BB' multiplet ^{1}H NMR resonance at δ 2.36-2.57 ppm, from the macrocyclic ring, was also observed in the spectrum. The cyclen based ligand (**45**) was found to have very similar physical characteristics to that of the tacn based ligand (**31**). Both ligands (**31**) and (**45**) are unstable to prolonged exposure to air and are soluble only in partially aqueous solvent systems.

The final step in the synthetic pathway was the hydrolysis of the methyl ester group to produce its water soluble derivative, ligand (**46**). The cyclen ester, ligand (**45**), was dissolved in a solution of THF and 0.1 mol dm^{-3} aqueous NEt_4OH and left to stir under nitrogen for 4 days. Purification in an analogous manner to that of ligand (**42**), resulted in the formation of the NEt_4^+ salt of ligand (**46**), $C_{52}H_{64}N_8O_{12}.4NEt_4$, in 80% yield. The ^1H NMR spectrum confirmed complete removal of the four methyl ester groups, by the disappearance of the resonance at δ 3.68 ppm. ^1H NMR integration also confirmed the number of incorporated NEt_4^+ ions. The cyclen acid (**46**) exhibited analogous properties to the tacn acid (**42**); both are water soluble at neutral pH 7 and are very hygroscopic. The hygroscopic nature of ligand (**46**) did not allow for its elemental confirmation by microanalysis; verification was achieved by the formation of its zinc triflate salt (**47**).

2.2.3 Tacn and cyclen series, L-tryptophan

The synthesis of the L-tryptophan based ligands followed an equivalent route to that of the L-phenylalanine amino acid derivatives, **Scheme 5**.

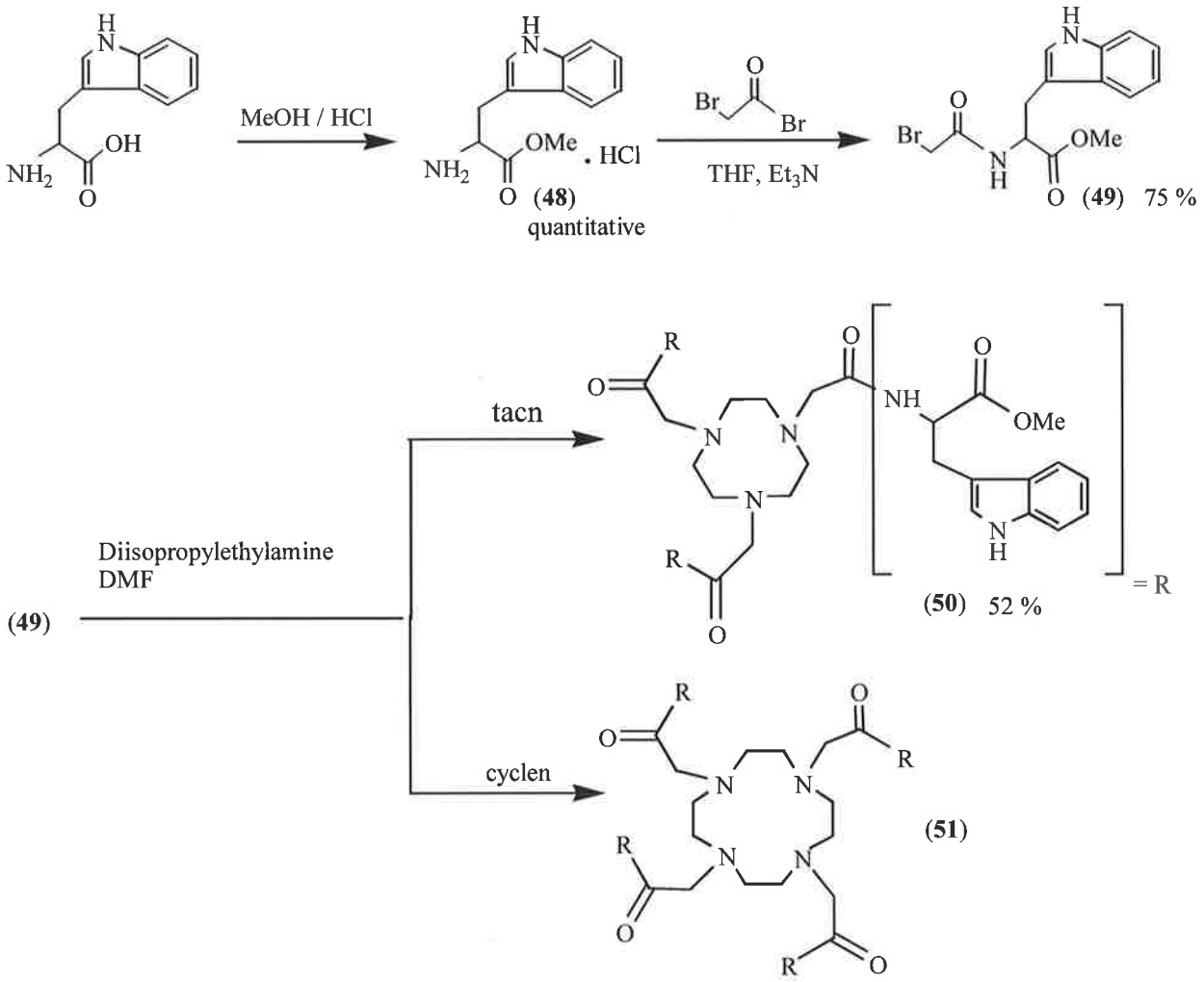

Scheme 5

The amino acid, L-tryptophan, was initially protected by acid catalysed esterification and the resultant HCl salt (**48**) was obtained in quantitative yield. Melting point and ^{1}H NMR analysis were consistent with literature values.[9] The salt (**48**) was reacted with bromoacetyl bromide and triethylamine in dry THF, to yield the bromoacetylated L-tryptophan methyl ester (**49**) in 75% yield. Confirmation of the acetylation was achieved by ^{13}C NMR spectroscopy and mass spectrometry. The appearance of two carbonyl resonances above δ 160 ppm, one at δ 165.2 and the other at δ 171.6 ppm, in the ^{13}C NMR spectrum, as well as the molecular ion at *m/z* 338 were

consistent with the formation of compound (**49**). The bromoaceylated amino acid (**49**) was used without further purification in the following reactions.

Functionalisation of the macrocyclic ring was achieved under a nitrogen atmosphere, in the presence of the bromoaceylated amino acid (**49**), *N*,*N*-diisopropylethylamine, and dry DMF. Tacn was added as a solid after the reagents were cooled to 0°C. The work-up and purification of the product was analogous to those of the previous esters, ligands (**31**) and (**45**), to afford ligand (**50**) as a white fluffy solid in 52% yield. The protons in the macrocyclic ring were observed as an AA'BB' multiplet at δ 2.45 ppm in the ^{1}H NMR spectrum. The macrocyclic ring carbons appeared as a single resonance at δ 56.5 ppm in the ^{13}C NMR spectrum in $CDCl_3$. A fast rate of decomposition was observed for this ligand; storage under vacuum over a suitable drying agent (P_4O_{10}) did not negate the problem. It was found that formation of a metal complex ion increased the stability of ligand (**50**). Microanalysis of the zinc triflate salt (**52**) was obtained in order to confirm the elemental composition of ligand (**50**). The instability of ligand (**50**) is believed to be due to the bulky nature of the aromatic groups present in the tryptophan amino acid pendant arms.

Concurrently to the synthesis of the tacn tryptophan ligand (**50**), the cyclen-based derivative ligand (**51**) was also investigated. The reaction was analogous to that of the tacn macrocycle ligand (**50**), differing only in the molar equivalents of the pendant arm used. Upon purification of the reaction it was found that the tetra-substituted ligand (**51**) was not formed. Electrospray mass spectrometry (LCQ) confirmed the presence of three molecular ions, *m/z* 947, 734 and 477, arising from the tri-, di- and mono-substituted macrocyclic rings, respectively (**Figure 2.1**). Separation of the three isomers was not possible by either column chromatography or recrystallisation. Varying the reaction time or the molar equivalents of the bromoaceylated amino acid (**49**), did not alter the outcome of the reaction. The steric bulkiness of the tryptophan derivative is thought to inhibit the addition of the fourth pendant arm to the ring.

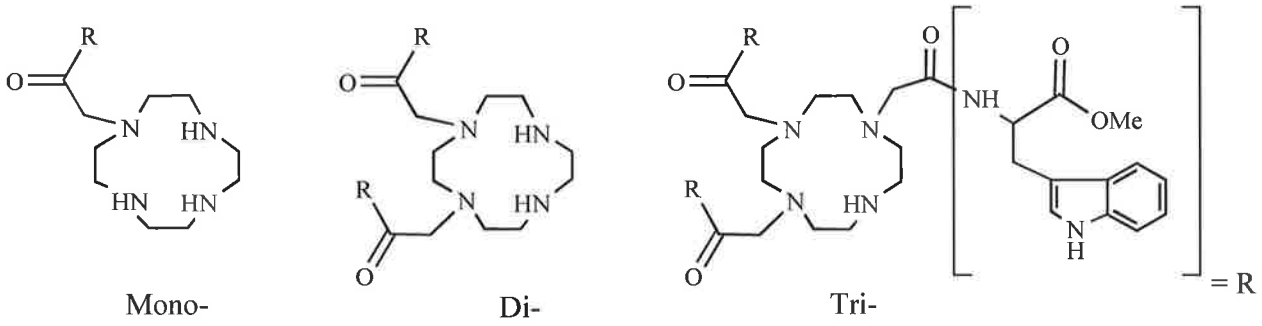

Figure 2.1. Diagrammatic representation of the three possible isomers formed in the synthesis of the tetraaza tryptophan derivative ligand (**51**).

The methyl ester ligand of the tacn tryptophan series ligand (**50**) was highly unstable thus making it difficult to utilise as a starting material for future preparations. The failure to produce the tetra-substituted amine ligand (**51**), or isolate the isomers formed, added to the unsuitability of the tryptophan series. Continued investigation into the tryptophan ligand series was therefore deemed to be inappropriate.

2.3 Synthesis of the anthracene substituted fluorescent sensors

The development of new fluorescent ligands for sensing metal ions, incorporating photoinduced electron transfer (PET), is of great interest, due to the ease with which fluorescence can be monitored. Previous work by Kimura *et al* has shown that the use of a cyclen based anthracene fluorophore, with an ethylamine linker, can improve fluorescence selectivity toward M^{2+} ions.[10] Based upon this type of fluorescent probe, two series of ligands were designed utilising the Fluorophore-Spacer-Receptor model.

2.3.1 Chiral amino acid anthracene substituted ligands

The synthetic pathway for the chiral amino acid anthracene substituted ligands, involved the initial functionalisation of anthracene. The fluorophore arm then underwent nucleophilic substitution onto the macrocyclic ring, which was then reacted further with the bromoacetylated amino acid derivative (**41**) seen previously (see section **2.2.1**). Due to the stability problems encountered with the L-tryptophan macrocycle, the amino acid L-phenylalanine was chosen as the primary focus of the investigation.

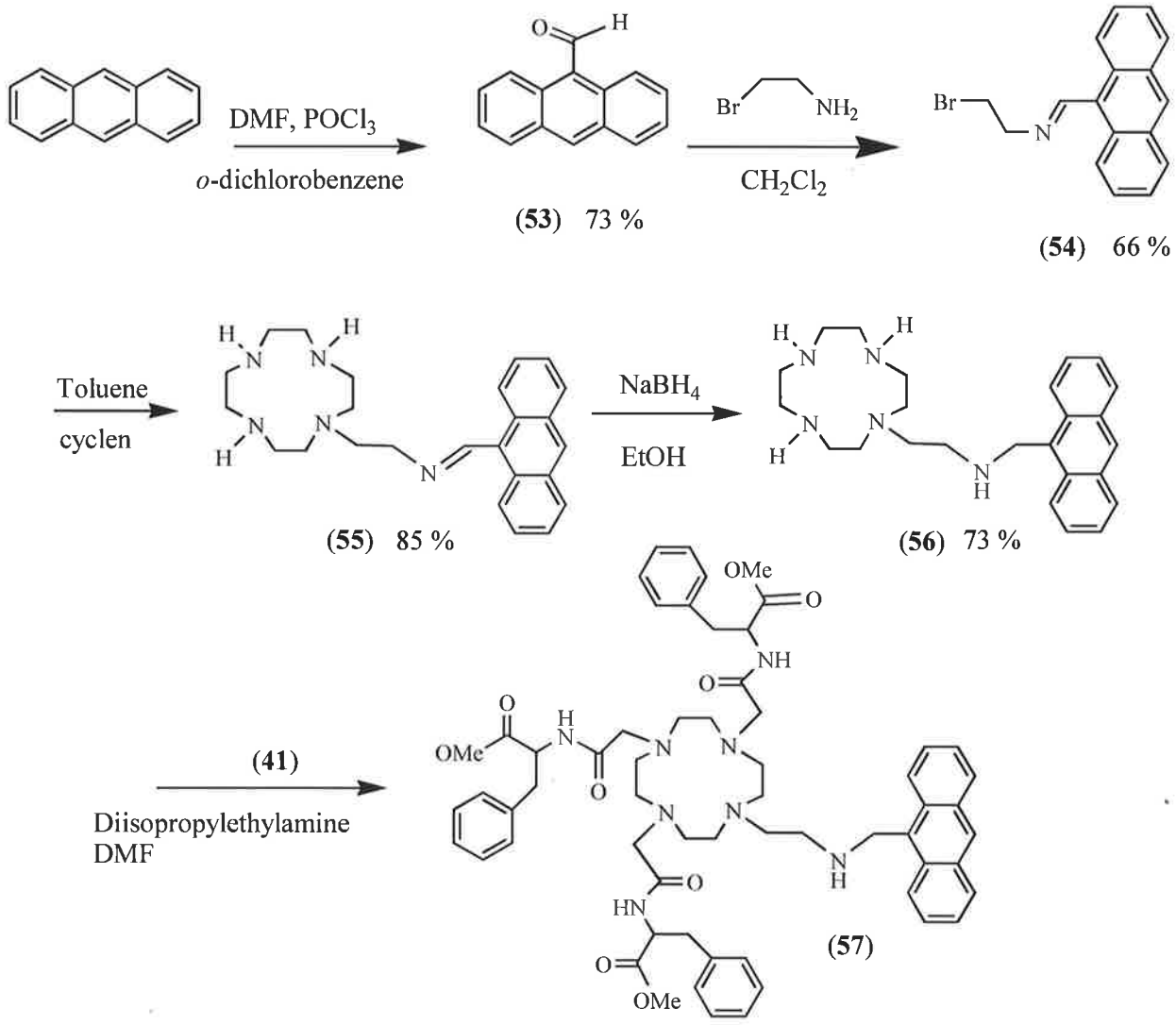

Scheme 6

Substitution of anthracene was carried out by the drop-wise addition of freshly distilled phosphorus oxychloride to a solution of anthracene, dry DMF, and *o*-dichlorobenzene. The reaction mixture was then left to stir at 90°C for one hour.

Recrystallisation from acetic acid produced 9-anthraldehyde (**53**) as a yellow crystalline solid in 73% yield. NMR spectroscopy and mass spectrometry of the product (**53**) was consistent with literature values.[11]

9-Anthraldehyde (**53**) was then reacted with a solution of 2-bromoethylamine in dichloromethane, at room temperature, for one hour. The 2-bromoethlyamine was purchased, as a hydrobromide salt, thus extraction with sodium hydroxide into a dichloromethane solution, prior to its use in the reaction, was required. Due to the volatility and toxicity of the neat amine, it was obtained as a solution in dichloromethane.[12] The resultant bromoethylimine anthracene (**54**) was recrystallised from ether/hexane to yield the product as a yellow crystalline solid in 66% yield. The melting point of the solid (84-87°C), ^{1}H and ^{13}C NMR spectra were consistent with the formation of product (**54**).

Compound (**54**) was then heated under reflux in hot toluene with 4 equivalents of cyclen to ensure only mono substitution occurred. After cooling, the reaction mixture was filtered and extracted with sodium hydroxide in order to remove the excess cyclen as an ammonium salt. This yielded the imine derivative (**55**) in 85% yield, which was used without further purification. Reduction of the imine bond, by $NaBH_4$ in ethanol, produced the cyclen amino anthracene derivative (**56**). Purification of ligand (**56**) was achieved by means of column chromatography to yield a yellow solid in 73% yield. Mono-substitution was confirmed by means of electrospray mass spectrometry (LCQ) and ^{1}H NMR spectroscopy.[10]

The final step in the synthesis of the anthracene substituted ligand (**57**) was the attachment of the amino acid pendant arms. The *N*-bromoacetyl-L-phenylalanine methyl ester (**41**) was reacted with the cyclen derivative (**56**), *N*,*N*-diisopropylethylamine, and DMF. Removal of the solvent, under high vacuum, yielded a dark brown oil, which was purified by means of a basic UG alumina column. Three products were obtained with R_f values of 0.15, 0.10 and 0.05, which suggested the possible formation of three different products (**Figure 2.2**).

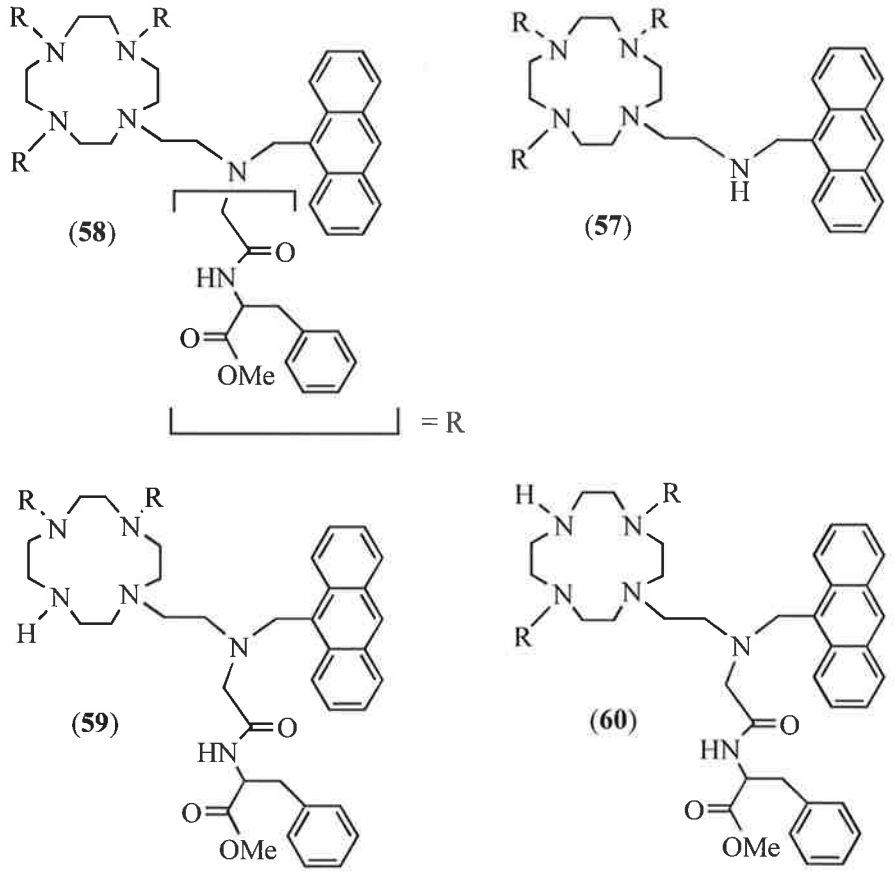

Figure 2.2. Diagrammatic representation of the possible products formed during the synthesis of the ligand (**57**).

Analysis of the high R_f fraction, by electrospray mass spectrometry (LCQ), showed a molecular ion at *m/z* 1282. Analysis of the other two fractions showed molecular ions for both at *m/z* 1063. The highest weight molecular ion was consistent with tetra-substitution; three substituents on the macrocyclic ring and one on the ethylamine nitrogen adjacent to the anthracene, ligand (**58**). The molecular ion at *m/z* 1063 was consistent with a tri-substituted arrangement; the two different R_f values obtained indicates the formation of isomers. There are three possible conformations for the tri-substituted ligand; (a) ligand (**57**) in which substitution occurred only on the macrocyclic ring; or (b) in either ligand (**59**) and (**60**), in which substitution occurred once on the ethylamine nitrogen adjacent to the anthracene, and twice on the ring structure, either *cis* or *trans* to each other. It could not be determined whether one, or both, of the ligands (**59**) and (**60**) were formed in the reaction. Physical and spectral analysis of the fraction was inconclusive. It was predicted that both the ligands (**59**) and (**60**) would have very similar chemical and physical properties.

The orientation of the substituted ligands was confirmed by NMR spectroscopy. The ^{13}C NMR spectra showed the most observable differences between the three fractions. The same chiral amino acid pendant arm had been used previously in the synthesis of ligand (**45**). The ^{13}C NMR spectrum of this ligand had shown 10 resonances, 6 sp^2 and 4 sp^3, due to the phenylalanine pendant arms. All four pendant arms of ligand (**45**) had been shown to exist in the same magnetic environment on the NMR time scale. The ^{13}C NMR spectrum for the tri-substituted ligand (**57**) showed the same number of ^{13}C NMR resonances, due to the amino acid pendant arms, as did the spectrum of ligand (**45**). This indicates that the three amino acid pendant arms in ligand (**57**) also all existed in the same magnetic environment on the NMR time scale. The ^{13}C NMR spectrum, obtained for the tetra-substituted ligand (**58**), showed twice as many signals for the amino acid pendant arms as did the spectra of ligands (**45**) and (**57**). This indicates that the pendant arm attached at the ethylamine nitrogen adjacent to the anthracene substituent, does not exist in the same magnetic environment as the pendant arms attached directly to the macrocyclic ring. The ^{13}C NMR spectrum of the fraction of unknown composition, containing ligands (**59**) and (**60**), exhibited three times as many ^{13}C NMR signals as did the spectra of ligands (**45**) and (**57**). The three sets of resonances arise from each of the three pendant arms, one at the amine adjacent to the anthracene, and the other two on the macrocyclic ring, either *cis* or *trans* to each other. An interesting feature of the ^{13}C NMR spectrum of the mixture of ligands (**59**) and (**60**) was that the number of signals indicates that the two pendant arms on the macrocyclic ring did not exist in the same magnetic environment. This would probably occur in either the *cis* or *trans* isomers, since the geometric conformational strain placed on the orientation of the arms would be much reduced, when compared with ligands (**57**) or (**58**). This allows the pendant arms to exist in different environments relative to each other. No other signals in the ^{13}C NMR spectrum for the ligand composition of (**59**) and (**60**) appeared to be duplicated. Unfortunately, this is not absolute proof that only one isomer existed in this sample because both isomers would be expected to have very similar spectral properties. Time constraints did not permit further investigations into the separation and characterisation of the two isomers. See **Chapter 5** for the individual resonance assignments.

The ^{1}H NMR spectrum was not as conclusive for identification as the ^{13}C NMR spectrum, due to the large overlap of signals. The integration of the resonances assigned to the protons from the phenyl rings and anthracene, however, were well separated and did support the formation of the tri- and tetra-substituted products. For the tri-substituted

ligands (**57**), (**59**), and (**60**), a ratio of 3:1 phenyl ring to anthracene protons was observed. For the tetra-substituted ligand (**58**), a 4:1 ratio of phenyl ring to anthracene protons was observed. Microanalysis of ligands (**57**) and (**58**) supported the proposed composition of the products formed.

The difference in the yields obtained for the three isomers was quite dramatic. The yield for ligand (**58**) was 58%. For the combination of ligands (**59**) and (**60**) a 20 % yield was obtained. Ligand (**57**) was obtained only with a 2.4% yield. The reaction was repeated with only three equivalents of the amino acid derivative (**41**) in an effort to avoid formation of the tetra-substituted ligand (**58**). Upon purification of the reaction mixture, two types of tri-substituted ligands were again observed. No significant change to the yield of the tri-substituted ligand (**57**) resulted; it was obtained in 2.6 % yield, whilst the mixture of the tri-substituted ligands (**59**) and (**60**) occurred in 60 % yield. This indicates that substitution at the ethylamine nitrogen adjacent to the anthracene substituent is more facile than substitution on the amines in the macrocyclic ring. There was no further attempt to improve the yield using different synthetic methods, since sufficient quantities were produced for the required physical measurements.

The two ligands (**57**) and (**58**) and the mixture of ligands (**59**) and (**60**), obtained from the reaction of the amino acid derivative (**41**) with the macrocycle (**56**), were soluble only in partially aqueous solutions. This was attributed to the high degree of conjugation in the both the anthracene substituent and phenyl rings. The ligands were, however, very stable to air and light.

2.3.2 Anthracene substituted fluorescent sensors with hydroxyethyl pendant arms

In an effort to improve the water solubility of the anthracene substituted fluorescent sensors, the pendant arms were changed to incorporate hydroxyethyl moieties. The same cyclen amino anthracene precursor (**56**) was used as for the ligands (**57**), (**58**), (**59**) and (**60**) (discussed previously), to allow comparisons of physical properties. However, the precursor was reacted with ethylene oxide in ethanol. The reaction of the substituted macrocycle (**56**) with ethylene oxide was predicted to form a composite of isomers. **Scheme 7** shows the possible isomers that may result from the reaction.

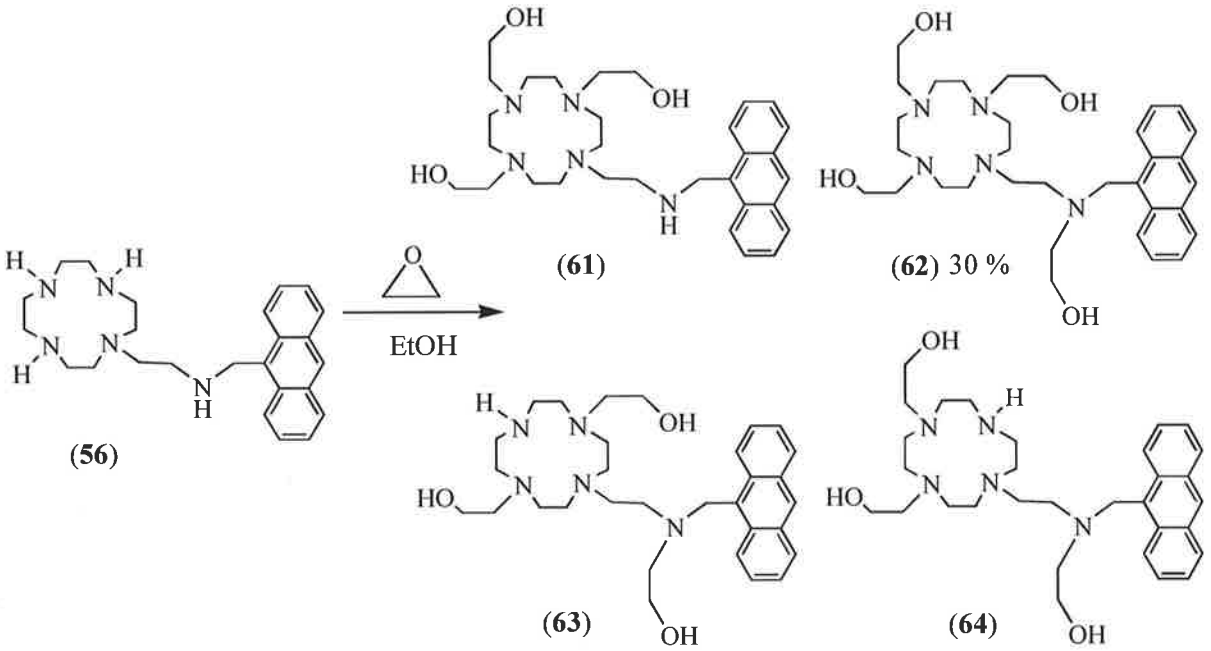

Scheme 7

The use of ethylene oxide in the reaction was rather difficult due to its low boiling point (10°C); all glassware involved in the handling of the reagent was chilled to 0°C. Two reactions were set up simultaneously involving varying quantities of ethylene oxide; one with four molar equivalents, and one with three molar equivalents. It was envisaged that incorporation of a pendant arm with less steric bulk would allow for the formation of only the ligands (**61**) and (**62**), dependent upon the number of equivalents of ethylene oxide used. The ethylene oxide was added to each reaction and the mixture left to rest in the dark for four days, followed by removal of any unreacted ethylene oxide and solvent, under reduced pressure. The products from both reactions were isolated as oils.

Electrospray mass spectrometry (LCQ) of the crude product obtained from the reaction of the anthracene substituted macrocycle (**56**), with four equivalents of ethylene oxide, showed the presence of numerous species. The oil was purified by means of a basic UG alumina column to give the tetra-substituted ligand (**62**) in 30% yield. Unfortunately the other products formed in this reaction, such as the tri-substituted ligands (**61**), (**63**) and (**64**), could not be isolated due to similarities in polarity. Ligand (**62**) was found to be highly light sensitive; decomposition occurred very quickly upon exposure to light, and this was accelerated after purification. The yield obtained was low, primarily due to the instability of ligand (**62**). Confirmation of the identity of the product was obtained by means of NMR spectroscopy, mass spectrometry, and microanalysis. The ^{13}C NMR spectrum showed 13 sp^3 resonance signals, consistent with the tetra-substituted ligand (**62**). Eight of the ^{13}C NMR resonances were assigned to the hydroxyethyl arms, three to the fluorophore spacer, and two to the macrocyclic ring. This indicates that the carbons in each of the hydroxyethyl pendant arms were magnetically inequivalent, in contrast to the amino acid pendant arms of ligand (**58**). This was attributed to the lack of chirality and steric bulkiness of the smaller hydroxyethyl arms in ligand (**62**). A molecular ion at *m/z* 604 ($M + Na^+$) was observed, which was consistent with the formation of the tetra-substituted product (**62**).

A variety of molecular ions was observed in the electrospray (LCQ) mass spectrum of the product, obtained from the reaction of only three molar equivalents of ethylene oxide with the macrocycle (**56**). Unfortunately, the products from this reaction had very similar physical properties and could not be isolated or further characterised. Time constraints meant that further investigation into the synthesis and characterisation of these isomers was not feasible. Therefore only one product was isolated from the reaction of ethylene oxide with the anthracene substituted macrocycle (**56**); the water soluble anthracene substituted ligand (**62**). The instability of ligand (**62**) to light when compared with the amino acid anthracene substituted ligands (**57**), (**58**), (**59**) and (**60**), which exhibit high stability to light, is attributed to the change in pendant arm. The amino acid anthracene substituted ligands (**57**), (**58**), (**59**) and (**60**) all contain phenyl rings, where ligand (**62**) does not. Charge transfer between the phenyl rings and the anthracene fluorophore may act to stabilise the ligands by reducing the amount of energy in the system. In the case of ligand (**62**) this results in fragmentation.

2.4 Conformational analysis of ligands by NMR spectroscopy

Elucidation of the diastereomeric conformation of the ligands was carried out by NMR spectroscopy. Investigation of the complexes by NMR spectroscopy was viable for only three of the ligands synthesised, ligands (**31**), (**45**) and (**50**). The anthracene substituted ligands (**57**), (**58**) and (**62**) were not investigated due to the complexity of their spectra, which did not allow for conclusive assignment of peak resonances; whilst the complexes of the chiral receptor ligands (**42**) and (**46**) were insufficiently soluble for NMR studies.

Only two metal ions (Zn^{2+} and Cd^{2+}) were investigated. The ligands were also expected to bind Cu^{2+}, but the resultant complexes cannot be investigated, as Cu^{2+} is paramagnetic. The main focus of this study was on the affect that the metal ion had on the magnetic environment of the carbons and protons in the macrocyclic ring. The two possible diastereomers of ligand (**31**), *Δ*-(*S,S,S*) and *Λ*-(*S,S,S*), are depicted in **Figure 2.3**, in the diagram the protons in the macrocyclic ring are assigned as H_a, H_b, H_c and H_d or H_a', H_b', H_c' and H_d', respectively.

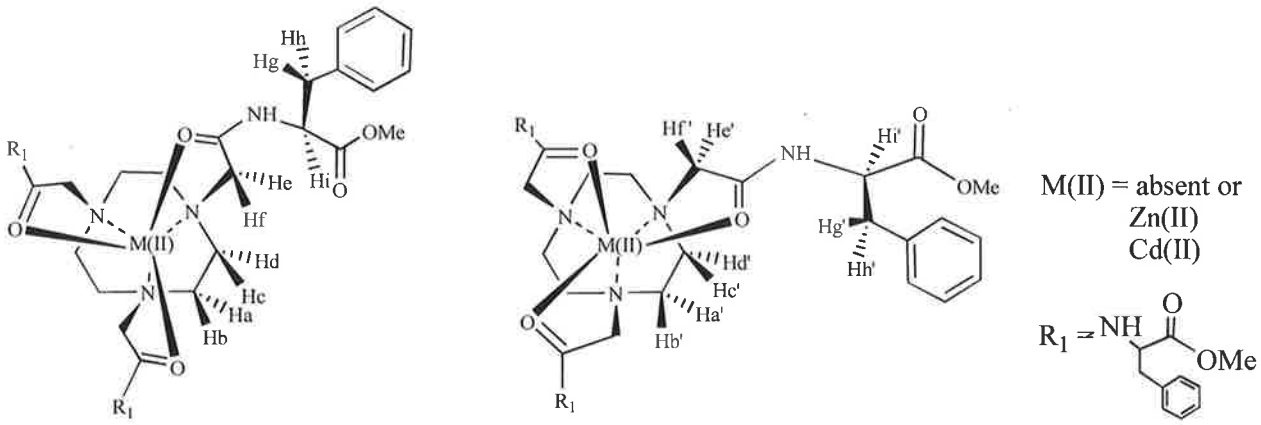

Δ-(*S,S,S*)-[M(**31**)]$^{2+}$ *Λ*-(*S,S,S*)-[M(**31**)]$^{2+}$

Figure 2.3. Two possible diastereomers of the triaza system ligand (**31**), *Δ*-(*S,S,S*) and *Λ*-(*S,S,S*).

The tacn macrocyclic ring methylene protons, H_a-H_d and H_a'-H_d', would be expected to be magnetically inequivalent in both possible diastereomers, due to the orientation of the chelate rings; thus for each diastereomer they should generate an AA'BB' quartet in a ^1H NMR spectrum. The two quartets for each diastereomer would be expected to have different chemical shifts since the protons for each isomer, Δ and Λ, are in different magnetic environments. This would also be expected for the H_e-H_i and H_e'-H_i' protons in the pendant arms for each diastereomer although due to the distance from the coordinating metal ion this may be somewhat diminished. The two diastereomeric complexes should also exhibit two sets of ^{13}C NMR resonances, because the macrocyclic ring carbons are also magnetically inequivalent. The information gained from both the ^1H and ^{13}C NMR should provide details about the stereochemistry of the uncomplexed ligands as well as upon metal ion coordination. It should be noted that the solvent in which these experiments were carried out, is different from that used in the characterisation of the ligands, from $CDCl_3$ to CD_3OD for ligands (**31**) and (**50**), and from $CDCl_3$ to CD_3CN for ligand (**45**).

The first ligand investigated was the L-phenylalanine tacn derivative, ligand (**31**). The ^1H NMR resonances for the macrocyclic ring methylene protons of ligand (**31**), in its uncomplexed state, are equivalent on a time average and gave rise to a single 12H AA'BB' multiplet at δ 2.45 ppm. The tacn macrocyclic ring carbons in the ^{13}C NMR spectrum existed as a broad signal at δ 58.1 ppm; only five sp^3 signals were observed. This indicates that the ligand is in a fast time averaged exchange, which causes the two macrocyclic ring carbons to appear as if in the same environment. The fast exchange could be between the two possible diastereomers or through the inversion around the amine nitrogens in a single diastereomer. On coordination with a metal ion, vast changes to the NMR spectra were observed. The macrocyclic ring methylene protons in the Zn(**31**)$^{2+}$ complex are inequivalent, and the H_a, H_b, H_c, and H_d protons are unique and gave rise to four sharp signals of 3H at δ 1.81, 2.45, 2.61 and 2.85 ppm, respectively. These are part of a well-resolved ABCD multiplet, as would be expected for a single diastereomer. Metal ion coordination also had a profound effect on the ^{13}C NMR spectrum; six sp^3 signals were visible. The macrocyclic ring carbons in the Zn(**31**)$^{2+}$ complex were unique and gave rise to two separate signals at δ 50.4 and 53.5 ppm, instead of the broad signal at δ 58.1 ppm. This pattern indicates that the complex existed as a single diastereomer. The coordination of ligand (**31**) with Cd^{2+} resulted in a similar splitting pattern in the NMR spectra as was observed for the Zn(**31**)$^{2+}$ complex. The macrocyclic methylene ring protons H_a, H_b, H_c

and H_d were also unique in the Cd(**31**)$^{2+}$ complex. Two of the proton signals overlapped to give a broad signal of 6H at δ 2.30 ppm; while the other two remaining proton resonances existed as 3H signals at δ 2.69 and 2.82 ppm. The macrocyclic ring carbons for the Cd(**31**)$^{2+}$ complex are inequivalent and gave rise to two resonances at δ 53.0 and 53.8 ppm.

The signals attributed to the protons on the pendant arms, H_e, H_f, H_g, H_h and H_i, also gave rise to different signals on metal ion compelxation. In the uncomplexed ligand (**31**) the proton signals for the pendant arms appeared as time averaged signals in the ^{1}H NMR spectrum. For example, in the uncomplexed ligand (**31**), the methylene protons adjacent to the phenyl ring H_g and H_h, are equivalent and gave rise to one signal at δ 3.18 ppm with an integration of 6H. On coordination of ligand (**31**) with Zn^{2+}, the methylene protons become inequivalent and gave rise to two separate signals at δ 2.85 and 3.33 ppm, each with a relative integration of 3H. A similar pattern of signal splitting was observed for the Cd^{2+} complex. If the metal complex ion existed in slow exchange around the nitrogen of a single diastereomer, the protons in the pendant arms would be expected to be inequivalent. No duplication in the ^{13}C NMR spectrum for the carbons in the pendant arms was observed in the spectra of either the Zn(**31**)$^{2+}$ or the Cd(**31**)$^{2+}$ complex. This indicates that each metal complex ion existed as a single diastereomer in solution, thus confirming the solid-state structure. X-Ray crystallography of the Cu^{2+} complex with ligand (**31**) had shown the ligand to adopt a single preferred geometry, *Λ*-(*S,S,S*).[6] The formation of a single diastereomeric species on complexation with Zn^{2+} can be seen in **Figure 2.4**.

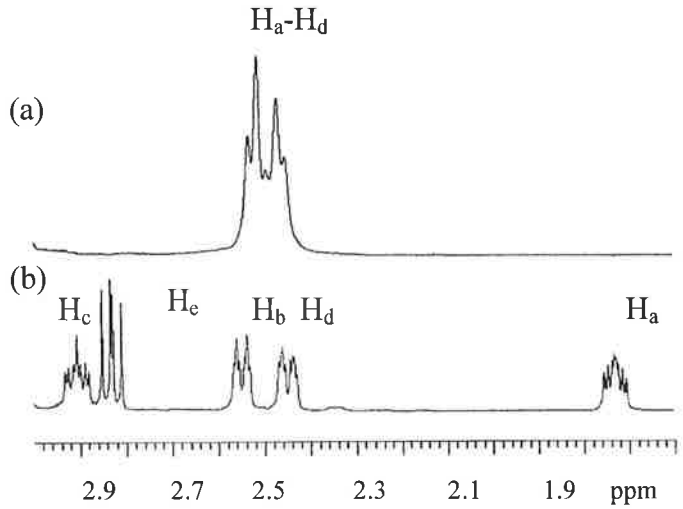

Figure 2.4. The ^{1}H NMR (600 MHz) spectra of the macrocyclic ring resonances of ligand (**31**), (a) alone, and (b) in the presence of Zn^{2+} in CD_3OD solution. The protons are labelled as in **Figure 2.3**; H_a-H_d represent the macrocyclic ring methylene protons and H_e represents a pendant arm proton.

The NMR spectra for the uncomplexed L-tryptophan tacn ligand (**50**) were very similar to those obtained for the L-phenylalanine tacn ligand (**31**). The ^{1}H NMR spectrum of the macrocyclic ring methylene protons of the uncomplexed ligand (**50**) showed a single 12H AA'BB' multiplet resonance at δ 1.89 ppm. This indicates that these protons are equivalent on a time average. The macrocyclic ring carbons were also equivalent in the uncomplexed ligand (**50**) and gave rise to a single resonance at δ 57.6 ppm in the ^{13}C NMR spectrum; only five sp^3 ^{13}C NMR resonances were observed. No duplication was observed to arise from the other atoms present in the pendant arms. On metal ion complexation, a noticeable change occurred in the ^{1}H NMR spectrum. The macrocyclic ring methylene protons in both the Zn(**50**)$^{2+}$ and Cd(**50**)$^{2+}$ complexes are inequivalent. The ring protons, H_a, H_b, H_c and H_d in the Zn^{2+} complex of ligand (**50**) gave rise to two sharp 3H signals at δ 1.00 and 1.10 and a single 6H multiplet at δ 2.23 ppm. In the Cd^{2+} complex of ligand (**50**), the macrocyclic ring methylene protons gave rise to four 3H multiplets at δ 1.20, 1.61, 2.12 and 2.40 ppm. The well-formed ABCD multiplets that were observed for both metal complex ions in solution for ligand (**50**) support the formation of only a single diastereomer. Six sp^3 resonances were observed for both the metal complex ions in the ^{13}C NMR spectra; the macrocyclic ring carbons were inequivalent and gave rise to two signals, at δ 51.9 and 52.4 ppm in the Zn^{2+} complex, and at δ 52.5 and 53.9 ppm in the Cd^{2+} complex. Again, as per the L-phenylalanine derivative ligand (**31**), the protons in the pendant arms of ligand (**50**) were also inequivalent on metal ion complexation.. No

duplication of the carbon signals in the ^{13}C NMR spectrum were observed due to the carbons in the pendant arms, which indicates that the complex existed as a single diastereomer.

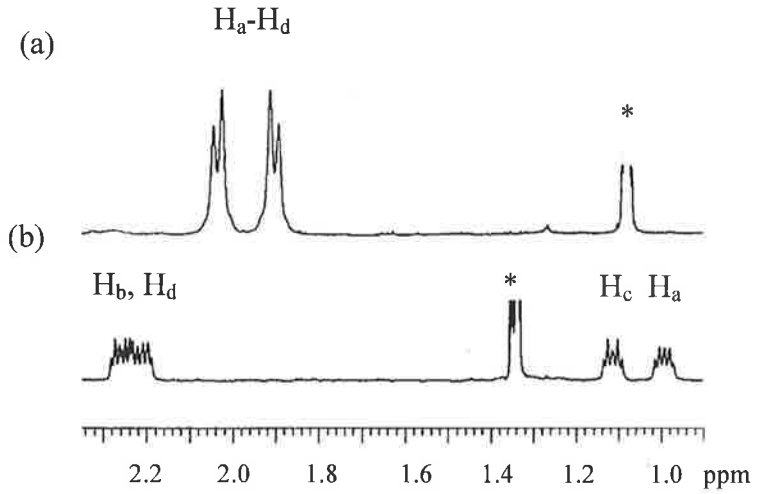

Figure 2.5. The ^1H NMR (600 MHz) spectra of the macrocyclic ring resonances of ligand (**50**), (a) alone, and (b) in the presence of Zn^{2+} in CD_3OD solution. The protons are labelled as in **Figure 2.3**; H_a-H_d represent the macrocyclic ring methylene protons. The asterisk indicates the solvent proton impurity resonances, which appear at differing δ due to the different dielectric constants of the solutions.

For the only cyclen system investigated, the L-phenylalanine cyclen derivative ligand (**45**), a similar splitting of proton and carbon resonances for the uncomplexed ligand were observed, as for that of ligands (**31**) and (**50**). The macrocyclic ring methylene proton resonances in the ^1H NMR spectrum of the uncomplexed ligand (**45**), gave rise to two 8H multiplets, which are part of a single 16H AA'BB' multiplet over the range δ 2.39 – 2.48 ppm. This indicates that they are equivalent on a time average. In the ^{13}C NMR spectrum, only five sp^3 ^{13}C NMR resonances were observed; the macrocyclic ring carbons are equivalent and gave rise to a single resonance at δ 54.3 ppm. On complexation with the metal ions, Zn^{2+} and Cd^{2+}, both the ^1H and ^{13}C NMR spectra of ligand (**45**) underwent changes. For the Zn^{2+} complex of ligand (**45**), the macrocyclic ring methylene protons are inequivalent and in the ^1H NMR spectrum gave rise to four 4H multiplets at δ 2.03, 2.35, 2.54 and 2.73 ppm. In the ^{13}C NMR spectrum, only six sp^3 resonances were observed; the two macrocyclic ring carbons gave rise to two signals at δ 50.1 and 51.6 ppm. The Cd^{2+} complex of ligand (**45**) also underwent a similar transformation; the macycrocyclic methylene ring protons are inequivalent and the H_a-H_d protons are unique and produce a

single well resolved ABCD multiplet as would exist for a single diastereomer. The ^{13}C NMR spectrum of the Cd^{2+} complex of ligand (**45**) showed two signals; at δ 47.5 and 51.1 ppm arising from the macrocyclic ring carbons. The protons in the pendant arms for both the $Zn(\mathbf{45})^{2+}$ and the $Cd(\mathbf{45})^{2+}$ complexes are inequivalent and gave rise to separate ^{1}H NMR resonances, but did not give rise to duplicate ^{13}C NMR resonances. This had been similarily observed with the various metal complex ions of ligands (**31**) and (**50**). This indicates that these types of chiral amino acid based ligands form only single diastereomers on metal ion complexation.

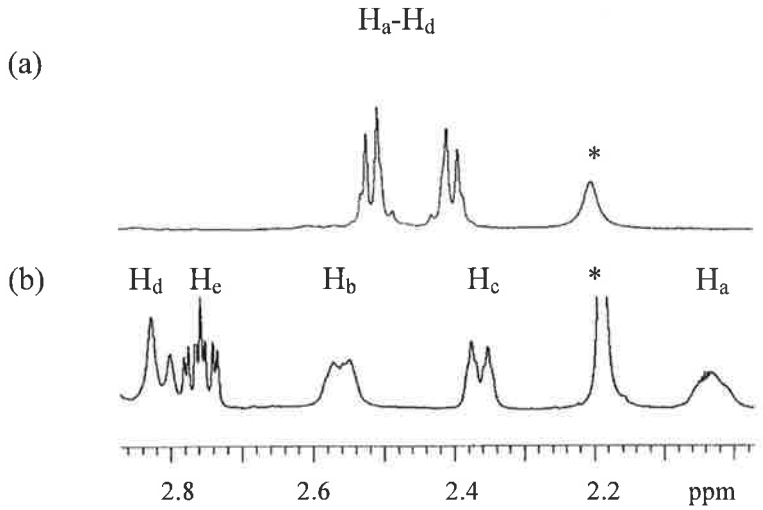

Figure 2.6. The ^{1}H NMR (600 MHz) spectra of the macrocyclic ring resonances of ligand (**45**), (a) alone, and (b) in the presence of Zn^{2+} in CD_3CN solution. The protons are labelled as per **Figure 2.3**; H_a-H_d represent the macrocyclic ring methylene protons, H_e represents the pendant arm proton. The asterisk indicates the solvent proton impurity resonances, which appear at differing δ due to the different dielectric constants of the solutions.

For detailed assignment of the peaks in the spectra, see **Appendix A.1**. All the analysed spectra were second order; hence *J* hertz coupling constants could not be elucidated. From the analysis of the NMR spectra of the ligands (**31**), (**45**) and (**50**), the stereochemistry can be rationalised for these systems. The lack of duplication in the ^{13}C NMR spectra as well as the separation of the macrocyclic methylene ring protons from AA'BB' multiplets into unique well-resolved ABCD multiplets on metal ion coordination, would indicate that all three ligands exist as single diastereomers. This is consistent with the X-ray crystal structure obtained for $[(\mathbf{31})Cu]^{2+}$.[6] As mentioned previously, work on

similar triazacyclononane and tetraazacyclododecane complexes with alkali metals, has shown that these types of macrocycles exist preferentially as single diastereomers.[13]

2.5 Discussion

The two types of target ligands, the chiral amino acid based ligands and the anthracene substituted ligands, have been successfully prepared and isolated by various synthetic procedures. The synthesis of the chiral amino acid based ligands was achieved through the alkylation of, either tacn, or cyclen with an amino acid derivative L-phenylalanine, or L-tryptophan, to give a diverse range of ligands. The ester derivatives synthesised, ligands (**31**), (**45**) and (**50**), were found to be unstable to prolonged exposure to air; this was most noticeable in the L-tryptophan derivative (**50**). Conversion of the two methyl ester L-phenylalanine ligands (**31**) and (**45**) to their carboxylic acid derivatives, gave the two water soluble ligands (**42**) and (**46**), respectively. The L-tryptophan derivative, ligand (**50**), was not converted to its corresponding acid, due to its poor stability on exposure to air. This is believed to be due to the steric bulk of the L-tryptophan amino acid derivative. The steric bulk of the L-tryptophan amino acid was also found to affect the synthesis of the cyclen derivative, ligand (**51**).

Analysis of the NMR spectra of the metal complex ions of ligands (**31**), (**45**) and (**50**), was used to probe the stereochemistry of the ligands. The ^{1}H NMR spectra of the macrocyclic methylene ring protons were observed to alter from AA'BB' multiplets, into unique, well-resolved ABCD multiplets on metal ion coordination. No duplication in the ^{13}C NMR spectra of the three ligands was observed. This indicates that all three ligands, (**31**), (**45**) and (**50**), exist as single diastereomers. This is supported by X-ray crystallography of the Cu^{2+} complex of ligand (**31**). Each diastereomer constitutes a part turn of either a triple helix for the tacn based ligands, or a quadruple helix for the cyclen based ligands. It is predicted that the attachment of peptide pendant arms to the macrocycles, instead of the single amino acid derivatives used in this investigation, may facilitate the study of multiple metal complexing by peptide helices.

The synthesis of the anthracene substituted ligands resulted in a variety of substituted ligands, with substitution appearing to occur most readily at the ethylamine nitrogen adjacent to the anthracene substituent. The incorporation of the chiral amino acid pendant arms into the anthracene substituted ligand, resulted in the formation of four

possible products. Only two could be isolated; the tri-substituted ligand (**57**) and the tetra-substituted ligand (**58**). Isolation of the other two ligands, (**59**) and (**60**), was not possible due to similarities in physical properties. NMR analysis of ligands (**57**), (**58**), (**59**) and (**60**), showed that when three pendant arms were present on the macrocyclic ring, they existed in the same magnetic environment. In contrast, when only two pendant arms were present, as in the case of ligands (**59**) and (**60**), they did not exist in the same magnetic environment. The pendant arms of the anthracene substituted ligand (**62**) each existed in their own magnetic environment, with the signals arising from all four pendant arms visible in the ^{13}C NMR spectrum. Comparison of the different pendant arms on the anthracene substituted ligands, showed that the larger pendant arms tend to exist preferentially in specific geometric conformations.

2.6 References

(1) Richman, J. E.; Atkins, T. J. *J. Am. Chem. Soc.* **1974**, *96*, 2268-2270.

(2) McAuley, A.; Norman, P. R.; Olubuyide, O. *Inorg. Chem.* **1994**, *23*, 1938-1943.

(3) Searle, G. H.; Geue, R. J. *Aust. J. Chem.* **1984**, *37*, 959-970.

(4) Yang, R.; Zompa, L. *Inorg. Chem.* **1976**, *15*, 1499-1502.

(5) Hancock, R. D.; Martell, A. E. *Chem. Rev.* **1989**, *89*, 1875-1914.

(6) Watson, A. A.; Willis, A. C.; Fairlie, D. P. *Inorg. Chem.* **1997**, *36*, 752-753.

(7) Pouchert, C. J.; Behnke, J. *The Aldrich Library of 13C and 1H FT NMR Spectra*; 1st ed.; Aldrich Chemical Company, 1993; Vol. 2.

(8) Aldrich *Catalogue Handbook of Fine Chemicals*, 2001.

(9) In *Beilstein*; Springer-Verlag: Berlin; Vol. 22, p 6771.

(10) Aoki, S.; Kaido, S.; Fujioka, H.; Kimura, E. *Inorg. Chem.* **2003**, *42*, 1023-1030.

(11) Fieser, L. F.; Hartwell, J. L.; Jones, J. E.; Wood, J. H.; Bost, R. W. In *Organic Syntheses*; Allen, F. H., VanAllan, J., Eds.; John Wiley and Sons: New York, 1955; Vol. Collective Volume 3, pp 98-99.

(12) Fabbrizzi, L.; Licchelli, M.; Perotti, A.; Poggi, A.; Rabaioli, G.; Sacchi, D.; Taglietti, A. *J. Chem. Soc., Perkin Trans. 2* **2001**, 2108-2113.

(13) Dhillion, R. S.; Madback, S. E.; Ciccone, F. G.; Buntine, M. A.; Lincoln, S. F.; Wainwright, K. P. *J. Am. Chem. Soc.* **1997**, *119*, 6126-6134.

Chapter 3. Potentiometric Titrations

3.1 Protonation constants

An area of major interest in polyaza macrocyclic ligands is their acid-base properties and metal ion binding affinities. This study is designed to produce selective metal ion receptors and to provide information about the thermodynamic characteristics of the receptors.

In aqueous solutions, macrocyclic ligands exist in an equilibrium mixture of their free and protonated forms due to their polybasic nature. The protonation constants of the protonated ligands (**31**), (**42**), (**45**), (**46**), (**50**), (**57**), (**58**) and (**62**), were determined in a methanol/water solvent system (80:20; v/v), with constant ionic strength, I = 0.1 mol dm^{-3} (NEt_4ClO_4), by potentiometric titration (see section **6.3**). The solvent system was chosen to ensure complete dissolution of the ligands whilst maintaining an adequate percentage of water to allow the pH electrode to function correctly. All solutions were acidified, to ensure complete protonation of all basic nitrogen donor atoms; gradual deprotonation was achieved by titration against NEt_4OH. The stepwise acid base equations for a tri-basic system can be expressed as follows,

$$[LH]^+ \xrightleftharpoons{K_{a1}} H^+ + L \qquad K_{a1} = \frac{[H^+][L]}{[LH^+]} \qquad (3.1)$$

$$[LH_2]^{2+} \xrightleftharpoons{K_{a2}} H^+ + [LH]^+ \qquad K_{a2} = \frac{[H^+][LH^+]}{[LH_2^{2+}]} \qquad (3.2)$$

$$[LH_3]^{3+} \xrightleftharpoons{K_{a3}} H^+ + [LH_2]^{2+} \qquad K_{a3} = \frac{[H^+][LH_2^{2+}]}{[LH_3^{3+}]} \qquad (3.3)$$

In these equations K_{a1}, K_{a2} and K_{a3} are the stepwise equilibrium constants (or acid dissociation constants) and L is the ligand under study. The negative logarithm of the equilibrium constant, K_a, can be used to obtain the pK_a of each nitrogen donor atom, as expressed below in Equations 3.4 - 3.6. The pK_a of an acid corresponds to the stepwise protonation constant of its conjugate base.

$$pK_{a1} = -\log K_{a1} \quad (3.4)$$

$$pK_{a2} = -\log K_{a2} \quad (3.5)$$

$$pK_{a3} = -\log K_{a3} \quad (3.6)$$

All the ligands synthesised previously, as described in **Chapter 2,** were subject to potentiometric titrations to determine the pK_a values associated with their donor atoms. In most cases, not all pK_a values were measurable, as some were below the detection limit for the method used. Since $pK_a \leq 2$ cannot be accurately measured using glass electrodes.

The partially aqueous solvent system, methanol/water (80:20; v/v), had a measured pH of 4.98, thus direct comparison between macrocycles of similar structures in aqueous solution cannot be made. The low pH was a reflection of the method used to calibrate the electrode and this, in turn, is reflected in the determined pK_a values.

3.1.1 Protonation constants for the amino acid pendant arm ligands (31), (42), (45), (46) and (50)

The pK_a values determined for ligands (**31**), (**42**), (**45**), (**46**) and (**50**), appear below in **Table 3.1**; the conditions for these titrations are listed below the table.

Table 3.1. pK_a values of the protonated amino acid pendant arm ligands (**31**), (**42**), (**45**), (**46**) and (**50**), obtained at 298.2 (± 0.2) K with I = 0.1 mol dm^{-3} (NEt_4ClO_4) in methanol/water (80:20; v/v).

pK_a of protonated site	(**31**)[a]	(**42**)[b]	(**45**)[c]	(**46**)[d]	(**50**)[e]
		(pK_a values in descending order from pK_{a1})			
pK_{a1}	8.69 ± 0.04	9.06 ± 0.02	8.50 ± 0.02	9.89 ± 0.03	8.79 ± 0.02
pK_{a2}	3.59 ± 0.07	6.13 ± 0.04	5.62 ± 0.04	7.06 ± 0.06	3.67 ± 0.03
pK_{a3}	low	4.93 ± 0.05	3.77 ± 0.08	5.53 ± 0.06	low
pK_{a4}		4.52 ± 0.06	low	5.46 ± 0.09	
pK_{a5}		low		4.44 ± 0.06	
pK_{a6}		low		4.26 ± 0.09	
pK_{a7}				low	
pK_{a8}				low	

[a] [**31**] = 9.3 x 10^{-4} mol dm^{-3}, [H$^+$] = 3.8 x 10^{-3} mol dm^{-3}, [NEt_4OH] = 0.109 mol dm^{-3}. [b] [**42**] = 8.9 x 10^{-4} mol dm^{-3}, [H$^+$] = 6.0 x 10^{-3} mol dm^{-3}, [NEt_4OH] = 0.104 mol dm^{-3}. [c] [**45**] = 8.8 x 10^{-4} mol dm^{-3}, [H$^+$] = 4.2 x 10^{-3} mol dm^{-3}, [NEt_4OH] = 0.103 mol dm^{-3}. [d] [**46**] = 1.1 x 10^{-3} mol dm^{-3}, [H$^+$] = 9.2 x 10^{-3} mol dm^{-3}, [NEt_4OH] = 0.109 mol dm^{-3}. [e] [**50**] = 7.3 x 10^{-4} mol dm^{-3}, [H$^+$] = 3.1 x 10^{-3} mol dm^{-3}, [NEt_4OH] = 0.114 mol dm^{-3}

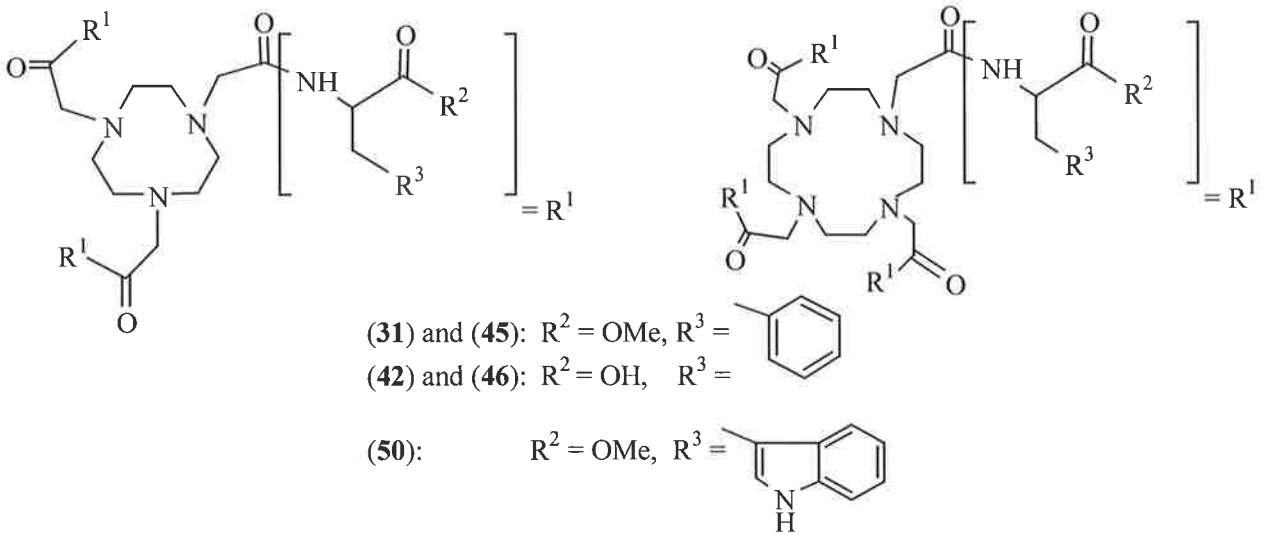

Figure 3.1 Structures of the chiral receptor ligands (**31**), (**42**), (**45**), (**46**) and (**50**).

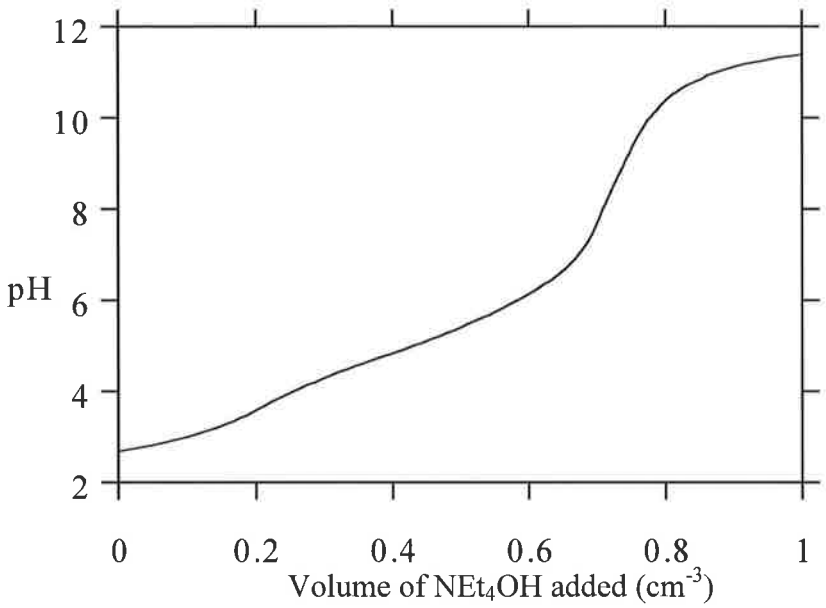

Figure 3.2. Typical titration curve of the protonated ligand (**46**) against NEt_4OH at 298.2 (± 0.2) K. $[\mathbf{46}]_{total} = 1.1 \times 10^{-3}$ mol dm^{-3}, $[H^+]_{total} = 9.2 \times 10^{-3}$ mol dm^{-3}, $[NEt_4OH] = 0.109$ mol dm^{-3}, $I = 0.10$ mol dm^{-3} (NEt_4ClO_4).

The pK_a values given in **Table 3.1** decrease from pK_{a1} to their lowest measureable pK_a value. In systems of multiple pK_as, it is generally observed and understood that the value of each sequential pK_a will decrease for two reasons; increasing charge and a statistical effect. Protonation of one nitrogen group results in a ligand having a 1+ charge, which coincides with a large pK_a value. The addition of a second proton causes repulsion between the two protons, which lowers the value for the second protonation constant, pK_{a2}. With ligands having more than two protonation sites, a larger electrostatic repulsion between the additional charges can be observed when protonation is increased, thus causing a large decrease to the pK_a value.[1]

The second reason for the decrease is a statistical effect. For a tri-basic ligand, such as ligand (**31**), there are three sites at which a proton can coordinate. The initial addition of a proton will leave only two remaining sites to which a proton can coordinate. Consequently, the probability with which the next proton will coordinate is decreased, resulting in a decrease in the pK_a value.

Acidity can also be affected by hydrogen bond formation between protonated amino groups and non-protonated amino groups. A proton involved in a hydrogen bond is more difficult to abstract, thus contributing to the difference in measurable pK_a values. Solvation of the ligand can have a large effect on the ability of the ligand to form hydrogen

bonds; a decrease in solvation can lead to weak coordination of the donor atom to the bound proton, and hence lower pK_a values may be observed.

For the three methyl esters studied, ligands (**31**), (**45**) and (**50**), protonation occurred on the nitrogens of the macrocyclic amine. In the case of the triamine ligands (**31**) and (**50**), only two pK_a values were measured. The third protonation occurred at very acidic pH, so measurement was not possible by this method; p$K_a \leq 2$ cannot be accurately measured using glass electrodes. The tetraamine ligand (**45**) has four possible protonation sites. Three pK_a values were measured, the fourth protonation being below the measurable range.

The pK_a values for all ligands studied increased on increasing ring size and steric bulk. The change in ring size between the tacn and the cyclen ring allows for a decrease in electrostatic repulsion between the positive charges, resulting in a noticeable decrease in acidity. Higher pK_a values were measured for the tryptophan triamine ligand (**50**), when compared with the phenylalanine triamine ligand (**31**). This was attributed to the tryptophan bulk and the increased hydrophobicity of the system.

From potentiometric studies on other acid based macrocyclic ligands, and the observed trends in their pK_a values,[2-5] the protonation sites for ligands (**42**) and (**46**) can be assigned. For ligand (**42**), the first protonation, assigned pK_{a1}, occurred at one of the ring amines, the acidity of which is decreased by the negative charge on the neighbouring ionised carboxylate group. The second and third protonation, assigned pK_{a2} and pK_{a3}, respectively, also occurred on the macrocyclic ring. The fourth protonation, assigned pK_{a4}, was the protonation of a carboxylic acid group. For the two pK_a values, pK_{a3} and pK_{a4}, protonation occurred simultaneously, therefore complete elucidation of the protonation sites is not possible. Protonation of the other possible sites, the two remaining carboxylic acid groups, occurred at a pH too low for measurement using a glass electrode. For the cyclen carboxylic acid ligand (**46**), the values of pK_{a1-4} arise from the protonation of the macrocyclic amine groups and pK_{a5-6} are due to the protonation of two carboxylic acid groups. For ligand (**46**), the protonation sites assigned to pK_{a3} and pK_{a4}, are identical within experimental error and so the pK_a values cannot be distinguished. The simultaneous protonation of the two sites, pK_{a3} and pK_{a4}, suggests that the two sites at which protonation occur are separated by distance, and probably occur at a position trans to each other across the ring. The protonation sites assigned to pK_{a5} and pK_{a6}, are also identical within

experimental error for ligand (**46**) and therefore cannot be distinguished. The two protonations, pK_{a5} and pK_{a6}, probably occur at a distance from each other. The higher pK_a values obtained for ligand (**46**), compared with ligand (**42**), are due to the larger ring size, which decreases the electrostatic repulsion and facilitates protonation.

3.1.2 Protonation constants for the anthracene substituted ligands (57), (58) and (62)

The pK_a values determined for the anthracene substituted ligands (**57**), (**58**) and (**62**), are listed in the following table, **Table 3.2.**

Table 3.2. pK_a values of the protonated anthracene substituted ligands (**57**), (**58**) and (**62**), obtained at 298.2 (± 0.2) K with I = 0.1 mol dm^{-3} (NEt_4ClO_4) in methanol/water (80:20; v/v).

pK_a of protonated site	(**57**) [a]	(**58**) [b]	(**62**) [c]
	(pK_a values in descending order from pK_{a1})		
pK_{a1}	9.84 ± 0.05	10.13 ± 0.04	9.99 ± 0.02
pK_{a2}	7.73 ± 0.09	9.24 ± 0.05	7.53 ± 0.04
pK_{a3}	5.88 ± 0.12	6.56 ± 0.06	6.67 ± 0.05
pK_{a4}	4.52 ± 0.09	4.90 ± 0.06	4.83 ± 0.06
pK_{a5}	low	4.51 ± 0.08	3.45 ± 0.09

[a] [**57**] = 3.3 x 10^{-4} mol dm^{-3}, [H$^+$] = 4.6 x 10^{-3} mol dm^{-3}, [NEt_4OH] = 0.111 mol dm^{-3}. [b] [**58**] = 5.3 x 10^{-4} mol dm^{-3}, [H$^+$] = 5.3 x 10^{-3} mol dm^{-3}, [NEt_4OH] = 0.111 mol dm^{-3}. [c] [**62**] = 4.0 x 10^{-4} mol dm^{-3}, [H$^+$] = 5.5 x 10^{-3} mol dm^{-3}, [NEt_4OH] = 0.102 mol dm^{-3}.

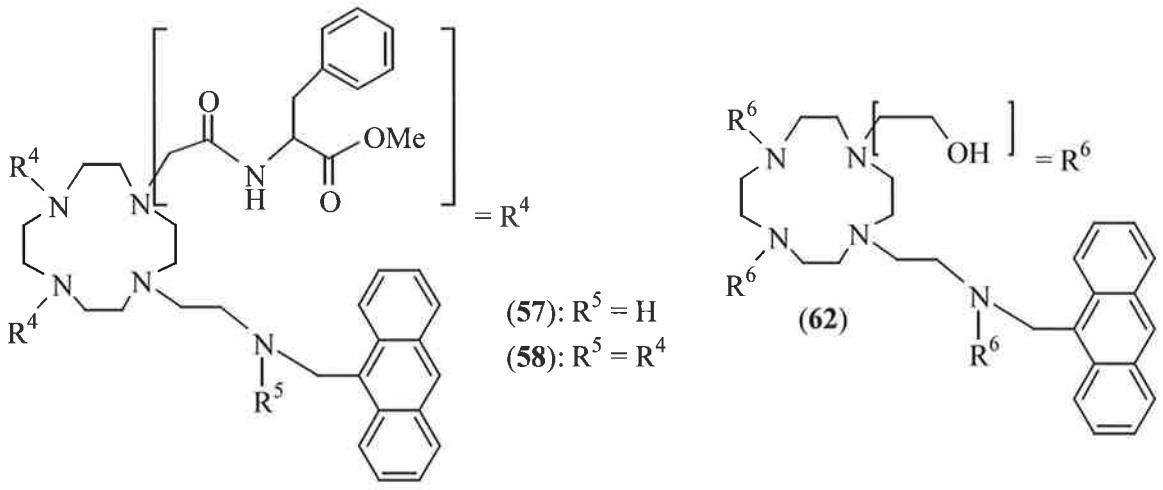

Figure 3.3 Structures of the anthracene substituted ligands (**57**), (**58**) and (**62**).

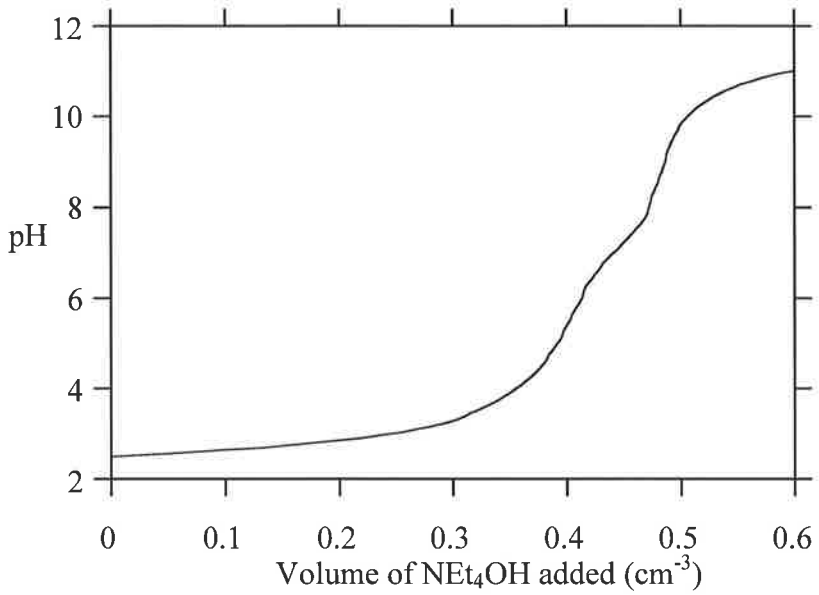

Figure 3.4. Typical titration curve of the protonated ligand (**62**) against NEt_4OH at 298.2 (± 0.2) K. $[\mathbf{62}]_{total} = 4.0 \times 10^{-4}$ mol dm^{-3}, $[H^+]_{total} = 5.5 \times 10^{-3}$ mol dm^{-3}, $[NEt_4OH] = 0.102$ mol dm^{-3}, $I = 0.10$ mol dm^{-3} (NEt_4ClO_4).

The trend observed in the pK_a values for the the anthracene substituted ligands (**57**), (**58**) and (**62**), was similar to that found for ligands (**31**), (**42**), (**45**), (**46**) and (**50**). The pK_a values decreased on increasing protonation, due to increasing charge and a statistical effect as discussed previously. Anthracene groups are known to affect pK_a values; their large steric bulk and hydrophobicity decreases the solvation of the amine group, and the electron withdrawing effect of the anthracene combines to decrease acidity.[6] In the case of ligands (**58**) and (**62**), in which pendant arm substitution occurs on the ethylamine nitrogen adjacent to the anthracene substituent, five pK_a values were measured for each of the ligands. Four of the pK_a values were attributed to the protonation of the macrocyclic ring amines, with the remaining pK_a value attributed to the protonation of the ethylamine nitrogen adjacent to the anthracene substituent. For ligand (**57**), four pK_a values were determined.

A trend can be observed when comparing the measured pK_a values for ligands (**57**) and (**58**). The pK_a values for ligand (**57**) are less than the measured pK_a values for ligand (**58**); this is attributed to the ethylamine nitrogen adjacent to the anthracene substituent being substituted in ligand (**58**) and not in ligand (**57**). This may be associated with the substitution either decreasing the electron withdrawing effect of the anthracene, increasing the hydrophobicity of the system, or a combination of these effects.

The trend observed in pK_a values for ligands (**58**) and (**62**), was similar to that found for ligands (**57**) and (**58**). The measured pK_a values for ligand (**62**) were less than those measured for ligand (**58**). This was attributed to pendant arm substitution; the amino acid based pendant arms in ligand (**58**) are much larger than the hydroxyethyl pendant arms of ligand (**62**). The larger pendant arms of ligand (**58**) may be associated with decreasing the electron withdrawing effect of the anthracene or increasing the hydrophobicity of the system. A difference between the ligands (**58**) and (**62**), was noticed at two protonation sites, pK_{a2} and pK_{a5}. The measured pK_a values for ligand (**62**) exhibited a significant increase in acidity compared with the pK_a values for ligand (**58**). Unfortunately, a detailed interpretation is not feasible due to the similarities between protonation sites for ligand (**62**).

Synthesis of the amino acid anthracene substituted ligands also resulted in the formation of two other possible isomers. These are the tri-substituted ligands (**59**) and (**60**), in which pendant arm substitution occurred once at the ethylamine nitrogen adjacent to the anthracene substituent, and twice on the macrocyclic ring either *cis* or *trans* to each other. As mentioned in **Chapter 2**, it was not known whether synthesis had resulted in formation of one or both isomers. If only one of the two possible isomers was present in the fraction, potentiometric titration of the fraction should result in four to five measurable pK_a values, as was seen for the analogous anthracene substituted ligands (**57**) and (**58**). From the curve, obtained from the data set, acquired from the titration of the acidified fraction with base, eight inflection points were observed. This confirms the presence of both isomers. In what percentage each was present was unknown and therefore pK_a values and metal complex ion stability constants could not be determined.

3.2 Determination of metal complex ion stability constants by potentiometric titrations

There are numerous methods that can be employed for the determination of metal complex ion stability constants. One method is that of potentiometric titrations. When a ligand complexes a metal ion in solution, an equilibrium is established between the ligand (L), the solvated metal ion (M^{n+}) and the metal complex ion (ML^{n+}), as can be seen below in Equation 3.7, where *K* represents the stability constant for metal ion complexation.

$$M^{n+} + L \underset{}{\overset{K}{\rightleftharpoons}} M^{n+}L \qquad K = \frac{[ML^{n+}]}{[M^{n+}][L]} \qquad (3.7)$$

In solution, the metal ion competes with the protons in the acidic media for ligand co-ordination sites, altering the pH of the solution. Therefore, a change in the titration curve on addition of a metal ion to the solution indicates the formation of a metal complex ion; the larger the change, the higher the metal complex ion stability constant. Determination of metal complex ion stability constants was achieved by adding a small aliquot (normally 1 equivalent of metal ion) to the acidic titration solution prior to titration with the relevant base. The calculation of the metal complex ion stability constants was achieved by means of the computer program SUPERQUAD.[7] The program allows for the fitting of a function or model to a data set. SUPERQUAD uses a non-linear least squares method to minimise the differences between the experimental data and the theoretical values calculated for the proposed model.

The factors that affect metal complex ion stability include, the relative sizes of the metal ion and the ligand cavity,[8] the solvation energy of the metal ion, the structure and flexibility of the macrocycle, and the number of donor atoms in the macrocycle. The coordination of the metal ion by the ligand involves the substitution of solvent molecules from the first coordination sphere of the metal ion. Consequently, the nature of the solvent affects the stability of the metal complex ion. The ligands in this work are based on two types of macrocycles, tacn and cyclen, with a variety of pendant arms; each ligand contains donor groups affording different metal complex ions. These ligands generally exist in a bi-facial arrangement in which all pendant arms delineate one face, above or below the plane

of the face, delineated by the macrocycle. The flexibility of the arms facilitates metal ion coordination.

In general terms, the formation of the metal complex ion by the pendant arm ligands (**31**), (**42**), (**45**), (**46**), (**50**), (**57**), (**58**) and (**62**), involves complexation by the amine nitrogens. Their disposition is substantially controlled by the macrocyclic ring size, as well as by the donor atoms of the pendant arms whose chelate ring size is determined by the number of ring atoms between them and the macrocyclic nitrogen atoms.[9,10] Upon complexation of the metal ion, the pendant arm ligand effectively forms a cavity, at the centre of which the metal ion is sited. In a given solvent, the overall stability of the complex is thus affected by the number of coordination sites occupied by the donor atoms of the pendant arm macrocycle, and by the 'fit' of the metal ion to the cavity formed by the coordinated pendant arm macrocycle.

The metal complex ion stability constants were determined in a methanol/water solvent system (80:20; v/v), with constant ionic strength $I = 0.1$ mol dm^{-3} (NEt_4ClO_4), by potentiometric titration (see section **6.3**). A large range of metal ions Zn^{2+}, Cd^{2+}, Cu^{2+}, Ni^{2+}, Co^{2+}, Ca^{2+} and Na^{+} were initially chosen for stability constant determination. However, only Zn^{2+}, Cd^{2+} and Cu^{2+} were found to alter the pH of the solutions to such an extent that stability constants could be determined. Equilibrium values (K) of less than K 200 dm^3 mol^{-1}, or $\log K < 2$,[11] cannot be measured using a glass electrode.

3.3 Stability constants for the metal complex ions of ligands (31), (42), (45) and (50)

Of the metal ions investigated, neither Na^+ nor Ca^{2+} showed any significant complexation. This is attributed to their hard acid behaviour in aqueous solution. Sodium(I) and Ca^{2+} tend to form weaker ionic bonds with donor atoms compared with the metal ions Zn^{2+}, Cd^{2+} and Cu^{2+}. The later metal ions are borderline hard acids and tend to form stronger covalent bonds with nitrogen donor atoms, resulting in higher metal complex ion stability constants. The Co^{2+} and Ni^{2+} complexes investigated both formed a precipitate at around pH 4, resulting in an insufficient number of data points for accurate measurement of metal complex ion stability constants. The stability constants for Zn^{2+}, Cd^{2+} and Cu^{2+} are given in **Tables 3.3** and **3.4**. The complexes of ligand (**46**) were insufficiently soluble to be studied under these conditions (see section **6.3**).

Table 3.3. The complexation constants expressed as log*K* values for the metal complex ions of Zn^{2+}, Cd^{2+} and Cu^{2+} with ligands (**31**), (**42**), (**45**) and (**50**), at 298.2 (± 0.2) with I = 0.1 mol dm^{-3} (NEt_4ClO_4) in methanol/water (80:20; v/v), (see **Table 3.4** for conditions)

Equilibrium Quotient	$M^{2+} = Zn^{2+}$ log*K*	$M^{2+} = Cd^{2+}$ log*K*	$M^{2+} = Cu^{2+}$ log*K*
$[M(\mathbf{31})^{2+}]/[M^{2+}][(\mathbf{31})]$	9.00 ± 0.09 [a]	6.49 ± 0.08 [a]	10.01 ± 0.05 [a]
$[M(H(\mathbf{31}))^{3+}]/[M^{2+}][H(\mathbf{31})^{+}]$		4.54 ± 0.06 [a]	
$[M(\mathbf{42})^{-}]/[M^{2+}][(\mathbf{42})^{3-}]$	10.68 ± 0.07 [b]	4.99 ± 0.08 [b]	12.55 ± 0.04 [b]
$[M(H(\mathbf{42}))]/[M^{2+}][H(\mathbf{42})^{2-}]$	6.60 ± 0.05 [b]	4.64 ± 0.07 [b]	7.66 ± 0.03 [b]
$[M(H_2(\mathbf{42}))^{+}]/[M^{2+}][H_2(\mathbf{42})^{-}]$	5.15 ± 0.04 [b]	3.99 ± 0.05 [b]	5.54 ± 0.02 [b]
$[M(H_3(\mathbf{42}))^{2+}]/[M^{2+}][H_3(\mathbf{42})]$		3.55 ± 0.05 [b]	
$[M(\mathbf{42})_2^{4-}]/[M(\mathbf{42})^{-}][(\mathbf{42})^{3-}]$			3.23 ± 0.05 [b]
$[M(\mathbf{45})^{2+}]/[M^{2+}][(\mathbf{45})]$	11.41 ± 0.02 [c]	9.16 ± 0.07 [c]	11.71 ± 0.02 [c]
$[M(H(\mathbf{45}))^{3+}]/[M^{2+}][H(\mathbf{45})^{+}]$		6.16 ± 0.04 [c]	
$[M(\mathbf{50})^{2+}]/[M^{2+}][(\mathbf{50})]$	10.19 ± 0.05 [d]	8.54 ± 0.09 [d]	10.77 ± 0.10 [d]

Table 3.4. The protonation constants expressed as pK_a values for the metal complex ions of Zn^{2+}, Cd^{2+} and Cu^{2+} with ligands (**31**), (**42**) and (**45**) at 298.2 (± 0.2) with I = 0.1 mol dm^{-3} (NEt_4ClO_4) in methanol/water (80:20; v/v).

Equilibrium Quotient	$M^{2+} = Zn^{2+}$ pK_a	$M^{2+} = Cd^{2+}$ pK_a	$M^{2+} = Cu^{2+}$ pK_a
$[M(\mathbf{31})^{2+}][H^+]/[M(H(\mathbf{31}))^{3+}]$		6.74 ± 0.06 [a]	
$[M(\mathbf{31})OH^+][H^+]/[M(\mathbf{31})^{2+}]$			5.83 ± 0.05 [a]
$[M(\mathbf{42})^-][H^+]/[M(H(\mathbf{42}))]$	4.98 ± 0.05 [b]	8.71 ± 0.07 [b]	4.17 ± 0.03 [b]
$[M((\mathbf{42})H)][H^+]/[M(H_2(\mathbf{42})^+)]$	4.68 ± 0.04 [b]	5.48 ± 0.05 [b]	4.01 ± 0.07 [b]
$[M(H_2(\mathbf{42}))^+][H^+]/[M(H_3(\mathbf{42}))^{2+})]$		4.49 ± 0.03 [b]	
$[M(\mathbf{42})OH^{2-}][H^+]/[M(\mathbf{42})^-]$	8.91 ± 0.06 [b]		
$[M(\mathbf{45})^{2+}][H^+]/[M(H(\mathbf{45}))^{3+}]$		5.50 ± 0.04 [c]	
$[M(\mathbf{45})OH^+][H^+]/[M(\mathbf{45})^{2+}]$			5.78 ± 0.06 [c]
$[MOH^+][H^+]/[M^{2+}]$	4.87 ± 0.04[e]	>7[e]	5.14 ± 0.04[e]

[a] $[\mathbf{31}]_{total}$ = 9.1 x 10^{-4} mol dm^{-3}, $[Zn^{2+}]_{total}$, $[Cd^{2+}]_{total}$ or $[Cu^{2+}]_{total}$ = 7.0 x 10^{-4} – 1.5 x 10^{-3} mol dm^{-3}, $[H^+]_{total}$ = 3.1 x 10^{-3} mol dm^{-3}, $[NEt_4OH]$ = 0.104 mol dm^{-3}. [b] $[\mathbf{42}]_{total}$ = 8.9 x 10^{-4} mol dm^{-3}, $[Zn^{2+}]_{total}$, $[Cd^{2+}]_{total}$ or $[Cu^{2+}]_{total}$ = 7.0 x 10^{-4} – 1.5 x 10^{-3} mol dm^{-3}, $[H^+]_{total}$ = 6.0 x 10^{-3} mol dm^{-3}, $[NEt_4OH]$ = 0.104 mol dm^{-3}. [c] $[\mathbf{45}]_{total}$ = 1.27 x 10^{-3} mol dm^{-3}, $[Zn^{2+}]_{total}$, $[Cd^{2+}]_{total}$ or $[Cu^{2+}]_{total}$ = 7.0 x 10^{-4} – 1.9 x 10^{-3} mol dm^{-3}, $[H^+]_{total}$ = 4.3 x 10^{-3} mol dm^{-3}, $[NEt_4OH]$ = 0.103 mol dm^{-3}. [d] $[\mathbf{50}]_{total}$ = 7.3 x 10^{-4} mol dm^{-3}, $[Zn^{2+}]_{total}$, $[Cd^{2+}]_{total}$ or $[Cu^{2+}]_{total}$ = 8.0 x 10^{-4} – 1.04 x 10^{-3} mol dm^{-3}, $[H^+]_{total}$ = 3.1 x 10^{-3} mol dm^{-3}, $[NEt_4OH]$ = 0.103 mol dm^{-3}. [e] $[M^{2+}]_{total}$ = 7.0 x 10^{-4} mol dm^{-3}, $[H^+]_{total}$ = 4.3 x 10^{-3} mol dm^{-3}, $[NEt_4OH]$ = 0.103 mol dm^{-3}.

Each of the three metal ions studied formed a metal hydroxide specie, due to their borderline hard acid behaviour.[12,13] The pH range of the titrations was limited due to the formation of these hydroxide species. For each metal ion a pK_a value for the coordinated water was determined.

A characteristic titration profile for ligand (**31**) with each of the metal ions is shown in **Figure 3.5**. The data collection was restricted to pH $\leq$ 6 due to metal hydroxide precipitation.

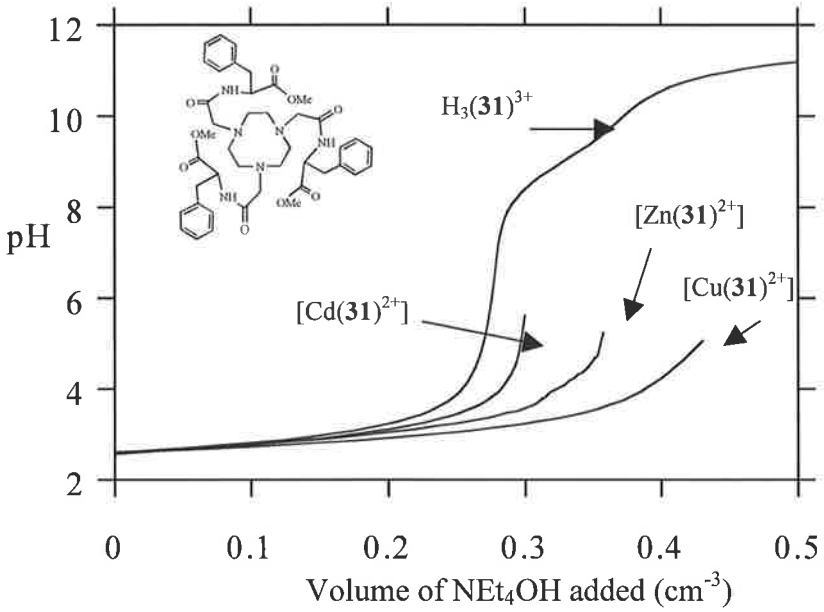

Figure 3.5, Typical titration curves of the protonated ligand (**31**), in the absence and presence of $Zn(ClO_4)_2$, $Cd(ClO_4)_2$ and $Cu(ClO_4)_2$ against NEt_4OH at 298.2 (± 0.2) K. $[(\mathbf{31})]_{total}$ = 9.1 x 10^{-4} mol dm^{-3}, $[Zn^{2+}]_{total}$, $[Cd^{2+}]_{total}$ and $[Cu^{2+}]_{total}$ = 7.0 x 10^{-4} mol dm^{-3}, $[H^+]_{total}$ = 3.1 x 10^{-3} mol dm^{-3}, $[NEt_4OH]$ = 0.104 mol dm^{-3}, I = 0.10 mol dm^{-3} (NEt_4ClO_4).

An overall trend for the metal complex ion stability constants $Cu^{2+}>Zn^{2+}>Cd^{2+}$ was observed for ligands (**31**), (**42**), (**45**) and (**50**). This is predicted by the Irving-Williams series,[14] and is also consistent with the Jahn-Teller effect enhancing the stability of Cu^{2+} over Zn^{2+}.[15] The Cd^{2+} complexes exhibit the lowest stability, which is attributed to the lower surface charge density of the large ion. For the tacn series, ligand (**31**) (**Figure 3.5**) and ligand (**50**) (**Figure 3.6**), the size of Cd^{2+} plays a role in the decreased stability that the ligand exhibits towards the metal ion. The cavity size of the tacn macrocycle is more closely matched to that of Zn^{2+} and Cu^{2+}, which have ionic radii of 0.73 and 0.74 Å respectively.[16] Cadmium(II) has a larger ionic radius of 0.96 Å,[16] which causes more steric strain within the ligand and decreases the stability of the complex.

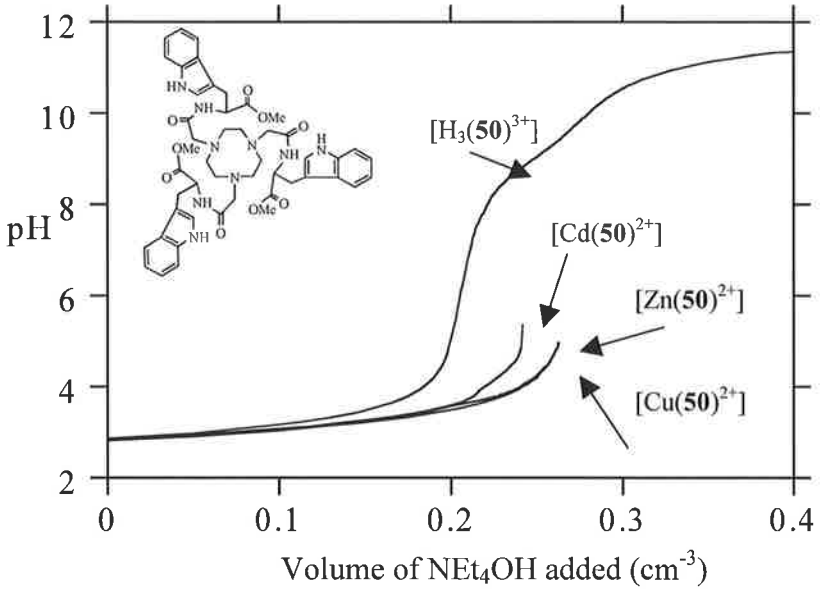

Figure 3.6. Typical titration curve of the protonated ligand (**50**), in the absence and presence of $Zn(ClO_4)_2$, $Cd(ClO_4)_2$ and $Cu(ClO_4)_2$ against NEt_4OH at 298.2 (± 0.2) K. $[(\mathbf{50})]_{total}$ = 7.3 x 10^{-4} mol dm^{-3}, $[Zn^{2+}]_{total}$, $[Cd^{2+}]_{total}$ or $[Cu^{2+}]_{total}$ = 8.0 x 10^{-4} mol dm^{-3}, $[H^+]_{total}$ = 3.1 x 10^{-3} mol dm^{-3}, $[NEt_4OH]$ = 0.103 mol dm^{-3}, I = 0.10 mol dm^{-3} (NEt_4ClO_4).

The tryptophan ligand, ligand (**50**), exhibited a trend towards more stable complexes when compared with its phenylalanine analogue, ligand (**31**). This is due to the change in steric bulk of the pendant arms. The larger aromatic structure of ligand (**50**) apparently interferes with the competitive complexing ability of water for the metal ion. The large bulk of ligand (**50**) may sterically hinder the ability of water to approach the complex, the increased hydrophobicity of ligand (**50**) may alter the hydration of the complex and affect its stability, or both effects may act in concert. Zinc(II) and Cu^{2+} form metal complex ions of similar stability with ligand (**50**): log$K$ (Zn^{2+}) 10.19 and (Cu^{2+}) 10.77. A lower metal complex ion stability constant was measured for Cd^{2+} and was attributed to the relative sizes of the macrocyclic cavity and the metal ion, which mismatched and destabilised the metal complex ion.

The metal complex ions of the cyclen based derivative ligand (**45**) (**Figure 3.7**) exhibited a higher stability when compared with their tacn analogues ligands (**31**) and (**50**). For Cu^{2+} and Zn^{2+}, which preferentially exist as 6-coordinate ions, the larger cyclen ring of ligand (**45**) may present a higher degree of flexibility. The configuration of the donor atoms and pendant arms may be altered to aid in metal ion complexation, with the structure favouring the stronger amine bonding of the four macrocyclic ring nitrogen atoms over the four weaker coordinating amide oxygen atoms. Work on similar macrocyclic ligands

indicates that the structure might be such that coordination to the metal ion is through the four amine nitrogen atoms as well as two of the amide oxygen atoms.[17] The cavity size of the cyclen based ligand (**45**) was expected to be better suited to the larger ionic radius of Cd^{2+} than that of Zn^{2+} or Cu^{2+} and thus exhibit stronger metal ion coordination. This was not observed and was attributed to the larger Cd^{2+} placing more steric strain on ligand (**45**), which decreases the stability of the metal complex ion.

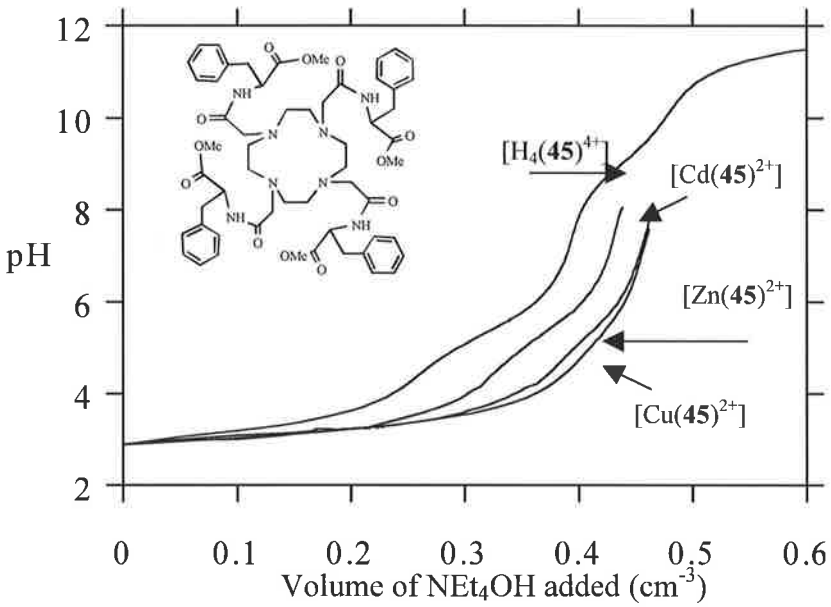

Figure 3.7. Typical titration curve of the protonated ligand (**45**), in the absence and presence of $Zn(ClO_4)_2$, $Cd(ClO_4)_2$ and $Cu(ClO_4)_2$ against NEt_4OH at 298.2 (± 0.2) K. $[(\mathbf{45})]_{total}$ = 1.27 x 10^{-3} mol dm^{-3}, $[Zn^{2+}]_{total}$, $[Cd^{2+}]_{total}$ or $[Cu^{2+}]_{total}$ = 7.0 x 10^{-4} mol dm^{-3}, $[H^+]_{total}$ = 4.3 x 10^{-3} mol dm^{-3}, $[NEt_4OH]$ = 0.103 mol dm^{-3}, I = 0.10 mol dm^{-3} (NEt_4ClO_4).

The larger size of Cd^{2+} is also associated with the formation of the $Cd(LH)^{3+}$ complexes that were obtained for ligands (**31**) and (**45**). The weak coordination of LH^+ by Cd^{2+} does not affect the pK_a value of ligand (**31**) (see **Tables 3.1** and **3.4**) to the same extent as that observed with Zn^{2+} and Cu^{2+} ($Zn(LH)^{3+}$ and $Cu(LH)^{3+}$ are too acidic to be present in detectable quantities.) The $M(LH)^{3+}$ for Cd^{2+} is a less stable complex for ligands (**31**) and (**45**) than that of the ML^{2+} complex. This is attributed to the charge repulsion that may occur between LH^+ and Cd^{2+}. A decrease in ligand denticity from 6 to 5 may also be a contributing factor.

Similar metal complex ion stability constants were observed for the coordination of ligand (**42**) with Cd^{2+} for the two metal complex ions ML^- and M(LH) (**Figure 3.8**). The di-protonated, $M(LH_2)^+$ and tri-protonated $M(LH_3)^{2+}$ metal complex ions were also detected for ligand (**42**) with Cd^{2+}. The similar stabilities of ML^- and M(LH) can be

ascribed to charge repulsion. The ML^- complex has a negative charge, decreasing stability, whilst the M(LH) complex is neutral thus increasing the stability of the metal complex ion. The complexes, $M(LH_2)^+$ and $M(LH_3)^{2+}$ show a decreasing stability towards formation as the charge on the complex increases, coinciding with increasing electrostatic repulsion.

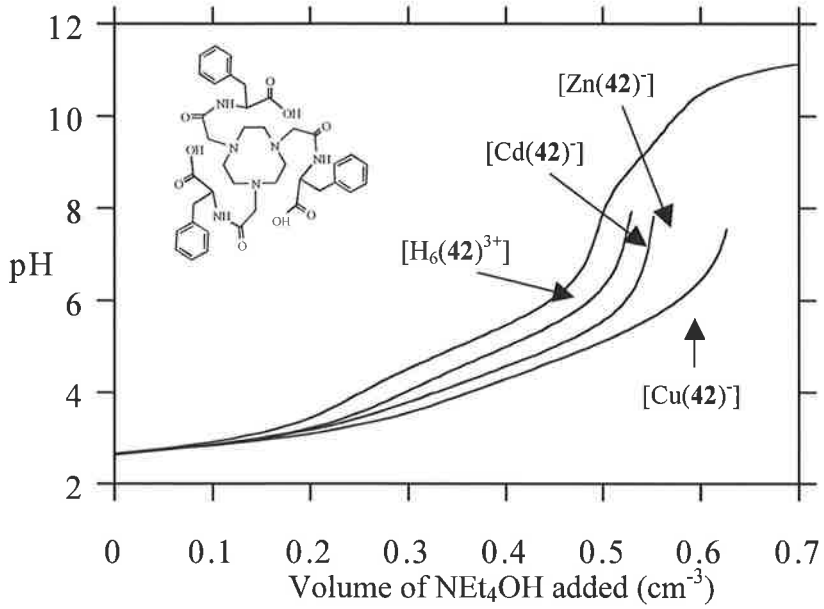

Figure 3.8. Typical titration curves of the protonated ligand (**42**), in the absence and presence of $Zn(ClO_4)_2$, $Cd(ClO_4)_2$ and $Cu(ClO_4)_2$ against NEt_4OH at 298.2 (± 0.2) K. $[(\mathbf{42})]_{total}$ = 8.9 x 10^{-4} mol dm^{-3}, $[Zn^{2+}]_{total}$, $[Cd^{2+}]_{total}$ or $[Cu^{2+}]_{total}$ = 7.0 x 10^{-4} mol dm^{-3}, $[H^+]_{total}$ = 6.0 x 10^{-3} mol dm^{-3}, $[NEt_4OH]$ = 0.104 mol dm^{-3}, I = 0.10 mol dm^{-3} (NEt_4ClO_4).

When a metal ion competes with protons for ligand coordination sites, the pH of the solution is altered, therefore a protonated amine, which is coordinated by a metal ion, will not have the same pK_a value as the protonated amine in the free state. When comparing the pK_{a3} and pK_{a4} values of the free ligand (**42**) with the pK_a values obtained for the Zn^{2+} complex ions, Zn(LH) and $Zn(LH_2)^+$, a close similarity was observed. This was also apparent for the pK_{a4} value of the free ligand (**42**) and the pK_a value of the Cd^{2+} complex ion, $Cd(LH_3)^{2+}$. These similarities suggest that the metal ion either does not coordinate through the atoms associated with these pK_a values, or that only weak coordination is occurring. Ligand (**42**) has nine donor atoms, whilst Zn^{2+} and Cd^{2+} preferentially form six and eight coordinate complexes respectively, reducing the probability that either metal ion coordinates through all available donor atoms. A similarity was also observed between the pK_{a2} value of the free ligand (**45**) and the pK_a value of $Cd(LH)^{3+}$. Ligand (**45**) has eight donor atoms and although Cd^{2+} can exist in an

eight-coordination sphere, the resultant complex may be highly strained and hence energetically disfavoured in comparison with a complex of lower coordination number.

Formation of the metal hydroxide complex $MLOH^+$ was detected for ligands (**31**) and (**45**) with Cu^{2+}. The metal hydroxide complexes were formed from the coordination of water to the ML complex to give the conjugate acid $ML(OH_2)$. The measured pK_a value for the $CuLOH^+$ complex of ligand (**31**), pK_a 5.83, was closely related to the measured pK_a of aquated Cu^{2+}, pK_a 5.17 (**Table 3.4**). The coordination of the water occurs through the displacement of one of the relatively weak donor amide oxygen atoms in the first coordination sphere of the six-coordinate Cu^{2+}. A similar rationale applies for the metal hydroxide complex detected for ligand (**45**).

The coordination of ligand (**42**) with Cu^{2+} was also found to form a 1:2 metal complex ion, ML_2^{4-}. The exact coordination of ligand (**42**) with Cu^{2+} could not be determined, but it is likely that the two ligands coordinate Cu^{2+} through each of their three amine donor nitrogen atoms, forming a six-coordinate metal complex ion (**Figure 3.9**). Such a structure requires that the amide donor oxygen atoms are not involved in complexation, reflecting the relative donor weakness of amide groups compared with the donor strength of amine groups. (The bis-coordination of tacn, the precursor to ligand (**42**) is well known.[18]) The d^9 electronic configuration of Cu^{2+}, and the effect this has on the stereochemical nature of the metal ion, may be the reason that the 1:2 metal complex ion was seen only for Cu^{2+} and not for d^{10} Zn^{2+}, which has more flexible stereochemical requirements.

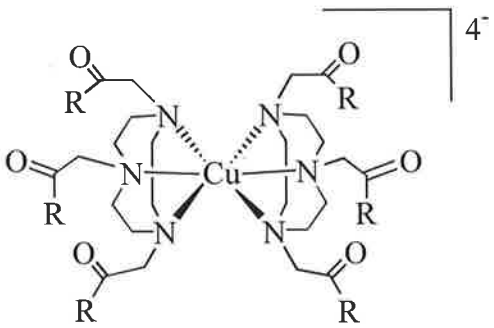

Figure 3.9. Diagrammatic representation of the coordination of Cu^{2+} by the macrocyclic ligand (**42**).

3.4 Speciation

The pK_a values of a ligand, in conjunction with metal complex ion stability constants, can be used to calculate the concentration of all species present in solution at any pH. The concentration of the species is expressed as a percentage relative to the total amount of ligand present in solution. The speciation diagrams for the various Zn^{2+} complexes formed at different pHs for each of the ligands (**31**), (**42**), (**45**) and (**50**), are shown in **Figures 3.10 - 3.13** (refer to **Appendix A.2** for speciation with Cd^{2+} and Cu^{2+} (**Figures A.1 – A.8**)).

The speciation diagram for ligand (**31**) (**Figure 3.10**) shows that the concentration of the ZnL^{2+} species increases with pH until pH 4.5, where a maximum percentage of formation is observed. From the measured pK_a value of the $ZnOH^+$ species, 4.87, it can be assumed that when the pH > p$K_{aZnOH}{}^+$ the later hydroxide species would be present. A precipitate was observed to appear above this pH, coinciding with the formation of the $Zn(OH_2)$ species.

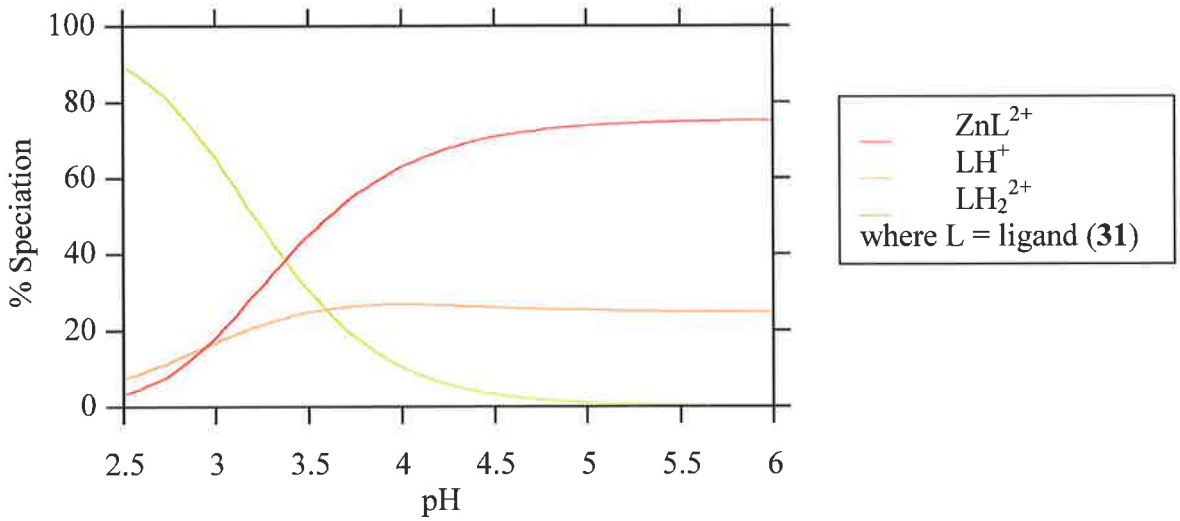

Figure 3.10. Speciation variation of ligand (**31**), showing the species present in a methanol/water (80:20; v/v) solution at various pH in which $[\mathbf{31}]_{total}$ = 9.1 x 10^{-4} mol dm^{-3}, $[Zn^{2+}]_{total}$ = 7.0 x 10^{-4} mol dm^{-3}, I = 0.10 mol dm^{-3} (NEt_4ClO_4) at 298.2 K. Speciation is shown relative to the total concentration of ligand (**31**).

The speciation diagram for the coordination of ligand (**42**) with Zn^{2+} is complicated, due to the number of species present in solution (**Figure 3.11**). The ligand initially coordinates Zn^{2+} as a di-protonated species $Zn(LH_2)^+$, which is sequentially

deprotonated to yield the mono-protonated species Zn(LH), followed by the unprotonated species ZnL^-. The stable ZnL^- species is observed to form predominantly at pH > 5; 100 % formation is not observed due to the high stability of the other metal complex ion species present over this pH range. On formation of the metal hydroxide species $ZnL(OH)^+$, the quantity of the ZnL^- species present is observed to decrease. (This is expected, since water coordinated to the ZnL^- species would be deprotonated at this high pH.)

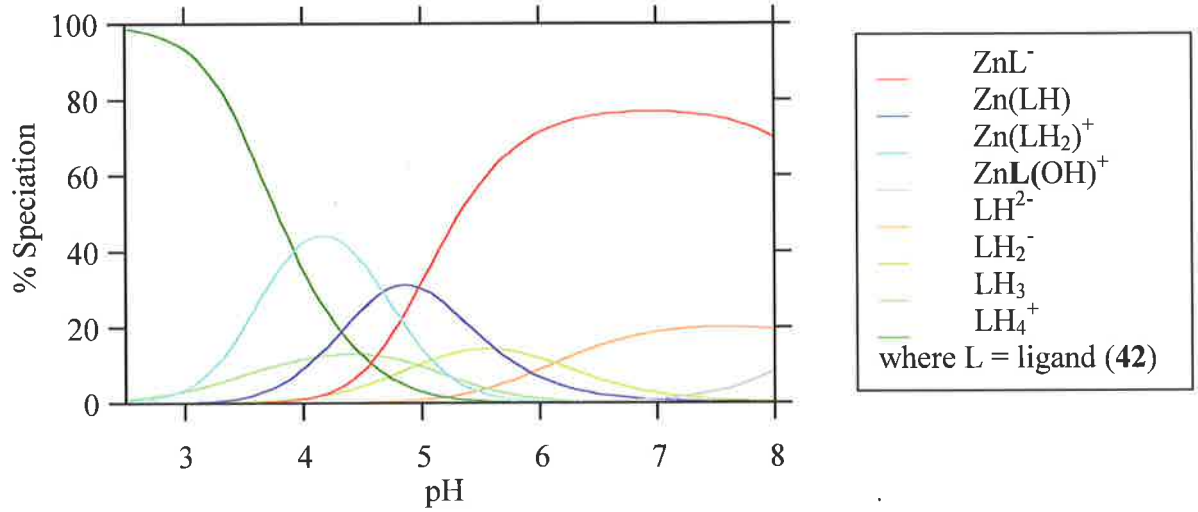

Figure 3.11. Speciation variation of ligand (**42**), showing the species present in a methanol/water (80:20; v/v) solution at various pH in which $[\mathbf{42}]_{total}$ = 8.9 x 10^{-4} mol dm^{-3}, $[Zn^{2+}]_{total}$ = 7.0 x 10^{-4} mol dm^{-3}, I = 0.10 mol dm^{-3} (NEt_4ClO_4) at 298.2 K. Speciation is shown relative to the total concentration of ligand (**42**).

The speciation diagram for the coordination of ligand (**45**) with Zn^{2+} shows the formation of the major species ZnL^{2+} above pH 3.5 (**Figure 3.12**). This reflects the high metal complex ion stability constant measured for ligand (**45**) with Zn^{2+}. A similar speciation diagram was seen for ligand (**50**) on coordination with Zn^{2+}, with the ZnL^{2+} species forming almost exclusively above pH 4 (**Figure 3.13**). This was expected as high metal complex ion stability constants were obtained for ligand (**50**).

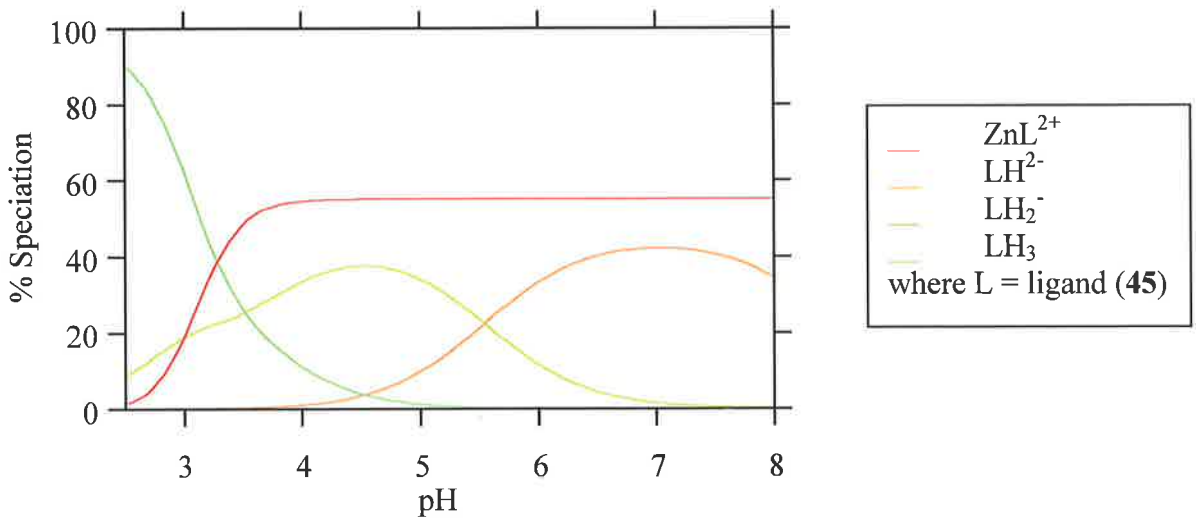

Figure 3.12. Speciation variation of ligand (**45**), showing the species present in a methanol/water (80:20; v/v) solution at various pH in which $[\mathbf{45}]_{total}$ = 1.2 x 10^{-3} mol dm^{-3}, $[Zn^{2+}]_{total}$ = 7.0 x 10^{-4} mol dm^{-3}, I = 0.10 mol dm^{-3} (NEt_4ClO_4) at 298.2 K. Speciation is shown relative to the total concentration of ligand (**45**).

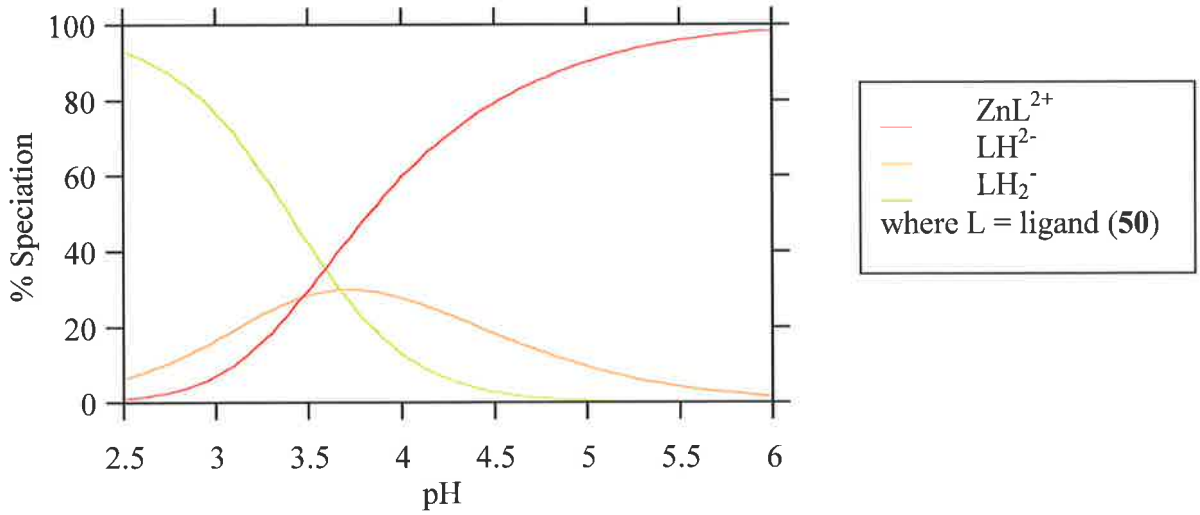

Figure 3.13. Speciation variation of ligand (**50**), showing the species present in a methanol/water (80:20; v/v) solution at various pH in which $[\mathbf{50}]_{total}$ = 7.3 x 10^{-4} mol dm^{-3}, $[Zn^{2+}]_{total}$ = 8.0 x 10^{-4} mol dm^{-3}, I = 0.10 mol dm^{-3} (NEt_4ClO_4) at 298.2 K. Speciation is shown relative to the total concentration of ligand (**50**).

3.5 Stability constants for the metal complex ions of ligands (57) and (58)

The metal complex ion stability constants for ligands (**57**) and (**58**), were determined in a methanol/water solvent system (80:20; v/v), with constant ionic strength I = 0.1 mol dm^{-3} (NEt_4ClO_4), by potentiometric titration (see section **6.3**). A range of metal ions was initially chosen for metal complex ion stability constant determination (Zn^{2+}, Cd^{2+}, Cu^{2+}, Ca^{2+} and Na^{+}). Similarly to ligands (**31**), (**42**), (**45**) and (**50**), no significant complexation was detected for Na^{+} or Ca^{2+} with ligands (**57**) or (**58**). This was attributed to their hard acid behaviour in aqueous solution.

Precipitation of the metal complex ions formed by ligand (**62**) occurred at a low pH (below pH < 4), thus an insufficient number of data points could be obtained. Similarly, ligand (**65**), with a shorter spacer group, was reported to form precipitates below pH 4.[19]

(**65**)

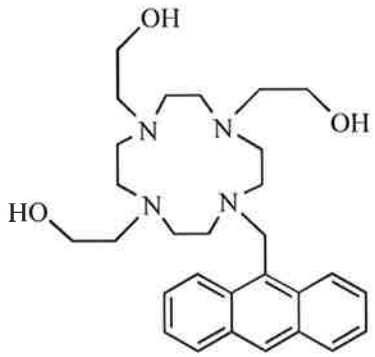

Ligands (**57**) and (**58**), also formed a precipitate at low pH on coordination with Zn^{2+} and so an insufficient number of data points were obtained to determine log$K$ values using a glass electrode. Refer to **Chapter 4** for the metal complex ion stability constants for ligand (**62**) with Zn^{2+}, Cd^{2+} and Cu^{2+}, and for the metal complex ion stability constants of ligands (**57**) and (**58**) with Zn^{2+}.

Table 3.5. The complexation constants expressed as log$K$ values for the metal complex ions of Cd^{2+} and Cu^{2+} with ligands (**57**) and (**58**), at 298.2 (± 0.2) with I = 0.1 mol dm^{-3} (NEt_4ClO_4) in methanol/water (80:20; v/v). (See **Table 3.6** for conditions).

Equilibrium Quotient	$M^{2+} = Cd^{2+}$ log$K$	$M^{2+} = Cu^{2+}$ log$K$
$[M(\mathbf{57})^{2+}]/[M^{2+}][(\mathbf{57})]$	11.46 ± 0.09[a]	14.00 ± 0.06[a]
$[M(H(\mathbf{57}))^{3+}]/[M^{2+}][H(\mathbf{57})^{+}]$	8.80 ± 0.09[a]	9.23 ± 0.06[a]
$[M(H_2(\mathbf{57}))^{4+}]/[M^{2+}][H(\mathbf{57})^{2+}]$	5.80 ± 0.07[a]	5.01 ± 0.06[a]
$[M(\mathbf{58})^{2+}]/[M^{2+}][(\mathbf{58})]$	14.61 ± 0.07[b]	19.42 ± 0.05[b]
$[M(H(\mathbf{58}))^{3+}]/[M^{2+}][H(\mathbf{58})^{+}]$	12.11 ± 0.06[b]	12.36 ± 0.04[b]
$[M(H_2(\mathbf{58}))^{4+}]/[M^{2+}][H_2(\mathbf{58})^{2+}]$	7.23 ± 0.04[b]	5.40 ± 0.06[b]

Table 3.6. The protonation constants expressed as pK_a values for the metal complex ions of Cd^{2+} and Cu^{2+} with ligands (**57**) and (**58**), at 298.2 (± 0.2) with I = 0.1 mol dm^{-3} (NEt_4ClO_4) in methanol/water (80:20, v/v).

Equilibrium Quotient	$M^{2+} = Cd^{2+}$ pK_a	$M^{2+} = Cu^{2+}$ pK_a
$[M(\mathbf{57})^{2+}][H^+]/[M(H(\mathbf{57}))^{3+}]$	7.56 ± 0.09[a]	8.40 ± 0.09[a]
$[MH(\mathbf{57})^{3+}][H^+]/[M(H_2(\mathbf{57}))^{4+}]$	5.10 ± 0.09[a]	5.52 ± 0.05[a]
$[M(\mathbf{58})^{2+}][H^+]/[M(H(\mathbf{58}))^{3+}]$	6.49 ± 0.07[b]	6.45 ± 0.03[b]
$[MH(\mathbf{58})^{3+}][H^+]/[M(H_2(\mathbf{58}))^{4+}]$	4.20 ± 0.05[b]	4.04 ± 0.07[b]
$[MOH^+][H^+]/[M^{2+}]$	>7[c]	5.14 ± 0.04[c]

[a] [**57**] = 3.3 x 10^{-4} mol dm^{-3}, $[Cd^{2+}]_{total}$ or $[Cu^{2+}]_{total}$ = 3.0 x 10^{-4} - 1.0 x 10^{-3} mol dm^{-3}, $[H^+]_{total}$ = 4.6 x 10^{-3} mol dm^{-3}, $[NEt_4OH]$ = 0.111 mol dm^{-3}. [b] [**58**] = 5.3 x 10^{-4} mol dm^{-3}, $[Cd^{2+}]_{total}$ or $[Cu^{2+}]_{total}$ = 4.0 x 10^{-4} - 1.0 x 10^{-4} mol dm^{-3}, $[H^+]_{total}$ = 5.3 x 10^{-3} mol dm^{-3}, $[NEt_4OH]$ = 0.111 mol dm^{-3}. [c] $[Cu^{2+}]_{total}$ = 7.0 x 10^{-4} mol dm^{-3}, $[H^+]_{total}$ = 4.3 x 10^{-3} mol dm^{-3}, $[NEt_4OH]$ = 0.103 mol dm^{-3}.

For the two anthracene substituted ligands, (**57**) and (**58**), subjected to metal complex ion stability constant determination, large log$K$ values were obtained, indicating that both ligand (**57**) and (**58**) formed stable metal complex ions. A stability variation of $Cu^{2+} > Cd^{2+}$ was observed for both ligands, (**57**) and (**58**). The observed stability variation is predicted by the Irving-Williams series.[14] The titration profiles for both ligands, (**57**) and (**58**), are shown in **Figures 3.14** and **3.15**.

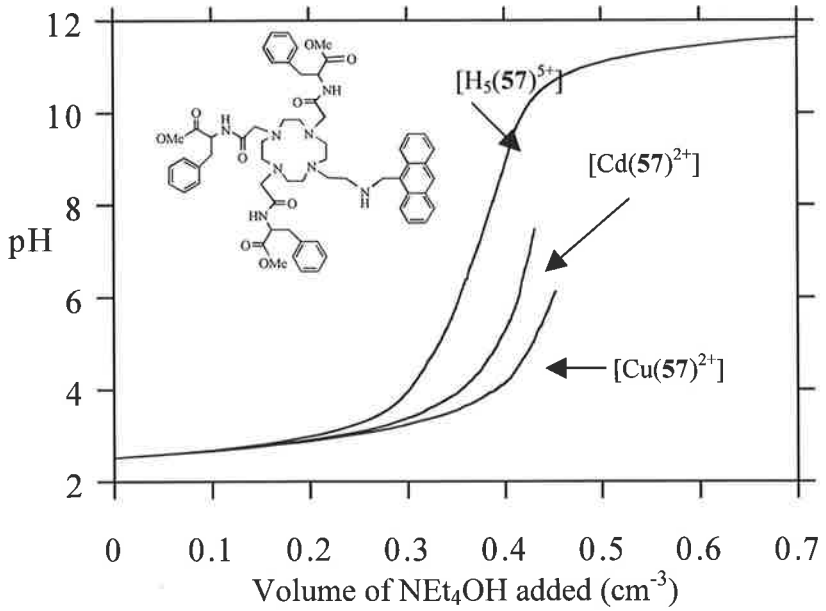

Figure 3.14. Typical titration curves of the protonated ligand (**57**), in the absence and presence of $Cd(ClO_4)_2$ and $Cu(ClO_4)_2$ against NEt_4OH at 298.2 (± 0.2) K. $[\mathbf{57}]_{total}$ = 3.3 x 10^{-4} mol dm^{-3}, $[Cd^{2+}]_{total}$ = 1.0 x 10^{-3} mol dm^{-3}, $[Cu^{2+}]_{total}$ = 1.0 x 10^{-3} mol dm^{-3} , $[H^+]_{total}$ = 4.6 x 10^{-3} mol dm^{-3}, $[NEt_4OH]$ = 0.111 mol dm^{-3}, I = 0.10 mol dm^{-3} (NEt_4ClO_4).

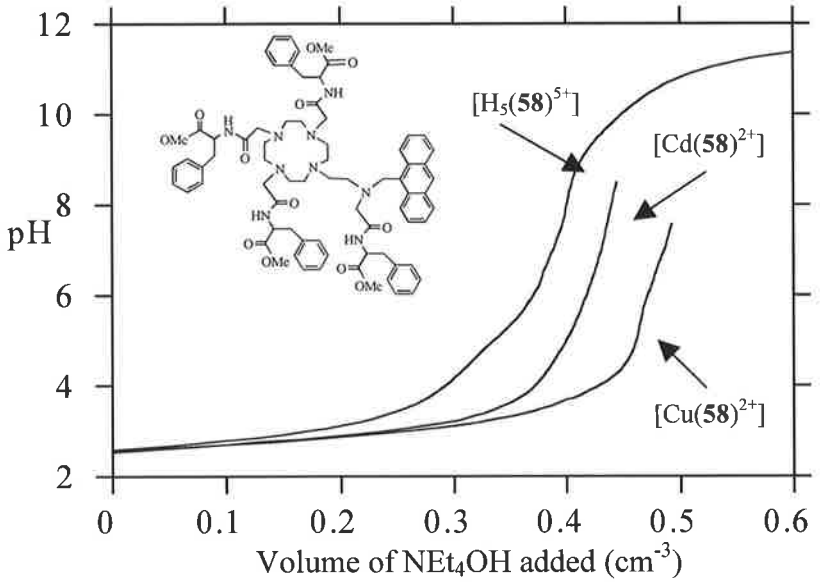

Figure 3.15. Typical titration curves of the protonated ligand (**58**), in the absence and presence of $Cd(ClO_4)_2$ and $Cu(ClO_4)_2$ against NEt_4OH at 298.2 (± 0.2) K. $[\mathbf{58}]_{total}$ = 5.3 x 10^{-4} mol dm^{-3}, $[Cd^{2+}]_{total}$ = 1.0 x 10^{-3} mol dm^{-3}, $[Cu^{2+}]_{total}$ = 1.0 x 10^{-3} mol dm^{-3} , $[H^+]_{total}$ = 5.3 x 10^{-3} mol dm^{-3}, $[NEt_4OH]$ = 0.111 mol dm^{-3}, I = 0.10 mol dm^{-3} (NEt_4ClO_4).

Higher metal complex ion stability constants were calculated for ligand (**58**) than for ligand (**57**). This is attributed to the ethylamine nitrogen adjacent to the anthracene substituent being substituted in ligand (**58**) but not in ligand (**57**). The extra pendant arm substituted in ligand (**58**) increases the number of donor atoms, decreases the electron withdrawing effect of the anthracene, and increases the hydrophobicity of the system. One or more of these effects may account for the increase in metal complex ion stability.

For the anthracene substituted ligands (**57**) and (**58**), both Cd^{2+} and Cu^{2+} were found to form mono-protonated and di-protonated metal complex ions, $M(LH)^{3+}$ and $M(LH_2)^{4+}$, respectively. The pK_{a2} and pK_{a3} values obtained for the free ligand (**57**) were similar to the pK_as of the protonated Cd^{2+} metal complex ions, $Cd(LH)^{3+}$ and $Cd(LH_2)^{4+}$. Similarly, the protonation assigned pK_{a3} for ligand (**57**) was comparable to the pK_a value of the protonated Cu^{2+} metal complex ion $Cu(LH_2)^{4+}$. A close similarity was also observed between the pK_{a3}, pK_{a4} and pK_{a5} values of the free ligand (**58**) and the pK_a values of both the protonated Cd^{2+} and Cu^{2+} complex ions, $M(LH)^{3+}$ and $M(LH_2)^{4+}$ (where pK_{a4} and pK_{a5} are indistinguishable, as discussed in section **3.1.2**) (see **Tables 3.2** and **3.6** for ligands (**57**) and (**58**)). These similarities suggest that not all amine groups are involved in metal ion coordination or are only weakly coordinated to the metal ion. Copper(II) tends to form only six coordinate complexes while both ligands (**57**) and (**58**) have eight and nine donor atoms respectively, increasing the probability that not all amine groups are involved in metal ion coordination. The same rationale applies for ligand (**58**) with Cd^{2+}. The usual coordination number of Cd^{2+} does, however, correspond with the number of donor atoms present in ligand (**57**); but the resultant complex may be highly strained, and hence energetically disfavoured by comparison with a complex of lower coordination number.

The stability constants calculated for the metal complex ions of ligand (**57**) were higher than the calculated stability constants for ligands (**31**), (**42**), (**45**) and (**50**) (see section **3.2.1**). In the case of ligands (**31**) and (**50**) this is attributed to ligand (**57**) possessing eight donor atoms, while ligands (**31**) and (**50**) have only six. The large number of donor atoms in ligand (**57**), coupled with the larger ring size, has probably created a more flexible coordination environment. The same rationale cannot be applied to ligands (**42**) and (**45**) however, as ligands (**42**) and (**45**) have eight and nine donor atoms respectively. The increased stability of the metal complex ions of ligand (**57**) over those of ligands (**42**) and (**45**), is attributed to the change in donor atoms present in ligand (**57**), which has an additional amine group. Hence, the higher metal complex ion stability

constants of ligand (**57**) reflect the increased strength of a coordinating amine nitrogen group compared with the relative weakness of a coordinating amide oxygen group. The higher metal complex ion stability constants may also be associated with the increased hydrophobicity of the system, due to the incorporation of the anthracene group. A similar rationale can also be applied to the difference between the metal complex ion stability constants of ligand (**58**) with those of ligands (**31**), (**42**), (**45**) and (**50**). Ligand (**58**) has a larger number of stronger coordinating atoms than ligands (**31**), (**42**), (**45**) and (**50**), with five amine donor nitrogen atoms, and four amide donor oxygen atoms. The hydrophobicity of the system in ligand (**58**) is also increased, due to the incorporation of the anthracene group. A combination of these factors is probably reflected in the difference between the stability constants of the metal complex ions formed by ligand (**58**) and those formed by ligands (**31**), (**42**), (**45**) and (**50**).

3.6 Speciation

The concentration of all species present in solution at any pH may be visualised by means of species distribution diagrams as mentioned previously (see section **3.3**). The speciation diagram **Figure 3.16** illustrates the effect varying pH has on the species present in solution for ligand (**57**) with Cu^{2+}. Copper(II) initially coordinates ligand (**57**) as the di-protonated species $Cu(LH_2)^{4+}$ up to pH 4, when sequential deprotonation of the metal complex ion occurs. All the detectable species for ligand (**57**) are seen in a large percentage relative to the total ligand concentration. This is a reflection of the large stability constants determined for the metal complex ions of ligand (**57**). A similar speciation diagram can be seen for ligand (**58**) with Cu^{2+} (**Figure 3.17**), as was seen for ligand (**57**), with initial complexation of Cu^{2+} forming a di-protonated species $Cu(LH_2)^{4+}$. Deprotonation of the $Cu(LH_2)^{4+}$ species results in the formation of the mono-protonated complex $Cu(LH)^{3+}$ and the unprotonated complex CuL^{2+}. The later species forms in predominance above pH 6.5 (refer to **Appendix A.2** for speciation with Cd^{2+} **Figures A.9** and **A.10**).

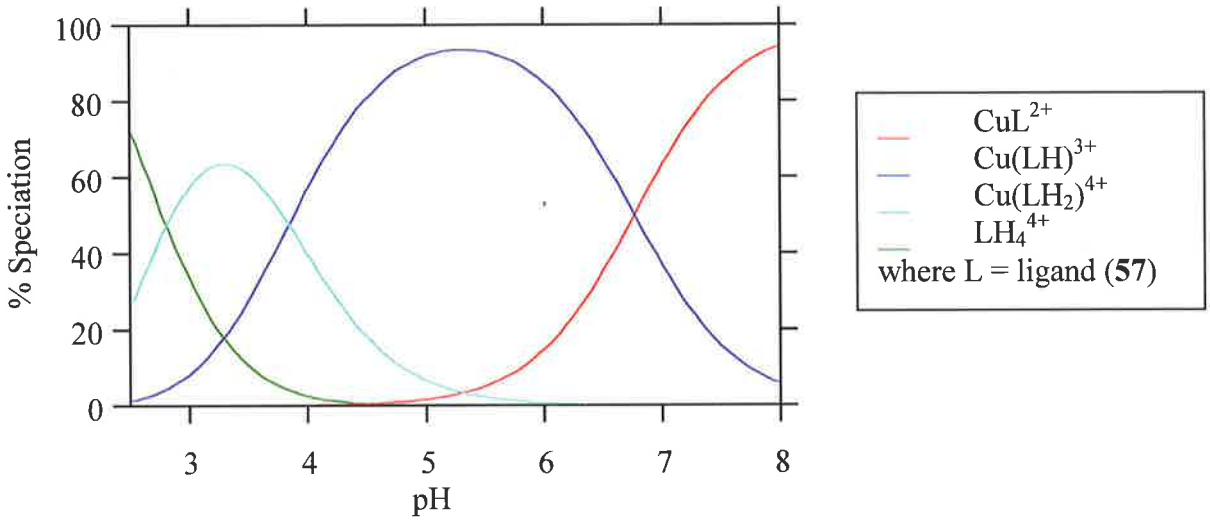

Figure 3.16. Speciation variation of ligand (**57**) showing the species present in a methanol/water (80:20; v/v) solution at various pH in which $[\mathbf{57}]_{total}$ = 3.3 x 10^{-4} mol dm^{-3}, $[Cu^{2+}]_{total}$ = 1.0 x 10^{-3} mol dm^{-3}, I = 0.10 mol dm^{-3} (NEt_4ClO_4) at 298.2 K. Speciation is shown relative to the total concentration of ligand (**57**).

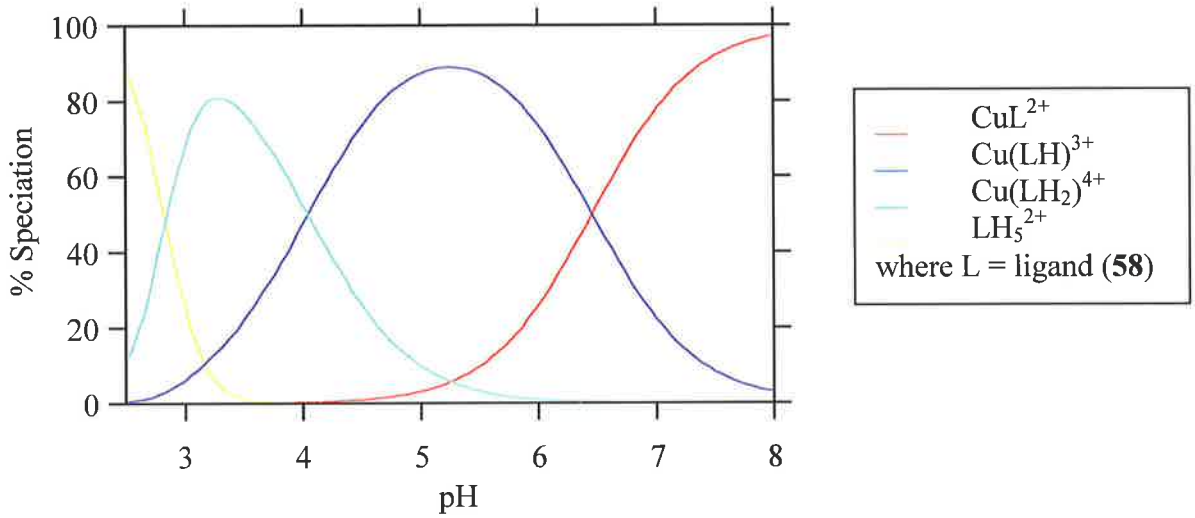

Figure 3.17. Speciation variation of ligand (**58**) showing the species present in a methanol/water (80:20; v/v) solution at various pH in which $[\mathbf{58}]_{total}$ = 5.3 x 10^{-4} mol dm^{-3}, $[Cu^{2+}]_{total}$ = 1.0 x 10^{-3} mol dm^{-3}, I = 0.10 mol dm^{-3} (NEt_4ClO_4) at 298.2 K. Speciation is shown relative to the total concentration of ligand (**58**).

3.7 Discussion

All of the ligands synthesised in **Chapter 2** were studied extensively using potentiometric titrations to determine their pK_a values and metal complex ion stability constants. All titrations were carried out in a partially aqueous solvent system, methanol/water (80:20; v/v), at constant ionic strength $I = 0.10$ mol dm^{-3} (NEt_4ClO_4).

It was found that increasing the steric bulk of the arms from phenylalanine to tryptophan yielded a ligand with higher pK_a values. Increasing the size of the ring from the 6-membered tacn to the 8-membered cyclen ring also had the effect of increasing the measured pK_a values. This was attributed to the greater charge separation achievable with the larger macrocyclic ring. It was also found that the pK_as, attributed to the carboxylic acids were the most acidic in the two ligands (**42**) and (**46**). The pK_a values for the anthracene substituted ligands (**57**), (**58**) and (**62**) showed the effect that the addition of an anthracene group had on the system. The pK_a values measured for ligand (**57**) were more acidic than for ligand (**58**); a similar trend was also observed between ligand (**62**) and ligand (**58**). The pK_a values measured for ligand (**62**) were more acidic than those for ligand (**58**). For the anthracene substituted ligands, these trends were attributed to the increased hydrophobicity of the system in ligand (**58**).

A trend in the metal complex ion stability constants $Cu^{2+} > Zn^{2+} > Cd^{2+}$ was observed, as predicted by the Irving Williams series. All three metal ions formed hydroxide species due to the deprotonation of coordinated water.

Higher metal complex ion stability constants were measured for the anthracene substituted ligands (**57**) and (**58**), than for those of ligands (**31**), (**42**), (**45**) and (**50**). This was attributed to both, the addition of the anthracene substituted arm with the extra amine donor nitrogen atom for coordination, as well as the increased hydrophobicity of the systems, which was associated with the anthracene substituent. The macrocyclic ring size was also found to affect the stability of the metal complex ions; higher stability constants were measured for the cyclen based ligands than for the tacn based ligands.

In some cases, similarities were observable between the pK_a values of the free ligands and the pK_a values of the protonated metal complex ions. This was most apparent

for the ligands with larger chelate rings and indicates that the metal ion may not be coordinated through all of the available donor atoms.

Three of the ligands that underwent potentiometric titration, ligands (**57**), (**58**) and (**62**) are designed as fluorescent sensors. To ascertain the usefulness of these ligands as fluorescent sensors their photophysical properties were investigated as described in **Chapter 4**.

3.8 References

(1) Bencini, A.; Bianchi, A.; Garcia-Espana, E.; Micheloni, M.; Ramirez, J. A. *Coord. Chem. Rev.* **1999**, *188*, 97-156.

(2) Desreux, J. F.; Merciny, E.; Loncin, M. F. *Inorg. Chem.* **1981**, *20*, 987-991.

(3) Geraldes, C. F. G.; Sherry, A. D.; Marques, M. P. M.; Alpoim, M. C.; Cortes, S. *J. Chem. Soc., Perkin Trans. 2* **1991**, 137-146.

(4) Cai, H.-Z.; Kaden, T. A. *Hel. Chim. Acta.* **1993**, *76*, 557-562.

(5) Cai, H.-Z.; Kaden, T. A. *Hel. Chim. Acta.* **1994**, *77*, 383-399.

(6) Greiner, G.; Maier, I. *J. Chem. Soc., Perkin Trans. 2* **2002**, 1005-1011.

(7) Gans, P.; Sabatini, A.; Vacca, A. *J. Chem. Soc., Dalton Trans.* **1985**, 1195-1200.

(8) Izatt, R. M.; Eatough, D. J.; Christensen, J. J. In *Structure and Bonding*, 1973, pp 161-189.

(9) Hancock, R. D.; Bhavan, R.; Wagner, C. A.; Hosken, G. D. *S. Afr. J. Chem.* **1986**, *39*, 238-242.

(10) Hay, B. P.; Hancock, R. D. *Coord. Chem. Rev.* **2001**, *212*, 61-78.

(11) Lehn, J.-M.; Sauvage, J. P. *J. Am. Chem. Soc.* **1975**, *97*, 6700-6707.

(12) Nieboer, E.; Richardson, D. H. S. *Enviro. Poll. B* **1980**, *1*, 3-26.

(13) Hancock, R. D.; Martell, A. E. *J. Chem. Ed.* **1996**, *73*, 654-661.

(14) Irving, H.; Williams, R. J. P. *J. Chem. Soc.* **1953**, 3192-3210.

(15) Shirver, D. F.; Atkins, P. W. *Inorganic Chemistry*; 3rd ed.; Oxford University Press: Oxford, UK, 1999.

(16) Shannon, R. D. *Acta. Crystallogr., Sect. A* **1976**, *32*, 751.

(17) Clarke, E. T.; Martell, A. E. *Inorg. Chim. Act.* **1991**, *190*, 27-36.

(18) Chaudhuri, P.; Wieghardt, K. *Prog. Inorg. Chem.* **1987**, *35*, 329.

(19) Ngo, H. T. In *Department of Chemistry*; The University of Adelaide: Adelaide, 2003.

Chapter 4 UV-visible Absorption and Fluorescence Studies

4.1 Introduction

There are many different types of electromagnetic radiation, from radio waves to gamma rays. The photon, which can be described as a small packet of energy, is an important part in the understanding of electromagnetic radiation or light. When the electronic energy of an atom is altered, it either absorbs or emits a photon. The energy of a photon is proportional to its frequency or wavelength as defined in Equation 4.1.

$$E = h\nu = hc/\lambda \qquad (4.1)$$

where h is Planck's constant (6.626×10^{-34} J s)

ν is the frequency of the radiation (s^{-1})

c is the velocity of light in a vacuum (3×10^{8} m s^{-1})

λ is the wavelength of the radiation (m)

When an electron absorbs a photon, it leaves a lower energy orbital to enter a higher energy orbital, and the atom or molecule thereby assumes an excited state. The various frequencies of light absorbed by atoms and molecules give rise to their absorption spectra and, more generally, absorption spectroscopy. When the electron in the excited state loses energy and returns to its ground state, a photon is emitted. This results in the emission spectra of atoms or molecules, a process that can generally be described as emission spectroscopy.

A useful technique, which harnesses the absorption of light, is ultraviolet-visible (UV-visible) spectroscopy. This technique produces a spectrum, which is the graphical representation of the intensity of light absorbed in producing electronic transitions in a molecule, as a function of the wavelength of light. The energy required to excite electrons between energy levels is characteristic of particular types of molecules. The relationship between the absorption spectra of molecules and their structure has been extensively studied.[1-3] The degree of absorption of a molecule is based on the Beer-Lambert law,

which defines the relationship between the absorbing substance and the incident, and transmitted radiation intensities. The Beer-Lambert equation is given in Equation 4.2.[3]

$$A = \log(I_0/I) = \varepsilon Cl \qquad (4.2)$$

where A is the absorbance of the sample

I_0 is the light intensity incident on the sample

I is the light intensity transmitted by the sample

ε is the molar extinction coefficient of the molecule ($dm^3\ mol^{-1}\ cm^{-1}$)

C is the concentration of absorbing molecules in solution ($mol\ dm^{-3}$)

l is the path length of light through the solution (cm)

Lambert's law states that the proportion of light absorbed by a transparent medium is independent of the intensity of the incident light, and that each successive layer of the medium absorbs an equal fraction of the incident light. Beer's Law is related to the concentration of the absorbing substance, and states that the amount of light absorbed is proportional to the number of absorbing molecules through which the light passes; that is, the absorption of a solution is directly proportional to its concentration.[2]

A spectrophotometer is used to measure absorbance as a quantity, which is expressed as the molar extinction coefficient or molar absorptivity of the molecule. The term molar absorptivity is used when the concentration is expressed as moles per litre and the path length is in centimetres. Molar absorptivity is an important concept, as it is independent of the concentration or sample size, and is related only to the absorption frequency. These laws can be applied only when the light source is monochromatic.

Emission spectroscopy is important in the study of photophysical effects; these types of experiments involve fluorescence or phosphorescence. The process of emission is slower than that of absorption and can take several pathways, such as vibrational relaxation, internal conversion, or intersystem crossing.[4,5] These electronic transitions are depicted in the energy level diagram, Figure 4.1, where S_0 is the ground state.

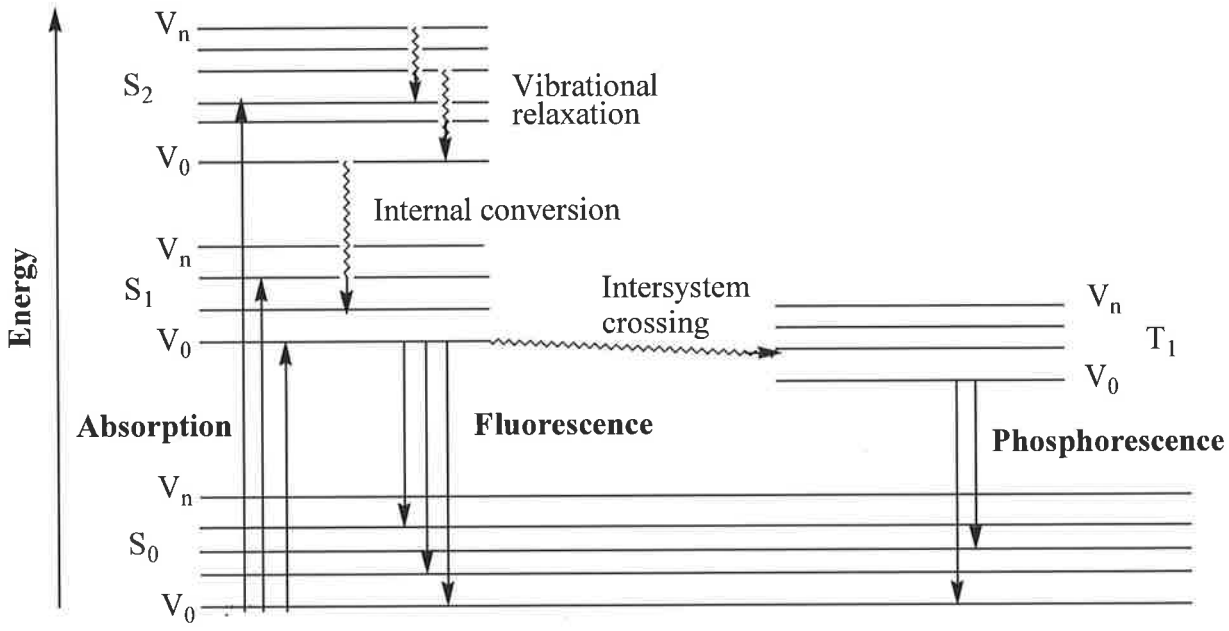

Figure 4.1. Schematic energy level diagram of the absorption and emission of energy from a molecule, indicating possible electronic transitions. S represents a singlet state, T represents a triplet state, V represents the various vibrational sublevels, and the wavy lines represent non-radiative energy transitions.

Vibrational relaxation occurs by the transfer of photons through collisions with other molecules in a stepwise fashion, which results in the electrons occupying the lowest vibrational level in the electronically excited state. The energy level diagram (Figure 4.1) illustrates the various vibrational energy levels associated with each excited state, V_0 - V_n (where n = 1,2…). The different vibrational energy levels in each state cannot be viewed individually for liquids at room temperature; but as a whole they contribute to the broad nature of the bands in both absorption and emission spectra.

Internal conversion occurs from the lowest vibrational level (V_0) in an excited state, S_2, to a lower electronic energy level, S_1. There are three different ways that this can be achieved. Firstly, if there is an overlap of vibrational levels between the upper electronic state (S_2) and the lower electronic state (S_1), then transient thermal equilibrium allows for the crossover between states. This is then followed by vibrational relaxation within the electronic energy level, until the next lowest vibrational level in that state is reached. Secondly, where the two electronic energy states do not overlap but the gap is small, a process called tunnelling can result, allowing for the decrease in energy. Thirdly, if the gap between the electronic energy states is large, radiative transmission then occurs

between the two states, upper and lower. The difference in energy is released as a photon, the frequency of which is proportional to the change in energy levels ($\upsilon = \Delta E/h$). This process is commonly referred to as fluorescence. Fluorescence is normally seen only between the energy levels S_1 to S_0. The above processes for relaxation are in effect only for singlet states or for those states in which all the electrons are spin paired.

In molecules that have one set of electrons unpaired, a triplet state results and intersystem crossing can occur. This can be rationalised by Hund's rule, which postulates that the triplet state will be at a lower energy than that of its corresponding singlet state, due to its unpaired electron. This allows for intersystem crossing between the two spin systems, singlet and triplet, S_1 to T_1. The conversion from the triplet state, T_1, to the lowest energy level, S_0, is referred to as phosphorescence. Phosphorescence has a lower probability of occurring than fluorescence because the change in spin state is classically forbidden. The spin-forbidden nature is reflected in the long radiative lifetime of phosphorescent transitions and occurs mostly in molecules with restricted vibrational freedom, such as aromatic groups.

Two types of spectra can be obtained when measuring fluorescence; emission and excitation. Emission spectra are obtained when the emission intensity is measured as a function of wavelength at a fixed excitation wavelength. This differs from excitation spectra, which are obtained by measuring the emission intensity at a fixed wavelength as the excitation wavelength is altered. In this work emission spectra only were measured.

Much interest has been expressed in the development of aminomethyl anthracene derivatives as fluorescent sensor systems for pH and metal ion detection.[6] They are often used for PET (photoinduced electron transfer) based detection, in which the lone pair of electrons from the amine nitrogen quenches the fluorescence of the anthracene substituent by electron transfer. The transfer of electrons by PET can be hindered by metal ion complexation or protonation of the amine group, which interrupts the PET mechanism and results in the restoration of fluorescence.[6-10] The focus of this study is to investigate how both protonation and metal ion complexation affect the UV-visible absorption and fluorescence properties of ligands (**57**), (**58**) and (**62**). These ligands have been devised as anthracene substituted sensors, designed to respond to the effects of protonation and metal ion complexation through PET. The ligands incorporate an anthracene substituent as a

fluorophore, and an ethylamine nitrogen adjacent to the anthracene substituent, which should act as the primary electron donor for PET.

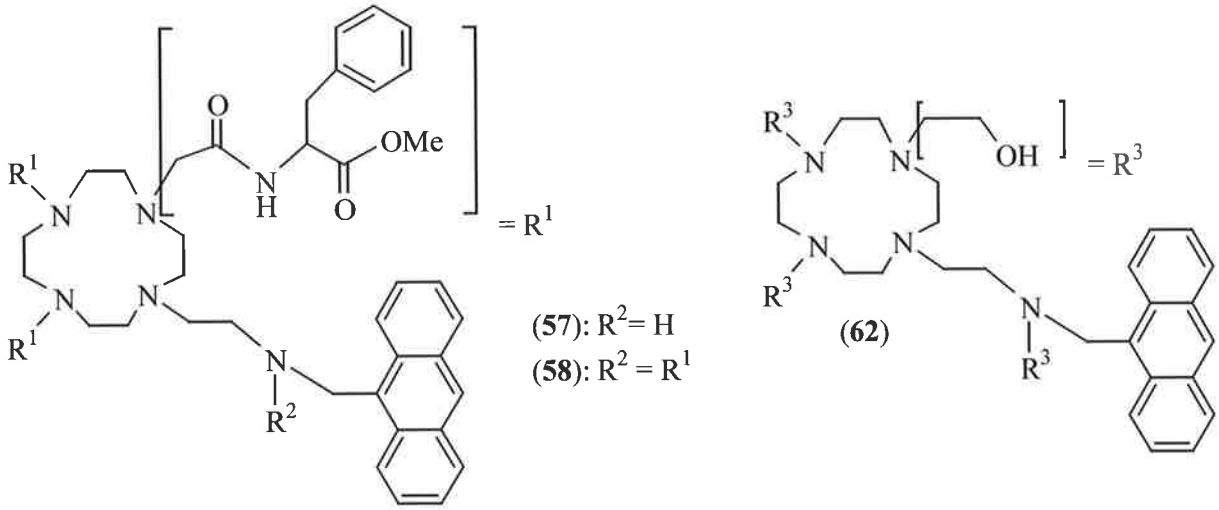

Figure 4.2 Structures of the anthracene substituted ligands (**57**), (**58**) and (**62**).

4.2 Photophysical pH titrations

All photophysical measurements were determined in a methanol/water solvent system (80:20; v/v) with constant ionic strength I = 0.1 mol dm^{-3} (NEt_4ClO_4). Methanol is a solvent of high transmittance (> 210.5 nm for a 1 cm path length),[11] which is highly miscible with water. The choice of solvent was governed by the solubility of ligands (**57**), (**58**) and (**62**) and allows for direct comparison with the data obtained from potentiometric titrations. The concentrations used for photophysical measurements however, differ from those used in the potentiometric titrations (see **Chapter 3**). Concentrations of the order of 10^{-5} and 10^{-6} mol dm^{-3} are compatible with UV-visible absorption and fluorescence measurements; the same solutions were used in both UV-visible absorption and fluorescence measurements.

4.2.1 UV-visible absorption pH titrations for ligands (57), (58) and (62)

To observe the influence of pH on the UV-visible absorption of ligands (**57**), (**58**) and (**62**), a dilute solution of the protonated ligand in a methanol/water solvent system (80:20; v/v), with constant ionic strength $I = 0.1$ mol dm^{-3} (NEt_4ClO_4), was titrated against a solution of tetraethylammonium hydroxide (NEt_4OH). The UV-visible absorption measurements were over the range of 300-450 nm.

9-substituted anthracene derivatives have been shown to yield characteristic four absorption band spectra;[12] hence similar absorption spectra were expected for the ligands in this study. The absorption spectra obtained from the titration of the protonated ligand (**57**) (**Figure 4.3**) show that the ligand underwent a change in absorption on titration with base; at higher pH the molar absorptivity of the ligand was increased. Three absorption bands were observed at 389, 368, and 325 nm for the protonated ligand (**57**).

The absorption spectra of ligand (**57**) show a large absorption band around 325 nm, consistent with a charge transfer, which may occur between the phenyl rings of the pendant arms and the anthracene substituent. The choice of solvent may have facilitated this, as charge transfer states are often seen in polar solvents.[13] The changes in absorption patterns for the individual spectra in the montage were in accordance with the mono to tetra protonated species present and hence also with the pK_a values obtained from the potentiometric titrations (see section **3.1.2**). On increasing pH, the two absorption bands at 389 and 368 nm underwent a hypsochromic shift (the absorption bands at 389 and 368 nm are associated with the electrons in the anthracene substituent). The band at 325 nm (associated with charge transfer between the phenyl rings and the anthracene substituent), however, underwent a slight bathochromic shift. A bathochromic shift indicates an increase in electron delocalisation, whilst a hypsochromic shift indicates a decrease in electron delocalisation. The absorption band shift suggests that as the pH of the solutions is increased, there is an increase in the charge transfer between the phenyl rings and the anthracene substituent. This increase coincides with a decrease in the electron delocalisation within the anthracene substituent.

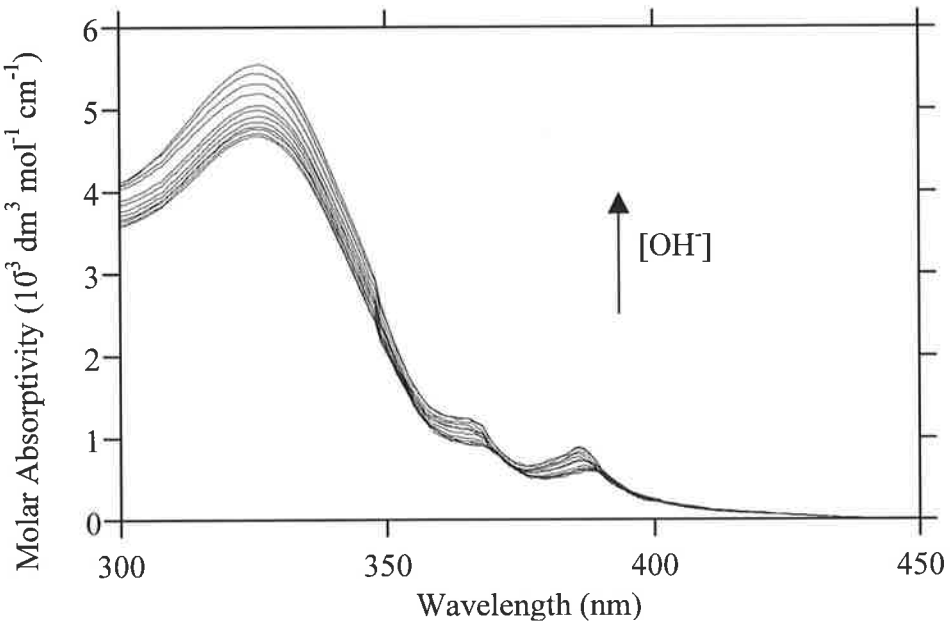

Figure 4.3. UV-visible absorption spectra for the titration of the protonated ligand (**57**) [3.3 x 10^{-5} mol dm^{-3}] against NEt_4OH in methanol/water (80:20; v/v) (I = 0.1 mol dm^{-3}, NEt_4ClO_4) at 298.2 K. $[H^+]_{total}$ = 4.6 x 10^{-4} mol dm^{-3}, $[NEt_4OH]_{total}$ = [0, 1.7 x 10^{-4}, 2.6 x 10^{-4}, 3.6 x 10^{-4}, 3.7 x 10^{-4}, 3.8 x 10^{-4}, 3.9 x 10^{-4}, 4.0 x 10^{-4}, 4.2 x 10^{-4}, 4.4 x 10^{-4}, 4.5 x 10^{-4}, 4.7 x 10^{-4} mol dm^{-3}] in ascending order of molar absorptivity and the corresponding pH values; 3.3, 3.4, 3.9, 4.2, 4.7, 5.1, 5.7, 6.4, 7.3, 8.2, 9.1, 10.1.

The absorption spectra obtained from the titration of the protonated ligand (**58**) with NEt_4OH are shown in **Figure 4.4**. Four absorption bands were observed at 387, 368, 346 and 331 nm for the protonated ligand (**58**). A significant difference in absorption patterns occurs between the absorption spectra of ligand (**57**) (**Figure 4.3**), and ligand (**58**) **Figure 4.4**). The difference in ratio of the molar absorptivity between the band at 331 nm (associated with charge transfer between the phenyl rings and the anthracene substituent) with the bands at 387, 368, and 346 nm (associated with the electrons in the anthracene substituent) is much smaller for ligand (**58**) than for ligand (**57**). This indicates that the extent to which charge transfer occurs in ligand (**58**) is decreased when compared with ligand (**57**). This is attributed to the ethylamine nitrogen adjacent to the anthracene substituent being substituted in ligand (**58**) but not in ligand (**57**). The steric bulk of the additional pendant arm may hinder the charge transfer between the phenyl rings and the anthracene substituent.

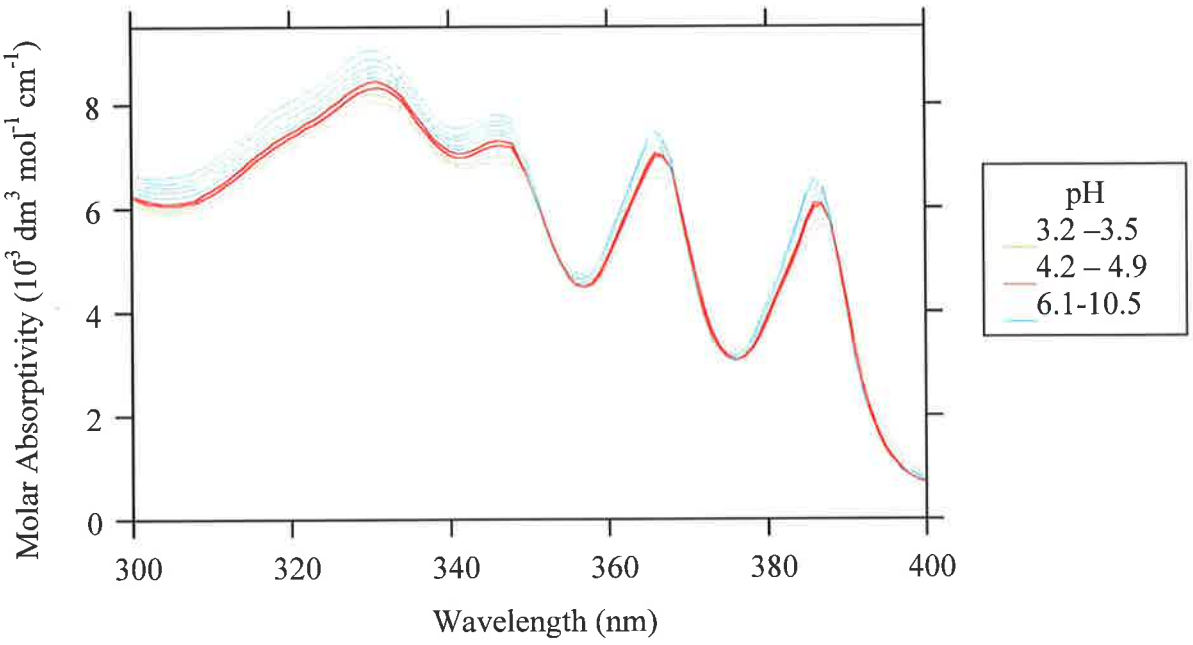

Figure 4.4. UV-visible absorption spectra for the titration of the protonated ligand (**58**) [8.6 x 10^{-5} mol dm^{-3}] against NEt_4OH in methanol/water (80:20; v/v) (I = 0.1 mol dm^{-3}, NEt_4ClO_4) at 298.2 K. $[H^+]_{total}$ = 1.1 x 10^{-3} mol dm^{-3}, $[NEt_4OH]_{total}$ = [0, 4.3 x 10^{-4}, 5.2 x 10^{-4}, 6.1 x 10^{-4}, 7.0 x 10^{-4}, 7.9 x 10^{-4}, 8.8 x 10^{-4}, 9.7 x 10^{-4}, 1.1 x 10^{-3} mol dm^{-3}] in ascending order of molar absorptivity and the corresponding pH values; 3.2, 3.5, 4.2, 4.9, 6.1, 7.3, 8.1, 9.1, 10.5.

A slight hypsochromic shift on titration with NEt_4OH was observed for the absorption spectra of ligand (**58**). This indicates that on deprotonation there is a decrease in electron delocalisation within this ligand. The change in the absorption pattern for the solutions, at which the individual spectra in the montage were measured, was in agreement with the mono to penta protonated species present, and hence also with the pK_a values obtained from the potentiometric titrations (see section **3.1.2**). The largest change in molar absorptivity occurs above pH 4.2. By comparing the change in molar absorptivity in **Figure 4.4** with the speciation plot and the various protonated species in **Figure 4.5**, the change in molar absorptivity above pH 4.2 is observed to coincide with the first deprotonations of ligand (**58**), (LH_4^{4+}, pK_{a4} 4.90 and LH_5^{5+}, pK_{a5} 4.51).

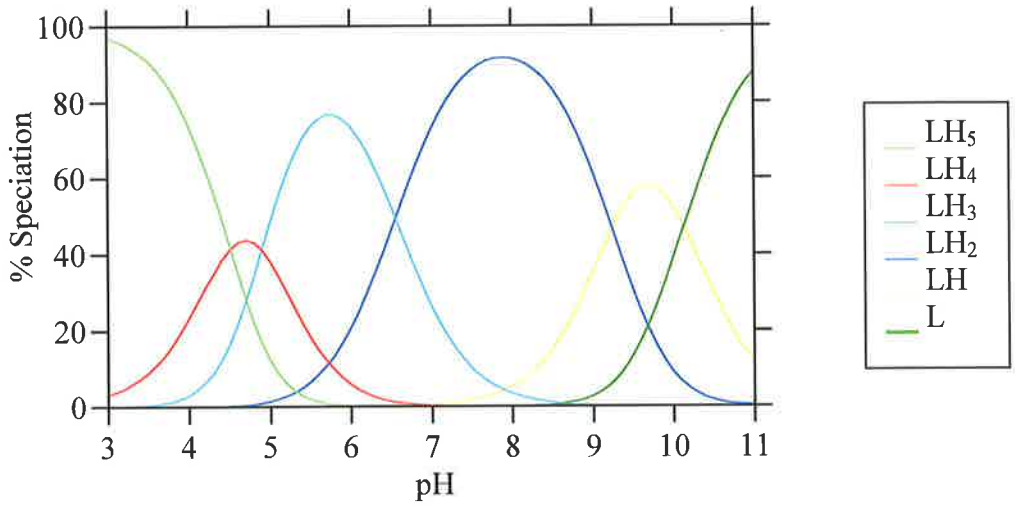

Figure 4.5 Speciation variation of ligand (**58**) showing the species present in methanol/water (80:20; v/v) at various pH (solid lines, —) in which $[\mathbf{58}]_{total} = 8.6 \times 10^{-5}$ mol dm^{-3}; where L = ligand (**58**) and speciation is shown relative to the total concentration of ligand (**58**).

The absorption spectra for the titration of the protonated hydroxyethyl pendant arm ligand (**62**) with NEt_4OH are shown in **Figure 4.6**. The absorption spectrum of the protonated ligand (**62**) at pH 2.8 displayed four bands at 388, 369, 351.5 and 337 nm. The absorption spectra for ligand (**62**) lacks the charge transfer band at around 330 nm, which was observed in the spectra of ligands (**57**) and (**58**). This is as a consequence of the absence of phenyl rings in the pendant arms of ligand (**62**), which minimises the opportunity for charge transfer. The absence of the charge transfer band allows the influence of pH on all four absorption bands of ligand (**62**) to be observed more clearly. The changes in absorption patterns, for the individual spectra in the montage, were in accordance with the variety of protonated species present, and hence also with the pK_a values obtained from the potentiometric titrations (see section **3.1.2**). Above pH 3.4 the absorption spectra underwent a significant change. This coincides with the second deprotonation of ligand (**62**) (LH_4^{4+}, pK_a 4.83) (**Figure 4.7**).

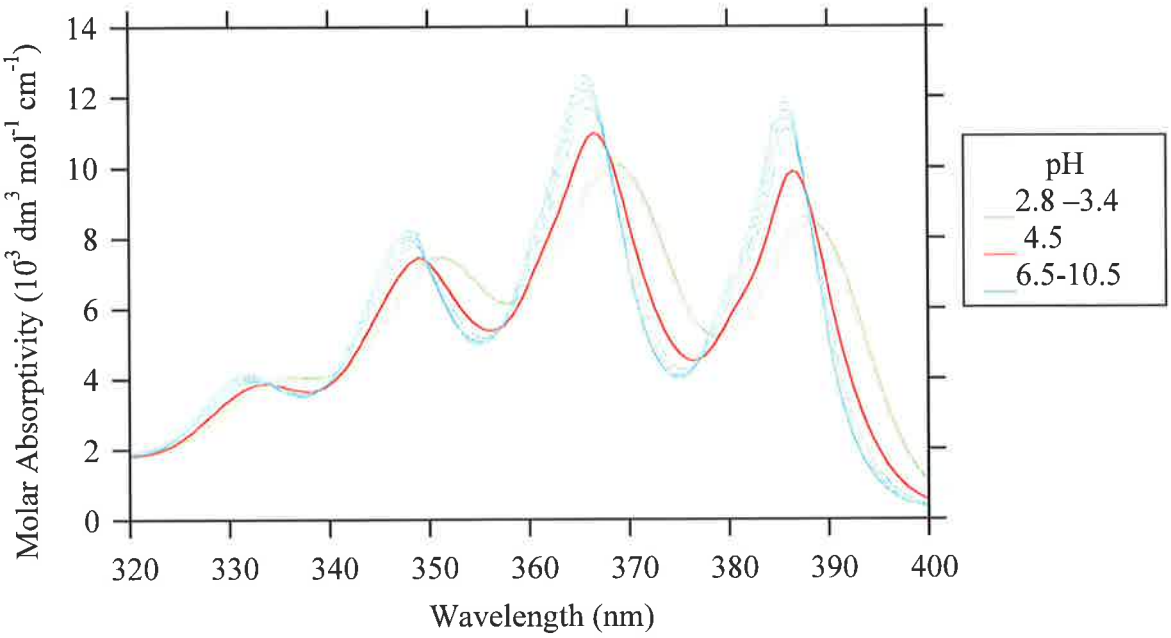

Figure 4.6. UV-visible absorption spectra for the titration of the protonated ligand (**62**) [1.2 x 10^{-4} mol dm^{-3}] against NEt_4OH in methanol/water (80:20; v/v) (I = 0.1 mol dm^{-3}, NEt_4ClO_4) at 298.2 K. $[H^+]_{total}$ = 1.8 x 10^{-3} mol dm^{-3}, $[NEt_4OH]_{total}$ = [0, 2.4 x 10^{-4}, 9.6 x 10^{-4}, 1.3 x 10^{-3}, 1.4 x 10^{-3}, 1.6 x 10^{-3}, 1.7 x 10^{-3}, 1.8 x 10^{-3}, 1.9 x 10^{-3}] in ascending order of molar absorptivity and the corresponding pH values; 2.8, 3.1, 3.4, 4.5, 6.5, 7.4, 9.1, 10.1, 10.5.

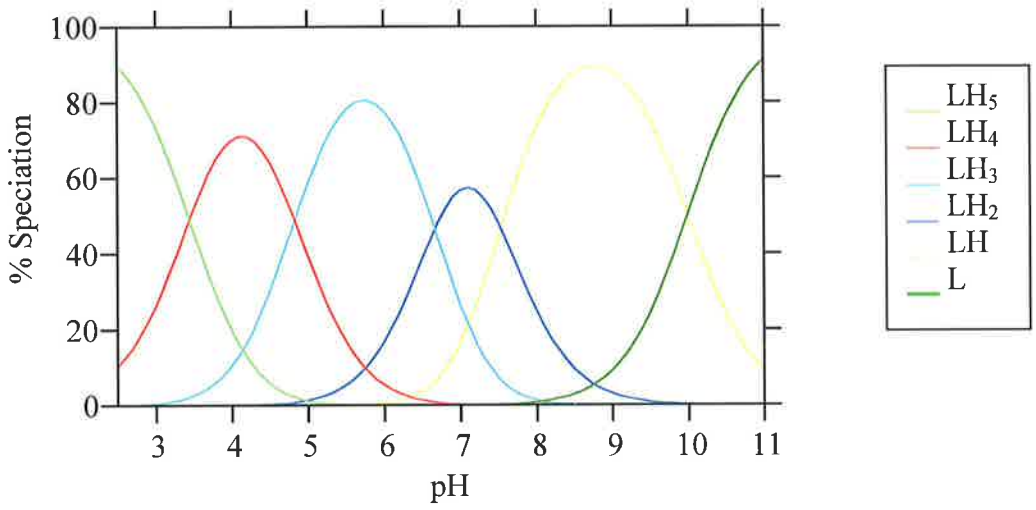

Figure 4.7 Speciation variation of ligand (**62**) showing the species present in methanol/water (80:20; v/v) at various pH (solid lines, —) in which $[\mathbf{62}]_{total}$ = 1.2 x 10^{-4} mol dm^{-3}; where L = ligand (**62**) and speciation is shown relative to the total concentration of ligand (**62**).

Table 4.1 The UV-visible absorption maximum wavelength and molar absorptivity (ε) values for ligands (**57**), (**58**) and (**62**) at indicated pH in methanol/water (80:20; v/v), (I = 0.1 mol dm^{-3}, NEt_4ClO_4) at 298.2 K

Ligand	Maximum wavelength (nm) (ε (10^{-4} mol dm^{-3}))
(**57**) at pH 3.3	389 (0.57) 368 (0.9) 325 (4.6)
(**57**) at pH 10.1	388 (0.79) 365 (1.2) 326 (5.5)
(**58**) at pH 3.2	387 (5.3) 368 (6.3) 346 (6.5) 331 (7.6)
(**58**) at pH 10.5	386 (6.6) 366 (7.5) 346 (5.8) 331 (9.0)
(**62**) at pH 2.8	388 (8.4) 369 (10.0) 351.5 (7.4) 337 (4.0)
(**62**) at pH 10.5	385.5 (11.8) 365.5 (12.6) 348 (8.2) 332 (4.1)

4.2.2 Fluorescence pH titrations for ligands (57), (58) and (62)

To observe the influence of pH on the fluorescence of ligands (**57**), (**58**) and (**62**), a dilute solution of the protonated ligand in a methanol/water solvent system (80:20; v/v), with constant ionic strength I = 0.1 mol dm^{-3} (NEt_4ClO_4), was titrated against a solution of NEt_4OH. The fluorescence measurements were over the range of 377-550 nm.

There are two options for determining the wavelength for excitation; (a) at the wavelength where the species of interest has the maximum molar absorbance, and (b) when the species present exhibit an isosbestic point, or identical molar absorbances. Due to the varied types of absorption spectra observed, the excitation wavelength was chosen from the second longest wavelength band at 368 nm.

The fluorescence spectra obtained for ligand (**57**) are shown in **Figure 4.8,** and are characteristic of a 9-substituted anthracene derivative.[2,12] Three emission maxima bands and a small shoulder were observed; the spectra underwent a small hypsochromic shift on titration of the protonated ligand (**57**) with NEt_4OH

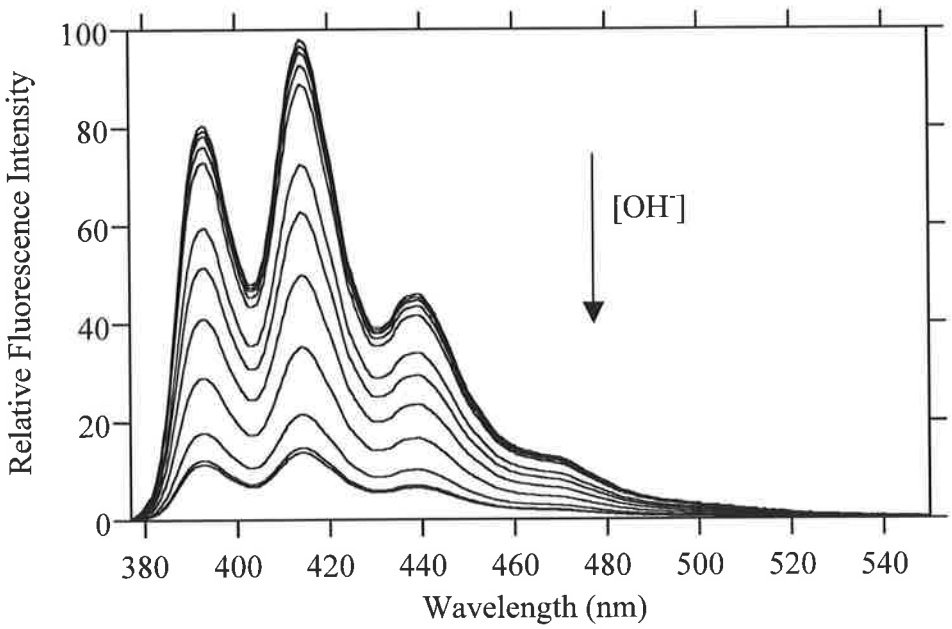

Figure 4.8. Fluorescence spectra for the titration of the protonated ligand (**57**) [3.3 x 10^{-5} mol dm^{-3}] against NEt_4OH in methanol/water (80:20; v/v) (I = 0.1 mol dm^{-3}, NEt_4ClO_4) at 298.2 K when excited at 368 nm. $[H^+]_{total}$ = 4.6 x 10^{-4} mol dm^{-3}, $[NEt_4OH]_{total}$ = [0, 1.7 x 10^{-4}, 2.6 x 10^{-4}, 3.6 x 10^{-4}, 3.7 x 10^{-4}, 3.8 x 10^{-4}, 3.9 x 10^{-4}, 4.0 x 10^{-4}, 4.2 x 10^{-4}, 4.4 x 10^{-4}, 4.5 x 10^{-4}, 4.7 x 10^{-4} mol dm^{-3}] in descending order of fluorescence intensity and the corresponding pH values; 3.3, 3.4, 3.9, 4.2, 4.7, 5.1, 5.7, 6.4, 7.3, 8.2, 9.1, 10.1.

In a PET type system, when the amine group involved in the transfer of electrons is protonated, the lone pair is not available to quench the fluorescence of the fluorophore. Only when the amine is deprotonated does the lone pair of electrons become available and fluorescence is quenched.[6-10] From **Figure 4.8** it can be observed that the highest fluorescence intensity corresponds with the fully protonated ligand (**57**). This indicates that the PET process is completely inhibited by protonation. The fluorescence of the anthracene substituent is then slowly quenched on titration with NEt_4OH, as ligand (**57**) is sequentially deprotonated. The change in fluorescence of ligand (**57**) as a function of pH is depicted in **Figure 4.9**.

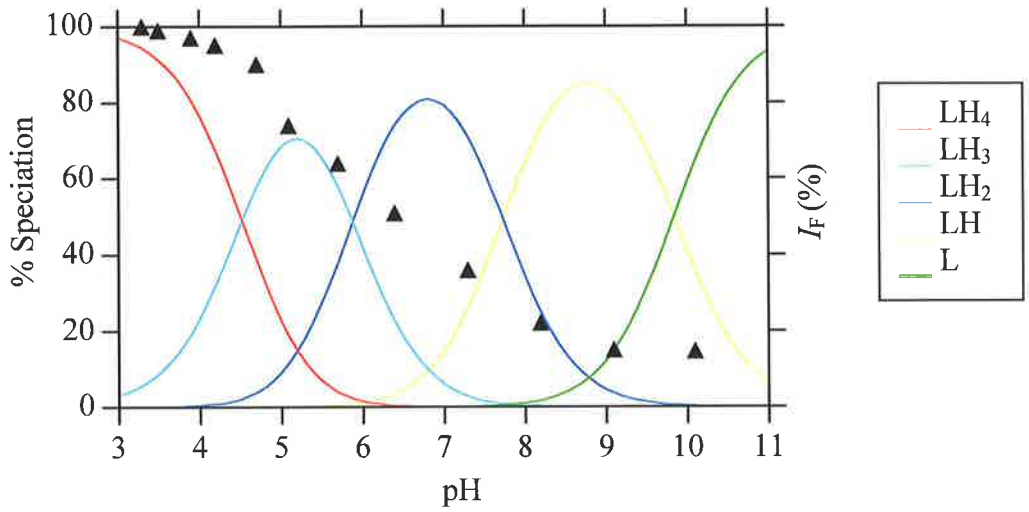

Figure 4.9 Left vertical axis; speciation variation of ligand (**57**) showing the species present in methanol/water (80:20; v/v) at various pH (solid lines, —) in which $[\mathbf{57}]_{total}$ = 3.3 x 10^{-5} mol dm^{-3}; Right vertical axis; dependence of the fluorescence intensity (I_F (%)) of the solution as a function of pH (black triangles, ▲); where L = ligand (**57**) and speciation is shown relative to the total concentration of ligand (**57**).

For ligand (**57**) the change in the intensity of the fluorescence is dominated by the relative proportions of $[LH_4]^{4+}$ and $[LH_3]^{3+}$, with a minor part played by LH_2, LH and L. Ligand (**57**) remained fluorescent even when fully deprotonated; this indicates that the fluorescence of the ligand is not fully quenched through PET.

There was a similar trend in the fluorescence spectra for the protonated ligand (**58**) on titration with NEt_4OH (**Figure 4.10**), as that observed for ligand (**57**). Fluorescence quenching occurred for ligand (**58**) on increasing pH. The fluorescence spectra obtained show three emission maxima bands and a small shoulder, which underwent small hypsochromic shifts on titration of the protonated ligand (**58**) with NEt_4OH.

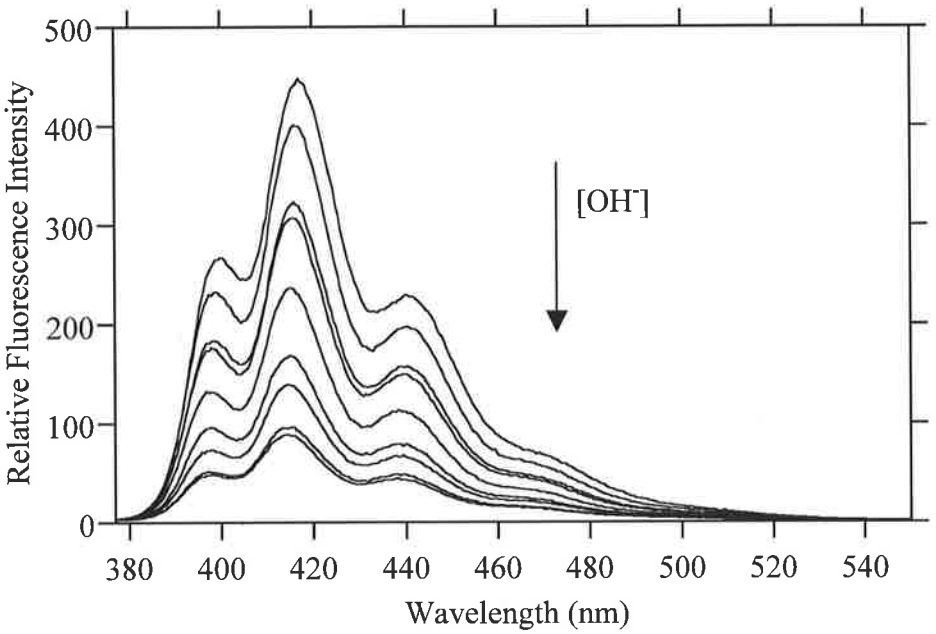

Figure 4.10. Fluorescence spectra for the titration of the protonated ligand (**58**) [8.6 x 10^{-5} mol dm^{-3}] against NEt_4OH in methanol/water (80:20; v/v) (I = 0.1 mol dm^{-3}, NEt_4ClO_4) at 298.2 K when excited at 368 nm. $[H^+]_{total}$ = 1.1 x 10^{-3} mol dm^{-3}, $[NEt_4OH]_{total}$ = [0, 4.3 x 10^{-4}, 5.2 x 10^{-4}, 6.1 x 10^{-4}, 7.0 x 10^{-4}, 7.9 x 10^{-4}, 8.8 x 10^{-4}, 9.7 x 10^{-4}, 1.1 x 10^{-3} mol dm^{-3}] in descending order of fluorescence intensity and the corresponding pH values; 3.2, 3.5, 4.2, 4.9, 6.1, 7.3, 8.1, 9.1, 10.5.

The change to the intensity of the fluorescence for ligand (**58**) is dominated by the relative proportions of $[LH_5]^{5+}$ and $[LH_4]^{4+}$, with a minor part played by LH_3, LH_2, LH and L. The change in fluorescence as a function of pH is depicted in **Figure 4.11**. The deprotonated ligand (**58**) remained fluorescent, which indicates that the fluorescence of the ligand was not fully quenched by PET; ligand (**57**) exhibited a similar behaviour. A small amount of quenching was observed under strongly acidic conditions for ligand (**58**). This type of quenching has been reported previously in other anthracene conjugated macrocycles. This has been attributed to both, protonation of the anthracene substituent, as well as an acid-catalysed photochemically induced decomposition.[14,15]

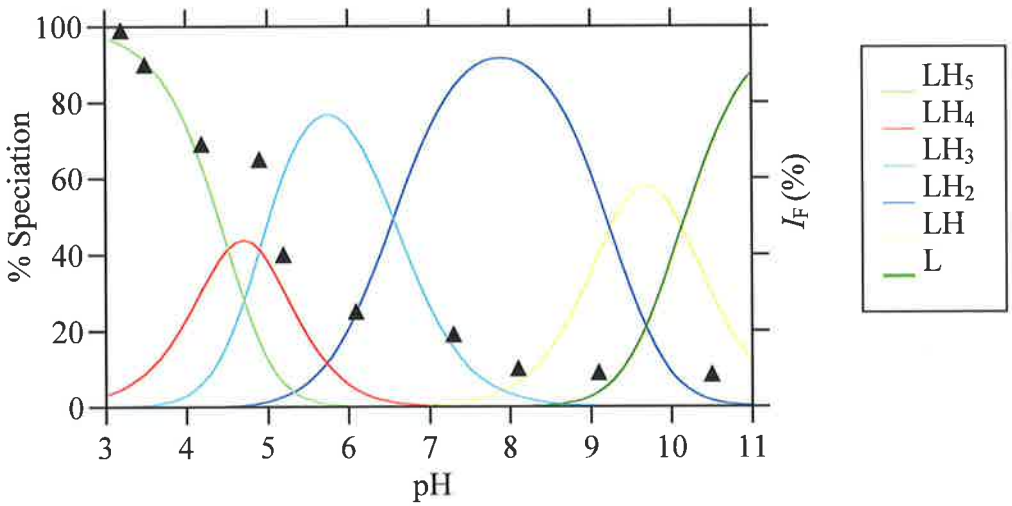

Figure 4.11 Left vertical axis; speciation variation of ligand (**58**) showing the species present in methanol/water (80:20; v/v) at various pH (solid lines, —) in which $[\mathbf{58}]_{total}$ = 8.6 x 10^{-5} mol dm^{-3}; Right vertical axis; dependence of the fluorescence intensity (I_F (%)) of the solution as a function of pH (black triangles, ▲); where L = ligand (**58**) and speciation is shown relative to the total concentration of ligand (**58**).

The fluorescence intensity of the solutions decreased markedly with the first deprotonation of LH_4^{4+} (pK_{a4} 4.52) for ligand (**57**), consistent with the deprotonation being that of the $-NH_2^+$- amine adjacent to the anthracene substituent. For ligand (**58**) the first two deprotonations are characterised by similar pK_as (pK_{a4} 4.90 and pK_{a5} 4.51), and therefore it is not obvious which deprotonation is having the greater effect on fluorescence. However, it is probable that deprotonation of the $-^+HNR^s$- group adjacent to the anthracene substituent, will have the greatest effect, and that this is characterised by the first or second pK_a.

The fluorescence spectra obtained from the titration of the protonated ligand (**62**) with NEt_4OH were also characteristic of an anthracene substituted ligand involving a PET mechanism; fluorescence quenching was observed on ligand deprotonation (**Figure 4.12**).

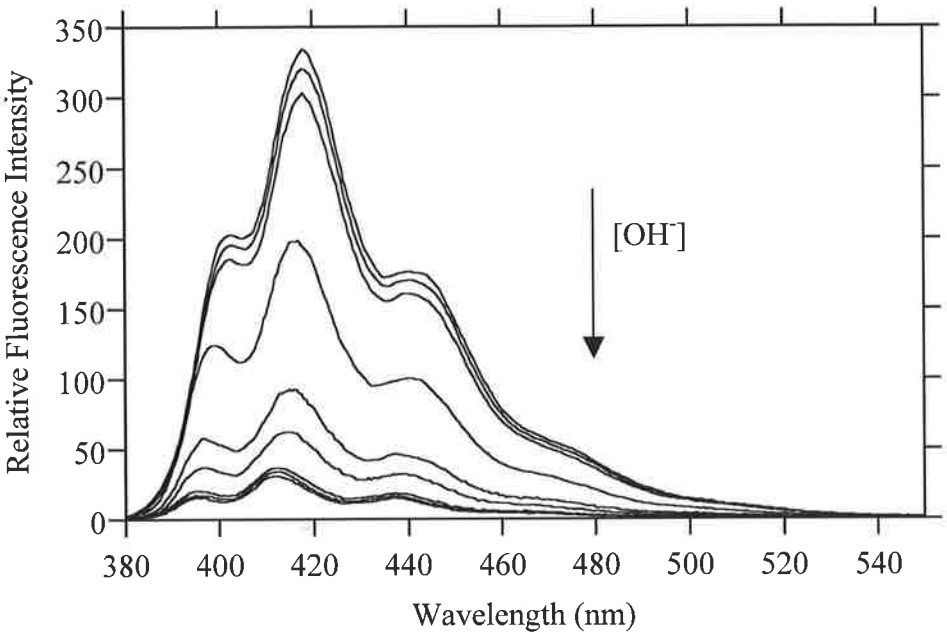

Figure 4.12. Fluorescence spectra for the titration of the protonated ligand (**62**) [1.2 x 10^{-4} mol dm^{-3}] against NEt_4OH in methanol/water (80:20; v/v) (I = 0.1 mol dm^{-3}, NEt_4ClO_4) at 298.2 K when excited at 368 nm. $[H^+]_{total}$ = 1.8 x 10^{-3} mol dm^{-3}, $[NEt_4OH]_{total}$ = [0, 2.4 x 10^{-4}, 9.6 x 10^{-4}, 1.3 x 10^{-3}, 1.4 x 10^{-3}, 1.6 x 10^{-3}, 1.7 x 10^{-3}, 1.8 x 10^{-3}, 1.9 x 10^{-3} mol dm^{-3}] in descending order of fluorescence intensity and the corresponding pH values; 2.8, 3.1, 3.4, 4.5, 6.5, 7.4, 9.1, 10.1, 10.5.

The intensity of the fluorescence for ligand (**62**) is dominated by the relative proportions of $[LH_5]^{5+}$ and $[LH_4]^{4+}$, with a minor part played by LH_3, LH_2, LH and L. No change in fluorescence intensity for ligand (**62**) was observed above pH 10.5. The change in fluorescence as a function of pH is depicted in **Figure 4.13**. The fluorescence spectra of ligand (**62**) were observed to undergo a slight hypsochromic shift on increasing pH. The fluorescence intensity of the solutions decreased markedly with the second deprotonation of LH_4^{4+} (pK_{a4} 4.83) for ligand (**62**), and was consistent with the deprotonation being that of the $-^+HNR^s-$ amine adjacent to the anthracene substituent.

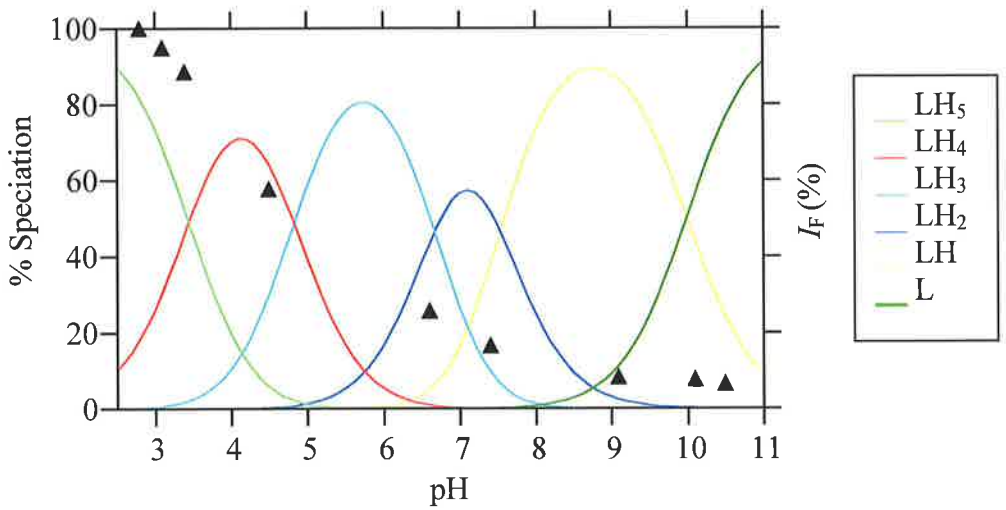

Figure 4.13 Left vertical axis; speciation variation of ligand (**62**) showing the species present in methanol/water (80:20; v/v) at various pH (solid lines, —) in which $[\mathbf{62}]_{total}$ = 1.2 x 10^{-4} mol dm^{-3}; Right vertical axis; dependence of the fluorescence intensity (I_F (%)) of the solution as a function of pH (black triangles, ▲); where L = ligand (**62**) and speciation is shown relative to the total concentration of ligand (**62**).

Table 4.2. Fluorescence values for emission maxima wavelength and the quantum yields for ligands (**57**), (**58**) and (**62**), at indicated pH in methanol/water (80:20, v/v), (I = 0.1 mol dm^{-3}, NEt_4ClO_4) at 298.2 K

	Emission Maxima (nm) (Quantum Yields)
Ligand (**57**) at pH 3.3	396.5, 418.5, 440, 474 (Φ_F 0.53)
Ligand (**57**) at pH 10.1	391.5, 414.5, 437.5, 471 (Φ_F 0.08)
Ligand (**58**) at pH 3.2	400.5, 417, 440.5, 469 (Φ_F 0.76)
Ligand (**58**) at pH 10.5	398, 414.5, 438, 468 (Φ_F 0.07)
Ligand (**62**) at pH 2.8	402.5, 418, 440.5, 480 (Φ_F 0.23)
Ligand (**62**) at pH 10.5	397, 412, 437, 478 (Φ_F 0.01)

4.3 Metal ion complexation studies

When designing fluorescent sensors as metal ion receptors, investigation into the influence that metal ion complexation has on fluorescence is vital for sensor evaluation. In this study a variety of metal ions were investigated for their influence on both the UV-visible absorption as well as the fluorescence properties of ligands (**57**), (**58**) and (**62**).

Due to the borderline hard acid behaviour of many of the metal ions to be evaluated for complexation, and the possible subsequent formation of metal hydroxy species,[16] the measurements were carried out in buffered solutions to help maintain a constant pH. There are numerous factors, which must be considered when choosing a buffer for metal ion complexation studies. Firstly, the buffer must not show any significant complexation with the metal ions of interest. Secondly, it is important that both the ligand and the chosen metal ions are soluble at the buffered pH. Thirdly, due to the manner in which PET works, it is advantageous for the pH of the solution to be above the pK_a of the protonated primary electron donor atom involved in PET; in the case of the ligands studied, this is the ethylamine nitrogen adjacent to the anthracene substituent. This ensures that any observed change to absorption or fluorescence is caused by metal ion complexation, and not by protonation of the primary electron donor. Fourthly, it is desirable that there be only one absorbing or emitting species present in the solution. This is generally the metal complex ion, LM.

The buffer systems for these studies were chosen in accordance with the above specifications. The speciation plots derived from the potentiometric titration of ligands (**57**) (**Figures 3.16** and **A.9**), (**58**) (**Figures 3.17** and **A.10**) and (**62**) (**Figure 4.7**), were used to determine the pH at which the metal complex ion LM was predominant, and the ethylamine nitrogen adjacent to the anthracene substituent was deprotonated. Unfortunately, in the case of ligands (**57**) and (**58**), the formation of the metal complex ion LM as the major species, coincided with precipitation in the potentiometric titrations. For ligand (**57**) the formation of the metal complex ion LM as the major species with Cu^{2+} and Cd^{2+}, occurs at pH 6.9 and 7.6, respectively. For ligand (**58**) the formation of the metal complex ion LM as the major species with Cu^{2+} and Cd^{2+}, occurs at pH 6.4 and 8.0, respectively. To ensure complete dissolution of ligands (**57**) and (**58**) whilst minimising the influence from the protonated ethylamine nitrogen adjacent to the anthracene substituent, (the primary electron donor involved in the PET process) the pH of the

buffered solutions was maintained at pH 5.6 by the buffer 4-morpholineethanesulfonic acid (MES). For both ligands (**57**) and (**58**), the major species present at this pH was the mono-protonated metal complex ion, $M(LH)^{3+}$.

Potentiometric titration of ligand (**62**) with metal ions was not possible due to the formation of precipitates at pH 4. Potentiometric titrations are carried out at much higher concentrations than photophysical measurements; thus problems normally associated with precipitate formation are often insignificant in photophysical measurements. Precipitation, however, was still observed for ligand (**62**) on addition of metal ions above pH 5. Below pH 5, precipitation was not observed; hence the pH of the buffered solutions was maintained at pH 4 by an acetic acid/acetate buffer. The pH at which measurements were feasible for ligand (**62**) coincided with the pK_a value assigned to the protonated ethylamine nitrogen adjacent to the anthracene substituent (LH_4^{4+}, pK_{a4} 4.83). Therefore for these solutions, the partially protonated amine would be expected to affect fluorescence spectra. The alternative to buffering the solutions at this pH was to filter the solutions containing the precipitate, prior to measurement. This, however, is undesirable because the concentrations of the species present in solution then become unknown.

4.3.1 UV-visible absorption properties in the presence of metal ions for ligands (57) and (58)

For ligands (**57**) and (**58**), the buffer system MES was chosen to maintain the pH of the solutions in the solvent system. The UV-visible measurements were carried out in a methanol/water solvent system (80:20; v/v), with constant ionic strength I = 0.1 mol dm^{-3} (NEt_4ClO_4), at pH 5.6 (MES buffer). The measurements were over the range of 300-450 nm.

Four metal ions (Zn^{2+}, Cd^{2+}, Cu^{2+} and Ca^{2+}) were investigated for their effect on the UV-visible absorption of ligands (**57**) and (**58**). The absorption spectra obtained for ligands (**57**) and (**58**) were characteristic of 9-substituted anthracene derivatives; the spectra obtained displayed four absorption bands and a small shoulder.[12] The absorption spectrum for ligand (**57**) alone shows four absorption bands at 387, 368, 349, 333 nm and a small shoulder at 319 nm (**Figure 4.14**). The absorption spectra observed for the buffered ligand (**57**) are different from those observed for the solutions in section **4.2.1**. This

indicates that the MES buffer, has an effect on the absorption of the ligand. This is attributed to the pH at which measurements were feasible, namely pH 5.6. At this pH, ligand (**57**) exists in a charged state, allowing for ion pairing interactions with the buffer, 4-morpholineethanesulfonic acid. This affects the absorbance of the ligand. Fortunately, the fluorescence spectra of ligand (**57**) were unaffected by the buffer; no change to the fluorescence spectra was observed between the buffered and unbuffered solutions.

The addition of Cu^{2+} to solutions containing ligand (**57**) had an effect on the absorption spectra; the absorption bands underwent hypsochromic shifts to 386, 367, 348, 332 and 319 nm (**Appendix, Figure A.11**). The absorption spectra obtained for Cu^{2+} complexation with ligand (**57**) show a large increase in molar absorptivity below 348 nm. The large increase is due to the nature of Cu^{2+}, which is capable of charge transfer processes, thus causing a ligand to metal electron transfer. In transitions like this the electrons move large distances, often resulting in large dipole moments, which give rise to intense absorption bands.[3] The shift in wavelength is due to the change in electron delocalisation on Cu^{2+} complexation, because the excited state becomes metal ion centred.[17] The formation of Cd^{2+} and Zn^{2+} complexes with ligand (**57**) had only a small effect on the absorption spectrum of the ligand (**Appendix, Figures A.12** and **A.13**). A slight increase in molar absorptivity accompanied by a small hypsochromic shift in the absorption maxima bands was observed. The influence of the complexation of ligand (**57**) by Ca^{2+} was negligible. The resultant spectra for ligand (**57**) alone, and in the presence of Zn^{2+}, Cd^{2+} and Cu^{2+} are shown in **Figure 4.14**.

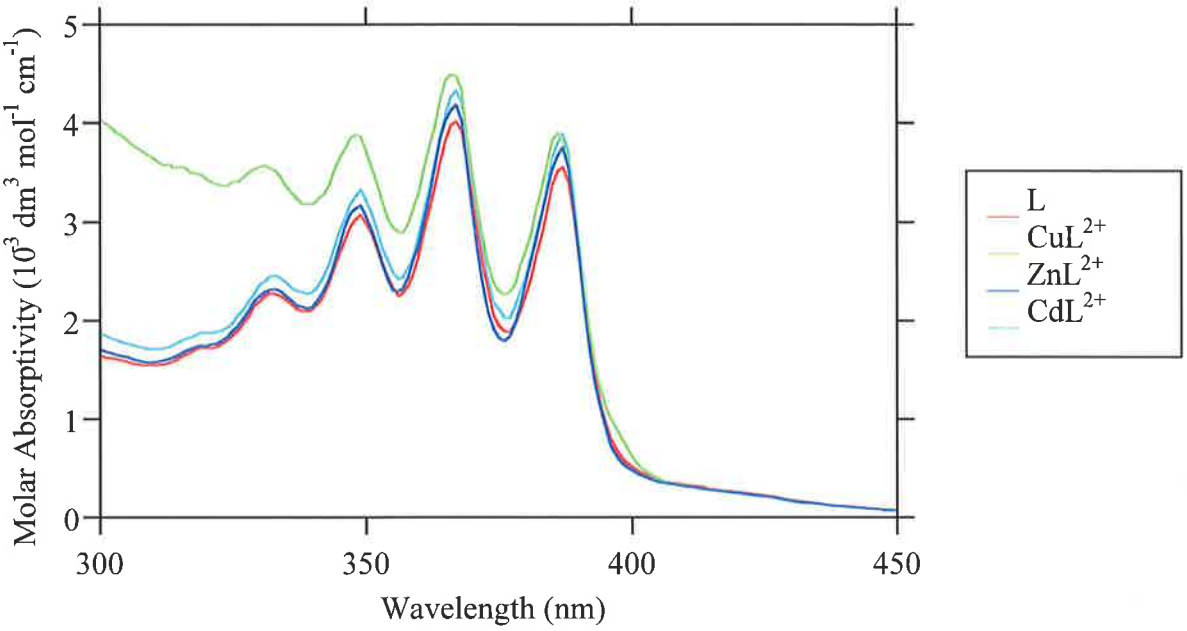

Figure 4.14. UV-visible absorption spectra of ligand (**57**) alone [4.1 x 10^{-5} mol dm^{-3}], and in the presence of Cu^{2+} [8.3 x 10^{-5} mol dm^{-3}], Zn^{2+} [8.3 x 10^{-5} mol dm^{-3}], or Cd^{2+} [8.3 x 10^{-5} mol dm^{-3}] at pH 5.6 (MES buffer) in methanol/water (80:20; v/v) (I = 0.1 mol dm^{-3}, $NEt_4(ClO_4)_2$) at 298.2 K, where L = ligand (**57**).

The UV-visible absorption spectrum of ligand (**58**) in an MES buffered solution displayed four absorption bands at 387, 368, 349, 333 nm and a shoulder at 319 nm (**Figure 4.15**). Similarly to ligand (**57**), the spectra obtained for the free ligand (**58**) in buffered solutions are different from those obtained in unbuffered solutions (see section **4.2.1**). This indicates that the MES buffer, also has an effect on the absorption of ligand (**58**). The change in absorption spectra between the buffered and unbuffered solutions is attributed to the pH at which measurements were feasible. At pH 5.6, ligand (**58**) exists in a charged state, which allows for ion pairing interactions with the buffer (MES), and consequently affects the absorption of the ligand. No changes to the fluorescence spectra of ligand (**58**) were observed between the buffered and unbuffered solutions. This indicates that the buffer has no influence on the fluorescence of ligand (**58**).

Upon addition of Cu^{2+} to solutions of ligand (**58**), significant changes to the absorption spectra were observed (**Appendix, Figure A.14**). The absorption bands underwent hypsochromic shifts to 386, 366, 348 and 331 nm and the shoulder to 316 nm. A decrease in molar absorptivity for the absorption bands above 348 nm was observed. For the absorption bands at shorter wavelengths, molar absorptivity was increased. The change in absorption pattern on complexation of Cu^{2+} by ligand (**58**) can be attributed to a

charge transfer transition from the ligand to the metal ion and the resultant dipole moments.[17]

Zinc(II) and Cd^{2+} did not have a significant influence on the absorption spectrum of ligand (**58**). Only a small increase in molar absorptivity occurred on metal ion complexation (**Appendix, Figures A.15** and **A.16**). This indicates that Zn^{2+} and Cd^{2+} have only a limited effect on the manner by which ligand (**58**) absorbs light. No spectral change was observed on titration of ligand (**58**) with Ca^{2+}.

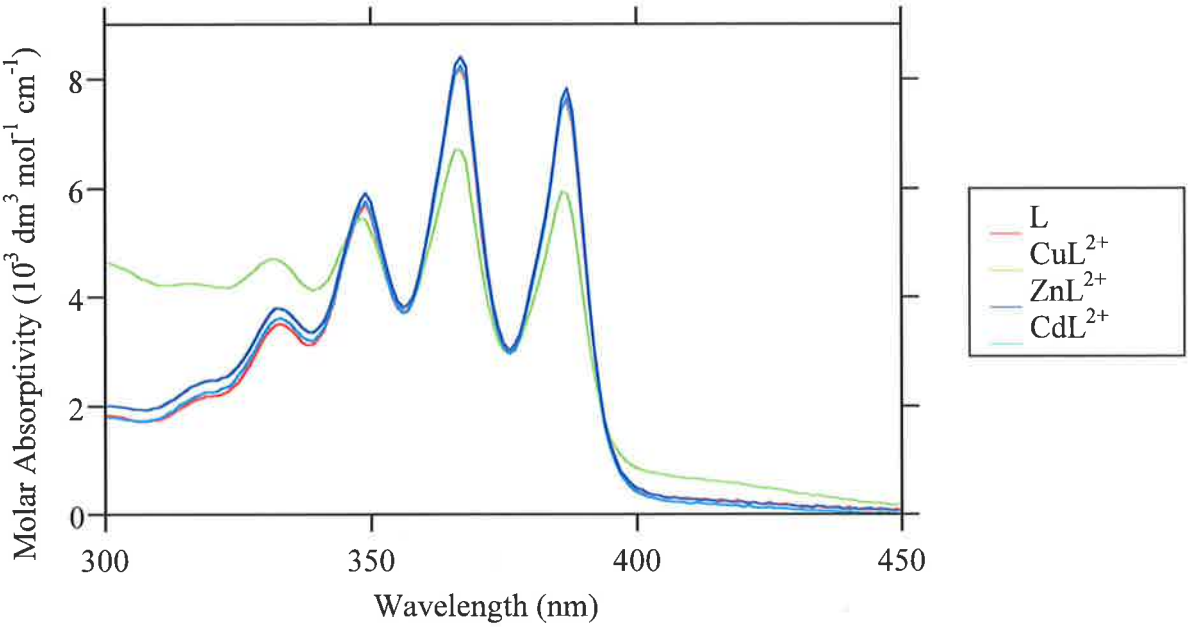

Figure 4.15. UV-visible absorption spectra of ligand (**58**) alone [4.7 x 10^{-5} mol dm^{-3}], and in the presence of Cu^{2+} [9.4 x 10^{-5} mol dm^{-3}], Zn^{2+} [9.4 x 10^{-5} mol dm^{-3}], or Cd^{2+} [9.4 x 10^{-5} mol dm^{-3}] at pH 5.6 (MES buffer) in methanol/water (80:20; v/v) (I = 0.1 mol dm^{-3}, NEt_4ClO_4) at 298.2 K, where L = ligand (**58**).

4.3.2 UV-visible absorption properties in the presence of metal ions for ligand (62)

For ligand (**62**), the buffer system of acetic acid/acetate was chosen to maintain the pH at 4.0 in the solvent system. The UV-visible measurements were carried out in a methanol/water solvent system (80:20; v/v), with constant ionic strength I = 0.1 mol dm^{-3} (NEt_4ClO_4). The measurements were over the range of 300-450 nm. Four metal ions (Zn^{2+}, Cd^{2+}, Cu^{2+} and Ca^{2+}) were investigated for their influence on the UV-visible absorption properties of ligand (**62**). Ligand (**62**) alone was found to have four absorption

bands at 386, 368, 349, 334 nm and a shoulder at 319 nm. The influence on the absorption spectra of ligand (**62**) upon addition of either Cd^{2+} or Ca^{2+} was negligible. However a slight increase in molar absorptivity on addition of Zn^{2+} was observed (**Appendix, Figure A.17**). The absorption spectra of ligand (**62**) underwent the largest change on addition of Cu^{2+} (**Appendix, Figure A.18**); a large increase in molar absorptivity occurred around 331 nm. This increase coincides with the area attributed to charge transfer between the ligand and the metal ion. The resultant absorption spectra for ligand (**62**) alone, and with Zn^{2+}, and Cu^{2+} are shown in **Figure 4.16**. The absorption bands for ligand (**62**) underwent hypsochromic shifts on formation of metal complex ions with Zn^{2+} and Cu^{2+}.

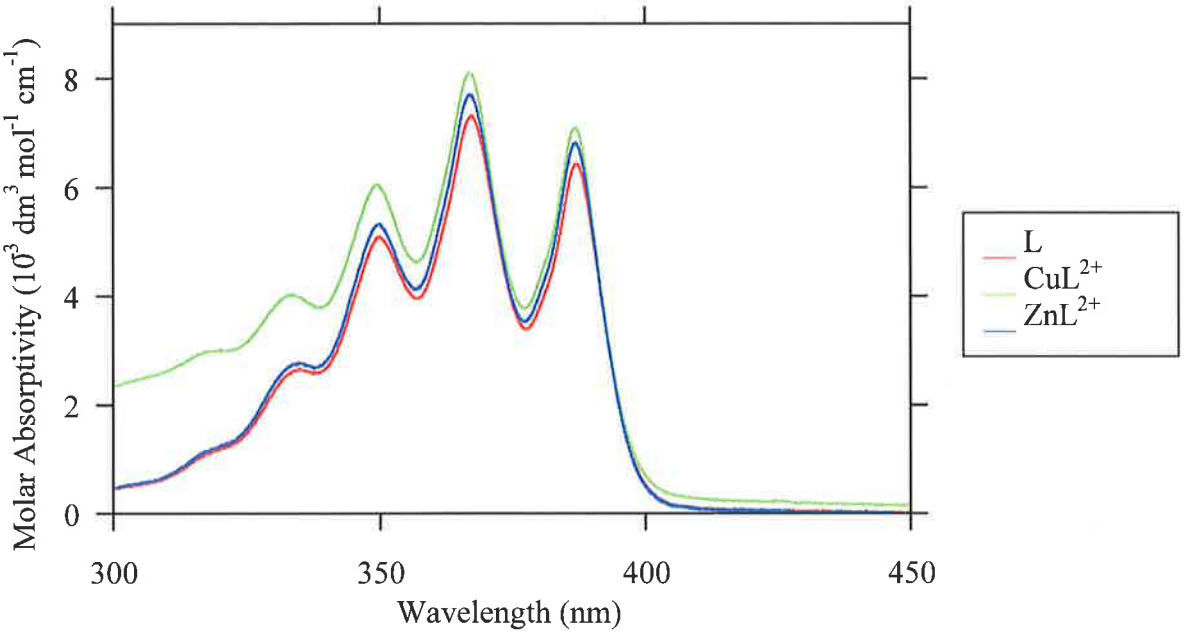

Figure 4.16. UV-visible absorption spectra of ligand (**62**) alone [5.5 x 10^{-5} mol dm^{-3}], and in the presence of Cu^{2+} [1.11 x 10^{-4} mol dm^{-3}], or Zn^{2+} [1.11 x 10^{-4} mol dm^{-3}] at pH 4.0 (acetate buffer) in methanol/water (80:20; v/v) (I = 0.1 mol dm^{-3}, NEt_4ClO_4) at 298.2 K, where L = ligand (**62**).

The wavelengths of the absorption bands for all three ligands, (**57**), (**58**) and (**62**), underwent hypsochromic shifts on metal ion complexation. Shifts of this nature have been associated with the participation of nitrogen lone pairs in metal ion coordination.[18] The UV-visible absorption spectra of ligands (**57**), (**58**) and (**62**), on addition of the various metal ions resulted in little or no spectral change. The ligands are designed as PET based fluorescent sensors so that these results are not unexpected or undesirable; fluorescence quenching only affects the excited state. The UV-visible maximum wavelength and molar absorptivity (ε) values are given in **Table 4.3**.

Table 4.3 The UV-visible absorption maximum wavelength and molar absorptivity (ε) values for ligands, (**57**), (**58**) and (**62**) alone, and in the presence of Cu^{2+}, Zn^{2+}, Cd^{2+} and Ca^{2+} in methanol/water (80/20; v/v), (I = 0.1 mol dm^{-3}, NEt_4ClO_4) at 298.2 K

	Maximum wavelength (nm)(ε (10^{-4} mol dm))
Ligand (**57**)	387 (3.55) 368 (4.01) 349 (3.07) 333 (2.27) 319 (1.72)
Cu(**57**)$^{2+}$	386 (3.90) 366 (4.49) 348 (3.88) 331 (3.57) 315 (3.55)
Zn(**57**)$^{2+}$	387 (3.75) 367 (4.18) 349 (3.16) 332 (2.31) 319 (1.74)
Cd(**57**)$^{2+}$	387 (3.89) 367 (4.32) 349 (3.32) 332 (2.45) 319 (1.87)
Ca(**57**)$^{2+}$	a
Ligand (**58**)	387 (7.59) 368 (8.18) 349 (5.69) 333 (3.51) 319 (2.17)
Cu(**58**)$^{2+}$	386 (5.92) 366 (6.71) 348 (5.44) 331 (4.70) 316 (3.55)
Zn(**58**)$^{2+}$	387 (7.83) 368 (8.40) 349 (5.90) 333 (3.79) 319 (2.43)
Cd(**58**)$^{2+}$	387 (7.65) 368 (8.24) 349 (5.70) 333 (3.62) 319 (2.24)
Ca(**58**)$^{2+}$	a
Ligand (**62**)	386 (6.41) 368 (7.21) 349 (5.07) 333 (2.68) 319 (1.12)
Cu(**62**)$^{2+}$	385 (6.82) 366 (8.10) 348 (6.02) 331 (3.94) 317 (3.09)
Zn(**62**)$^{2+}$	385 (7.09) 367 (7.82) 349 (5.32) 332 (2.75) 319 (1.13)
Cd(**62**)$^{2+}$	a
Ca(**62**)$^{2+}$	a

[a] Absorbance unchanged in the presence of metal ion.

4.4 Determination of metal complex ion stability constants by fluorescence spectroscopy

The ligands in this study, (**57**), (**58**) and (**62**), have been designed as fluorescent sensors which respond to PET. As mentioned previously, the PET process is hindered by protonation of the electron donor or by metal ion complexation; interruptions to the PET pathway restore fluorescence. To evaluate the ability of these ligands to act as sensors, studies into the influence that metal ions have on the PET process for each ligand are paramount. The determination of stability constants is often used to gain a better understanding of the factors controlling metal ion complexation. A variety of techniques can be used in the determination of metal complex ion stability constants. Potentiometric titrations have already been used in this study (see **Chapter 3**). There are, however, some limitations involved with potentiometric titrations. Firstly, large concentrations are required which can lead to problems with precipitates. Secondly, the technique is best suited to higher stability constants ($K \geq 100$ dm^3 mol^{-1}), which can lead to sensitivity issues. Potentiometric titrations are not the only method available for the determination of metal complex ion stability constants. NMR spectroscopy,[19-21] UV-visible absorption spectroscopy[22-25] and fluorescence spectroscopy can all be utilised.[26,27] The determination of metal complex ion stability constants by NMR spectroscopy was not a viable option for this study, due to the complicated ^{13}C and ^{1}H NMR spectra obtained for ligands (**57**), (**58**) and (**62**). In contrast to potentiometric titrations, fluorescence and UV-visible absorption measurements require only relatively small concentrations and they are both sensitive to small changes, especially in the case of fluorescence measurements. The ligands in this study, (**57**), (**58**) and (**62**), have been designed as fluorescent sensors so that larger changes would be expected for the fluorescence spectra when compared with the UV-visible absorption spectra. Therefore metal complex ion stability constants were determined with fluorescence spectroscopy.

The complexation of a ligand with a metal ion can be expressed as the equilibrium seen in Equation 4.3. Equation 4.4 represents the complexation of a second metal ion.

$$M^{n+} + L \underset{}{\overset{K_1}{\rightleftharpoons}} [ML]^{n+} \quad (4.3)$$

$$M^{n+} + [ML]^{n+} \underset{}{\overset{K_2}{\rightleftharpoons}} [M_2L]^{2n+} \quad (4.4)$$

where K_1 and K_2 represent the stepwise stability constants, as seen in Equations 4.5 and 4.6.

$$K_1 = \frac{[ML^{n+}]}{[M^{n+}]\,[L]} \quad (4.5)$$

$$K_2 = \frac{[M_2L^{2n+}]}{[M^{n+}][ML^{n+}]} \quad (4.6)$$

An overall stability constant, β_2, can also be derived which is the product of the stepwise formation constants of K_1 and K_2, as appears in Equations 4.7 and 4.8.

$$2\,M^{n+} + L \underset{}{\overset{\beta_2}{\rightleftharpoons}} [M_2L]^{2n+} \quad (4.7)$$

$$\beta_2 = \frac{[M_2L^{2n+}]}{[M^{n+}]^2[L]} = K_1.K_2 \quad (4.8)$$

A mole ratio method was used in the determination of metal complex ion stability constants by fluorescence spectroscopy. This involved varying the metal ion concentration relative to a constant ligand concentration.[26,28] Measurements at different metal ion concentration were performed incrementally until no further spectral change was observed, since this was assumed to coincide with completion of ligand metal ion complexation. The data obtained was fitted with a non-linear least-squares regression programme, DATAFIT/SPECFIT[29,30] which was run through MATLAB (see section **6.6**). Different stoichiometries can be tested by this method, as exemplified by the complexation of the metal complex ions to form 1:1 (ML) or 2:1 (M_2L) complexes. The programme also takes into account the ability of the theoretical data to fit well with the experimental data, in the form of the sum of the squared standard deviation (SSD). This is determined along with the metal complex ion stability constants for each complexation model. SPECFIT cannot

accurately fit data when $K \geq 10^7$ dm^3 mol^{-1}, because, at equilibrium, the ratio of the product metal complex ion concentration to those of it precursors, becomes very large. Therefore the minor error in the stability of the former constitutes a very large error in the latter, and so the overall error in the determined K becomes extremely large.

4.4.1 Fluorescence properties of ligands (57), (58) and (62) in the presence of metal ions

The influences of metal ion complexation on the fluorescence of ligands (**57**), (**58**) and (**62**), in the appropriate buffer system, are discussed in this section. The measurements for ligands (**57**) and (**58**) were determined in a methanol/water solvent system (80:20; v/v), with constant ionic strength I = 0.1 mol dm^{-3} (NEt_4ClO_4), at pH 5.6 (MES buffer). For ligand (**62**) measurements were determined in a methanol/water solvent system (80:20; v/v), with constant ionic strength I = 0.1 mol dm^{-3} (NEt_4ClO_4), at pH 4.0 (acetate buffer). The fluorescence measurements for all ligands were over the range of 377-550 nm.

4.4.2 Metal ion complexation by ligand (57)

As stated previously, typical fluorescence spectra for 9-substituted anthracene derivatives consist of three bands and a shoulder.[2,12] The fluorescence spectra for ligand (**57**) displayed this pattern, with emission maxima bands at 393, 414 and 438.5 nm and a small shoulder at 465.5 nm. Ligand (**57**) alone was fluorescent (Φ_F = 0.32, $\lambda_{excitation}$ 368 nm). The same range of metal ions (Zn^{2+}, Cd^{2+}, Cu^{2+} and Ca^{2+}) were investigated for their influence on the ligand's fluorescence as were used for the UV-visible absorption measurements (see section **4.3.1**). Complexation of ligand (**57**) by Ca^{2+} was found not to alter the fluorescence spectra significantly.

The spectrofluorimetric titration of ligand (**57**) with Cu^{2+} (ranging from 8.3 x 10^{-6} to 8.3 x 10^{-4} mol dm^{-3}) resulted in ligand fluorescence quenching (Φ_F = 0.05) (**Figure 4.17**). This was expected, because Cu^{2+} is normally associated with fluorescence quenching. Such behaviour is typical of d^9 Cu^{2+}, and is due to the charge transfer transitions between the ligand and Cu^{2+}.[31] This is consistent with the charge transfer band obtained in the absorption spectra for ligand (**57**) with Cu^{2+} (**Figure 4.14**). On addition of Cu^{2+} to ligand (**57**), a slight hypsochromic shift was observed, with the three emission

maxima bands shifted to 392, 413, 438 nm and the shoulder to 467 nm. In cases where high metal complex ion stability constants are obtained, the ligand is generally fully complexed after the addition of one equivalent of metal ion, with no further spectral changes observed. Fluorescence quenching for the Cu^{2+} complex of ligand (**57**) occurred only until one equivalent of metal ion was added. Continued titration with Cu^{2+} beyond this did not result in further changes to ligand fluorescence. This result suggests that ligand (**57**) forms very stable complexes with Cu^{2+}, with a 1:1 complexation model most suitable.

The fluorescence of ligand (**57**) diminished linearly with concentration of added Cu^{2+} to the point where a 1:1 ratio was reached, and thereafter no significant changes were observed. This is consistent with the stability constant being greater than $K = 10^7$ dm^3 mol^{-1}, and with the value of $K = 10^{14}$ dm^3 mol^{-1} determined potentiometrically (see section **3.4**). It confirms the formation of a dominant 1:1 metal complex ion. The fluorescence variation at 415 nm is shown in **Figure 4.18**.

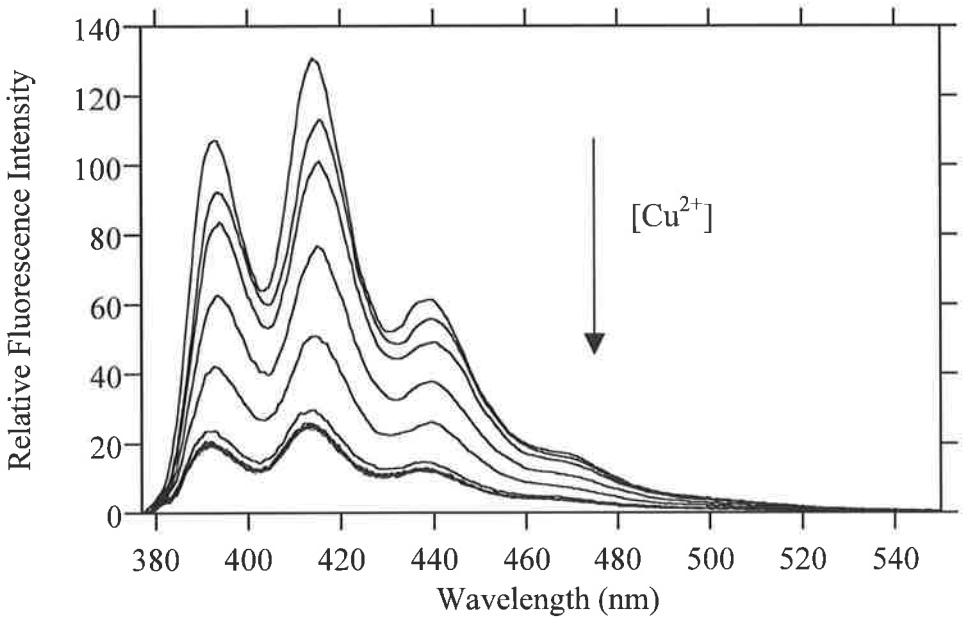

Figure 4.17. Fluorescence spectra of ligand (**57**) alone [4.1 x 10^{-5} mol dm^{-3}], and in the presence of increasing concentrations of Cu^{2+} [8.3 x 10^{-6}, 1.6 x 10^{-5}, 2.5 x 10^{-5}, 3.3 x 10^{-5}, 4.1 x 10^{-5}, 4.9 x 10^{-5}, 5.8 x 10^{-5}, 6.7 x 10^{-5}, 7.4 x 10^{-5}, 8.3 x 10^{-5} mol dm^{-3}] at pH 5.6 (MES buffer) in methanol/water (80:20; v/v) (I = 0.1 mol dm^{-3}, NEt_4ClO_4) at 298.2 K when excited at 368 nm. The fluorescence of the ligand alone is the highest intensity curve. Fluorescence decreases with increase in [Cu^{2+}].

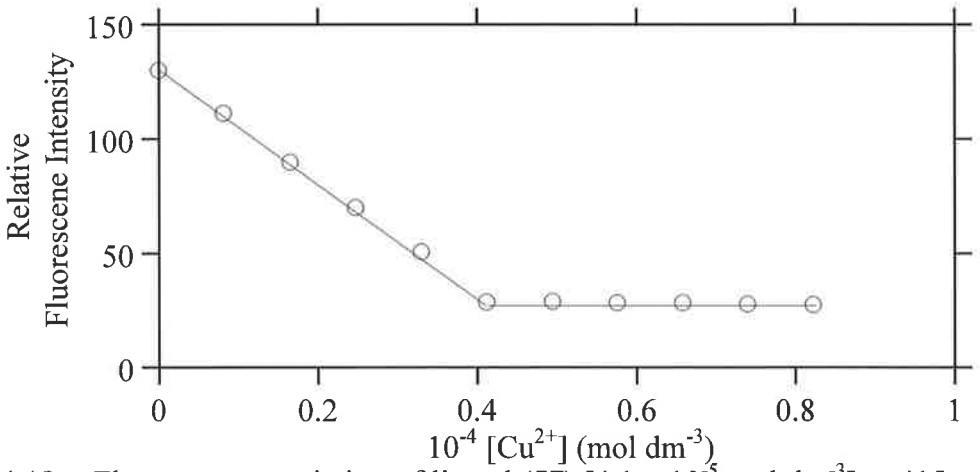

Figure 4.18. Fluorescence variation of ligand (**57**) [4.1 x 10^{-5} mol dm^{-3}] at 415 nm in the presence of increasing concentrations of Cu^{2+} [ranging from 8.3 x 10^{-6} to 8.3 x 10^{-5} mol dm^{-3}] at pH 5.6 (MES buffer) in methanol/water (80:20; v/v) (I = 0.1 mol dm^{-3}, NEt_4ClO_4) at 298.2 K when excited at 368 nm, and when fitted for a 1:1 complexation model. The circles represent the experimentally obtained data points, and the solid lines indicate the stoichiometric change in fluorescence.

The fluorescence spectrum of ligand (**57**) was only slightly perturbed on addition of either Zn^{2+} or Cd^{2+} (**Appendix**, **Figure A.19** and **A.20**). Complexation of either Zn^{2+} or Cd^{2+} by ligand (**57**) resulted in a slight increase in fluorescence intensity. The increase in fluorescence intensity is consistent with the PET mechanism being hindered by metal ion complexation. The emission maxima underwent hypsochromic shifts to 392, 413.5, 437.5 and 465.5 nm on Zn^{2+} complexation; and to 392.5, 413, 437.5 and 465.5 nm on Cd^{2+} complexation. The hypsochromic shift indicates a decrease in electron delocalisation within the system which can be attributed to (a) metal ion complexation hindering the PET process, or (b) the participation of the nitrogen lone pairs in metal ion coordination. A combination of these affects can also influence the emission maxima shift. For PET to be hindered, Zn^{2+} and Cd^{2+} complexation probably occurs through the ethylamine nitrogen adjacent to the anthracene substituent. Quantum yields measured for Zn^{2+} and Cd^{2+} complexation were Φ_F = 0.33 and Φ_F = 0.34, respectively.

No change to the fluorescence spectra for either Zn^{2+} or Cd^{2+} was observed beyond addition of more than one equivalent of metal ion. This indicates that a 1:1 complexation model would probably be the most suitable for these complexes. Owing to the fact that the fluorescence change was small, metal complex ion stability constants could not be accurately determined. The stability constants and quantum yields for metal ion complexation by ligand (**57**) appear in **Table 4.4**.

Table 4.4. Stability constants (fitted to a 1:1 complexation model) and quantum yields for metal ion complexation of ligand (**57**) in methanol/water (80:20; v/v) at pH 5.6 (MES buffer), (I = 0.1 mol dm^{-3}, NEt_4ClO_4) at 298.2 K

	K_1 (dm^3 mol^{-1})	SSD	Φ_F
Ligand (**57**)	-	-	0.32
Zn^{2+}	-	-	0.33
Cd^{2+}	-	-	0.34
Cu^{2+}	$> 10^7$	-	0.05

4.4.3 Metal ion complexation by ligand (58)

Ligand (**58**) alone was fluorescent (Φ_F = 0.19, $\lambda_{excitation}$ 368 nm), with emission maxima at 395.5, 415.5, 440.5 nm and a small shoulder at 468 nm. Cadmium(II) and Ca^{2+} did not alter the ligand's fluorescence significantly. The fluorescence of ligand (**58**) was completely extinguished in the presence of Cu^{2+} (**Figure 4.19** and **Figure 4.20**). The results obtained from the potentiometric titration of ligand (**58**) with Cu^{2+} had indicated that the resultant complexes were very stable; only the ML^{2+}, $M(LH)^{3+}$ and $M(LH_2)^{4+}$ complexes were detected (log$K$ = 19.42, log$K$ = 12.36 and log$K$ = 5.40, respectively). The $M(LH)^{3+}$ complexwas predominant at the pH at which fluorescence measurements were made (pH 5.6 MES buffer) (see **Figure 3.17**). It was expected, due to the high metal complex ion stability constant, which was determined from the potentiometric titrations for the $M(LH)^{3+}$ complex, that the ligand would be fully complexed after the addition of one equivalent of Cu^{2+}. This was not observed for the spectrofluorimetric titration of ligand (**58**) with Cu^{2+}. Fluorescence quenching was still observed on continued titration of Cu^{2+} with ligand (**58**) past one equivalent. The quenching continued until 3.5 equivalents of Cu^{2+} had been added, and this coincided with the fluorescence of the ligand being extinguished. The data obtained from the spectrofluorimetric titration of Cu^{2+} with ligand (**58**) could not be fitted to any of the available models, and is not in agreement with the values determined from potentiometric titration. The data could not be fitted accurately to the following complexation models; 1:1 (ML), 2:1 (M_2L), 1:2 (ML_2), 3:1 (M_3L) or a 2:1 (M_2L) in one step. The discrepancy cannot be explained through human error, since the results obtained in both the fluorimetric and potentiometric titrations were repeatable. Unfortunately the reason behind the unusual response of ligand (**58**) to Cu^{2+} complexation

could not be determined. This may be an area, which warrants further investigation in future studies.

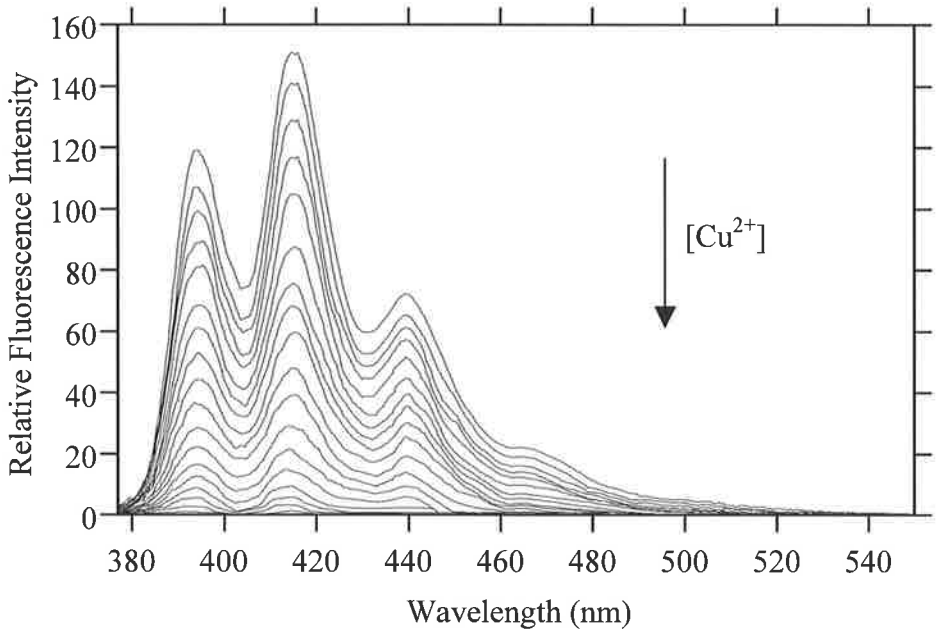

Figure 4.19. Fluorescence spectra of ligand (**58**) alone [4.7 x 10^{-5} mol dm^{-3}], and in the presence of increasing concentrations of Cu^{2+} [9.4 x 10^{-6}, 1.9 x 10^{-5}, 2.8 x 10^{-5}, 3.7 x 10^{-5}, 4.7 x 10^{-5}, 5.6 x 10^{-5}, 6.6 x 10^{-5}, 7.5 x 10^{-5}, 8.5 x 10^{-5}, 9.4 x 10^{-5}, 1.0 x 10^{-4}, 1.1 x 10^{-4}, 1.2 x 10^{-4}, 1.3 x 10^{-4}, 1.4 x 10^{-4}, 1.5 x 10^{-4}, 1.6 x 10^{-4} mol dm^{-3}] at pH 5.6 (MES buffer) in methanol/water (80:20; v/v) (I = 0.1 mol dm^{-3}, NEt_4ClO_4) at 298.2 K when excited at 368 nm. The fluorescence of the ligand alone is the highest intensity curve. Fluorescence decreases with increase in [Cu^{2+}].

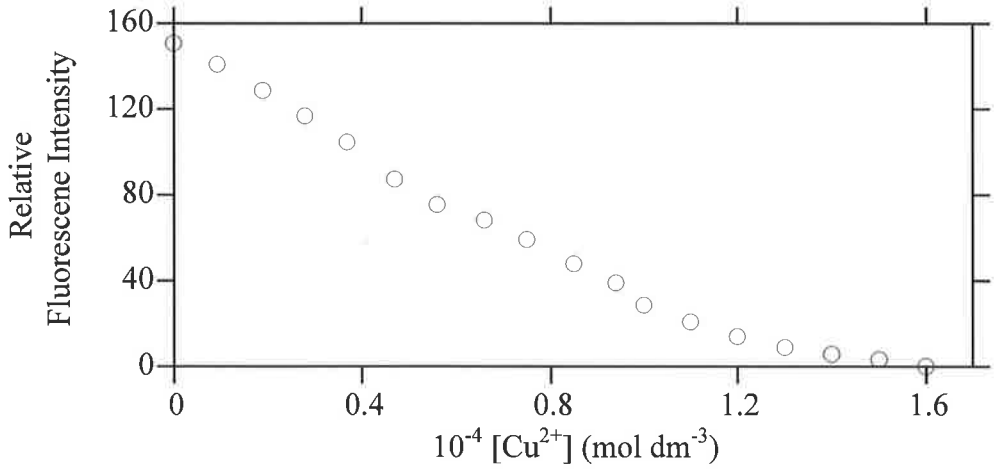

Figure 4.20. Fluorescence variation of ligand (**58**) [4.7 x 10^{-5} mol dm^{-3}] at 415 nm in the presence of increasing concentrations of Cu^{2+} [ranging from 9.4 x 10^{-5} to 1.6 x 10^{-4} mol dm^{-3}] at pH 5.6 (MES buffer) in methanol/water (80:20; v/v) (I = 0.1 mol dm^{-3}, NEt_4ClO_4) at 298.2 K when excited at 368 nm. The circles represent the experimentally obtained data points.

The spectral data obtained for the spectrofluorimetric titration of ligand (**58**) with Zn^{2+} (ranging from 9.4 x 10^{-5} to 9.4 x 10^{-4} mol dm^{-3}) are shown in **Figure 4.21**. Titration with Zn^{2+} had a quenching effect on the fluorescence intensity of ligand (**58**) with a quantum yield of Φ_F = 0.14 measured for the metal complex ion. It had been originally postulated that, on addition of Zn^{2+} to a solution of ligand (**58**), the intensity of the fluorescence of the ligand would be increased, in accordance with metal ion complexation hindering PET. This however was not observed. Previous reports of fluorescence quenching by Zn^{2+} have been attributed to a charge transfer between aromatic groups.[32-34] For ligand (**58**), charge transfer may occur between the phenyl rings present in the pendant arms and the anthracene substituent. Metal ion complexation may cause the phenyl rings to be brought closer to the anthracene substituent, facilitating charge transfer and subsequent fluorescence quenching.[35-37]

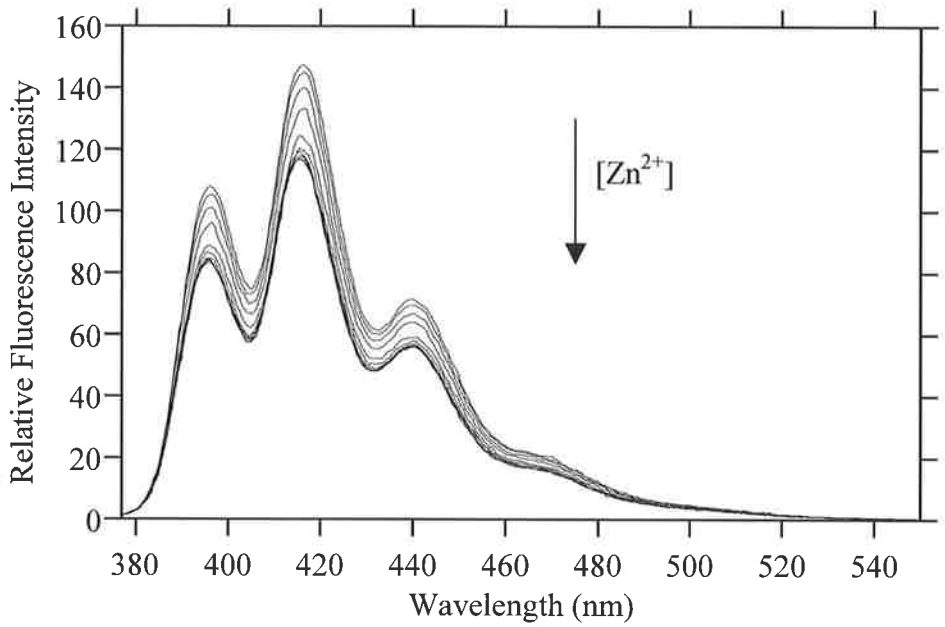

Figure 4.21. Fluorescence spectra of ligand (**58**) alone [4.7 x 10^{-5} mol dm^{-3}], and in the presence of increasing concentrations of Zn^{2+} [9.4 x 10^{-6}, 1.9 x 10^{-5}, 2.8 x 10^{-5}, 3.7 x 10^{-5}, 4.7 x 10^{-5}, 5.6 x 10^{-5}, 6.6 x 10^{-5}, 7.5 x 10^{-5}, 8.5 x 10^{-5}, 9.4 x 10^{-5} mol dm^{-3}] at pH 5.6 (MES buffer) in methanol/water (80:20; v/v) (I = 0.1 mol dm^{-3}, NEt_4ClO_4) at 298.2 K when excited at 368 nm. The fluorescence of the ligand alone is the highest intensity curve. Fluorescence decreases with increase in $[Zn^{2+}]$.

As discussed earlier, and in contrast to the observations for ligand (**58**), a small fluorescence increase was observed for ligand (**57**) upon complexation by Zn^{2+}. This was attributed to Zn^{2+} complexation of the ethylamine nitrogen adjacent to the anthracene substituent decreasing PET, thereby hindering fluorescence quenching to a small extent. The contrasting decrease in fluorescence of ligand (**58**) upon complexation by Zn^{2+}, is consistent with the steric hindrance induced by the amino acid substituent virtually precluding its involvement in Zn^{2+} complexation (and thereby decreasing PET), as well as an additional mechanism operating for fluorescence quenching.

The ligand (**58**) complex formed is predominantly $[ZnLH]^{3+}$, in which the protonation site is most probably the ethylamine nitrogen adjacent to the anthracene substituent. This is despite its substantially linear fluorescence by comparison with LH_5^{5+}, in which complete PET cancellation is expected. It is possible that hydrogen bonding between the proton of $[ZnLH]^{3+}$ and the adjacent amide oxygen may lessen the PET cancellation effect to a greater extent than is the case in LH_5^{5+} (**Figure 4.10** and **Table 4.2**). This leaves the fluorescence quenching of complexed LH^+ in $[ZnLH]^{3+}$ to be

explained. The most obvious effect of Zn^{2+} complexation on ligand (**58**) is that the three amide oxygens of the amino acid residues, attached to the macrocyclic ring carbons, exert a constraint on the motion of the three associated phenyl groups, compared with the situations in the free ligand. This, in turn, affects their interactions with the anthracene substituent on charge transfer between these four entities. It also affects the fourth amino acid residue attached to the ethylamine nitrogen adjacent to the anthracene substituent. If this results in fluorescence quenching, the extent of this quenching will be proportionate to the fraction of ligand (**58**) complexed, and thus provides a plausible explanation for the observed decrease in fluorescence.

The fluorescence variation of ligand (**58**) with Zn^{2+} fitted only a 1:1 complexation model. This resulted in the determination of $K_1 = 2.0 \pm 0.2 \times 10^6$ dm^3 mol^{-1} over the wavelength range 377 – 550 nm; a fit of the fluorescence data at 415 nm is shown in **Figure 4.22**. The SSD for this fit was 2.4×10^3. The relatively large error value obtained for K_1 can be ascribed to the stability constant approaching the upper limit for this method; $K = 10^7$ dm^3 mol^{-1} is the upper limit. Potentiometric titration of ligand (**58**) with Zn^{2+} was not possible due to the early formation of precipitate. This precipitation was avoided by the reduction in concentration for the fluorescence measurements. It was expected, however, that Zn^{2+} would exhibit a high metal complex ion stability constant, similar to those calculated for Cd^{2+} and Cu^{2+}, following the Irving-Williams series. In cases where a high metal complex ion stability constant is obtained, the ligand is generally almost fully complexed after the addition of one equivalent of metal ion. The fluorescence of ligand (**58**) decreased steeply until the first equivalent of Zn^{2+} had been added, upon which a fluorescence minimum was observed. No shift to either a shorter or longer wavelength occurred on metal ion complexation. The stability constants, and quantum yields, for the metal complex ions with ligand (**58**) can be found in **Table 4.5**.

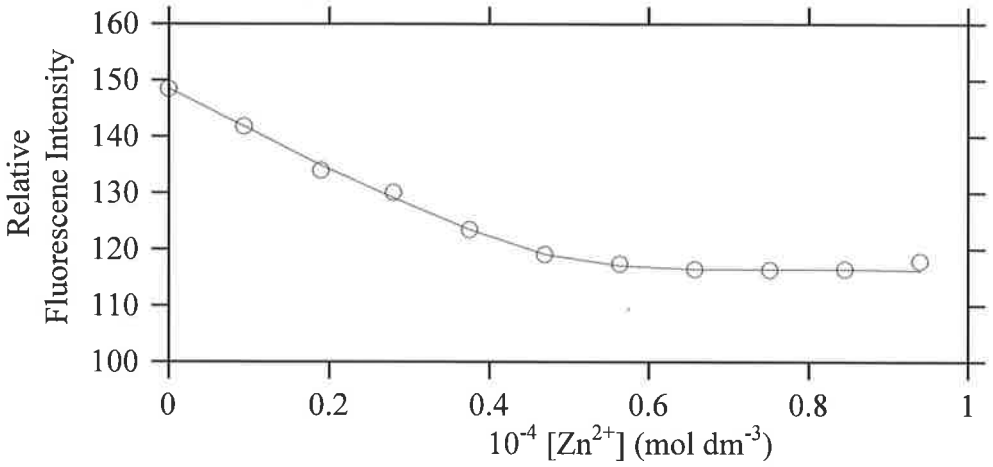

Figure 4.22. Fluorescence variation of ligand (**58**) [4.7 x 10^{-5} mol dm^{-3}] at 415 nm in the presence of increasing concentrations of Zn^{2+} [ranging from 9.4 x 10^{-5} to 9.4 x 10^{-4} mol dm^{-3}] at pH 5.6 (MES buffer) in methanol/water (80:20; v/v) (I = 0.1 mol dm^{-3}, NEt_4ClO_4) at 298.2 K when excited at 368 nm, when fitted for a 1:1 complexation model. The circles represent the experimentally obtained data points, and the solid line indicates the stoichiometric change in fluorescence.

Table 4.5. Stability constants (fitted to a 1:1 complexation model) and quantum yields for the metal ion complexation of ligand (**58**) in methanol/water (80:20; v/v) at pH 5.6 (MES buffer), (I = 0.1 mol dm^{-3}, NEt_4ClO_4) at 298.2 K

	K_1 (dm^3 mol^{-1})	SSD	Φ_F
Ligand (**58**)	-	-	0.19
Zn^{2+}	2.04 x 10^6 $\pm$ 2.04 x 10^5	2.42 x 10^3	0.14
Cu^{2+}	-	-	0

4.4.4 Metal ion complexation by ligand (62)

The fluorescence of ligand (**62**) on titration with metal ions, Zn^{2+}, Cd^{2+}, Cu^{2+} and Ca^{2+}, was measured in a solution of methanol/water (80:20; v/v), at constant ionic strength I = 0.1 mol dm^{-3} (NEt_4ClO_4), at pH 4.0 (acetate buffer). The consequence of the pH chosen for fluorescence measurements is that a number of fluorescent species may be present in solution. This will have a significant influence on the measured fluorescence. The species present at the buffered pH (pH 4.0 acetate buffer) prior to metal ion addition include the protonated species LH_5^{5+}, LH_4^{4+} and LH_3^{3+} (see **Figure 4.7**). Potentiometric titration of ligand (**62**) with metal ions was not possible due to the formation of precipitates, as discussed in **Chapter 3**. Therefore the complexes formed on metal ion complexation are unknown for ligand (**62**) but may include the unprotonated metal complex ion LM^{2+} and the protonated metal complex ion, $M(LH)^{3+}$.

Ligand (**62**) was fluorescent (Φ_F = 0.14, $\lambda_{excitation}$ 368 nm) with emission maxima at 397.5, 417.5, 440 nm and a shoulder at 469 nm. The fluorescence spectra of ligand (**62**) were not significantly altered in the presence of Ca^{2+}. Titration of ligand (**62**) with increasing concentrations of Cu^{2+} (ranging from 5.45 x 10^{-6} mol dm^{-3} to 1.11 x 10^{-4} mol dm^{-3}) resulted in the expected fluorescence quenching (**Figure 4.23**), with a small bathochromic shift of the emission maxima to 398, 418, 441.5 and 470 nm observed. The quenching of the ligand's fluorescence with Cu^{2+} is attributable to charge transfer transitions, and is in agreement with the charge transfer band observed in the absorption spectra of ligand (**62**) with Cu^{2+} (**Figure 4.16**)

Fluorescence quenching of ligand (**62**) decreases steeply on addition of one equivalent of Cu^{2+}, at which a fluorescence minimum was observed. The fluorescence variation of ligand (**62**) fitted only a 1:1 complexation model. A metal complex ion stability constant of $K_1 = 1.8 \pm 0.2 \times 10^6$ dm^3 mol^{-1} with an SSD of 3.18 x 10^3 was found on fitting a 1:1 complexation model over the wavelength range 377 – 550 nm. A fit of the fluorescence data at 418 nm is shown in **Figure 4.24**. The data did not fit for a 2:1 metal complex ion.

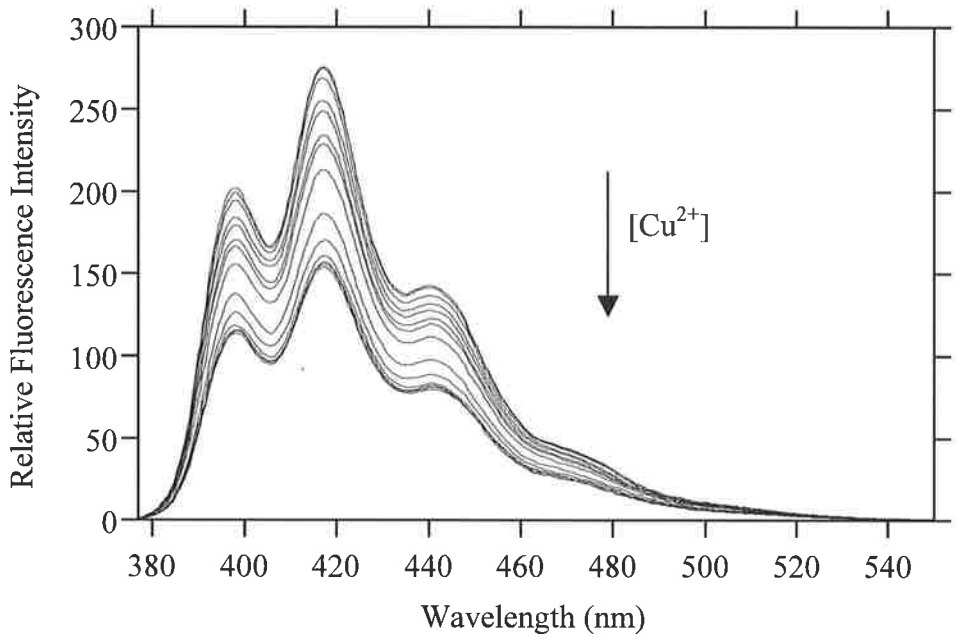

Figure 4.23. Fluorescence spectra of ligand (**62**) alone [5.5 x 10^{-5} mol dm^{-3}], in the presence of increasing concentrations of Cu^{2+} [5.45 x 10^{-6}, 1.1 x 10^{-5}, 1.6 x 10^{-5}, 2.2 x 10^{-5}, 2.7 x 10^{-5}, 3.8 x 10^{-5}, 4.9 x 10^{-5}, 6.0 x 10^{-5}, 7.0 x 10^{-5}, 8.1 x 10^{-5}, 9.2 x 10^{-5}, 1.0 x 10^{-5}, 1.11 x 10^{-4} mol dm^{-3}] at pH 4.0 (acetate buffer) in methanol/water (80:20; v/v) (I = 0.1 mol dm^{-3}, NEt_4ClO_4) at 298.2 K when excited at 368nm. The fluorescence of the ligand alone is the highest intensity curve. Fluorescence decreases with increase in $[Cu^{2+}]$.

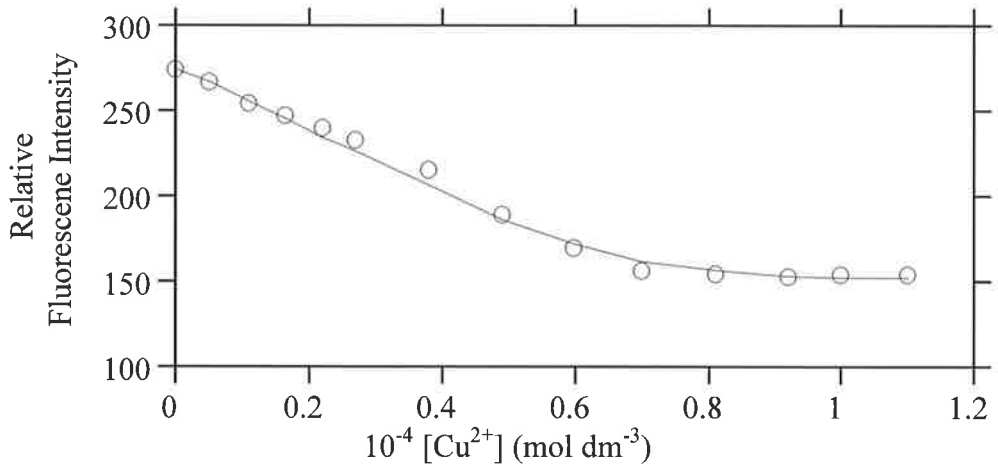

Figure 4.24. Fluorescence variation of ligand (**62**) [5.5 x 10^{-5} mol dm^{-3}] at 418 nm in the presence of increasing concentrations of Cu^{2+} [ranging from 5.45 x 10^{-6} mol dm^{-3} to 1.11 x 10^{-4} mol dm^{-3}] at pH 4.0 (acetate buffer) in methanol/water (80:20; v/v) (I = 0.1 mol dm^{-3}, NEt_4ClO_4) at 298.2 K when excited at 368nm, when fitted for a 1:1 complexation model. The circles represent the experimentally obtained data points, and the solid line indicates the stoichiometric change in fluorescence.

Titration of ligand (**62**) with increasing concentrations of Zn^{2+} (ranging from 5.45 x 10^{-6} mol dm^{-3} to 1.11 x 10^{-4} mol dm^{-3}) resulted in a small decrease to ligand fluorescence intensity (**Figure 4.25**). A quantum yield of Φ_F = 0.13 was measured. This can be attributed to the pH, and hence species present, at which fluorescence measurements were feasible, pH 4.0 (acetate buffer). From the speciation plots obtained from the potentiometric titration of the protonated ligand (**62**) with base (**Figure 4.7**), the LH_5^{5+}, LH_4^{4+} and the LH_3^{3+} species are observed to be present at this pH. This results in the primary electron donor being protonated (the ethylamine nitrogen adjacent to the anthracene substituent (LH_4^{4+}, pK_a 4.83)). The PET mechanism is affected only by either protonation or metal ion complexation of the primary electron donor. It is well known that the protonation of an amine is far more efficient at interrupting the transfer of electrons by PET than by metal ion complexation,[7] due to the formation of a covalent bond which alters the oxidation potential of the amine.[38] This suggests that when Zn^{2+} complexation displaces the proton, from the ethylamine nitrogen adjacent to the anthracene substituent, there is less hindrance to the transfer of electrons from the lone pair thus enhancing the PET process; hence the observed fluorescence quenching.[39,40]

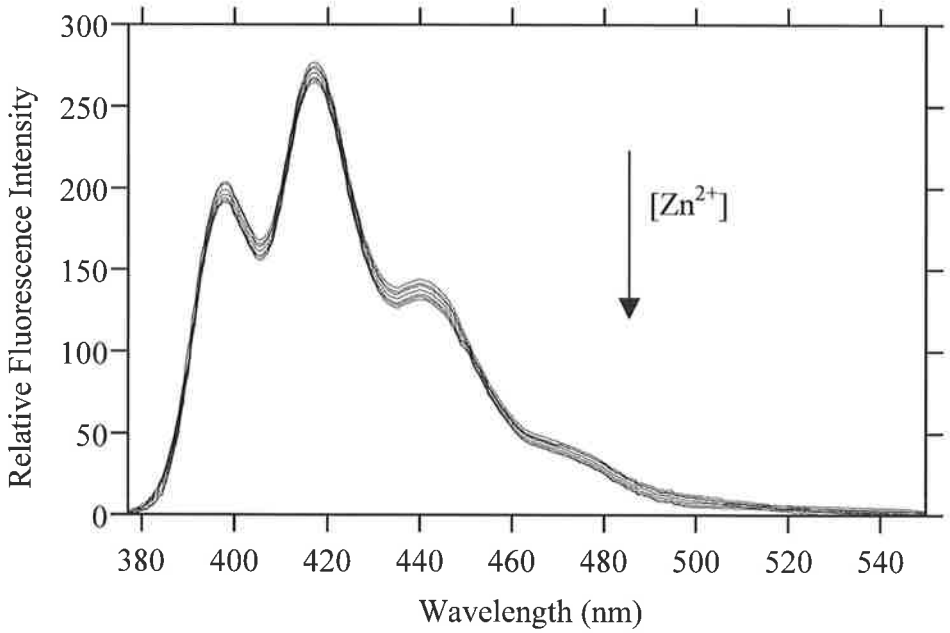

Figure 4.25. Fluorescence spectra of ligand (**62**) alone [5.5 x 10^{-5} mol dm^{-3}], and in the presence of increasing concentrations of Zn^{2+} [5.45 x 10^{-6}, 1.1 x 10^{-5}, 1.6 x 10^{-5}, 2.2 x 10^{-5}, 2.7 x 10^{-5}, 3.8 x 10^{-5}, 4.9 x 10^{-5}, 6.0 x 10^{-5}, 7.0 x 10^{-5}, 8.1 x 10^{-5}, 9.2 x 10^{-5}, 1.0 x 10^{-5}, 1.11 x 10^{-4} mol dm^{-3}] at pH 4.0 (acetate buffer) in methanol/water (80:20; v/v) (I = 0.1 mol dm^{-3}, NEt_4ClO_4) at 298.2 K when excited at 368nm. The fluorescence of the ligand alone is the highest intensity curve. Fluorescence decreases with increase in $[Zn^{2+}]$.

No change in fluorescence intensity was observed after the addition of one equivalent of Zn^{2+} to ligand (**62**). The spectral data for Zn^{2+} complexation fitted only a 1:1 complexation model (**Figure 4.26**). A stability constant of $K_1 = 9.0 \pm 0.2 \times 10^5$ dm^3 mol^{-1} was obtained, with a SSD of 3.08×10^3 over the wavelength range 377 – 550 nm. The relatively large error value for the metal complex ion stability constant can be attributed to the small intensity range over which spectral change occurred. A slight bathochromic shift was observed with the emission maxima bands shifted to 397.5, 418, 441 and 470 nm for Zn^{2+} complexation by ligand (**62**).

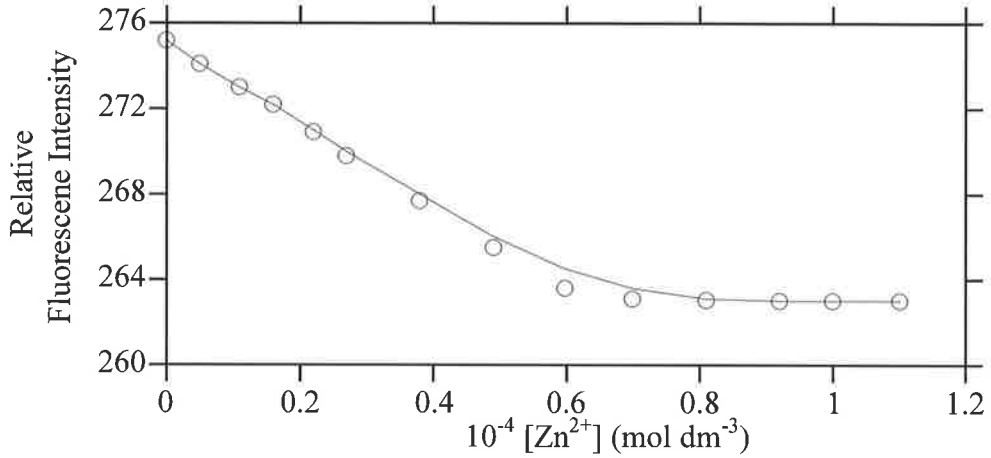

Figure 4.26. Fluorescence variation of ligand (**62**) [5.5×10^{-5} mol dm^{-3}] at 418 nm in the presence of increasing concentrations of Zn^{2+} [ranging from 5.45×10^{-6} mol dm^{-3} to 1.11×10^{-4} mol dm^{-3}] at pH 4.0 (acetate buffer) in methanol/water (80:20; v/v) (I = 0.1 mol dm^{-3}, NEt_4ClO_4) at 298.2 K when excited at 368nm, when fitted for a 1:1 complexation model. The circles represent the experimentally obtained data points, and the solid line indicates the stoichiometric change in fluorescence.

Similarly to Zn^{2+} complexation by ligand (**62**), spectrofluorimetric titration of ligand (**62**) with Cd^{2+} (ranging from 5.45×10^{-6} mol dm^{-3} to 1.11×10^{-4} mol dm^{-3}) resulted in a decrease in ligand fluorescence intensity (**Figure 4.27**). The rationale applied for the influence of Zn^{2+} on the fluorescence intensity of ligand (**62**) can be applied to Cd^{2+} complexation. The displacement of the proton, at the ethylamine nitrogen adjacent to the anthracene substituent by Cd^{2+}, causes an increase in PET; this results in the observed fluorescence quenching. A slight bathochromic shift was observed on metal ion complexation; the emission maxima were shifted to 398.5, 418, 440.5 and the shoulder to 470 nm. A quantum yield of $\Phi_F = 0.13$ was obtained. The data obtained from Cd^{2+} complexation by ligand (**62**) fitted only a 1:1 complexation model to yield a $K_1 = 4.3 \pm 0.3 \times 10^5$ and a SSD of 2.35×10^3 over the wavelength range 377 – 550 nm (**Figure 4.28**).

The relatively large error value obtained may be attributed to the small effect the metal ion complexation has on the fluorescence of ligand (**62**).

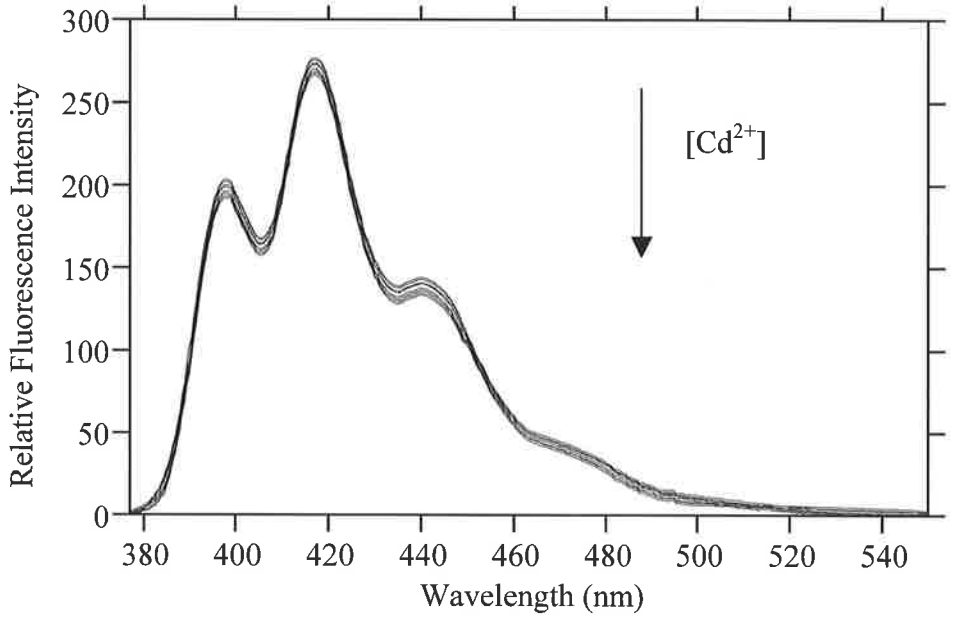

Figure 4.27. Fluorescence spectra of ligand (**62**) alone [5.5 x 10^{-5} mol dm^{-3}], and in the presence of increasing concentrations of Cd^{2+} [5.45 x 10^{-6}, 1.1 x 10^{-5}, 1.6 x 10^{-5}, 2.2 x 10^{-5}, 2.7 x 10^{-5}, 3.8 x 10^{-5}, 4.9 x 10^{-5}, 6.0 x 10^{-5}, 7.0 x 10^{-5}, 8.1 x 10^{-5}, 9.2 x 10^{-5}, 1.0 x 10^{-5}, 1.11 x 10^{-4} mol dm^{-3}] at pH 4.0 (acetate buffer) in methanol/water (80:20; v/v) (I = 0.1 mol dm^{-3}, NEt_4ClO_4) at 298.2 K when excited at 368nm. The fluorescence of the ligand alone is the highest intensity curve. Fluorescence decreases with increase in $[Cd^{2+}]$.

The bathochromic shifts observed for the coordination of ligand (**62**) with Cu^{2+}, Zn^{2+} and Cd^{2+} are indicative of an increase in electron delocalisation for the excited state of ligand (**62**). For Zn^{2+} and Cd^{2+} complexation, the wavelength shift may be due to the increase in electron transfer through the PET mechanism. For Cu^{2+} complexation the wavelength shift can be attributed to the resultant charge transfer from ligand to metal ion. Metal ion coordination may also cause ligand (**62**) to adopt a more rigid structure, which would favour the increase in electron delocalisation within the excited state. A combination of these factors may also contribute to the observed wavelength shift for each of the metal complex ions formed with ligand (**62**). An overall trend for the metal complex ion stability constants was observed for ligand (**62**); Cu^{2+}>Zn^{2+}>Cd^{2+}. This is predicted by the Irving-Williams series.[41] It is also consistent with the Jahn-Teller effect, enhancing the stability of Cu^{2+} over Zn^{2+}.[42] The stability constants and quantum yields for the metal complex ions with ligand (**62**) appear in **Table 4.6**.

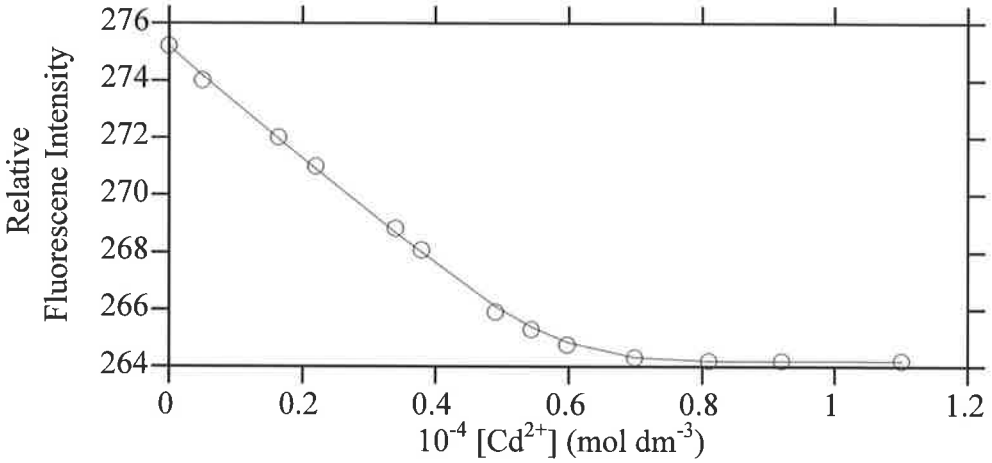

Figure 4.28. Fluorescence variation of ligand (**62**) [5.5 x 10^{-5} mol dm^{-3}] at 418 nm in the presence of increasing concentrations of Cd^{2+} [ranging from 5.45 x 10^{-6} mol dm^{-3} to 1.11 x 10^{-4} mol dm^{-3}] at pH 4.0 (acetate buffer) in methanol/water (80:20; v/v) (I = 0.1 mol dm^{-3}, NEt_4ClO_4) at 298.2 K when excited at 368nm, when fitted for a 1:1 complexation model. The circles represent the experimentally obtained data points, and the solid line indicates the stoichiometric change in fluorescence.

Table 4.6. Stability constants (fitted to a 1:1 complexation model) and quantum yields for the metal ion complexation of ligand (**62**) in methanol/water (80:20; v/v) at pH 5.6 (MES buffer), (I = 0.1 mol dm^{-3}, NEt_4ClO_4) at 298.2 K

	K_1 (dm^3 mol^{-1})	SSD	Φ_F
Ligand (**62**)	-	-	0.14
Zn^{2+}	9.0 x 10^5 ± 2.3 x 10^4	3.0 x 10^3	0.13
Cd^{2+}	4.3 x 10^5 ± 3.3 x 10^4	2.3 x 10^3	0.13
Cu^{2+}	1.8 x 10^6 ± 2.0 x 10^5	3.2 x 10^3	0.07

4.5 Discussion

The three ligands (**57**), (**58**) and (**62**), studied for their UV-visible absorption and fluorescence properties, were quite varied in behaviour. All three ligands, (**57**), (**58**) and (**62**), exhibited some background fluorescence, which was attributed to the partially protonated species present at the pH at which measurements were made, as was discussed earlier. Due to the solubility of the ligands and the formation of precipitates, the pH at which measurements were feasible was not ideal for the monitoring of UV-visible absorption or fluorescence. The high background fluorescence is readily noted in the large quantum yields obtained for the ligands alone; Φ_F (**57**) = 0.32 at pH 5.6, Φ_F (**58**) = 0.19 at pH 5.6, Φ_F (**62**) = 0.14 at pH 4.0.

The consequence of a change in pendant arm functionality, and substitution pattern was readily apparent in the absorption spectra of ligands (**57**), (**58**) and (**62**). The incorporation of pendant arms containing aromatic substituents resulted in charge transfer, which occurred between the phenyl rings and the anthracene substituent for ligands (**57**) and (**58**). The change in substitution pattern of the pendant arms was seen to have a significant effect on electron mobility between the two types of aromatic groups. Pendant arm substitution at the ethylamine nitrogen adjacent to the anthracene substituent in ligand (**58**), decreased the extent to which charge transfer occurred. The addition of a buffer to solutions of the partially charged ligands, (**57**) and (**58**), was observed to influence ligand absorption pattern by stabilising the charge transfer between aromatic groups; the fluorescence spectra of the ligand were unaffected.

The influence of pH on the fluorescence of the protonated ligands (**57**), (**58**) and (**62**) exemplified the PET mechanism. Protonation of the electron donors coincided with a restoration of ligand fluorescence. Fluorescence pH titrations allowed the assignment of pK_a values associated with the protonation of the primary electron donor (the ethylamine nitrogen adjacent to the anthracene substituent) for ligand (**57**) pK_{a4} 4.52, for ligand (**58**) pK_{a4} 4.90 or pK_{a5} 4.51, and for ligand (**62**) pK_a 4.83.

The complexation of Zn^{2+}, Cu^{2+}, Cd^{2+} and Ca^{2+} with the three ligands (**57**), (**58**) and (**62**) did not have a large effect on their respective absorption spectra. The ligands were designed to respond to PET; therefore the small size of the observed spectral change in the

absorption spectra on metal ion complexation is neither unexpected nor necessarily undesirable, because fluorescence quenching only affects the excited state.

Pendant arm substitution pattern was observed to affect the manner in which metal ion complexation influenced fluorescence. The fluorescence of ligand (**57**) was enhanced on complexation with either Zn^{2+} or Cd^{2+}, consistent with the operation of a PET mechanism for fluorescence quenching. The fluorescence of ligand (**58**), with the same type of pendant arm as ligand (**57**), but different substitution pattern, was observed to decrease on complexation with Zn^{2+}; Cd^{2+} complexation did not alter the fluorescence spectra significantly. Fluorescence quenching of ligand (**58**) on complexation with Zn^{2+} was attributed to a charge transfer between the phenyl rings in the pendant arms and the anthracene substituent. The difference in fluorescence response between the two ligands, (**57**) and (**58**), is attributable to the ethylamine nitrogen adjacent to the anthracene, being substituted in ligand (**58**) but not in ligand (**57**).

The change in fluorescence on either Zn^{2+} or Cd^{2+} complexation by ligand (**62**) highlights the lower efficiency that metal ion complexation has on hindering the PET process in comparison with that of protonation. Metal ion complexation displaces the proton from the ethylamine nitrogen adjacent to the anthracene substituent. This results in less hindrance to the transfer of electrons from the amine nitrogens lone pair, thus enhancing the PET process. The fluorescence of ligand (**62**) was influenced by the presence of the protonated ethylamine nitrogen adjacent to the anthracene substituent.

Not all metal ions resulted in spectral changes. This lack of fluorescence variation does not necessarily signify that complexation does not occur, but only that if metal ion complexation does occur, there is no alteration to ligand fluorescence. The lack of spectral response can be ascribed to two reasons. Firstly metal ion coordination may not occur through all available donor atoms; and secondly to the pH at which measurements were feasible. At pH 5.6 for ligands (**57**) and (**58**), and pH 4.0 for ligand (**62**), the monoprotonated or diprotonated metal complex ion species may also be present. These species may not be significantly different spectroscopically from the free ligand.

4.6 References

(1) Birks, J. B. *Photophysics of Aromatic Molecules*; Wiley-Interscience: London, 1970.

(2) Berlman, I. B. *Handbook of Fluorescence Spectra of Aromatic Compounds*; Academic Press: London, 1965.

(3) Jaffe, H. H.; Orchin, M. *Theory and Applications of Ultraviolet Spectroscopy*; John Wiley and Sons, Inc: New York, 1962.

(4) Schulman, S. G. *Fluorescence and Phosphorescence Spectroscopy: Physicochemical Principles and Practice*; Pergamon Press: Oxford, 1977.

(5) Suppan, P. *Chemistry and Light*; Royal Society of Chemistry: London, 1994.

(6) Bissell, R. A.; Calle, E.; de Silva, A. P.; de Silva, S. A.; Gunarantne, H. Q. N.; Habib-Jiwan, J.-L.; Peiris, S. L. A.; Rupasinghe, R. A. D. D.; Samarashinghe, T. K. S. D.; Sandanayake, K. R. A. S.; Soumillion, J.-P. *J. Chem. Soc., Perkin Trans. 2* **1992**, 1559-1564.

(7) Huston, M. E.; Haider, K. W.; Czarnik, A. W. *J. Am. Chem. Soc.* **1988**, *110*, 4460-4462.

(8) de Silva, A. P.; Zavaleta, A.; Baron, D. E.; Allam, O.; Isidor, E. V.; Kashimura, N.; Percarpio, J. M. *Tet. Lett.* **1997**, *38*, 2237-2240.

(9) Fabbrizzi, L.; Francese, G.; Pallavicini, P.; Parodi, L. *New J. Chem.* **1998**, 1403-1407.

(10) Konopelski, J. P.; Kotzyba-Hubert, F.; Lehn, J.-M.; Desvergne, J.-P.; Fages, F.; Castellan, A.; Boaus-Laurent, H. *J. Chem. Soc., Chem. Commun.* **1985**, 433-436.

(11) Burgess, C.; Knowles, A., Eds. *Standards in Absorption Spectrometry*; Chapman and Hall: London, 1981.

(12) Murov, S. L.; Carmichael, I. *Handbook of Photochemistry*; 2nd ed.; Dekker: New York, 1993.

(13) Laguitton-Pasquier, H.; Pansu, R.; Chauvet, J.-P.; Collet, A.; Faure, J.; Lapouyade, R. *Chem. Phys.* **1996**, *212*, 437-455.

(14) Akkaya, E. U.; Huston, M. E.; Czarnik, A. W. *J. Am. Chem. Soc.* **1990**, *112*, 3590-3593.

(15) Czarnik, A. W. In *Frontiers in Supramolecular Organic Chemistry and Photochemistry*; Schnieder, H. J., Durr, H., Eds.; VCH: Germany, 1991, pp 109-122.

(16) Burgess, J. *Metal Ions in Solution*; Halsted Press: New York, 1978.

(17) Horvath, O.; Stevenson, K. L. *Charge-Trasfer Photochemistry of Coordination Comopunds*; VCH: Weinheim, Germany, 1993.

(18) Mizukami, S.; Nagano, T.; Urano, Y.; Odani, A.; Kikuchi, K. *J. Am. Chem. Soc.* **2002**, *124*, 3920-3925.

(19) Geraldes, C. F. G.; Alpoim, M. C.; Marques, M. P. M.; Sherry, A. D.; Singh, M. *Inorg. Chem.* **1985**, *24*, 3876-3881.

(20) Reido, T. J.; Kaden, T. A. *Hel. Chim. Acta.* **1979**, *62*, 1089-1096.

(21) Reido, T. J.; Kaden, T. A. *Chimia* **1977**, *31*, 220-222.

(22) Renfrew, R. W.; Jamison, R. S.; Weatherburn, D. C. *Inorg. Chem.* **1979**, *18*, 1584-1589.

(23) Thom, V. J.; Hosken, G. D.; Hancock, R. D. *Inorg. Chem.* **1985**, *24*, 3378-3381.

(24) Hinz, F. P.; Margerum, D. W. *Inorg. Chem.* **1974**, *13*, 2941-2949.

(25) Halfiger, H.; Kaden, T. A. *Hel. Chim. Acta.* **1979**, *62*, 683-688.

(26) Tsukube, H.; Furuta, H.; Odani, A.; Takeda, Y.; Kudo, Y.; Inoue, Y.; Y, L.; Sakamoto, H.; Kimura, K. *Comprehensive Supramolecular Chemistry: Physical Methods in Supramolecular Chemsitry*; Pergamon: New York, 1996; Vol. 8.

(27) Martell, A. E.; Motekaitis, R. J. *The Determination and Use of Stability Constants*; VCH Publishers: Weinheim, 1988.

(28) Beck, M.; Hagypal, I. *Chemistry of Complex Equilibria*; Ellis Horwood: Chichester, 1990.

(29) Kuruscev, T., Private Communication.

(30) Maeder, M.; Zuberbuhler, A. D. *Anal. Chem.* **1990**, *62*, 2220-2224.

(31) Lakowicz, J. R. *Principles of Fluorescence Spectrometry*; 2nd ed.; Kluwer Academic/Plenum Publishers: New York, 1999.

(32) Bruseghini, I.; Fabbrizzi, L.; Licchelli, M.; Taglietti, A. *Chem. Commun.* **2002**, 1348-1349.

(33) De Santis, G.; Fabbrizzi, L.; Faravelli, I.; Licchelli, M.; Poggi, A.; Taglietti, A. *Angew. Chem. Int. Ed.* **1996**, *35*, 202-204.

(34) Fabbrizzi, L.; Licchelli, M.; Perotti, A.; Poggi, A.; Rabaioli, G.; Sacchi, D.; Taglietti, A. *J. Chem. Soc., Perkin Trans. 2* **2001**, 2108-2113.

(35) Haenel, M. W.; Schweitzer, D. *Adv. Chem. Ser.* **1988**, *217*, 333-355.

(36) Baldes, R.; Schnieder, H.-J. *Angew. Chem. Int. Ed. Eng.* **1995**, *34*, 321.

(37) Inoue, M. B.; Velazquez, E. F.; Medrano, F.; Ochoa, K. L.; Galvez, J. C.; Inoue, M.; Fernando, Q. *Inorg. Chem.* **1998**, *37*, 4070-4075.

(38) de Silva, A. P.; Gunaratne, H. Q. N. *J. Chem. Soc., Chem. Commun.* **1990**, 186-188.

(39) Bernardo, M. A.; Pina, F.; Garcia-Espana, E.; Latorre, J.; Luis, S. V.; Llinares, J. M.; Ramierez, J. A.; Soriano, C. *Inorg. Chem.* **1998**, *37*, 3935-3942.

(40) Pina, F.; Bernardo, A.; Garcia-Espana, E. *Eur. J. Inorg. Chem.* **2000**, 2143-2157.

(41) Irving, H.; Williams, R. J. P. *J. Chem. Soc.* **1953**, 3192-3210.

(42) Shirver, D. F.; Atkins, P. W. *Inorganic Chemistry*; 3rd ed.; Oxford University Press: Oxford, UK, 1999.

Chapter 5. Conclusions

This study describes the investigation into a series of pendant arm substituted macrocycles. They are designed to act as either chiral receptors through the use of chiral amino acid pendant arms, or as fluorescent metal ion sensors, incorporating a photoinduced electron transfer (PET) pathway. Two types of polyaza macrocycles, tacn and cyclen, were used in the course of the investigation.

Synthesis of the two types of target ligands, amino acid pendant arm and the anthracene substituted fluorescent sensors, yielded a variety of products. For the chiral amino acid based ligands, the size of the pendant arm incorporated was found to affect both the extent to which substitution occurred as well as the stability of the ligand. The macrocyclic ligands incorporating L-phenylalanine pendant arms were found to be more stable than those incorporating the larger L-tryptophan pendant arms. Synthesis of the anthracene substituted sensors yielded a variety of ligands with varying substitution patterns. Pendant arm substitution occurred more readily at the ethylamine nitrogen adjacent to the anthracene substituent.

NMR spectroscopy was used to probe the stereochemistry of the chiarl amino acid based ligands (**31**), (**45**) and (**50**). The ligands were found to exist in a preferred diastereomeric conformation on metal ion coordination. Each diastereomer forms a part turn in a triple or quadruple helix, depending on the parent macrocycle. The extension of the pendant arms, from single amino acids to peptides, may allow the study of peptide helices, and the formation of multiple metal complex ions.

The protonation constants and metal complex ion stability constants, for all of the ligands synthesised, were determined in a solution of methanol/water (80:20; v/v) by potentiometric titration. The values obtained for the amino acid pendant arm ligands followed similar patterns to other pendant arm substituted polyaza macrocycles. Increasing the macrocyclic ring size, or the steric bulk of the pendant arms, was found to yield ligands with higher protonation constants. The protonation constants obtained for the anthracene substituted ligands showed the effects that, (a) varying the pendant arm functionality and substitution pattern, and (b) the incorporation of the hydrophobic anthracene moiety, had on amine basicity. Larger metal complex ion stability constants

were observed for the anthracene substituted ligands over the amino acid pendnat arm ligands. These were attributed to the change in coordination number and donor atom type, which led to the formation of preferential stereochemical environments around the metal ions, for the anthracene substituted ligands.

The UV-visible absorption and fluorescence behaviour of the anthracene substituted ligands (**57**), (**58**) and (**62**), was evaluated through protonation and metal ion complexation studies. The change in pendant arm functionality and substitution pattern had a significant effect on the photophysical properties of the ligands. Charge transfer bands were observed in the absorption spectra for the chiral amino acid pendant arm anthracene substituted ligands (**57**) and (**58**). These were attributed to the transfer of electrons between the phenyl rings and the anthracene substituent. Substitution at the ethylamine nitrogen adjacent to the anthracene substituent, was seen to affect the transfer of electrons between the aromatic groups. For all three ligands, (**57**), (**58**) and (**62**), changes in absorbance were in agreement with the protonated species present, and hence pK_a values. Investigation into the protonation behaviour of the three ligands (**57**), (**58**) and (**62**), in relation to their fluorescence, showed that full protonation restored ligand fluorescence. Changes in fluorescence on titration of the protonated ligands with base, facilitated the determination of the pK_a value for the protonated ethylamine nitrogen adjacent to the anthracene substituent, (the primary electron donor) in each ligand. These were coincident with those determined by potentiometric titration. Such pK_a determination by fluorescence change, for the protonated macrocyclic ring nitrogens, was not possible due to their greater distance from the anthracene fluorophore.

For all three anthracene substituted ligands, (**57**), (**58**) and (**62**), only limited changes to the UV-visible absorption spectra were observed on metal ion complexation, in accordance with excited state quenching, the mechanism by which PET occurs. The three ligands (**57**), (**58**) and (**62**), exhibited very different fluorescence behaviour on metal ion complexation. All three ligands (**57**), (**58**) and (**62**), complexed the metal ions investigated with a high degree of stability, a desirable property of a fluorescent metal ion sensor. For most of the complexes formed, changes in fluorescence were observed only for the addition of the first equivalent of metal ion; this coupled with the metal complex ion stability constants determined, indicated preferential formation of 1:1 metal complex ions. The fluorescence of ligand (**57**) was enhanced on addition of either one equivalent of Zn^{2+}, or Cd^{2+}, indicating that metal ion coordination hindered the PET process. The fluorescence

of ligand (**58**), however, was quenched on titration with Zn^{2+}, indicating that the effect of the coordination of Zn^{2+} on the PET process was dominant in determining the overall fluorescence. The complexation of Zn^{2+}, in the case of ligand (**58**), brought the phenyl rings and anthracene substituent closer. This facilitated charge transfer, which resulted in fluorescence quenching. Fluorescence quenching was also observed for ligand (**62**) with Zn^{2+} and Cd^{2+}. Displacement of the proton by the metal ion enhanced the transfer of electrons from the lone pair of the nitrogen. Metal ions do not hinder the PET process to the same extent as protons. Titration of all three ligands with Cu^{2+} resulted in fluorescence quenching.

All ligands synthesised in this study showed a high degree of affinity towards transition metal ions over group I or II metal ions, with stability trends consistent with the Irving Williams series. The generation of water soluble ligands was successful, for both the chiral amino acid receptor ligands and the anthracene substituted fluorescent sensors. The carboxylic acid derivatives of L-phenylalanine, both the tacn ligand (**42**) and the cyclen ligand (**46**), were soluble at neutral pH 7. The anthracene substituent ligand (**62**) with hydroxyethyl pendant arms was also soluble at neutral pH 7. However, the metal complex ions of both ligand (**46**) and ligand (**62**) were found to be insoluble in aqueous and partially aqueous solvent systems.

A good basis for future investigations would be provided by the enhanced stability of both anthracene substituted ligands (**57**) and (**58**), with chiral amino acid pendant arms, to air and light accompanied by the high metal complex ion stability constants determined, with respect to the other ligands investigated. Future studies should focus on the design of these ligands and the role that different functional groups play in altering specificity and selectivity towards metal ions through responses in fluorescence.

The incorporation of an additional amine group (through the addition of the spacer arm in the anthracene substituted ligands) significantly increased the specificity towards metal ions; this however, did not induce large fluorescence enhancements. Future investigations should focus on determining the metal ion coordination sites in these ligands, as this may play a role in the observed fluorescence response. The information obtained from that study could be used to design highly specific fluorescent sensors, which respond to metal ion coordination with significant alterations in fluorescence signals, which is a desirable property when designing fluorescent sensors. Increasing the water

solubility of the metal complex ions is also desirable. This may be achieved through the incorporation of hydrophilic pendant arms of a similar structure to phenylalanine and tryptophan, such as L-tyrosine. The incorporation of carboxylic acid based arms, with the carbonyl groups β to the macrocyclic amines, into the anthracene substituted ligands, may also provide for highly stable and selective fluorescent probes for aqueous solutions.

Chapter 6. Experimental

6.1 General synthetic methods

^{1}H NMR spectra were recorded at 200 MHz on a Varian Gemini spectrometer (50.28 MHz for ^{13}C) with a dual 5mm ^{13}C/^{1}H probe, 300 MHz Varian Gemini NMR spectrometer (75.5 MHz for ^{13}C) or at 600 MHz on a Varian Nova NMR spectrometer (150.8 MHz for ^{13}C). All spectra were recorded as dilute solutions in $CDCl_3$ with tetramethylsilane as an internal standard for non aqueous solvents, and in D_20 against the HOD resonance (δ 4.72 ppm), at 25°C, unless otherwise stated. Chemical shifts are quoted on the δ-scale in parts per million (ppm), followed by multiplicity, coupling constant(s) and assignment. All multiplicities for proton NMR are abbreviated: s, singlet; d, doublet; t, triplet; q, quartet; m, multiplet and br, broad.

Melting points were determined on a Kofler hot-stage micro-melting point apparatus equipped with a Reichart microscope, and are uncorrected. Infrared spectra were recorded on a ATI Matson Genesis FTIR spectrometer as nujol mulls between sodium chloride plates. Combustion analyses were carried out by the Microanalytical Division of the Chemistry Department, University of Otago, New Zealand. Mass Spectra were recorded as electron impact (EI) mass spectra on a VG ZAB 2HF mass spectrometer. Electrospray ionisation mass spectra were recorded in positive ion mode on a Finnigan MAT ion trap LC-Q octapole mass spectrometer (LCQ).

Thin layer chromatography (tlc) was carried out with Merck Silica gel (Kieselgel) $60F_{254}$ on aluminium backed plates, or on Merck Aluminium oxide $150F_{254}$ neutral (type T) plates. The plates were visualised by 253 nm ultraviolet light, or by staining with iodine. Flash chromatography was carried out with either generic basic UG alumina or with Merck Silica gel 60 (particle size 0.040-0.063 nm). Squat column chromatography was performed with Merck Kieslgel 60 PF_{254}. Solvents were purified and dried using standard laboratory procedures.[1] All organic extracts were dried over anhydrous sodium sulfate.

6.2 General physical methods

Deionised water that had been purified with the MilliQ-Reagent system to produce water with a specific resistance of >15 MΩ cm^{-1}, boiled for 30 min to remove CO_2, and cooled under a drying tube filled with soda lime, was used in the preparation of all aqueous solutions. All volumetric glassware was "A-grade".

Methanol (AR, B.D.H) was dried by distillation under nitrogen. The metal salts $NaClO_4$ (B.D.H), $Ca(ClO_4)_2$ (Aldrich), $Zn(ClO_4)_2$ (Aldrich), $Cu(ClO_4)_2$ (Aldrich), $Ni(ClO_4)_2$ (Aldrich), $Co(ClO_4)_2$ (Aldrich), and $Cd(ClO_4)_2$ (Aldrich) were purchased and dried under high vacuum over P_4O_{10}. *Caution: Anhydrous perchlorate salts can be explosive and should be handled with care.* All metal salts were standardized in triplicate by means of cation exchange chromatography. A Dowex AG 50W-X2 cation exchange column (2 x 20 cm) in its H^+ form was loaded with 1.0 cm^3 of a 0.1 mol dm^{-3} aqueous solution of the metal salt to be standardized, and the column eluted with water until the eluant was neutral. Bromothymol Blue (3 drops) was added to the eluant and the solution titrated against 0.1 mol dm^{-3} NaOH (previously standardized by titration against potassium hydrogen phthalate).

Tetraethylammonium perchlorate (NEt_4ClO_4) was prepared by addition of excess $HClO_4$ (1.0 mol dm^{-3}, 1.7 dm^3) (Ajax) to NEt_4Br (300 g, 1.4 mol) (Aldrich) in H_2O. The resulting NEt_4ClO_4 was recrystallised from H_2O until free of bromide and acid. The white crystalline NEt_4ClO_4 was then dried under high vacuum over P_4O_{10}.

The two buffer solutions utilised in this study, MES ([2-(*N*-morpholino)-ethane-sulfonic acid] sodium salt, pK_a 6.15) and acetic acid/ sodium acetate (pK_a 4.52) were prepared as described in the literature,[2] by means of a pH-electrode calibrated in a methanol/water (80:20; v/v) solvent system. The pH of the solution was adjusted by the addition of $HClO_4$ until the desired pH 5.6 (MES) or pH 4.0 (acetate) was obtained. The ionic strength was maintained at $I = 0.1$ mol dm^{-3} with NEt_4ClO_4.

The ligands used were prepared as described in **Chapter 2**, they were dried over P_4O_{10} containing indicator (Sicapent) under vacuum for a minimum of 6 hr prior to use.

6.3 Partially aqueous potentiometric titrations in methanol/water solvent system

Potentiometric titrations were carried out by means of a Metrohm E665 Dosimat Autoburette which was equipped with a 5 cm^3 burette interfaced to a Laser XT/3-8086 PC. Changes in hydrogen ion concentration were monitored by means of an Orion Ross Sureflow 81-72 BN combination electrode connected to an Orion 720 Digital Voltmeter. The titrations were carried out at 298.2 $\pm$ 0.1 K in a water-jacketed vessel. High purity nitrogen was bubbled through a solution of 0.1 mol dm^{-3} NEt_4ClO_4 and then through the cell. Methanol, Milli-Q water and NEt_4ClO_4 were prepared as described in section **6.2**. All solutions were prepared as a methanol/water (80:20; v/v) solvent system, with constant ionic strength I = 0.1 mol dm^{-3} (NEt_4ClO_4).

The glass electrode was calibrated daily by titrating 0.1 mol dm^{-3} NEt_4OH with 10 cm^3 of a solution of 0.1 mol dm^{-3} NEt_4ClO_4 and 0.0038 mol dm^{-3} $HClO_4$. The resulting data was fitted to the Nernst equation to determine E_0 and pK_w, Equation 6.1.

$$E = E_o + \frac{RT}{F} \ln[H^+] \qquad (6.1)$$

where E = observed potential (V)

E_0 = standard electrode potential (V)

R = gas constant (8.314 J mol^{-1} K^{-1})

T = temperature (K)

F = Faraday's constant (9.6487 x 10^4 Coulombs mol^{-1})

At 298.2 K, with E in millivolts and converting to logarithm base 10:

$$pH = \frac{(E_o - E)}{59.15} \qquad (6.2)$$

where E = observed potential (mV)

$pH = -\log[H^+]$

and

$$pK_w = \frac{(E_o - E)}{59.15} + pOH \qquad (6.3)$$

The program MacCalib[3] was used to calculate the endpoint of the titration (and hence the exact concentration of H^+ used) and the calibration parameters E_0 and pK_w. Diffusion correction terms used for aqueous methanol were E_0 = 3.15 and pK_w = 1.311. Three titrations were performed for each system. The protonation constants were determined by the titration of a 0.1 mol dm^{-3} NEt_4OH with a 10 cm^3 solution of a ligand and $HClO_4$. The NEt_4OH was previously standardised against potassium hydrogen phthalate. The concentration of the ligand of interest and $HClO_4$ in solution varied for each ligand, the following concentrations were used [ligand, ($HClO_4$)]; [(**31**), 9.3 x 10^{-4} mol dm^{-3} (3.8 x 10^{-3} mol dm^{-3})], [(**42**), 8.9 x 10^{-4} mol dm^{-3} (6.0 x 10^{-3} mol dm^{-3})], [(**45**), 8.8 x 10^{-4} mol dm^{-3}, (4.2 x 10^{-3} mol dm^{-3})], [(**46**), 1.1 x 10^{-3} mol dm^{-3}, (9.2 x 10^{-3} mol dm^{-3})], [(**50**), 7.3 x 10^{-4} mol dm^{-3}, (3.1 x 10^{-3} mol dm^{-3})], [(**57**), 3.3 x 10^{-4} mol dm^{-3}, (4.6 x 10^{-3} mol dm^{-3})], [(**58**), 5.3 x 10^{-4} mol dm^{-3}, (5.3 x 10^{-3} mol dm^{-3})] and [(**62**), 4.0 x 10-4 mol dm^{-3}, (5.3 x 10^{-3} mol dm^{-3})].

The determination of metal complex ion stability constants for each ligand was carried out by the addition of a metal salt solution (varying concentration) to the acidified titration solution. [Ligand, M^{2+} range, $HClO_4$]; [(**31**)] 9.1 x 10^{-4} mol dm^{-3}, [M^{2+}] 7.0 x 10^{-4} – 1.5 x 10^{-3} mol dm^{-3}, [$HClO_4$] 3.1 x 10^{-3} mol dm^{-3}, [(**42**)] 8.9 x 10^{-4} mol dm^{-3}, [M^{2+}] 7.0 x 10^{-4} – 1.5 x 10^{-3} mol dm^{-3}, [$HClO_4$] 6.0 x 10^{-3} mol dm^{-3}, [(**45**)] 1.27 x 10^{-3} mol dm^{-3}, [M^{2+}] 7.0 x 10^{-4} – 1.9 x 10^{-3} mol dm^{-3}, [$HClO_4$] 4.3 x 10^{-3} mol dm^{-3}, [(**50**)] 7.3 x 10^{-4} mol dm^{-3}, [M^{2+}] 8.0 x 10^{-4} – 1.04 x 10^{-3} mol dm^{-3}, [$HClO_4$] 3.1 x 10^{-3} mol dm^{-3}, [(**57**)] 3.3 x 10^{-4} mol dm^{-3}, [M^{2+}] 3.0 x 10^{-4} – 1.0 x 10^{-3} mol dm^{-3}, [$HClO_4$] 4.6 x 10^{-3} mol dm^{-3}, [(**58**)] 5.3 x 10^{-4} mol dm^{-3}, [M^{2+}] 4.0 x 10^{-4} – 1.0 x 10^{-3} mol dm^{-3}, [$HClO_4$] 5.3 x 10^{-3} mol dm^{-3}. Where M^{2+} = $Zn(ClO_4)_2$, $Cd(ClO_4)_2$ or $Cu(ClO_4)_2$ for ligands (**31**), (**42**), (**45**) and (**50**) and for ligands (**57**) and (**58**) M^{2+} = $Cd(ClO_4)_2$ or $Cu(ClO_4)_2$.

By means of the Dosimat Autoburette, either constant volume aliquots of the titrant were delivered, or variable successive additions of titrant were added during the titrations, during which the emf decreased by 4 mV. For all titrations, a maximum delay of 300 seconds between each titrant addition was sufficient for equilibrium to be established.

The stability constants for each metal complex ion were determined by means of the Fortran programme SUPERQUAD.[4] The final constants represent an average from at least two calculated titrations where the χ^2 of each run was less than 12.6 at the 95% confidence level.

6.4 Ultraviolet-visible spectroscopy

UV-visible absorbance spectra were recorded by means of a Varian CARY 300 Bio spectrophotometer equipped with matched 1.0 cm path length quartz cells over the wavelength range 300-450 nm at 0.083 nm intervals, with a scan rate of 49.8 nm min^{-1}. The blank used contained all species present in the solutions of interest except for the ligand and metal salt, where applicable. Baseline correction measurements were used for all spectra. All solutions were equilibrated at 298.2 $\pm$ 0.2 K in a thermostatted block throughout the measurements. The concentration of ligand solutions used varied depending on the solubility of the ligand. The concentrations of the ligands for metal binding studies were [(**57**)] 4.1 x 10^{-5} mol dm^{-3}, [(**58**)] 4.7 x 10^{-5} mol dm^{-3} and [(**62**)] 5.5 x 10^{-5} mol dm^{-3}. For the pH titrations the concentrations of the ligands were [(**57**)] 3.3 x 10^{-5} mol dm^{-3}, [(**58**)] 8.6 x 10^{-5} mol dm^{-3} and [(**62**)] 1.2 x 10^{-4} mol dm^{-3}; these solutions were obtained by direct dilution from those used in the potentiometric titrations. All solutions were prepared freshly prior to measurement.

6.5 Fluorescence spectroscopy

Fluorescence measurements were made with a Perkin-Elmer LS-50B spectrofluorimeter equipped with a 1.0 cm path length quartz cell. Data was obtained between 377 and 550 nm with excitation and emission slit widths of 10 nm and 5 nm respectively, by means of a 1 % transmittance emission filter. Two scans at 0.5 nm intervals, with a scan rate of 200 nm min^{-1}, were recorded and averaged. Baseline correction measurements were used for all spectra; a solution containing the solvent, supporting electrolyte and buffer (where applicable) was used. All solutions were equilibrated at 298.2 $\pm$ 0.2 K in a thermostatted block throughout the measurements. The concentrations of the ligands investigated were the same as that used for the UV-visible absorbance measurements, (see section **6.4**). The excitation wavelength for each system studied was selected from within the second longest wavelength absorbance band.

6.6 Stability constants from fluorescence

The metal complex ion stability constants of ligands (**57**), (**58**) and (**62**), were also determined with fluorescence measurements, where the concentrations of metal ions used varied from 0.1 – 4.0 molar equivalents of the ligand depending on the fluorescence observed. The observed fluorescence of a single (metal)•(ligand) complex is given by Equation 6.4,

$$F = \varepsilon_L[\text{ligand}] + \varepsilon_M[\text{metal ion}] + \varepsilon_{M\bullet L}[(\text{metal})\bullet(\text{ligand})] \qquad (6.4)$$

where F = total fluorescence

ε_L, ε_M and $\varepsilon_{M\bullet L}$ = molar fluorescence of the ligand, metal ion and (metal ion)•(ligand) complex

[ligand], [metal] and [(metal ion)•(ligand)] = the equilibrium ligand, metal ion and (metal ion)•(ligand) complex concentrations.

A simultaneous fit over a range of recorded spectral data in Equation 6.4, using a non-linear least squares regression routine, based on Method 5 of Pitha and Jones,[5] by means of the MATLAB programme DATAFIT/SPECFIT[6] was used to determine the metal complex ion stability constants. SPECFIT is designed to calculate stability constants, and their standard deviations from fluorescence spectra, followed by the emission spectra of each species. The experimental data was not weighted.

6.7 Quantum yields

The use of the optically dilute method[7] was employed for the determination of the quantum yields (Φ_F). Equation 6.5 relates the quantum yield of an unknown to that of a reference standard.

$$\Phi_x = \Phi_r \cdot \frac{A_r}{A_x} \cdot \frac{F_x}{F_r} \cdot \frac{(n_x)^2}{(n_r)^2} \qquad (6.5)$$

where x refers to the unknown

r refers to the reference

Φ is the quantum yield

A is the absorbance of the solution at the excitation wavelength

F is the integrated area under the emission spectrum

n is the index of refraction of the solvent

The reference standard used was quinine sulphate (Φ_r = 0.542 in 0.1 mol dm^{-3} sulphuric acid).[8,9] Due to the close proximity of the refractive indices of methanol and water, the refractive index was omitted from calculations. Analytical reagent grade anhydrous quinine sulphate in sulphuric acid (Convol, BDH) at 0.1 mol dm^{-3} was used to prepare the standard solutions.

UV-visible absorbance spectra and fluorescence emission spectra of the standard (quinine sulphate) (5.0 x 10^{-6} mol dm^{-3}) were recorded as described in sections **6.4** and **6.5**. The excitation wavelength for quinine sulphate was matched to that used for the unknown, in each case, to ensure that the intensity of the exciting light was identical. The concentrations for the fluorescence measurements corresponded to absorbances of < 0.03 at the excitation wavelength. Thus corrections for self-absorption, of incident and emitted light on the emission intensities, were not required. Computerised integration was used to calculate the area under each curve, between 377 and 550 nm. Errors in quantum yield values obtained are approximately 10 %.

6.8 Synthesis

1,2-Di(*p*-toluensulfonyloxy)ethane, $TsOCH_2CH_2OTs$, (34).[10]

Triethylamine (98.7 cm^3, 708 mmol) was added dropwise to a stirred solution of ethylene glycol (17.9 cm^3, 322 mmol) in dichloromethane (130 cm^3) at 0°C. A solution of *p*-toluenesulfonyl chloride (128.9 g, 676 mmol) in dichloromethane (390 cm^3) was then added to the reaction mixture in a dropwise manner to maintain the lower temperature. The reaction mixture was then stirred for 2 hrs at room temperature, the solid triethylamine hydrochloride salt was then filtered off and the filtrate was concentrated under reduced pressure to yield a white precipitous slurry. This was washed with ether (500 cm^3) and the remaining solid collected by vacuum filtration. Recrystallisation with ethanol afforded the compound as white crystals (109 g, 90 %), mp 123-125°C (Lit[10] 123-125°C); δ_H(300 MHz, $CDCl_3$) 2.46 (6H, s, 2 x Ar**C**$\mathbf{H}_3$), 4.19 (4H, s, 2 x **C**$\mathbf{H}_2$O), 7.34 (4H, AA' portion of AA'XX', Ar**H**), 7.75 (4H, XX' portion of AA'XX', Ar**H**); δ_C (75.5 MHz) 22.3 (2 x **C**H_3Ar), 67.3 (2 x **C**H_2O), 128.6 (4 x Ar**C**H), 130.6 (4 x Ar**C**H), 132.4 (2 x Ar**C**), 145.2 (2 x Ar**C**); *m/z* (EI) 370 (M^+, 32%), 301 (9), 277 (2), 196 (10), 153 (63), 136 (20).

1,4,7-Tris(*p*-toluensulfonyl)diethylenetriamine, $TsN(CH_2CH_2NHTs)_2$, (35).[11]

Triethylamine (152 g, 1.51 mol) was added dropwise to a stirred solution of diethylenetriamine (50 g, 485 mmol) in dichloromethane (500 cm^3) at 0°C. A solution of *p*-toluensulfonyl chloride (276 g, 1.45 mol) in dichloromethane (300 cm^3) was then added to the stirred reaction mixture in a dropwise manner to maintain the lower temperature. After the addition the reaction mixture was allowed to warm to room temperature where it was left to stir overnight. The resulting white precipitate was filtered off and retained, the filtrate was concentrated under reduced pressure to afford a white solid. Both solids where combined and recrystallised from methanol to afford the title compound as white crystals (243 g, 89 %), mp 174-176°C (Lit[11] mp 173-175°C); δ_H (200 MHz, $CDCl_3$) 2.40 (9H, s, 3 x Ar**C**$\mathbf{H}_3$), 3.14 (8H, m, **C**$\mathbf{H}_2$N and **C**$\mathbf{H}_2$NH) 5.21 (2H, bs, N**H**), 7.23 (2H, AA' portion of AA'XX', Ar**H**), 7.28 (4H, BB' portion of BB'YY', 2 x Ar**H**), 7.60 (2H, XX' portion of AA'XX', Ar**H**), 7.75 (4H, YY' portion of BB'YY', Ar**H**); δ_C (50.28 MHz) 22.2 (3 x Ar**C**H_3), 42.6 (2 x **C**H_2NH), 51.2 (2 x TsN**C**H_2), 127.8 (4 x Ar**C**H), 127.9 (2 x Ar**C**H), 130.5 (4 x Ar**C**H), 130.7 (2 x Ar**C**H), 134.9, 136.9, 143.7, 144.2 (6 x Ar**C**); m/z (EI) 566

[$(M + H)^+$, 70 %), 550 (2), 500 (1), 458 (1), 412 (25), 381 (18), 369 (2), 308 (10), 290 (10), 228 (60), 198 (12), 154 (88).

1,4,7-Tris(*p*-toluenesulfonyl)diethylenetriamine-1,7-disodium salt, (36).[10]

1,4,7,-Tris(*p*-toluenesulfonyl)diethylenetriamine (**35**) (40.95 g, 72.3 mmol) was dissolved in a stirred solution of absolute ethanol (500 cm^3) at 0°C. Sodium metal (4.65 g, 202 mmol) was then added slowly to the reaction mixture under nitrogen to ensure the maintenance of the low temperature. The reaction was then left to stir overnight. The resulting precipitate was collected by vacuum filtration and washed with ethanol (100 cm^3). The solid was then dried under high vacuum to yield a white solid (41 g, 93 %), mp 293-294°C (Lit[10] mp 294-295°C).

1,4,7-Tris(*p*-toluenesulfonyl)-1,4,7-triazacyclononane, (37).[10,12]

1,2-Di(*p*-toluenesulfonyloxy)ethane (**34**) (19 g, 51.4 mmol) in DMF (100 cm^3) was added dropwise to a solution of 1,4,7-tris(*p*-toluenesulfonyl)diethylenetraimine-1,7-disodium salt (**36**) (30 g, 51.4 mmol) in DMF (200 cm^3) at 65 °C. The reaction was then left to stir at 110°C for 12 hours under nitrogen. The solvent was then removed under reduced pressure to yield a thick slurry that was suspended with rapid stirring in ice cold water (100 cm^3), this was left to stir for 30 minutes. The resulting white precipitate was then filtered off and washed successively with water, ethanol and ether. The solid was then dried and recrystallised from acetone/water to yield a white crystalline solid (18 g, 60 %). δ_H (200 MHz, $CDCl_3$) 2.43 (9H, s, 3 x ArCH_3), 3.42 (12H, s, 6 x CH_2N), 7.30 (6H, AA' portion of AA'XX', Ar**H**), 7.68 (6H, XX' portion of AA'XX', Ar**H**); δ_C (50.28 MHz) 21.5 (3 x Ar**C**H_3), 51.9 (3 x N(CH_2)$_2$N ring), 127.5 (6 x Ar**C**H), 129.9 (6 x Ar**C**H), 134.7 (3 x Ar**C**), 143.9 (3 x Ar**C**); *m/z* (EI) 592 [$(M + H)^+$, 4 %], 566 (2), 484 (14), 438 (13), 436 (30), 381 (4), 281 (10).

1,4,7-Triazacyclononane Trihydrobromide, (38).[13]

1,4,7-Tris(*p*-toluenesulfonyl)-1,4,7-triazacyclononane (**37**) (12 g, 20.2 mol) was dissolved in conc. sulphuric acid (80 cm^3) and heated at 110 °C for 3 days under nitrogen. The reaction was then cooled to room temperature and added dropwise to a solution of ethanol (100 cm^3) and ether (35 cm^3) at 0°C. The resulting grey precipitate was collected

and then dissolved in a solution of hot water (10 cm^3). Hydrobromic acid (6 cm^3) was added dropwise to yield a white solid. The mixture was cooled to 0°C and precipitate collected under a constant stream of nitrogen to yield a pale grey solid (6.05 g, 80 %), mp 269-276°C (Lit[11,13] mp 277-278°C); δ_H (200 MHz, D_2O) 4.1 (12H, s, 3 x N($C\mathbf{H}_2$)$_2$N ring); δ_C (50.28 MHz) 44.2 (3 x N($\mathbf{C}H_2$)$_2$N ring); *m/z* (EI) 130 [$(M + H)^+$, 100%), 114 (6), 102 (10), 94 (20), 86 (10), 76 (19), 63 (12).

1,4,7-Triazacyclononane, (39).[11]

1,4,7-Triazacyclononane trihydrobromide (**38**) (6.05 g, 16.2 mmol) was dissolved in a solution of sodium hydroxide (2.07 g, 51 mmol) to give a clear brown solution. Benzene (100 cm^3) was added and the reaction fitted with a dean stark apparatus and left to reflux at 100°C for 2 days to remove water. The reaction was then filtered to remove the precipitate, which was then washed with warm benzene. The filtrate was concentrated under reduced pressure to yield a white oil, which on standing at 0°C formed a white amorphous solid (1.66 g, 80%), mp 43-44°C (Lit[11] mp 42-46°C); δ_H (200 MHz, $CDCl_3$) 1.94 (3H, bs, 3 x N**H**), 2.74 (12H, s, 3 x N($C\mathbf{H}_2$)$_2$N ring); δ_C (50.28 MHz) 47.5 (3 x N($\mathbf{C}H_2$)$_2$N ring); *m/z* (EI) 129 (M^+, 16%), 114 (20), 88 (65), 56 (78).

L-phenylalanine methyl ester, (40).[14]

L-phenylalanine (1 g, 6.05 mmol) was refluxed in a solution of 1.8 mol dm^{-3} hydrochloric acid dissolved in methanol (13.4 cm^3, 12.1 mmol) for 4 hrs. The reaction was then concentrated under reduced pressure to yield a white solid in quantitative yield, m.p.158-160°C, (Lit[14] 158-162°C). δ_H (300 MHz, $CDCl_3$), 3.42 (2H, d, ArC$\mathbf{H}_2$CH), 3.68 (3H, s, OC$\mathbf{H}_3$), 4.38 (1H, m, αC**H**), 7.27-7.30 (5H, m, Ar**H**); δ_C (75.5 MHz) 34.02 (Ar$\mathbf{C}H_2$), 51.99 (O$\mathbf{C}H_3$), 53.35 (α**C**H), 127.00, 128.04, 128.97, 134.20 (**C**=C), 168.79 (**C**=O); *m/z* (EI) 180 [$(M + H)^+$, 4%)], 163 (1), 147 (1), 131 (1), 103 (15), 88 (95).

_N_-bromoacetyl-L-phenylalanine methyl ester, (41).[15]

L-phenylalanine methyl ester (**40**) (10 g, 46.5 mmol) was dissolved in a solution of dry THF (50 cm^3) and triethylamine (13 cm^3, 93 mmol) under nitrogen, the mixture was then cooled to 0°C. A solution of bromoacetyl bromide (4.0 cm^3, 46.0 mmol) in dry THF (50 cm^3) was then added dropwise to the reaction mixture at 0°C, the temperature was not allowed to rise above 10°C. The reaction was left to warm to room temperature over a 1 hr period. The reaction was quenched with a dropwise addition of water (20 cm^3) then extracted with ethyl acetate (40 cm^3) and the organic layer washed with 1 mol dm^{-3} hydrochloric acid (20 cm^3) and saturated solution of sodium bicarbonate (20 cm^3). The organic layer was then dried and the solvent removed under reduced pressure to give a crystalline solid (9.0 g, 65 %) of N-bromoacetyl-L-phenylalanine methyl ester which was used without further purification, mp 55-57°C, δ_H (300 MHz), 3.14 (2H, m, Ar**C**$\mathbf{H}_2$), 3.73 (3H, s, O**C**$\mathbf{H}_3$), 3.84 (2H, s, Br**C**$\mathbf{H}_2$), 4.85 (1H, m, α-C**H**), 6.86 (1H, bs, N**H**), 7.1-7.3 (5H, m Ar**H**); δ_C (75.5 MHz) 28.54 (Ar**C**H_2), 37.6 (O**C**H_3), 52.3 (α**C**H), 53.6 (Br**C**H_2), 127.2, 128.6, 129.2, 135.2 (**C**=C), 165.0, 171.2 (**C**=O); *m/z* (EI) 300 (M^+, 10 %), 178 (5), 162 (60), 131 (20), 91 (95).

_N_-bromoacetyl-L-phenylalanine methyl ester-dimer, (43).

δ_H (300 MHz), 3.14-3.6 (6H, m, C$\mathbf{H}_2$), 3.68 (3H, s, O**C**$\mathbf{H}_3$), 3.74 (3H, s, O**C**$\mathbf{H}_3$), 4.71 (1H, m, α-C**H**), 4.75 (1H, m, α-C**H**), 7.04-7.34 (10H, m Ar**H**); δ_C (75.5 MHz) 28.7, 29.8 (Ar**C**H_2), 37.8, 38.1 (O**C**H_3), 52.4, 52.9 (α**C**H), 53.2 (N**C**H_2), 127.4, 127.8, 128.7, 128.9, 129.3,130.1, 135.7, 136.0 (**C**=C), 166.2, 172.4 (**C**=O); *m/z* (LCQ) 437 (MK^+, 10 %), 398 (30), 367 (28), 339.

1,4,7-*tris*[(2'S)-acetamido-2'-(methyl-3'-phenylpropionate)]-1,4,7-triazacyclononane, (31).[15]

N-bromoacetyl-L-phenylalanine methyl ester (**41**) (470 mg, 1.56 mmol) was dissolved in a solution of diisopropylethylamine (0.49 cm^3, 2.82 mmol) and dry DMF (2 cm^3) under nitrogen and cooled to 0°C. Solid 1,4,7-triazacylcononane (62 mg, 0.487 mmol) was then added and the reaction left to stir overnight under nitrogen. The reaction was diluted in water and extracted with dichloromethane. The solvent was removed under

reduced pressure and the resulting oil washed with water. Purification by means of column chromatography [basic UG alumina, dichloromethane / methanol 10/0.4 (v/v) R_f 0.25] yielded a yellow oil. The oil was re-dissolved in dichloromethane and diethyl ether was then added forming a milky solution which was filtered off and concentrated under reduced pressure to yield a white fluffy solid (250 mg, 65 %), mp 43°C, δ_H (600 MHz, $CDCl_3$) 2.45 (12H, AA'BB', 3 x N(CH_2)$_2$N ring), 3.09 (6H, s, CH_2C=O), 3.16 (6H, m, ArCH_2), 3.72 (9H, s, OCH_3), 4.87 (3H, m, α**C**H), 7.06-7.25 (15H, m, **Ar**H); δ_C (150.8 MHz) 37.5 (ArCH_2), 52.3 (OCH_3), 52.6 (α**C**H), 56.5 (N(CH_2)$_2$)N ring), 62.5 (CH_2C=O), 127.1 (**Ar**H), 128.6 (**Ar**H), 129.2 (**Ar**H), 136.0 (**Ar**H), 170.8 (**C**=ONH), 172.0 (**C**=OCH); *m/z* (LCQ) 786 (M^+ 8%).

Tris(Tetraethylammonium)1,4,7-_tris_[(2'S)-acetamido-2'-(1'-carboxyl-3'-phenylpropane)]-1,4,7-triazacyclononane, (NEt_4)$_3$.(42).

An aqueous solution of 0.1 mol dm^{-3} tetraethylammoniumhydroxide (20 cm^3) was added dropwise to a solution of ligand (**31**) (400 mg, 0.53 mmol) in a solvent mixture of THF / water (10 cm^3 1:1 (v/v)) and stirred under nitrogen at room temperature for 4 days. The solvent was then removed to yield an oil, subsequent washings with acetone and ether removed excess hydroxide to yield a white crystalline product (369 g, 80 %), δ_H (600 MHz, D_2O) 1.21 (36H, t, (CH_3CH_2)$_4$N), 2.40-2.70 (12H, AA'BB', 3 x N(CH_2)$_2$N ring), 2.96 (6H, s, CH_2C=O), 3.14 (6H, m, ArCH_2), 3.17 (24H, q, (CH_3CH_2)$_4$N), 4.50 (3H, m, α**C**H), 7.56-7.97 (15H, m, **Ar**H); δ_C (150.8 MHz) 6.4 ((CH_3CH_2)$_4$N), 37.2 (ArCH_2), 51.8 ((CH_3CH_2)$_4$N), 55.2 (α**C**H), 55.5 (N(CH_2)$_2$)N ring), 61.2 (CH_2C=O), 127.2 (**Ar**H), 129.0 (**Ar**H), 129.4 (**Ar**H), 137.2 (**Ar**H), 173.5 (**C**=ONH), 178.0 (**C**=OCH); *m/z* (LCQ) $C_{63}H_{105}O_9N_9$ 1132 (65 %).

1,4,7-_tris_[(2'S)-acetamido-2'-(1'-carboxyl-3'-phenylpropane)]-1,4,7-triazacyclononane-zinc(II)tetraethylammoniumtriflate·4CH_3OH, [Zn(H_2(42)]NEt_4·2(CF_3SO_3)·4CH_3OH, (44).

A solution of $Zn(CF_3SO_3)_2$ (16 mg, 4.4 x 10^{-5} mol) in methanol (1 cm^3) was added to a solution of ligand (**42**) (50 mg, 4.4 x 10^{-5} mol) in methanol (2 cm^3). A layer of ether (1 cm^3) was then added and the solution was left overnight. The resulting precipitate was then collected by filtration under reduced pressure and dried over P_4O_{10} under reduced

pressure to yield a yellow solid (55 mg, 84 %). (Found: C, 45.83; H, 6.54; N, 7.17. $C_{49}H_{65}N_7O_{15}F_6S_2Zn.(CH_3OH)_4$ requires C,46.65; H, 6.14; N, 7.19 %)

1,4,7,10-*tetrakis*[(2'S)-acetamido-2'-(methyl-3'-phenylpropionate)]-1,4,7,10-tetraacycldodecane, (45).

N-Bromoacetyl-L-phenylalaninemethylester (**41**) (500 mg, 1.66 mmol) was dissolved in diisopropylethylamine (0.46 cm^3, 26.5 mmol) and DMF (5 cm^3) under nitrogen. The solution was cooled to 0° and solid 1,4,7,10-tetraazacyclododecane (57 mg, 0.32 mmol) added. The reaction was left to stir overnight at room temperature and was then diluted with water (20 cm^3) and extracted with dichloromethane. The solvent was removed under reduced pressure and the resulting oil washed with water. Purification by means of column chromatography [basic UG alumina, dichloromethane / methanol 10/0.4 (v/v) R_f 0.25] yielded a yellow oil. The oil was re-dissolved in dichloromethane and diethyl ether was then added forming a milky solution which was filtered off and concentrated under reduced pressure to yield a white fluffy solid (250 mg, 50 %), δ_H (600 MHz, $CDCl_3$) 2.36-2.57 (16H, m, AA'BB', 4 x N(C**H**$_2$)$_2$N ring), 3.01 (8H, s, C**H**$_2$C=O), 3.09 (8H, m, ArC**H**$_2$), 3.68 (12H, s, OC**H**$_3$), 4.87 (4H, m, αC**H**), 7.08-7.24 (20H, m, Ar**H**); δ_C (150.8 MHz) 37.5 (Ar**C**H$_2$), 52.2 (O**C**H$_3$), 53.1 (α**C**H), 56.3 (N(**C**H$_2$)$_2$)N ring), 62.3 (**C**H$_2$C=O), 127.0 (**Ar**H), 128.4 (**Ar**H), 129.0 (**Ar**H), 136.0 (**Ar**H), 170.7 (**C**=ONH), 172.0 (**C**=OCH); *m/z* (LCQ) 1071.6 (M + Na^+)(95 %); (Found: C, 62.95; H, 6.95; N, 10.51. $C_{56}H_{72}N_8O_{12}.H_2O$ requires C, 63.01; H, 6.99; N, 10.50%)

Tetrakis(tetraethylammonium)1,4,7,10-*tetrakis*[(2'S)-acetamido-2'-(1'-carboxy-3'-phenylpropane)]-1,4,7,10-tetraazacyclododecane, $(NEt_4)_4$.(46).

An aqueous solution of 0.1 mol dm^{-3} tetraethylammoniumhydroxide (42 cm^3) was added dropwise to a solution of ligand (**45**) (600 mg, 0.57 mmol) in a solvent mixture of THF/water (20 cm^3 1:1 (v/v)) and stirred under nitrogen at room temperature for 4 days. The solvent was then removed under reduced pressure to yield an oil, subsequent washings with acetone and ether removed excess hydroxide to yield a white crystalline product (410 mg, 80%), δ_H (600 MHz, D_2O) 1.21 (48H, t, (C**H**$_3$CH$_2$)$_4$N), 2.10-2.40 (16H, AA'BB', 4 x N(C**H**$_2$)$_2$N ring), 2.86-3.14 (16H, m, C**H**$_2$C=O and ArC**H**$_2$), 3.19 (32H, q, (CH$_3$C**H**$_2$)$_4$N), 4.50 (4H, m, αC**H**), 7.09-7.48 (20H, m, Ar**H**); δ_C (150.8 MHz) 8.45 ((**C**H$_3$CH$_2$)$_4$N), 37.2 (Ar**C**H$_2$), 53.9 ((CH$_3$**C**H$_2$)$_4$N), 55.2 (α**C**H), 55.5 (N(**C**H$_2$)$_2$)N ring), 61.2 (**C**H$_2$C=O), 127.2

(**Ar**H), 129.0 (**Ar**H), 129.4 (**Ar**H), 137.2 (**Ar**H), 173.5 (**C**=ONH), 178.0 (**C**=OCH); *m/z* (LCQ) $C_{52}H_{64}N_8O_{12}$, 993.5 (98 %).

Bis(tetraethylammonium)1,4,7,10-*tetrakis*[(2'S)-acetamido-2'-(1'-carboxy-3'-phenylpropane)]-1,4,7,10-tetraazacyclododecanezinc(II)ditriflate·6CH_3OH, (NEt_4)$_2$[Zn(H_2(46)](CF_3SO_3)$_2$·6CH_3OH, (47).

A solution of $Zn(CF_3SO_3)_2$ (11 mg, 3 x 10^{-5} mol) in methanol (1 cm^3) was added to a solution of ligand (**46**) (50 mg, 3 x 10^{-5} mol) in methanol (2 cm^3). A layer of ether (1 cm^3) was then added and the solution was left overnight. The resulting precipitate was then collected by means of vacuum filtration and dried to yield a yellow solid (51 mg, 85 %). (Found: C, 50.45; H, 7.45; N, 7.60. $C_{70}H_{104}N_{10}O_{18}F_6S_2Zn.(CH_3OH)_6$ requires C, 50.50; H, 7.04; N, 7.76%).

L-tryptophan methyl ester hydrochloride, (48).[16]

L-tryptophan (5 g, 24.5 mmol) was refluxed in a solution of 1.8 mol dm^{-3} hydrochloric acid dissolved in methanol (37 cm^3, 49 mmol) for 3 hrs. The reaction was then concentrated under reduced pressure to yield a white solid in quantitative yield, m.p.217-218°C, (Lit[16] 218-220°C). δ_H (200 MHz, DMSO), 3.57 (2H, d, ArC**H**$_2$CH), 3.85 (3H, s, OC**H**$_3$), 4.49 (1H, m, αC**H**), 7.21-7.73 (5H, m, Ar**H**), 8.97 (2H, s, N**H**), 11.33 (1H, s, N**H**); δ_C (50.28 MHz) 26.4 (Ar**C**H$_2$), 52.6 (O**C**H$_3$) 52.9 (α**C**H), 106.6, 111.9, 118.3, 118.9, 121.5, 125.3, 127.2, 136.5 (**Ar**H), 170 (**C**=OCH); *m/z* (EI) 218 [(M + H)$^+$, 20%)], 158 (6), 130 (95).

***N*-bromoacetyl-L-Tryptophan methyl ester, (49).**

L-tryptophan methyl ester hydrochloride (**48**) (9 g, 35.4 mmol) was dissolved in a solution of dry THF (100 cm^3) and triethylamine (18.7 cm^3, 134.5 mmol) under nitrogen and cooled to 0°C. A solution of bromoacetyl bromide (3.99 cm^3, 46 mmol) in dry THF (50 cm^3) was then added dropwise to the reaction mixture at 0°C. The reaction was allowed to warm to room temperature over a 1 hr period and was then quenched with a dropwise addition of water (20 cm^3). The solution was extracted with ethyl acetate (40 cm^3) and the organic layer washed with 1 mol dm^{-3} hydrochloric acid (20 cm^3) followed by a saturated solution of sodium bicarbonate (20 cm^3). The organic layer was then dried and

solvent removed under reduced pressure to give a crystalline solid (9.9 g, 75 %) of *N*-bromoacetyl-L-phenylalanine methyl ester which was used without further purification, mp 56-63°C, δ_H (200 MHz), 3.33 (2H, d, ArC**H**$_2$), 3.68 (3H, s, OC**H**$_3$), 3.82 (2H, s, BrC**H**$_2$), 4.87 (1H, m, α-C**H**), 7.00-7.55 (5H, m Ar**H**) 8.34 (1H, bs, N**H**); δ_C (50.28 MHz) 27.0 (Ar**C**H$_2$), 28.6 (O**C**H$_3$), 52.4 (α**C**H), 53.4 (Br**C**H$_2$), 109.3, 111.2, 118.3, 118.4, 119.6, 122.2, 127.3, 136.0, (**Ar**H), 165.2, 171.6 (**C**=O); *m/z* (EI) 338 (M^+), 258 (20), 201 (19), 170 (9), 130 (98).

1,4,7-*tris*[(2'S)-acetamido-2'-(methyl-3'-(1*H*-3-indolyl)propionate)]-1,4,7-triazacyclonane, (50).

N-bromoacetyl-L-tryptophan methyl ester (**49**) (3.43 mg, 9.0 mmol) was dissolved in a solution of diisopropylethylamine (2.72 cm^3, 15.6 mmol) and dry DMF (6 cm^3) under nitrogen and cooled to 0°C. Solid 1,4,7-triaazacyclononane (358 mg, 2.7 mmol) was then added and the solution was left to stir overnight under nitrogen. The solution was diluted in water and extracted with dichloromethane. The solvent was removed under reduced pressure and the resulting oil washed with water. Purification by means of column chromatography [basic UG alumina, dichloromethane / methanol 10/0.4 (v/v) R_f 0.25] yielded a white fluffy solid (1.19 g, 52 %), δ_H (600 MHz, $CDCl_3$) 2.45 (12H, AA'BB', 3 x N(C**H**$_2$)$_2$N ring), 3.09 (6H, s, C**H**$_2$C=O), 3.16 (6H, m, ArC**H**$_2$), 3.72 (9H, s, OC**H**$_3$), 4.87 (3H, m, α**C**H), 7.06-7.25 (15H, m, Ar**H**); δ_C (150.8 MHz) 37.5 (Ar**C**H$_2$), 52.3 (O**C**H$_3$), 52.6 (α**C**H), 56.5 (N(**C**H$_2$)$_2$)N ring), 62.5 (**C**H$_2$C=O), 109.5, 111.4, 118.4, 119.5, 122.1, 123.0, 127.7, 136.0 (**Ar**H), 170.8 (**C**=ONH), 172.0 (**C**=OCH); *m/z* (LCQ) 904 (M^+ 95%).

1,4,7-*tris*[(2'S)-acetamido-2'-(methyl-3'-(1*H*-3-indolyl)propionate)]-1,4,7-triazacyclonane zinc ditriflate.CH_3OH, [Zn(50)]·$(CF_3SO_3)_2$·CH_3OH, (52).

A solution of $Zn(CF_3SO_3)_2$ (5.8 mg, 0.0016 mmol) in methanol (1 cm^3) was added to a solution of ligand (**50**) (20 mg, 0.0022 mmol) in methanol (2 cm^3). A layer of ether (1 cm^3) was then added and the resulting solution was left overnight. The resulting precipitate was then collected by means of vacuum filtration and dried to yield a yellow solid (12 mg, 60 %). (Found: C, 47.27; H, 4.57; N, 9.58. $C_{50}H_{57}N_9O_{15}F_6S_2Zn.CH_3OH$ requires C, 47.18; H, 4.74; N, 9.71 %).

1,4,7,10-*tetrakis*[(2'S)-acetamido-2'-(methyl-3'-(1*H*-3-indolyl)propionate)]-1,4,7,10-tetraacyclododecane, (51).

N-bromoacetyl-L-tryptophan methyl ester (**49**) (2.7 g, 8.0 mmol) was dissolved in a solution of diisopropylethylamine (2.63 cm^3, 14.4 mmol) and dry DMF (5 cm^3) under nitrogen and cooled to 0°C. Solid 1,4,7,10-tetraazacycdodecane (522 mg, 3.0 mmol) was then added and the reaction left to stir overnight under nitrogen. The reaction was diluted in water and extracted with dichloromethane. The solvent was removed *in vacuo* and the resulting oil washed with water. Purification by means of column chromatography [basic UG alumina, dichloromethane / methanol 10/0.4 (v/v) R_f 0.25] did not result in the desired product. Three inseparable isomers, the tri-, di- and mono- substituted ligands were obtained, *m/z* (LCQ) 947 (M^+ 62%), 734 (M^+ 98 %) and 477 (M^+ 99 %) respectively.

9-Anthraldehyde, (53).[17]

Anthracene (17.8 g, 0.1 mol), DMF (20 cm^3, 0.26 mol) and *o*-dichlorobenzene (20 cm^3) were placed in a two neck round bottom flask fitted with a reflux condenser, pressure equalizing dropping funnel and a calcium chloride guard tube. Freshly distilled phosphorous oxychloride (16 cm^3, 0.175 mol) was then added dropwise, after addition the reaction was heated at 95°C for an hour. The resulting solution was cooled and neutralised with a solution of sodium acetate trihyrdrate (100 g in 175 cm^3). On standing a yellow precipitate formed, this was collected and washed with conc. sulfuric acid (100 cm^3) and water (1 m^3). The remaining solid was then recrystallised with acetic acid to yield a yellow solid (15.04 g, 73 %) mp 103-104°C [Lit[17] 104-105°C]; δ_H (300 MHz, $CDCl_3$) 7.53 (2H, q, Anth**H**), 7.66 (2H, q, Anth**H**), 8.06 (2H, d, Anth**H**), 8.72 (1H, s, Anth**H**), 9.02 (2H, d, Anth**H**), 11.55 (1H, s, C=O**H**); δ_C (75.5 MHz) 123.5, 124.5, 125.7, 129.1, 129.2, 131.1, 132.1, 135.2 (Anth), 192.9 (**C**=O); *m/z* (EI) 206 (M^+ 80 %), 205 (30), 177 (57).

2-Bromoethyl-9-methylimino anthracene, (54).[18]

2-Bromoethylamine hydrobromide (5.96 g, 0.029 mol) was dissolved in a solution of 1 mol dm^{-3} NaOH (30 cm^3) and extracted with CH_2Cl_2 (5 x 30 cm^3). The organic extracts were combined and concentrated under reduced pressure to approximately 30 cm^3, this then was added dropwise to a solution of 9-anthraldehyde (**53**) (5 g, 0.024 mol) in CH_2Cl_2 (30 cm^3). The reaction was left to stir at room temperature for an hour then dried

over sodium sulphate, filtered and concentrated under reduced pressure and recrystallised from ether/hexane to yield a yellow solid (5 g, 66 %) mp 84-87°C; δ_H (300 MHz, $CDCl_3$) 3.92 (2H, t, C**H**$_2$N) 4.39 (2H, t, C**H**$_2$Br), 7.47 (4H, m, Anth**H**), 8.01 (2H, m, Anth**H**), 8.58 (3H, m, Anth**H**), 9.47 (1H, s, N=C**H**); δ_C (75.5 MHz) 33.0 (**C**H$_2$), 63.9 (**C**H$_2$), 122.7, 123.6, 124.8, 125.3, 126.8, 128.8, 130.0, 131.1 (Anth), 131.2 (**C**=N); *m/z* (EI) 312 (M^+, 98 %), 218 (87), 204 (70), 177 (40).

_N_-(2-(9-anthracenylmethyl)iminoethyl)-1,4,7,10-tetraazcyclodecane, (55).[19]

1,4,7,10-tetraazacyclododecane (2.85 g, 16 mmol) was dissolved in hot toluene (10 cm^3) and 2-bromoethyl-9-methylimino anthracene (**54**) (1 g, 3 mmol) added as a solid. The solution was heated at reflux for 3 hrs after which the reaction was cooled and filtered to remove excess ammonium salt, the filtrate was then washed with 0.1 mol dm^{-3} NaOH (100 cm^3). The organic layer dried and concentrated *in vacuo* to yield a yellow solid (4.38 g, 85 %); δ_H (300 MHz, $CDCl_3$) 2.50 (4H, m, N(C**H**$_2$)$_2$N ring), 2.67 (14H, m, N(C**H**$_2$)$_2$N ring and C**H**$_2$) 3.07 (2H, m, C**H**$_2$), 7.48 (4H, m, Anth**H**), 8.00 (2H, m, Anth**H**), 8.63 (3H, m, Anth**H**), 9.54 (1H, s, N=C**H**). This was used unpurified in the next step.

_N_-(2-(9-anthracenylmethyl)aminoethyl)-1,4,7,10-tetraazcyclodecane, (56).[19]

Crude (**55**) (2.25 g, 5.7 mmol) was dissolved in ethanol (20 cm^3) and $NaBH_4$ (240 mg, 6.3 mmol) added portion-wise, the reaction was left to stir overnight at room temperature. The reaction was then diluted with water (20 cm^3) and extracted with CH_2Cl_2, the organic layer dried and concentrated under reduced pressure to yield a brown oil. Purification by means of column chromatography [basic UG alumina, dichloromethane / methanol 10/0.2 (v/v) R_f 0.2] yielded a yellow solid. (1.6 g, 73 %); δ_H (300 MHz, $CDCl_3$) 2.24 (4H, m, N(C**H**$_2$)$_2$N ring), 2.40 (12H, m, N(C**H**$_2$)$_2$N ring), 2.55 (2H, m, C**H**$_2$), 2.92 (2H, m, C**H**$_2$), 4.62 (2H, m, C**H**$_2$), 7.40 (4H, m, Anth**H**), 7.85 (2H, m, Anth**H**), 8.29 (3H, m, Anth**H**); δ_C (75.5 MHz) 44.9, 45.6, (N(**C**H$_2$)$_2$N ring), 45.7 (**C**H$_2$), 46.6 (N(**C**H$_2$)$_2$N ring), 48.0 (**C**H$_2$), 52.0 (N(**C**H$_2$)$_2$N ring), 54.8 (**C**H$_2$), 122.8, 123.4, 124.9, 125.0, 126.9, 128.7, 130.1, 131.0 (Anth), ; *m/z* (LCQ) 468 ($M^+ + Na^+ + K^+$ 95%).

Synthesis of the anthracene substituted ligands (57), (58), (59) and (60).

To a solution of N-bromoacetyl-L-phenylalanine methyl ester (**41**) (1 g, 3 mmol) and diisopropylethylamine (0.86 cm^3, 5 mmol) in DMF (3 cm^3) a solution of ligand (**56**) (338 mg, 8 x 10^{-4} mol) in DMF (2 cm^3) was added. The reaction was stirred under an atmosphere of nitrogen overnight. The reaction was subsequently diluted in water and extracted with dichloromethane. The solvent was removed under reduced pressure and the resulting oil washed with water. Purification by means of column chromatography [basic UG alumina, dichloromethane / methanol 10/0.2 (v/v) R_f 0.15, 0.10 and 0.05] yielded three compounds as yellow oils. Each was redissolved in dichloromethane and a small quantity of diethylether added, they were then dried under high vacuum. The yields obtained for the (**57**), (**58**) and the composite of (**59**) and (**60**) are 2.4 %, 58 % and 20 % respectively.

1,4,7-*tris*[(2'S)-acetamido-2'-(methyl-3'-phenylpropionate)]-10-(2-*N*-(9-anthrylmethylamino)ethyl-1,4,7,10-tetraacycldodecane, (57).

δ_H (600 MHz, $CDCl_3$) 2.28-2.43 (20H, m, 4 x N(C**H**$_2$)$_2$N ring and 2 x C**H**$_2$), 2.75-3.19 (12H, m, C**H**$_2$), 3.68 (9H, m, OC**H**$_3$), 4.69 (2H, s, C**H**$_2$Anth), 4.75-4.82 (3H, m, αC**H**), 7.04-7.26 (15H, m, Ar**H**) 7.34-8.40 (9H, m, Anth**H**); δ_C (150.8 MHz) 29.9 (Anth**C**H$_2$), 37.9 (Ar**C**H$_2$), 51.5 (Anth**C**H$_2$) 52.4 (O**C**H$_3$), 52.9 (α**C**H), 53.8 (N(**C**H$_2$)$_2$)N ring), 57.8 (Anth**C**H$_2$) 59.5 (**C**H$_2$C=O), 124.5, 125.3, 126.7 (**Anth**H), 127.1 (**Ar**H), 128.4 (**Anth**H), 128.6 129.2 (**Ar**H), 129.7, 131.5, 131.7 (**Anth**H), 136.4 (**Ar**H), 171.2 (**C**=ONH$_2$), 172.0 (**C**=OCH); *m/z* (LCQ) 1063 (M^+ 95%), (Found: C, 64.69; H, 6.83; N, 9.55. $C_{61}H_{74}N_8O_9.4H_2O$ requires C, 64.52; H, 7.28; N, 9.87 %).

1,4,7-*tris*[(2'S)-acetamido-2'-(methyl-3'-phenylpropionate)]-10-(2-*N*-(9-anthrylmethyl)-*N*-[(2'S)-acetamido-2'-(methyl-3'-phenylpropionate)]-1,4,7,10-tetraacycldodecane, (58).

δ_H (600 MHz, $CDCl_3$) 2.02-2.58 (20H, m, 4 x N(C**H**$_2$)$_2$N ring 2 x C**H**$_2$), 2.71-3.26 (16H, m, C**H**$_2$), 3.57-3.74 (12H, m, OC**H**$_3$), 4.56-4.62 (2H, d, C**H**$_2$Anth), 4.71-4.83 (4H, m, αC**H**) 6.94-7.28 (20H, m, Ar**H**) 7.43-8.47 (9H, m, Anth**H**); δ_C (150.8 MHz) 29.9 (Anth**C**H$_2$), 37.7, 38.3 (Ar**C**H$_2$), 51.5 (Anth**C**H$_2$) 52.4, 52.5 (O**C**H$_3$), 52.9. 53.0 (α**C**H), 53.6, 54.1 (N(**C**H$_2$)$_2$)N ring), 57.8 (Anth**C**H$_2$) 59.1, 59.7 (**C**H$_2$C=O), 124.5, 125.3, 126.7 (**Anth**H), 127.0, 127.3 (**Ar**H), 128.4 (**Anth**H), 128.5, 128.8, 129.0, 129.4 (**Ar**H), 129.7,

131.5, 131.7 (**Anth**H), 136.1, 136.5 (**Ar**H), 171.2, 171.3 (**C**=ONH$_2$), 172.0, 172.4 (**C**=OCH); *m/z* (LCQ) 1282 (M^+ 95%), (Found: C, 66.04; H, 6.83; N, 9.02. $C_{73}H_{87}N_9O_{12}.2H_2O$ requires C, 66.48; H, 6.96; N, 9.56 %).

1,4-*di*[(2'S)-acetamido-2'-(methyl-3'-phenylpropionate)]-10-(2-*N*-(9-anthrylmethyl)-*N*-[(2'S)-acetamido-2'-(methyl-3'-phenylpropionate)]-1,4,7,10-tetraacycldodecane, (59).

Or

1,7-*di*[(2'S)-acetamido-2'-(methyl-3'-phenylpropionate)]-10-(2-*N*-(9-anthrylmethyl)-*N*-[(2'S)-acetamido-2'-(methyl-3'-phenylpropionate)]-1,4,7,10-tetraacycldodecane, (60).

δ_H (600 MHz, $CDCl_3$) 2.22-2.73 (20H, m, 4 x N(C**H**$_2$)$_2$N ring and 2 x C**H**$_2$), 2.78-3.23 (12H, m, C**H**$_2$), 3.51-3.74 (9H, m, OC**H**$_3$), 4.51-4.70 (2H, d, C**H**$_2$Anth), 4.82-4.84 (3H, m, αC**H**), 6.51 (1H, d, N**H**), 6.88-7.27 (15H, m, Ar**H**) 7.39-8.48 (9H, m, Anth**H**); δ_C (150.8 MHz) 29.9 (Anth**C**H$_2$), 38.1, 38.2, 38.7 (Ar**C**H$_2$), 51.5 (Anth**C**H$_2$) 52.8, 52.9, 53.0 (O**C**H$_3$), 53.3, 53.4, 53.5 (α**C**H), 53.9, 54.0, 54.3, 54.6 (N(**C**H$_2$)$_2$)N ring), 55.5 (Anth**C**H$_2$) 59.7, 59.8, 60.0 (**C**H$_2$C=O), the assignment of the aromatic region was difficult due to overlay, 171.5, 171.6, 171.7 (**C**=ONH$_2$), 172.74, 172.79, 172.8 (**C**=OCH); *m/z* (LCQ) 1063 (M^+ 99 %)

1,4,7-*tris*[2-hydroxyethyl]-10-(2-*N*-(9-anthrylmethyl)-*N*-(2-hydroxyethyl)amino-ethyl)-1,4,7,10-tetraacyclododecane, (62).

Ethylene oxide (0.229 cm^3, 4.59 mmol) at 0°C was added to a solution of ligand (**56**) (453 mg, 1.12 mmol) in ethanol (20 cm^3). The reaction was then left in the dark for 4 days. The solvent was removed under reduced pressure. Purification by means of column chromatography [basic UG alumina, dichloromethane / methanol 10/0.2 (v/v) R_f 0.15] yielded the product (**62**) (200 mg, 30 % yield). δ_H (600 MHz, $CDCl_3$) 2.22-2.53 (20H, m, 4 x N(C**H**$_2$)$_2$N ring and 2 x C**H**$_2$), 2.72 (3H, t, C**H**$_2$), 2.82 (3H, t, C**H**$_2$), 2.93 (2H, t, C**H**$_2$), 3.47 (3H, t, C**H**$_2$), 3.55 (3H, t, C**H**$_2$), 3.61 (2H, t, C**H**$_2$), 4.63 (2H, d, C**H**$_2$), 7.42-7.56 (4H, m, Anth**H**), 7.97 (2H, d, Anth**H**), 8.38 (3H, m, Anth**H**); δ_C (150.8 MHz) 51.1, 51.5, 51.6, 52.0, 52.6, 52.8, 54.2, 57.0, 57.4, 59.3, 59.6, 60.2, 66.4 (**C**H$_2$), 125.3, 125.5, 126.6, 128.4,

129.7, 130.2, 131.9, 132.0 (**Anth**H); *m/z* (LCQ) 604 (M^+ + Na^+ 99 %) 582 (M^+ 35%), (Found: C, 67.55; H, 8.90; N, 11.53. $C_{33}H_{51}N_5O_4$ requires C, 68.11; H, 8.84; N, 12.04 %).

6.9 References

(1) Perrin, D. D.; Aramego, W. L. F.; Perrin, D. R. *Purificiation of Laboratory Chemicals*; 2nd ed.; Permagon: Oxford, UK, 1980.

(2) Perrin, D. D.; Dempsey, B. *Buffers for pH and Metal Ion Control*; Chapman and Hall: London, 1974.

(3) Duckworth, P., Private Communication.

(4) Gans, P.; Sabatini, A.; Vacca, A. *J. Chem. Soc., Dalton Trans.* **1985**, 1195-1200.

(5) Pitha, J.; Jones, R. N. *Can. J. Chem.* **1966**, *44*, 3031-3050.

(6) Kuruscev, T., Private Communication.

(7) Demas, J. N.; Crosby, G. A. *J. Phys. Chem.* **1971**, *75*, 991-1024.

(8) Olmsted, J. *J. Phys. Chem.* **1979**, *83*, 2581-2584.

(9) Melhuish, W. H. *J. Phys. Chem.* **1961**, *65*, 229-235.

(10) McAuley, A.; Norman, P. R.; Olubuyide, O. *Inorg. Chem.* **1994**, *23*, 1938-1943.

(11) Searle, G. H.; Geue, R. J. *Aust. J. Chem.* **1984**, *37*, 959-970.

(12) Richman, J. E.; Atkins, T. J. *J. Am. Chem. Soc.* **1974**, *96*, 2268-2270.

(13) Yang, R.; Zompa, L. *Inorg. Chem.* **1976**, *15*, 1499-1502.

(14) In *Beilstein*; Springer-Verlag: Berlin; Vol. 14, p 499.

(15) Watson, A. A.; Willis, A. C.; Fairlie, D. P. *Inorg. Chem.* **1997**, *36*, 752-753.

(16) In *Beilstein*; Springer-Verlag: Berlin; Vol. 22, p 6771.

(17) Fieser, L. F.; Hartwell, J. L.; Jones, J. E.; Wood, J. H.; Bost, R. W. In *Organic Syntheses*; Allen, F. H., VanAllan, J., Eds.; John Wiley and Sons: New York, 1955; Vol. Collective Volume 3, pp 98-99.

(18) Fabbrizzi, L.; Licchelli, M.; Perotti, A.; Poggi, A.; Rabaioli, G.; Sacchi, D.; Taglietti, A. *J. Chem. Soc., Perkin Trans. 2* **2001**, 2108-2113.

(19) Aoki, S.; Kaido, S.; Fujioka, H.; Kimura, E. *Inorg. Chem.* **2003**, *42*, 1023-1030.

Appendix A

A.1 NMR spectral data

Ligand (31)

δ_H (600 MHz, CD_3OD) 2.45 ([H_a, H_b, H_c, H_d], 12H, AA'BB', 3 x N($C\mathbf{H}_2$)$_2$N ring), 3.05 ([H_f, H_e], 6H, s, $C\mathbf{H}_2$C=O), 3.18 ([H_g, H_h], 6H, m, Ar$C\mathbf{H}_2$), 3.71 (9H, s, O$C\mathbf{H}_3$), 4.74 ([H_i], 3H, m, α$C\mathbf{H}$), 7.06-7.25 (15H, m, Ar**H**); δ_C (150.8 MHz) 38.6 (Ar$C\mathbf{H}_2$), 53.3 (O$C\mathbf{H}_3$), 55.0 (α**C**H), 58.1 (N($C\mathbf{H}_2$)$_2$)N ring), 63.0 ($C\mathbf{H}_2$C=O), 128.3 (**Ar**H), 130.8 (**Ar**H), 133.0 (**Ar**H), 138.4 (**Ar**H), 173.8 (**C**=ONH_2), 174.4 (**C**=OCH_3).

[Zn(31)]$^{2+}$

δ_H (600 MHz, CD_3OD) 1.81 ([H_a], 3H, m, N($C\mathbf{H}_2$)$_2$N ring), 2.45 ([H_c], 3H, m, N($C\mathbf{H}_2$)$_2$N ring), 2.61 ([H_b], 3H, m, N($C\mathbf{H}_2$)$_2$N ring), 2.85 ([H_g], 3H, m, Ar$C\mathbf{H}_2$), 2.89 ([H_d], 3H, m, N($C\mathbf{H}_2$)$_2$N ring), 3.16 ([H_f], 3H, d, J = 16.5 Hz, $C\mathbf{H}_2$C=O), 3.33 ([H_h], 3H, m, Ar$C\mathbf{H}_2$), 3.55 ([H_e], 3H, d, J = 16.5 Hz, $C\mathbf{H}_2$C=O), 3.83 (9H, s, O$C\mathbf{H}_3$), 4.98 ([H_i], 3H, m, α$C\mathbf{H}$), 7.17-7.29 (15H, m, Ar**H**); δ_C (150.8 MHz) 39.4 (Ar$C\mathbf{H}_2$), 50.4 (N($C\mathbf{H}_2$)$_2$)N ring), 53.5 (N($C\mathbf{H}_2$)$_2$)N ring), 53.7 (O$C\mathbf{H}_3$), 56.7 (α**C**H), 59.5 ($C\mathbf{H}_2$C=O), 128.6 (**Ar**H), 130.1 (**Ar**H), 131.2 (**Ar**H), 138.5 (**Ar**H), 172.2 (**C**=OCH_3), 174.7 (**C**=ONH_2).

[Cd(31)]$^{2+}$

δ_H (600 MHz, CD_3OD) 2.30 ([H_a, H_c], 6H, m, N($C\mathbf{H}_2$)$_2$N ring), 2.69 ([H_d], 3H, m, N($C\mathbf{H}_2$)$_2$N ring), 2.82 ([H_b], 3H, m, N($C\mathbf{H}_2$)$_2$N ring), 2.95 ([H_g], 3H, m, Ar$C\mathbf{H}_2$), 3.22 ([H_h], 3H, m, Ar$C\mathbf{H}_2$), 3.43 ([H_e, H_f], 6H, bs, $C\mathbf{H}_2$C=O), 3.71 (9H, s, O$C\mathbf{H}_3$), 4.89 ([H_i], 3H, m, α$C\mathbf{H}$), 7.17-7.28 (15H, m, Ar**H**); δ_C (150.8 MHz) 38.9 (Ar$C\mathbf{H}_2$), 53.0 (N($C\mathbf{H}_2$)$_2$)N ring), 53.5 (O$C\mathbf{H}_3$), 53.8 (N($C\mathbf{H}_2$)$_2$)N ring), 56.3 (α**C**H), 61.6 ($C\mathbf{H}_2$C=O), 128.6 (**Ar**H), 130.0 (**Ar**H), 130.9 (**Ar**H), 138.3 (**Ar**H), 172.8 (**C**=OCH_3), 173.9 (**C**=ONH_2).

Ligand (45)

δ_H (600 MHz, CD_3CN) 2.39 ([H_a, H_c], 8H, AA'BB', 4 x N($C\mathbf{H}_2$)$_2$N ring), 2.48 ([H_b, H_d], 8H, AA'BB', 4 x N($C\mathbf{H}_2$)$_2$N ring), 2.88 ([H_e, H_f], 8H, m, $C\mathbf{H}_2$C=O), 3.02 ([H_g], 4H, m, Ar$C\mathbf{H}_2$), 3.10 ([H_h], 4H, m, Ar$C\mathbf{H}_2$), 3.61 (12H, s, O$C\mathbf{H}_3$), 4.62 ([H_i], 4H, m, α$C\mathbf{H}$), 7.14-7.43 (20H, m, Ar**H**); δ_C (150.8 MHz) 37.9 (Ar$C\mathbf{H}_2$), 52.7 (O$C\mathbf{H}_3$), 53.6 (α**C**H), 54.3

(N($\mathbf{C}H_2)_2$)N ring), 59.5 ($\mathbf{C}H_2$C=O), 127.6 (**Ar**H), 129.3 (**Ar**H), 130.4 (**Ar**H), 138.0 (**Ar**H), 171.8 (**C**=ONH_2), 173.1 (**C**=OCH_3).

[Zn(45)]$^{2+}$

δ_H (600 MHz, CD_3CN) 2.03 ([H_a], 4H, m, N($C\mathbf{H}_2)_2$N ring), 2.35 ([H_c], 4H, m, N($C\mathbf{H}_2)_2$N ring), 2.54 ([H_b], 4H, m, N($C\mathbf{H}_2)_2$N ring), 2.73 ([H_d], 4H, m, N($C\mathbf{H}_2)_2$N ring), 2.82 ([H_e], 4H, m, $C\mathbf{H}_2$C=O), 2.88 ([H_f], 4H, m, $C\mathbf{H}_2$C=O), 2.92 ([H_g], 4H, m, Ar$C\mathbf{H}_2$), 3.14 ([H_h], 4H, m, Ar$C\mathbf{H}_2$), 3.65 (12H, s, O$C\mathbf{H}_3$), 4.64 ([H_i], 4H, m, α**C**H), 7.18-7.40 (20H, m, Ar**H**); δ_C (150.8 MHz) 38.3 (Ar$\mathbf{C}H_2$), 50.1 (N($\mathbf{C}H_2)_2$)N ring), 51.6 (N($\mathbf{C}H_2)_2$)N ring), 53.1 (O$\mathbf{C}H_3$), 55.2 (α**C**H), 56.4 ($\mathbf{C}H_2$C=O), 128.0 (**Ar**H), 129.6 (**Ar**H), 130.4 (**Ar**H), 137.7 (**Ar**H), 171.8 (**C**=OCH_3), 172.0 (**C**=ONH_2).

[Cd(45)]$^{2+}$

δ_H (600 MHz, CD_3CN) 1.28 ([H_a], 4H, m, N($C\mathbf{H}_2)_2$N ring), 1.96 ([H_c], 4H, m, N($C\mathbf{H}_2)_2$N ring), 2.03 ([H_e], 4H, m, $C\mathbf{H}_2$C=O) 2.12 ([H_b], 4H, m, N($C\mathbf{H}_2)_2$N ring), 2.49 ([H_f], 4H, m, $C\mathbf{H}_2$C=O), 2.65 ([H_d], 4H, m, N($C\mathbf{H}_2)_2$N ring), 2.88 ([H_g], 4H, m, Ar$C\mathbf{H}_2$), 3.27 ([H_h], 4H, m, Ar$C\mathbf{H}_2$), 3.84 (12H, s, O$C\mathbf{H}_3$), 4.76 ([H_i], 4H, m, α**C**H), 7.21-7.40 (20H, m, Ar**H**); δ_C (150.8 MHz) 38.3 (Ar$\mathbf{C}H_2$), 47.5 (N($\mathbf{C}H_2)_2$)N ring), 51.1 (N($\mathbf{C}H_2)_2$)N ring), 53.3 (O$\mathbf{C}H_3$), 54.6 (α**C**H), 55.4 ($\mathbf{C}H_2$C=O), 128.0 (**Ar**H), 129.7 (**Ar**H), 130.6 (**Ar**H), 138.2 (**Ar**H), 171.6 (**C**=OCH_3), 172.1 (**C**=ONH_2).

Ligand (50)

δ_H (600 MHz, CD_3OD) 1.89 ([H_a, H_b], 6H, d, N($C\mathbf{H}_2)_2$N ring), 2.02 ([H_c, H_d], 6H, d, N($C\mathbf{H}_2)_2$N ring), 2.77 ([H_e, H_f], 6H, s, $C\mathbf{H}_2$C=O), 3.33 ([H_g, H_h], 6H, m, Ar$C\mathbf{H}_2$), 3.70 (9H, s, O$C\mathbf{H}_3$), 4.76 ([H_i], 3H, m, α**C**H), 6.93 (6H, t, Ar**H**), 7.03 (3H, t, Ar**H**), 7.26 (3H, d, Ar**H**), 7.39 (3H, d, Ar**H**); δ_C (150.8 MHz) 28.3 (Ar$\mathbf{C}H_2$), 53.4 (O$\mathbf{C}H_3$), 54.6 (α**C**H), 57.6 (N($\mathbf{C}H_2)_2$)N ring), 63.6 ($\mathbf{C}H_2$C=O), 110.6 (**Ar**H), 112.8 (**Ar**H), 119.5 (**Ar**H), 120.4 (**Ar**H), 123.0 (**Ar**H), 125.4 (**Ar**H), 129.5 (**Ar**H), 138.5 (**Ar**H), 174.2 (**C**=ONH_2), 174.4 (**C**=OCH).

[Zn(50)]$^{2+}$

δ_H (600 MHz, CD_3OD) 1.00 ([H_a], 3H, m, N($C\mathbf{H}_2)_2$N ring), 1.10 ([H_c], 3H, m, N($C\mathbf{H}_2)_2$N ring), 2.23 ([H_b, H_d], 6H, m, N($C\mathbf{H}_2)_2$N ring), 2.91 ([H_g], 3H, m, Ar$C\mathbf{H}_2$), 3.33 ([H_e, H_f], 6H, s, $C\mathbf{H}_2$C=O), 3.44 ([H_h], 3H, m, Ar$C\mathbf{H}_2$), 3.93 (9H, s, O$C\mathbf{H}_3$), 5.09 ([H_i], 3H, m, α**C**H), 6.99 (3H, t, Ar**H**), 7.05 (3H, s, Ar**H**), 7.17 (3H, t, Ar**H**), 7.34 (3H, d, Ar**H**), 7.49 (3H, d, Ar**H**); δ_C (150.8 MHz) 29.4 (Ar$\mathbf{C}H_2$), 50.3 (O$\mathbf{C}H_3$), 51.9 (N($\mathbf{C}H_2)_2$)N ring), 52.4

(N(**C**H_2)$_2$)N ring), 53.8 (**C**H_2C=O), 55.0 (α**C**H), 111.0 (**Ar**H), 113.3 (**Ar**H), 119.5 (**Ar**H), 120.5 (**Ar**H), 123.0 (**Ar**H), 125.4 (**Ar**H), 128.6 (**Ar**H), 138.2 (**Ar**H), 172.6 (**C**=OCH_3), 174.4 (**C**=ONH_2).

[Cd(50)]$^{2+}$

δ_H (600 MHz, CD_3OD) 1.20 ([H_a], 3H, m, N(C**H**$_2$)$_2$N ring), 1.61 ([H_c], 3H, m, N(C**H**$_2$)$_2$N ring), 2.12 ([H_b], 3H, m, N(C**H**$_2$)$_2$N ring), 2.31 ([H_e], 3H, m, C**H**$_2$C=O), 2.40 ([H_d], 3H, m, N(C**H**$_2$)$_2$N ring), 2.95 ([H_f], 3H, m, C**H**$_2$C=O), 3.01 ([H_g], 3H, m, ArC**H**$_2$), 3.37 ([H_h], 3H, m, ArC**H**$_2$), 3.77 (9H, s, OC**H**$_3$), 5.05 ([H_i], 3H, m, α**CH**), 6.93 (3H, t, Ar**H**), 7.06 (3H, s, Ar**H**), 7.09 (3H, t, Ar**H**), 7.32 (3H, d, Ar**H**), 7.49 (3H, d, Ar**H**); δ_C (150.8 MHz) 29.5 (Ar**C**H_2), 52.5 (N(**C**H_2)$_2$)N ring), 53.6 (O**C**H_3), 53.9 (N(**C**H_2)$_2$)N ring), 55.0 (α**C**H), 62.0 (**C**H_2C=O), 111.0 (**Ar**H), 113.2 (**Ar**H), 119.8 (**Ar**H), 120.5 (**Ar**H), 123.0 (**Ar**H), 125.8 (**Ar**H), 128.8 (**Ar**H), 138.8 (**Ar**H), 173.1 (**C**=OCH_3), 173.5 (**C**=ONH_2).

A.2 Speciation

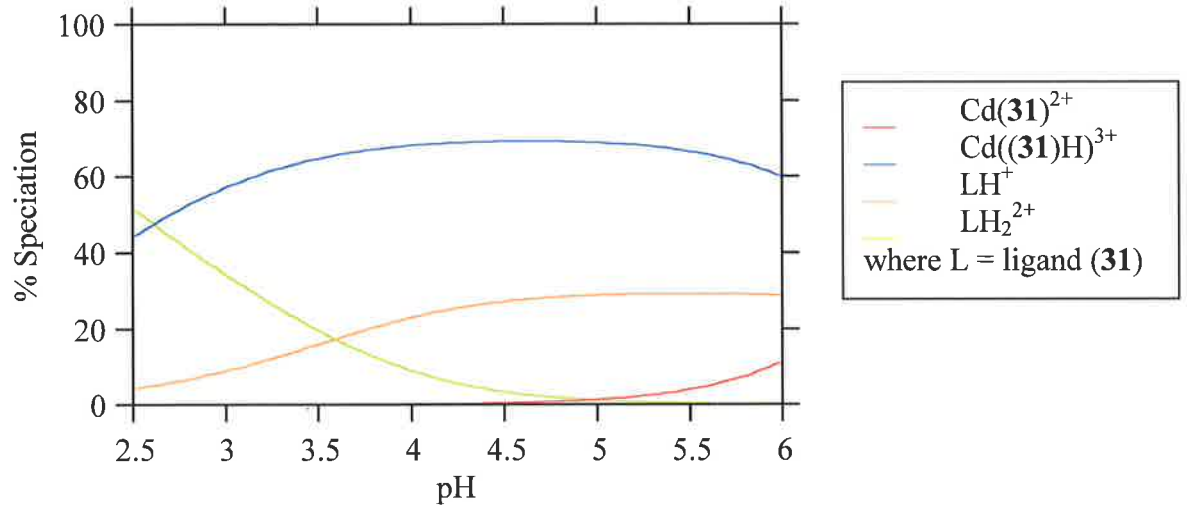

Figure A.1. Speciation variation of ligand (**31**) showing the species present in methanol/water (80:20); v/v) at various pH in which $[\mathbf{31}]_{total}$ = 9.1 x 10^{-4} mol dm^{-3}, $[Cd^{2+}]_{total}$ = 7.0 x 10^{-4} mol dm^{-3}, I = 0.10 mol dm^{-3} (NEt_4ClO_4) at 298.2 K. Speciation shown relative to the total concentration of ligand (**31**).

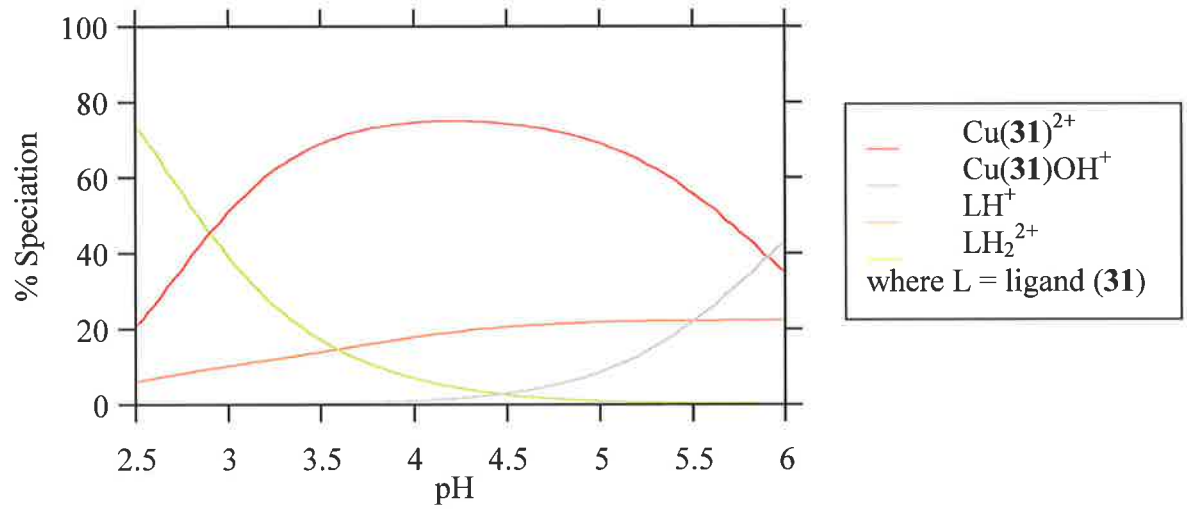

Figure A.2. Speciation variation of ligand (**31**) showing the species present in methanol/water (80:20); v/v) at various pH in which $[\mathbf{31}]_{total}$ = 9.1 x 10^{-4} mol dm^{-3}, $[Cu^{2+}]_{total}$ = 7.0 x 10^{-4} mol dm^{-3}, I = 0.10 mol dm^{-3} (NEt_4ClO_4) at 298.2 K. Speciation shown relative to the total concentration of ligand (**31**).

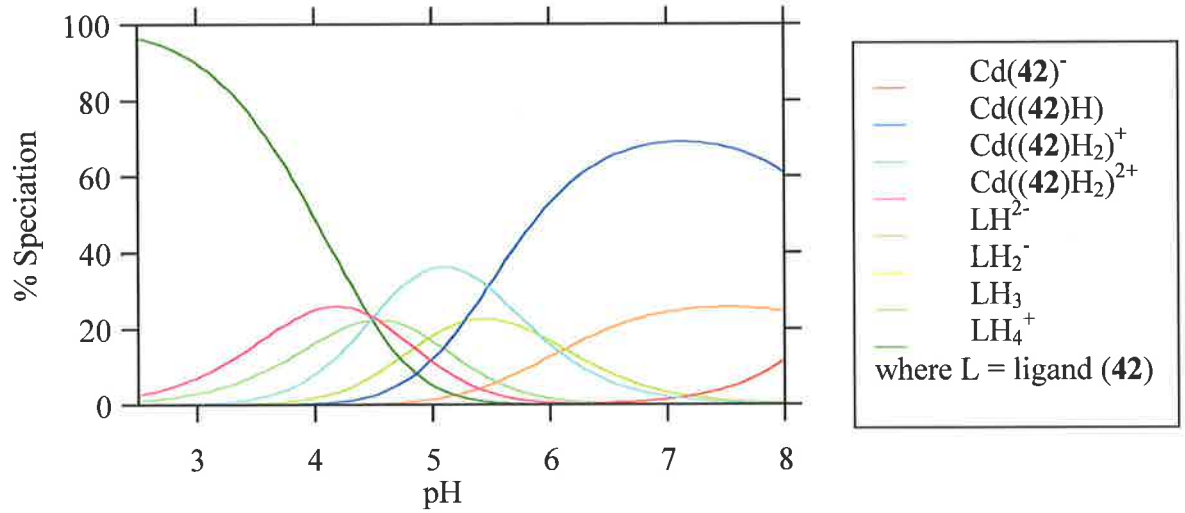

Figure A.3. Speciation variation of ligand (**42**) showing the species present in methanol/water (80:20); v/v) at various pH in which $[\mathbf{42}]_{total}$ = 8.9 x 10^{-4} mol dm^{-3}, $[Cd^{2+}]_{total}$ = 7.0 x 10^{-4} mol dm^{-3}, I = 0.10 mol dm^{-3} (NEt_4ClO_4) at 298.2 K. Speciation shown relative to the total concentration of ligand (**42**).

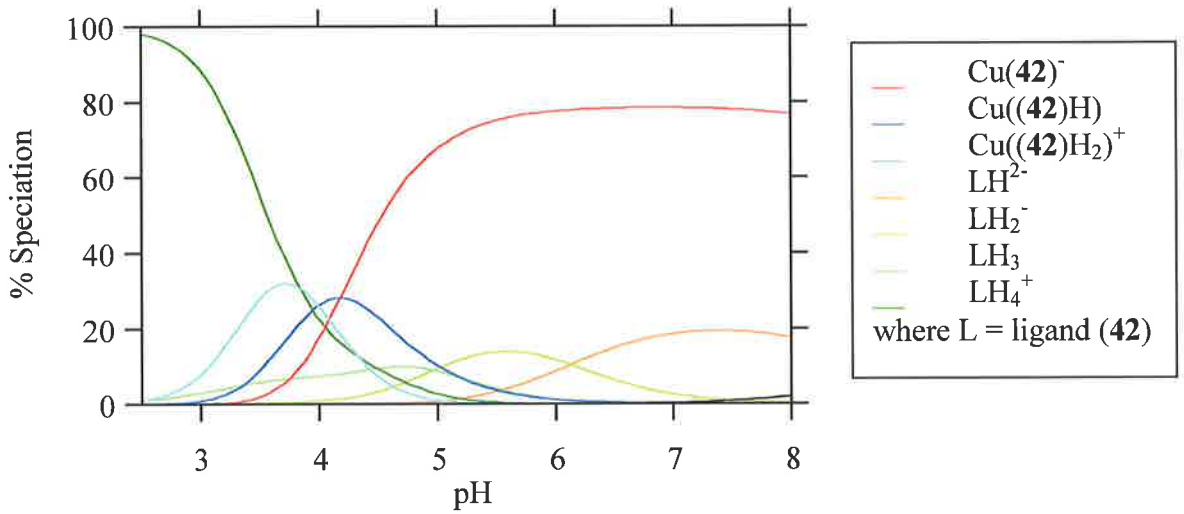

Figure A.4. Speciation variation of ligand (**42**) showing the species present in methanol/water (80:20); v/v) at various pH in which $[\mathbf{42}]_{total}$ = 8.9 x 10^{-4} mol dm^{-3}, $[Cu^{2+}]_{total}$ = 7.0 x 10^{-4} mol dm^{-3}, I = 0.10 mol dm^{-3} (NEt_4ClO_4) at 298.2 K. Speciation shown relative to the total concentration of ligand (**42**).

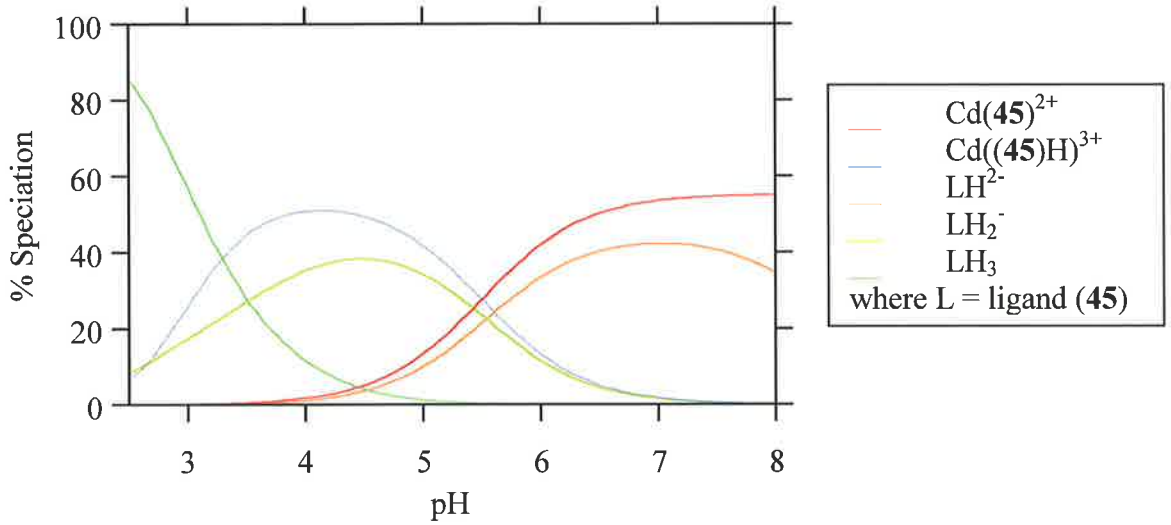

Figure A.5. Speciation variation of ligand (**45**) showing the species present in methanol/water (80:20); v/v) at various pH in which $[\mathbf{45}]_{total}$ = 1.2 x 10^{-3} mol dm^{-3}, $[Cd^{2+}]_{total}$ = 7.0 x 10^{-4} mol dm^{-3}, I = 0.10 mol dm^{-3} (NEt_4ClO_4) at 298.2 K. Speciation shown relative to the total concentration of ligand (**45**).

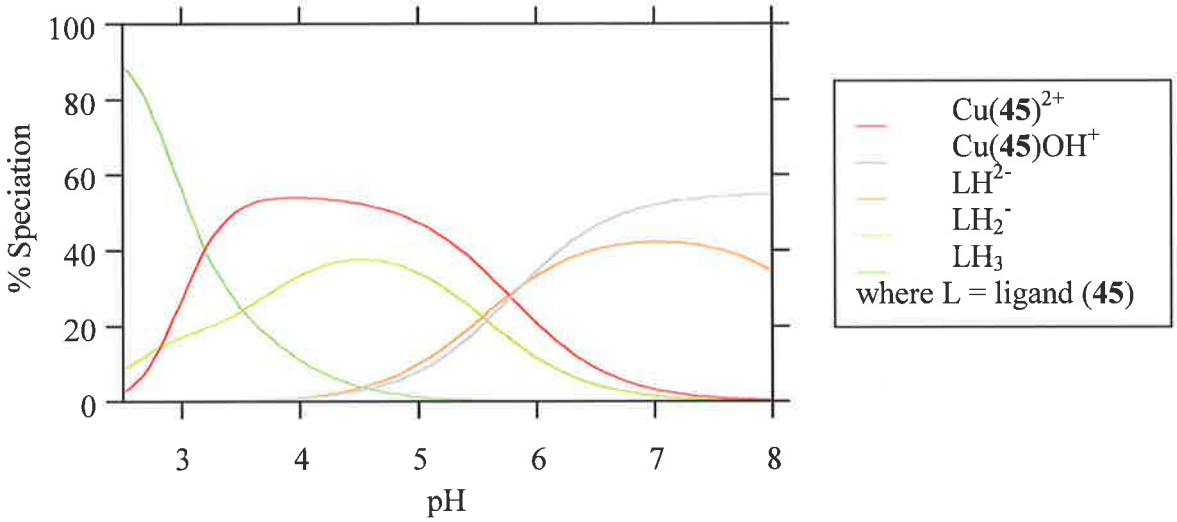

Figure A.6. Speciation variation of ligand (**45**) showing the species present in methanol/water (80:20); v/v) at various pH in which $[\mathbf{45}]_{total}$ = 1.2 x 10^{-3} mol dm^{-3}, $[Cu^{2+}]_{total}$ = 7.0 x 10^{-4} mol dm^{-3}, I = 0.10 mol dm^{-3} (NEt_4ClO_4) at 298.2 K. Speciation shown relative to the total concentration of ligand (**45**).

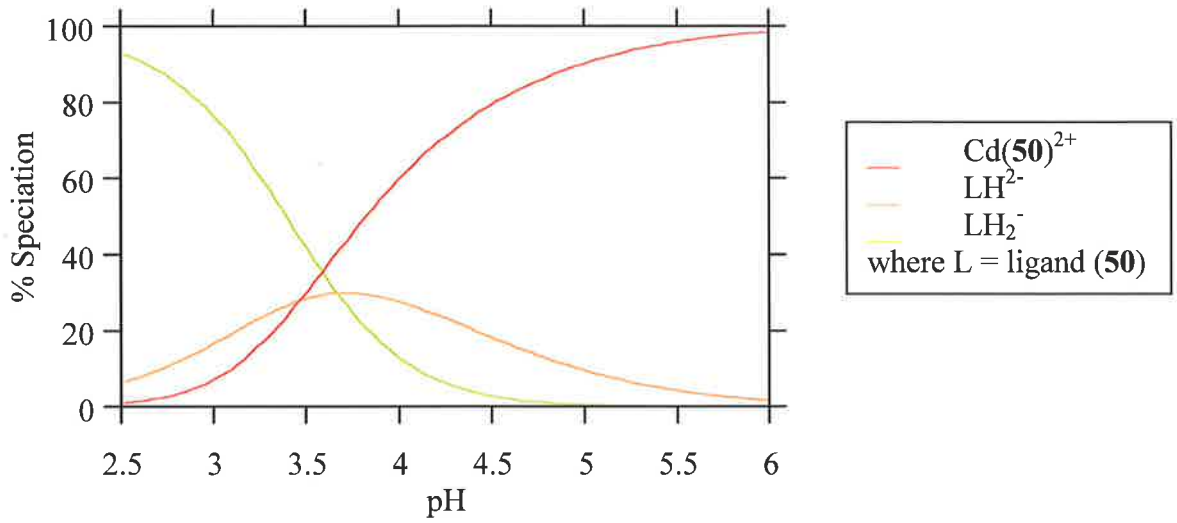

Figure A.7. Speciation variation of ligand (**50**) showing the species present in methanol/water (80:20); v/v) at various pH in which $[\mathbf{50}]_{total}$ = 7.3 x 10^{-4} mol dm^{-3}, $[Cd^{2+}]_{total}$ = 8.0 x 10^{-4} mol dm^{-3}, I = 0.10 mol dm^{-3} (NEt_4ClO_4) at 298.2 K. Speciation shown relative to the total concentration of ligand (**50**).

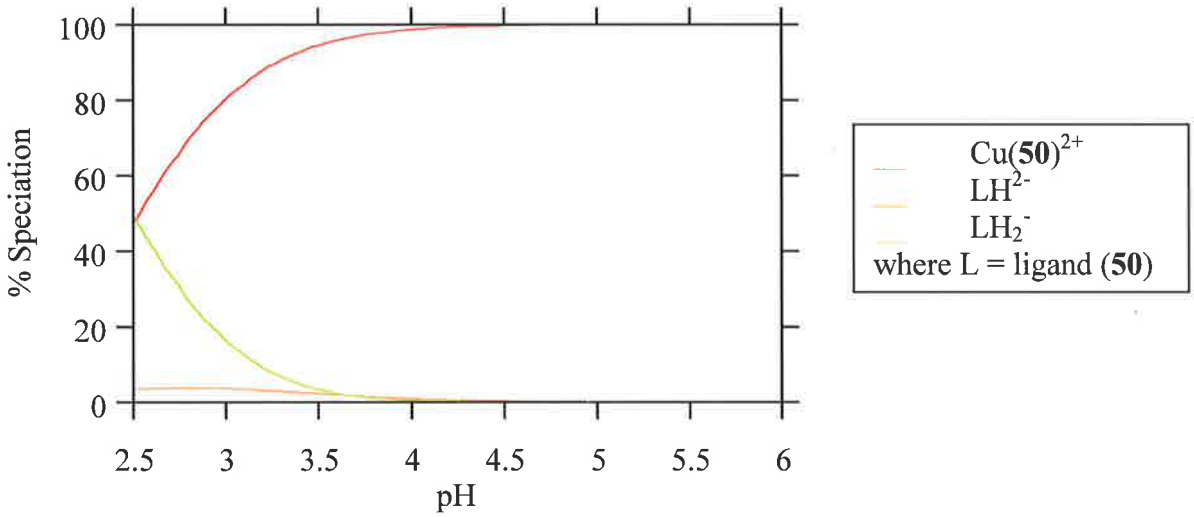

Figure A.8. Speciation variation of ligand (**50**) showing the species present in methanol/water (80:20); v/v) at various pH in which $[\mathbf{50}]_{total}$ = 7.3 x 10^{-4} mol dm^{-3}, $[Cu^{2+}]_{total}$ = 8.0 x 10^{-4} mol dm^{-3}, I = 0.10 mol dm^{-3} (NEt_4ClO_4) at 298.2 K. Speciation shown relative to the total concentration of ligand (**50**).

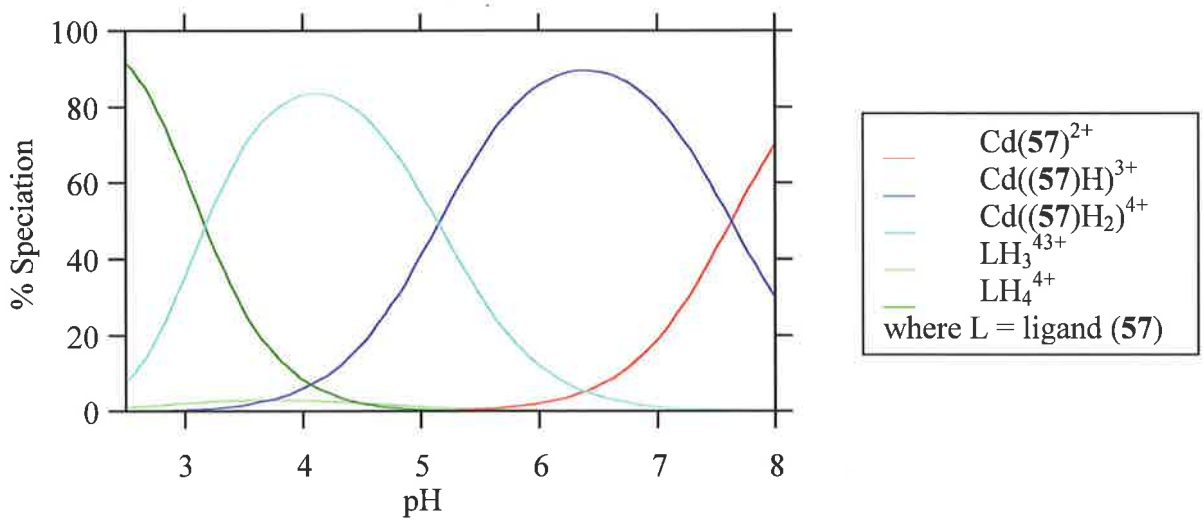

Figure A.9. Speciation variation of ligand (**57**) showing the species present in methanol/water (80:20); v/v) at various pH in which $[\mathbf{57}]_{total}$ = 3.3 x 10^{-4} mol dm^{-3}, $[Cd^{2+}]_{total}$ = 1.0 x 10^{-3} mol dm^{-3}, I = 0.10 mol dm^{-3} (NEt_4ClO_4) at 298.2 K. Speciation shown relative to the total concentration of ligand (**57**).

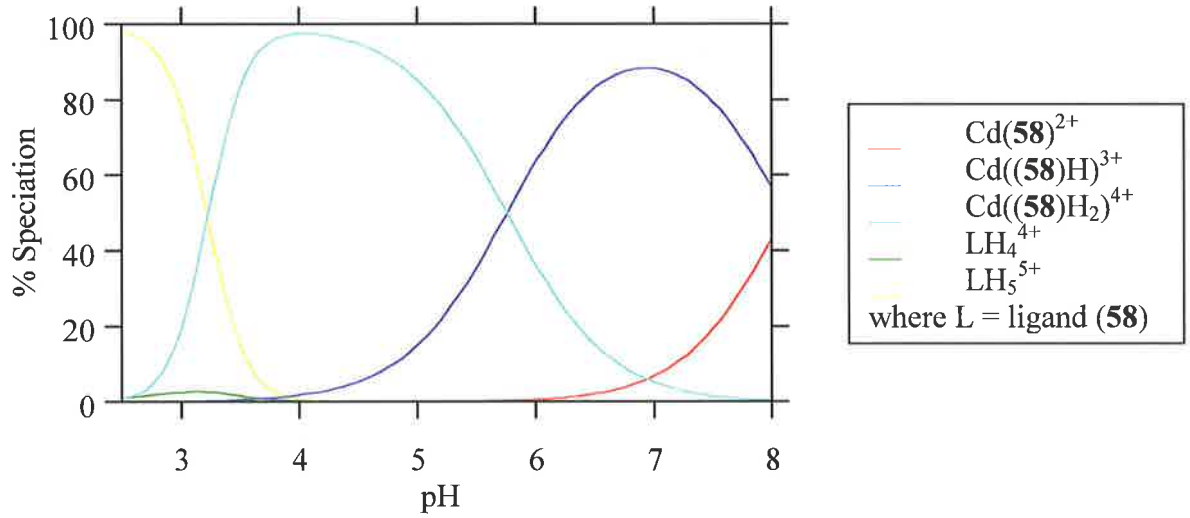

Figure A.10. Speciation variation of ligand (**58**) showing the species present in methanol/water (80:20); v/v) at various pH in which $[\mathbf{58}]_{total}$ = 5.3 x 10^{-4} mol dm^{-3}, $[Cd^{2+}]_{total}$ = 1.0 x 10^{-3} mol dm^{-3}, I = 0.10 mol dm^{-3} (NEt_4ClO_4) at 298.2 K. Speciation shown relative to the total concentration of ligand (**58**).

A.3 UV-visible absorption spectra

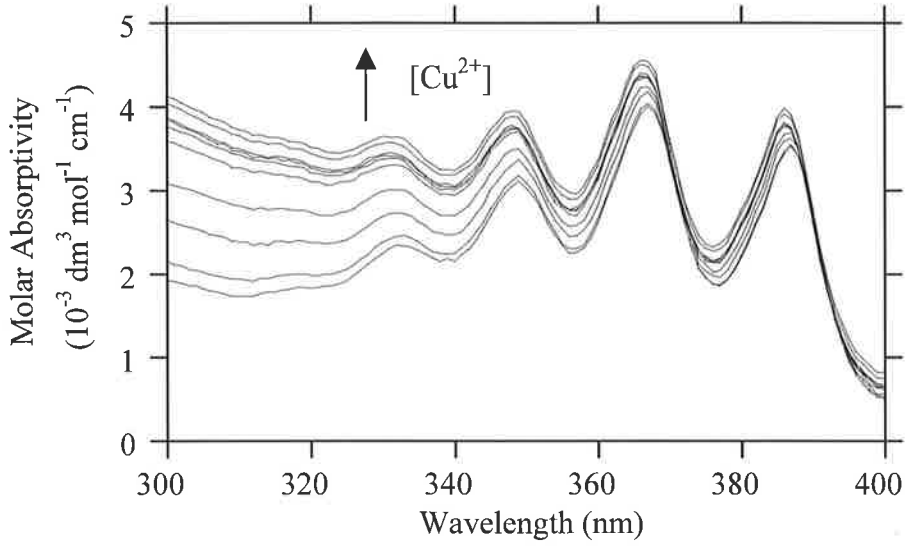

Figure A.11. UV-visible absorption spectra of ligand (**57**) alone [4.1 x 10^{-5} mol dm^{-3}] and in the presence of Cu^{2+} [8.3 x 10^{-6}, 1.6 x 10^{-5}, 2.5 x 10^{-5}, 3.3 x 10^{-5}, 4.1 x 10^{-5}, 4.9 x 10^{-5}, 5.8 x 10^{-5}, 6.7 x 10^{-5}, 7.4 x 10^{-5}, 8.3 x 10^{-5} mol dm^{-3}] at pH 5.6 (MES buffer) in methanol/water (80:20; v/v) (I = 0.1 mol dm^{-3}, NEt_4ClO_4) at 298.2 K. The absorption of the ligand alone is the lowest intensity absorption curve. Molar absorptivity increases with increase in $[Cu^{2+}]$.

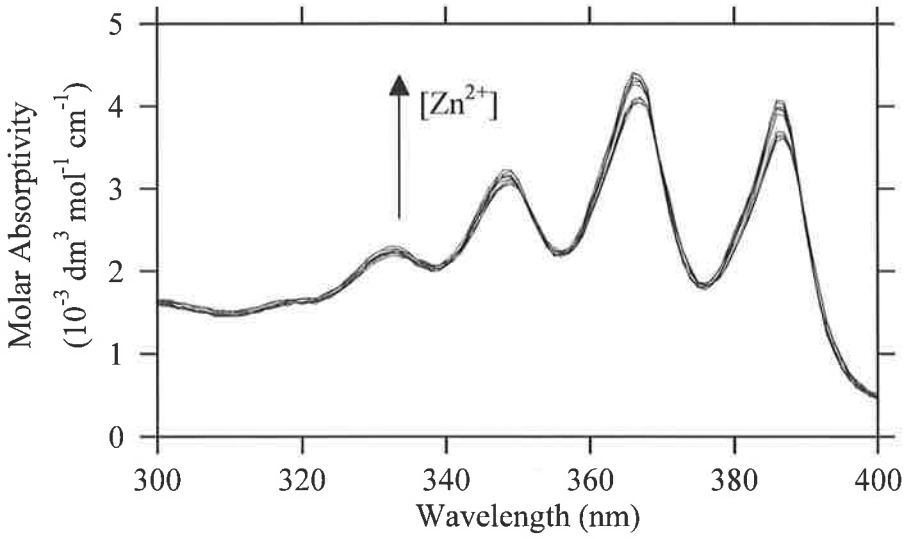

Figure A.12. UV-visible absorption spectra of ligand (**57**) alone [4.1 x 10^{-5} mol dm^{-3}] and in the presence of Zn^{2+} [8.3 x 10^{-6}, 1.6 x 10^{-5}, 2.5 x 10^{-5}, 3.3 x 10^{-5}, 4.1 x 10^{-5}, 4.9 x 10^{-5}, 5.8 x 10^{-5}, 6.7 x 10^{-5}, 7.4 x 10^{-5}, 8.3 x 10^{-5} mol dm^{-3}] at pH 5.6 (MES buffer) in methanol/water (80:20; v/v) (I = 0.1 mol dm^{-3}, NEt_4ClO_4) at 298.2 K. The absorption of the ligand alone is the lowest intensity absorption curve. Molar absorptivity increases with increase in $[Zn^{2+}]$.

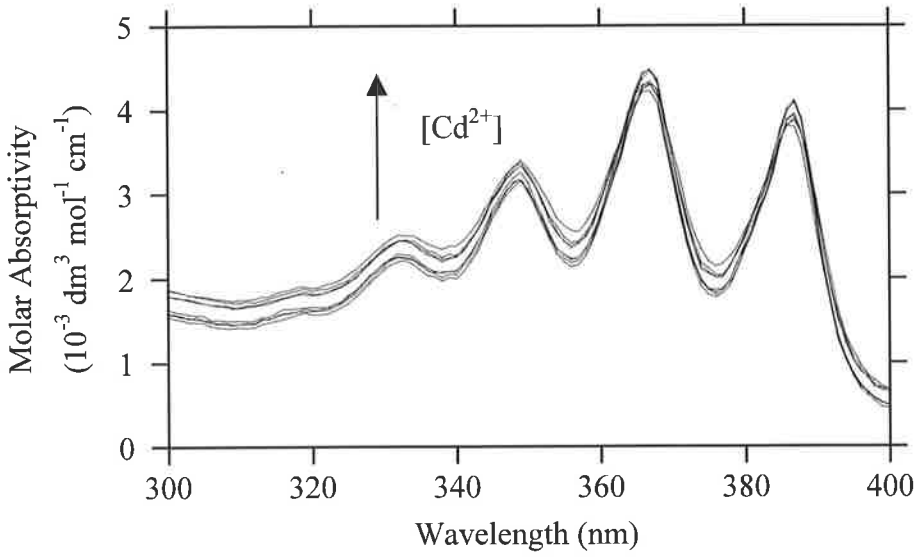

Figure A.13. UV-visible absorption spectra of ligand (**57**) alone [4.1 x 10^{-5} mol dm^{-3}] and in the presence of Cd^{2+} [8.3 x 10^{-6}, 1.6 x 10^{-5}, 2.5 x 10^{-5}, 3.3 x 10^{-5}, 4.1 x 10^{-5}, 4.9 x 10^{-5}, 5.8 x 10^{-5}, 6.7 x 10^{-5}, 7.4 x 10^{-5}, 8.3 x 10^{-5} mol dm^{-3}] at pH 5.6 (MES buffer) in methanol/water (80:20; v/v) (I = 0.1 mol dm^{-3}, NEt_4ClO_4) at 298.2 K. The absorption of the ligand alone is the lowest intensity absorption curve. Molar absorptivity increases with increase in [Cd^{2+}].

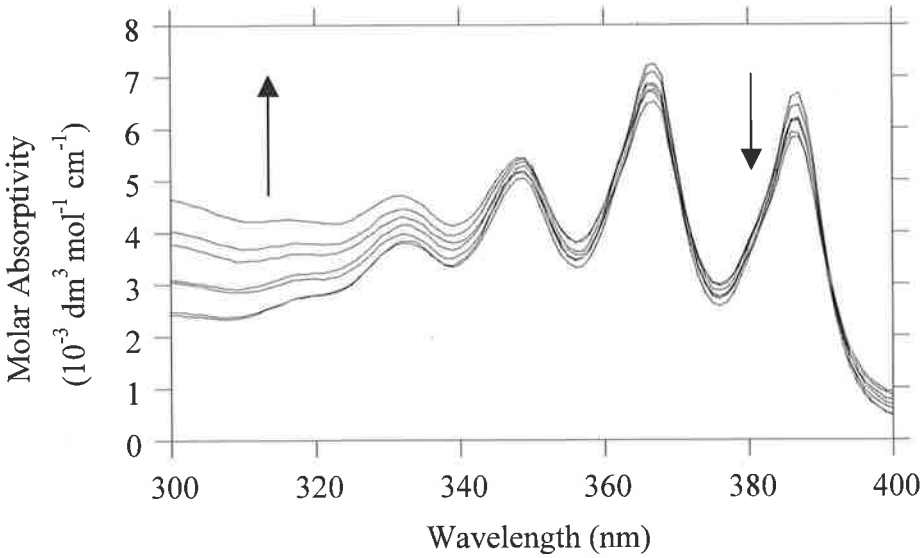

Figure A.14. UV-visible absorption spectra of ligand (**58**) alone (4.7 x 10^{-5} mol dm^{-3}) and in the presence of Cu^{2+} [9.4 x 10^{-6}, 1.9 x 10^{-5}, 2.8 x 10^{-5}, 3.7 x 10^{-5}, 4.7 x 10^{-5}, 5.6 x 10^{-5}, 6.6 x 10^{-5}, 7.5 x 10^{-5}, 8.5 x 10^{-5}, 9.4 x 10^{-5} mol dm^{-3}] at pH 5.6 (MES buffer) in methanol/water (80:20; v/v) (I = 0.1 mol dm^{-3}, NEt_4ClO_4) at 298.2 K. Molar absorptivity decreases with increase in [Cu^{2+}] above 348 nm, and increases with increase in [Cu^{2+}] below 348 nm.

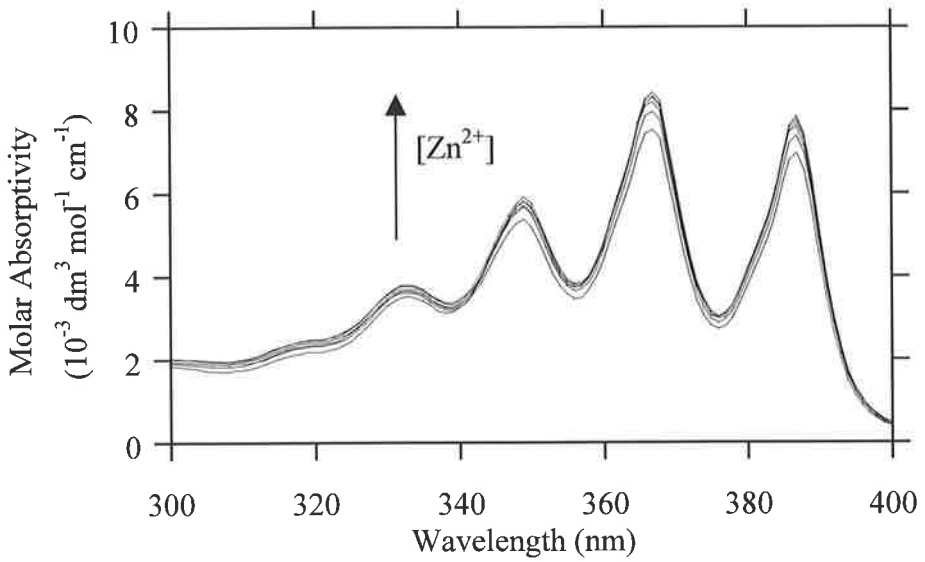

Figure A.15. UV-visible absorption spectra of ligand (**58**) alone (4.7 x 10^{-5} mol dm^{-3}) and in the presence of Zn^{2+} [9.4 x 10^{-6}, 1.9 x 10^{-5}, 2.8 x 10^{-5}, 3.7 x 10^{-5}, 4.7 x 10^{-5}, 5.6 x 10^{-5}, 6.6 x 10^{-5}, 7.5 x 10^{-5}, 8.5 x 10^{-5}, 9.4 x 10^{-5} mol dm^{-3}] at pH 5.6 (MES buffer) in methanol/water (80:20; v/v) (I = 0.1 mol dm^{-3}, NEt_4ClO_4) at 298.2 K. The absorption of the ligand alone is the lowest intensity absorption curve. Molar absorptivity increases with increase in [Zn^{2+}].

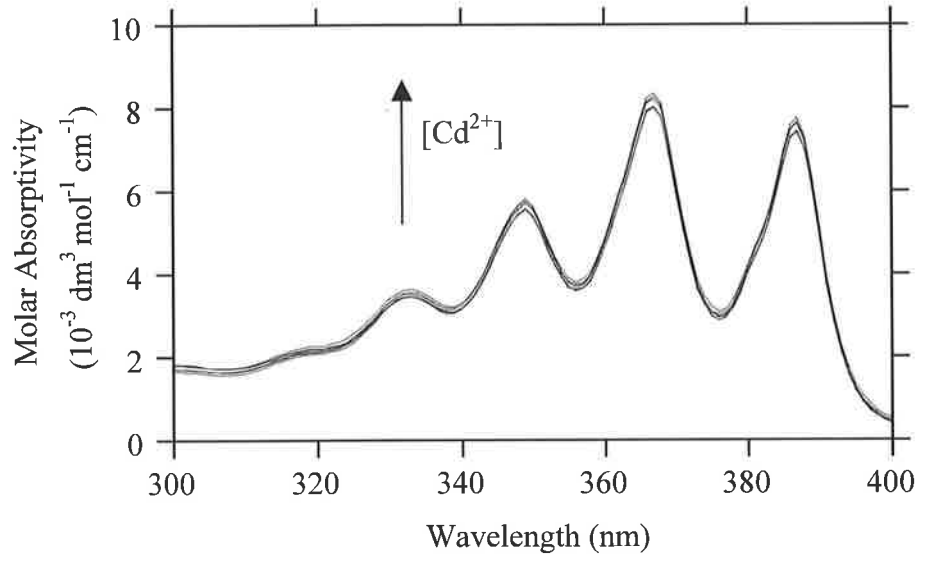

Figure A.16. UV-visible absorption spectra of ligand (**58**) alone (4.7 x 10^{-5} mol dm^{-3}) and in the presence of Cd^{2+} [9.4 x 10^{-6}, 1.9 x 10^{-5}, 2.8 x 10^{-5}, 3.7 x 10^{-5}, 4.7 x 10^{-5}, 5.6 x 10^{-5}, 6.6 x 10^{-5}, 7.5 x 10^{-5}, 8.5 x 10^{-5}, 9.4 x 10^{-5} mol dm^{-3}] at pH 5.6 (MES buffer) in methanol/water (80:20; v/v) (I = 0.1 mol dm^{-3}, NEt_4ClO_4) at 298.2 K. The absorption of the ligand alone is the lowest intensity absorption curve. Molar absorptivity increases with increase in [Cd^{2+}].

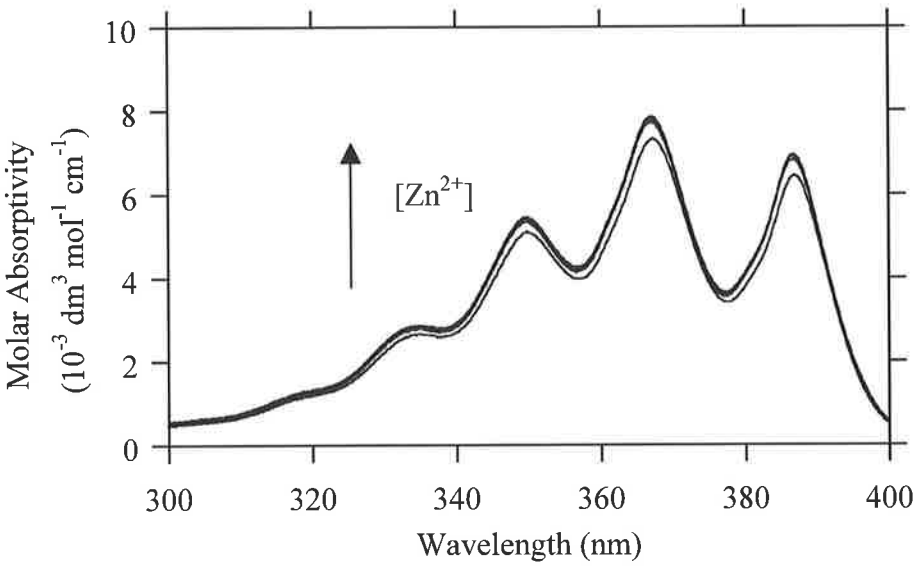

Figure A.17. UV-visible absorption spectra of ligand (**62**) alone (5.5 x 10^{-5} mol dm^{-3}) and in the presence of Zn^{2+} [5.45 x 10^{-6}, 1.1 x 10^{-5}, 1.6 x 10^{-5}, 2.2 x 10^{-5}, 2.7 x 10^{-5}, 3.8 x 10^{-5}, 4.9 x 10^{-5}, 6.0 x 10^{-5}, 7.0 x 10^{-5}, 8.1 x 10^{-5}, 9.2 x 10^{-5}, 1.0 x 10^{-5}, 1.11 x 10^{-4} mol dm^{-3}] at pH 4.0 (acetate buffer) in methanol/water (80:20; v/v) (I = 0.1 mol dm^{-3}, NEt_4ClO_4) at 298.2 K. The absorption of the ligand alone is the lowest intensity absorption curve. Molar absorptivity increases with increase in [Zn^{2+}].

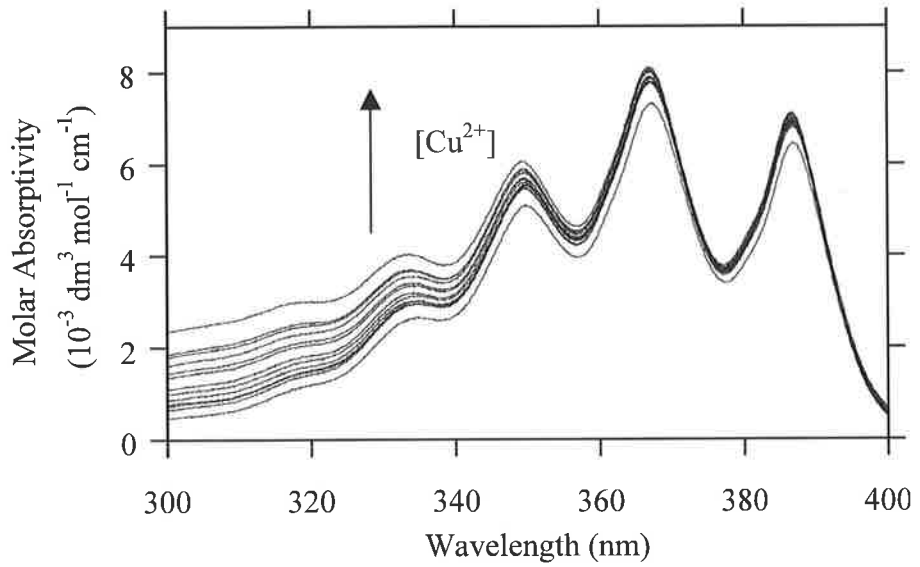

Figure A.18. UV-visible absorption spectra of ligand (**62**) alone (5.5 x 10^{-5} mol dm^{-3}) and in the presence of Cu^{2+} [5.45 x 10^{-6}, 1.1 x 10^{-5}, 1.6 x 10^{-5}, 2.2 x 10^{-5}, 2.7 x 10^{-5}, 3.8 x 10^{-5}, 4.9 x 10^{-5}, 6.0 x 10^{-5}, 7.0 x 10^{-5}, 8.1 x 10^{-5}, 9.2 x 10^{-5}, 1.0 x 10^{-5}, 1.11 x 10^{-4} mol dm^{-3}] at pH 4.0 (acetate buffer) in methanol/water (80:20; v/v) (I = 0.1 mol dm^{-3}, NEt_4ClO_4) at 298.2 K. The absorption of the ligand alone is the lowest intensity absorption curve. Molar absorptivity increases with increase in [Cu^{2+}].

A.3 Fluorescence spectra

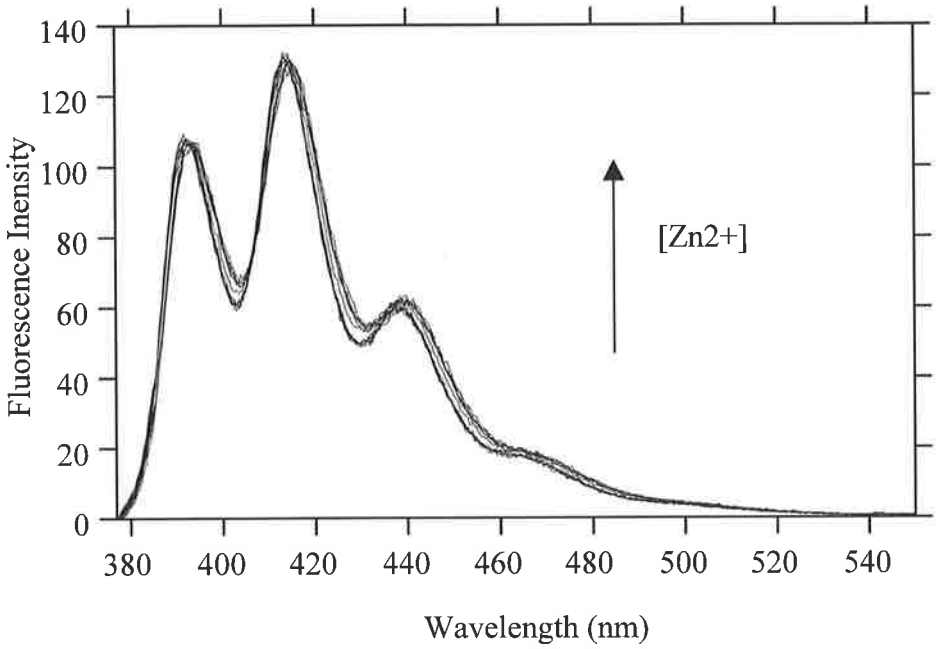

Figure A.19 Fluorescence spectra of ligand (**57**) alone [4.1 x 10^{-5} mol dm^{-3}] and in the presence of increasing concentrations of Zn^{2+} [8.3 x 10^{-6}, 1.6 x 10^{-5}, 2.5 x 10^{-5}, 3.3 x 10^{-5}, 4.1 x 10^{-5}, 4.9 x 10^{-5}, 5.8 x 10^{-5}, 6.7 x 10^{-5}, 7.4 x 10^{-5}, 8.3 x 10^{-5} mol dm^{-3}] at pH 5.6 (MES buffer) in methanol/water (80:20; v/v) (I = 0.1 mol dm^{-3}, NEt_4ClO_4) at 298.2 K when excited at 368 nm. The fluorescence of the ligand alone is the highest intensity curve. Fluorescence increases with increase in [Zn^{2+}].

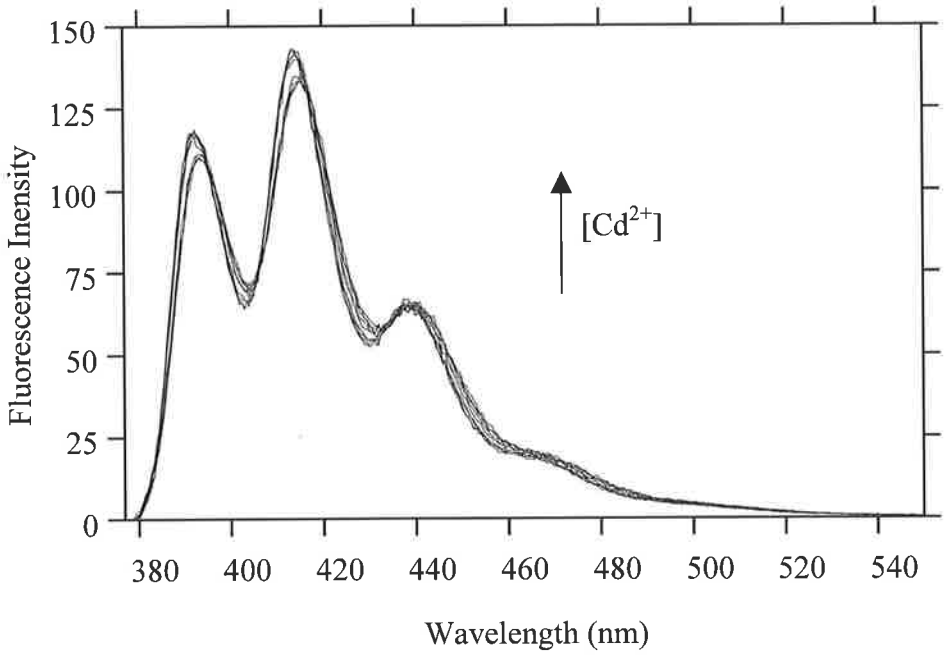

Figure A.20 Fluorescence spectra of ligand (**57**) alone [4.1 x 10^{-5} mol dm^{-3}] and in the presence of increasing concentrations of Cd^{2+} [8.3 x 10^{-6}, 1.6 x 10^{-5}, 2.5 x 10^{-5}, 3.3 x 10^{-5}, 4.1 x 10^{-5}, 4.9 x 10^{-5}, 5.8 x 10^{-5}, 6.7 x 10^{-5}, 7.4 x 10^{-5}, 8.3 x 10^{-5} mol dm^{-3}] at pH 5.6 (MES buffer) in methanol/water (80:20; v/v) (I = 0.1 mol dm^{-3}, NEt_4ClO_4) at 298.2 K when excited at 368 nm. The fluorescence of the ligand alone is the highest intensity curve. Fluorescence increases with increase in $[Cd^{2+}]$.

A.5 Publications arising from this thesis

"Aminoacid *N*-substituted 1,4,7-triazacyclonoane and 1,4,7,10-tetraazacyclododecane Zn^{2+}, Cd^{2+} and Cu^{2+} complexes. A preparative and potentiometric titration and NMR spectroscopic study." Sally E. Plush, Stephen F. Lincoln and Kevin P. Wainwright, *Dalton Transactions*, 2004, 1410-1417.

FULL PAPER

Dalton
www.rsc.org/dalton

Aminoacid *N*-substituted 1,4,7-triazacyclononane and 1,4,7,10-tetraazacyclododecane Zn^{2+}, Cd^{2+} and Cu^{2+} complexes. A preparative, potentiometric titration and NMR spectroscopic study †

Sally E. Plush,[a] Stephen F. Lincoln *[a] and Kevin P. Wainwright [b]

[a] *Department of Chemistry, The University of Adelaide, Adelaide, SA 5005, Australia. E-mail: Stephen.Lincoln@adelaide.edu.au*

[b] *School of Chemistry, Physics and Earth Sciences, The Flinders University of South Australia, GPO Box 2100, Adelaide, SA 5001, Australia*

Received 5th February 2004, Accepted 12th March 2004
First published as an Advance Article on the web 26th March 2004

The pK_as and Zn^{2+}, Cd^{2+} and Cu^{2+} complexation constants (K) for 1,4,7-tris[(2″*S*)-acetamido-2″-(methyl-3″-phenylpropionate)]-1,4,7-triazacyclononane, **1**, 1,4,7-tris[(2″*S*)-acetamido-2″-(1″-carboxy-3″-phenylpropane)]-1,4,7-triazacyclononane, H_3**2**, 1,4,7-tris[(2″*S*)-acetamido-2″-(methyl-3″-(1*H*-3-indolyl)propionate)]-1,4,7-triazacyclononane, **3**, and 1,4,7,10-tetrakis[(2″*S*)-acetamido-2″-(methyl-3″-phenylpropionate)]-1,4,7,10-tetraazacyclododecane, **4**, 1,4,7,10-tetrakis[(2″*S*)-acetamido-2″-(1″-carboxy-3″-phenylpropane)]-1,4,7,10-tetraazacyclododecane, H_4**5**, in 20 : 80 v/v water–methanol solution are reported. The pK_as within the potentiometric detection range for H_3**1**$^{3+}$ = 8.69 and 3.59, for H_6**2**$^{3+}$ = 9.06, 6.13, 4.93 and 4.52, H_3**3**$^{3+}$ = 8.79 and 3.67, H_4**4**$^{4+}$ = 8.50, 5.62 and 3.77 and for H_8**5**$^{4+}$ = 9.89, 7.06, 5.53, 5.46, 4.44 and 4.26 where each tertiary amine nitrogen is protonated. The complexes of **1**: [Zn(**1**)]$^{2+}$ (9.00), [Cd(**1**)]$^{2+}$ (6.49), [Cd(H**1**)]$^{3+}$ (4.54) and [Cu(**1**)]$^{2+}$ (10.01) are characterized by the log(K/dm^3 mol^{-1}) values shown in parentheses. Analogous complexes are formed by **3** and **4**: [Zn(**3**)]$^{2+}$ (10.19), [Cd(**3**)]$^{2+}$ (8.54), [Cu(**3**)]$^{2+}$ (10.77), [Zn(**4**)]$^{2+}$ (11.41) [Cd(**4**)]$^{2+}$ (9.16), [Cd(H**4**)]$^{3+}$ (6.16) and [Cu(**4**)]$^{2+}$ (11.71). The tricarboxylic acid H_3**2** generates a greater variety of complexes as exemplified by: [Zn(**2**)$^-$] (10.68) [Zn(H**2**)] (6.60) [Zn(H_2**2**)$^+$] (5.15), [Cd(**2**)]$^-$ (4.99), [Cd(H**2**)] (4.64), [Cd(H_2**2**)]$^+$ (3.99), [Cd(H_3**2**)]$^{2+}$ (3.55), [Cu(**2**)]$^-$ (12.55) [Cu(H**2**)] (7.66), [Cu(H_2**2**)]$^+$ (5.54) and [Cu_2(**2**)]$^{4-}$ (3.23). The complexes of H_4**5** were insufficiently soluble to study in this way. The ^{1}H and ^{13}C NMR spectra of the ligands are consistent with formation of a predominant Zn^{2+} and Cd^{2+} Δ or Λ diastereomer. The preparations of the new pendant arm macrocycles H_3**2**, **3**, **4** and H_4**5** are reported.

Introduction

The complexation of metal ions by macrocyclic polyaza pendant arm ligands[1,2] facilitates a wide range of chemistry including that of luminescent sensors,[3] MRI relaxation agents[4] and chiral receptor systems.[5,6] Frequently, the pendant arms have terminated in either alcohol, amine, amide, carboxylate or phosphate coordinating groups which, together with the tertiary amines in the macrocyclic ring, constitute the polydentate ligand donor set. It is usually observed that metal complexation of such ligands based on pendant arm substitution on all ring nitrogens of 1,4,7-triazacyclononane, 1,4,7,10-tetraazacyclododecane and 1,4,7,10,13-pentaazacyclopentadecane causes the three, four or five pendant arms, respectively, to adopt orientations which give two enantiomeric complexes when the arms are achiral and one of the possible diastereomeric complexes to predominate when the arms incorporate a chiral centre.[7] This raises the possibility of attaching amino acids as pendant arms to polyaza macrocyclic platforms to study the effects of their close proximity on their metal ion coordination properties and the overall chirality of the metal complex formed.

The complex, 1,4,7-tris[(2″*S*)-acetamido-2″-(methyl-3″-phenylpropionate)]-1,4,7-triazacyclononane copper(II), [Cu(**1**)]$^{2+}$, has been shown to form the Λ-(*S*,*S*,*S*) diastereomer in the solid state where the coplanar trio of amine nitrogens are rotated clockwise relative to the coplanar trio of amide oxygens when viewed from the latter plane down the C_3 axis as shown for its Zn^{2+} analogue in Scheme 1.[8] In this study, the new ligands 1,4,7-tris[(2″*S*)-acetamido-2″-(1″-carboxy-3″-phenylpropane)]-1,4,7-triazacyclononane, H_3**2**, 1,4,7-tris[(2″*S*)-acetamido-2″-(methyl-3″-(1*H*-3-indolyl)propionate)]-1,4,7-triazacyclononane, **3**, 1,4,7,10-tetrakis[(2″*S*)-acetamido-2″-(methyl-3″-phenylpropionate)]-1,4,7,10-tetraazacyclododecane, **4** and 1,4,7,10-tetrakis[(2″*S*)-acetamido-2″-(1″-carboxy-3″-phenylpropane)]-1,4,7,10-tetraazacyclododecane, H_4**5**, have been prepared (Scheme 2). These ligands are of two types, those which contain an ester function (**1**, **3** and **4**) and those in which the ester function has been hydrolysed (H_3**2** and H_4**5**). Their protonation and metal ion complexing characteristics in 20 : 80 v/v water–methanol solution have been determined (the complexes of H_4**5** were insufficiently soluble to be studied in this way). The method of preparation was similar to that described for **1** in the literature.[8] 1,4,7-Triazacyclononane, **6**, was substituted at each nitrogen with either *N*-bromoacetyl-(*S*)-phenylalanine methyl ester or *N*-bromoacetyl-(*S*)-tryptophan methyl ester in dry dimethylformamide under basic conditions to give **1** and **3**, respectively, and H_3**2** was obtained by hydrolysing **1** with NEt_4OH in aqueous tetrahydrofuran (Scheme 2). Similar methods were used to prepare **4** and H_4**5** from 1,4,7,10-tetraazacyclododecane, **7**.

Zinc(II) and Cd^{2+} were chosen for the complexation studies as both are in the same group, have d^{10} electronic configurations and thereby have no electronically directed preferred stereochemistry, with the consequence that differences in their complexation are likely to be dominantly because of their differing ionic radii, r_M.[9] Their diamagnetism permits high resolution NMR studies. Copper(II) was chosen to provide a comparison for Zn^{2+} with an adjacent first row transition metal ion.

† Electronic supplementary information (ESI) available: Titration curve for H_3**3**$^{3+}$ alone and in the presence of Zn^{2+}, Cd^{2+} and Cu^{2+}. Fig. S2: Distribution variation of **3** and derived species with pH in the presence of Zn^{2+}. See http://www.rsc.org/suppdata/dt/b4/b401763c/

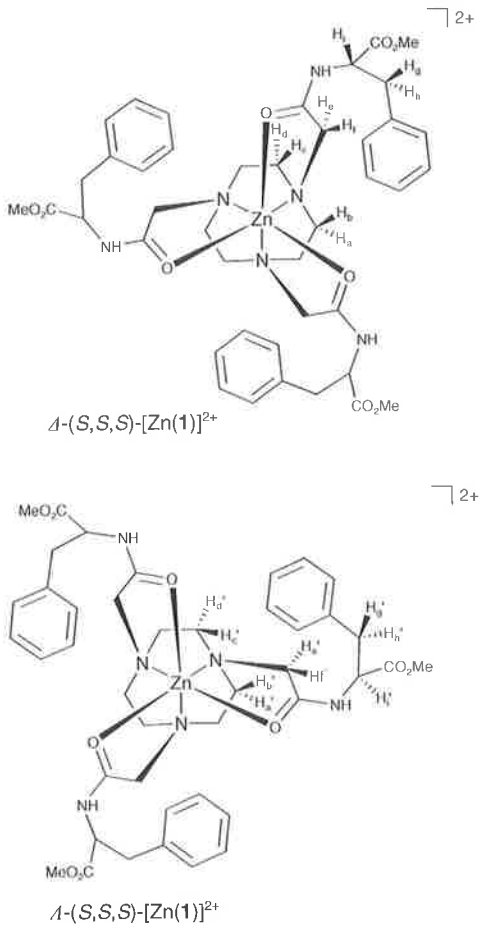

Scheme 1 Illustration of the rotation of the triaza plane relative to the trioxa plane, which is exaggerated for clarity.

Results and discussion

Ligand pK_as

The pK_as of the protonated ligands were determined in 20 : 80 v/v water–methanol solution by adding approximately three to seven equivalents of $HClO_4$ to solutions of **1**, H_3**2** and **3** and five equivalents to solutions of **4** and H_4**5**, to protonate the macrocyclic ring tertiary amines, followed by titration with NEt_4OH to obtain a potentiometric titration curve from which the pK_as were calculated (The titration curves for **1**, H_3**2**, **4** and **3** are shown in Figs. 1–3 and S1 (ESI†), respectively.) The two pK_as determined for $H_3\mathbf{1}^{3+}$and $H_3\mathbf{3}^{3+}$ are assigned to the protonated macrocyclic amines of **1** and **3** and it is assumed

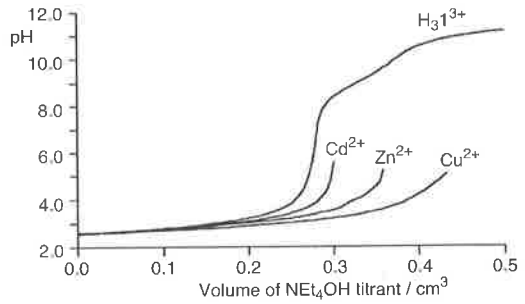

Fig. 1 Titration curve for $H_3\mathbf{1}^{3+}$, formed in a solution, where $[\mathbf{1}]_{total}$ = 9.10×10^{-4} and $[HClO_4]_{total} = 3.10 \times 10^{-3}$ mol dm^{-3} at 298.2 K and I = 0.10 mol dm^{-3} (NEt_4ClO_4). The titration curve is also shown for the same solution, except that it was also 7.00×10^{-4} mol dm^{-3} in $[Zn^{2+}]_{total}$. Titration curves are also shown where either $[Cd^{2+}]_{total}$ or $[Cu^{2+}]_{total}$ = 7.00×10^{-4} mol dm^{-3}, $[\mathbf{1}]_{total} = 9.00 \times 10^{-4}$ and $[H^+]_{total} = 3.10 \times 10^{-3}$ mol dm^{-3}. For the three metal ions the titration curves are shown up to the pH just below that at which precipitation of the metal complex or hydroxide occurred. Titrant $[NEt_4OH]$ = 0.104 mol dm^{-3}.

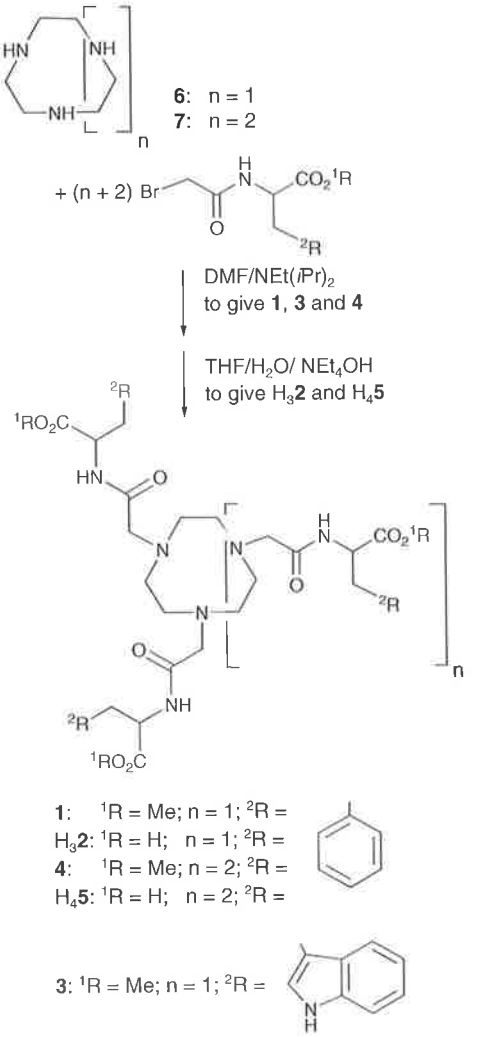

Scheme 2

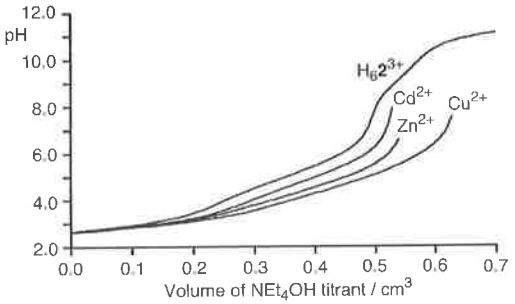

Fig. 2 Titration curve for $H_6\mathbf{2}^{3+}$, formed in a solution, where $[H_3\mathbf{2}]_{total}$ = 8.90×10^{-4} and $[HClO_4]_{total} = 6.00 \times 10^{-3}$ mol dm^{-3} at 298.2 K and I = 0.10 mol dm^{-3} (NEt_4ClO_4). Titration curves are also shown for the same solution, except that it was also 7.00×10^{-4} mol dm^{-3} in either $[Zn^{2+}]_{total}$, $[Cd^{2+}]_{total}$ or $[Cu^{2+}]_{total}$, up to the pH just below that at which precipitation of the metal complex or hydroxide occurred. Titrant $[NEt_4OH]$ = 0.104 mol dm^{-3}.

that the third pK_a is too small to be determined potentiometrically (Table 1). The three pK_as determined for H_4**4** are assigned to three protonated macrocyclic amines of **4** and it is assumed that the fourth pK_a is too small to be determined. The three larger pK_as of $H_6\mathbf{2}^{3+}$ are assigned to the three protonated macrocyclic amines, the smallest pK_a is assigned to a carboxylic acid and it is assumed that the pK_as of the other two carboxylic acids are too small to be determined. Similarly, the four larger pK_as of $H_8\mathbf{5}^{4+}$ are assigned to the four protonated macrocyclic amines, the two smaller pK_as are assigned to carboxylic acids and it is assumed that the pK_as of the other carboxylic acids are too small to be determined. The pH variations observed in the

Table 1 pK_as of the protonated forms of ligands **1**, H_3**2**, **3**, **4** and H_4**5** at 298.2 K and I = 0.10 mol dm^{-3} (NEt_4ClO_4) in 20 : 80 v/v water–methanol solution

Equilibrium quotient	pK_a
$[\mathbf{1}][H^+]/[H\mathbf{1}^+]^a$	8.69 ± 0.04
$[H\mathbf{1}^+][H^+]/[H_2\mathbf{1}^{2+}]$	3.59 ± 0.07
$[H_2\mathbf{1}^{2+}][H^+]/[H_3\mathbf{1}^{3+}]$	Low
$[\mathbf{2}^{3-}][H^+]/[H\mathbf{2}^{2-}]^b$	9.06 ± 0.02
$[H\mathbf{2}^{2-}][H^+]/[H_2\mathbf{2}^-]$	6.13 ± 0.04
$[H_2\mathbf{2}^-][H^+]/[H_3\mathbf{2}]$	4.93 ± 0.05
$[H_3\mathbf{2}][H^+]/[H_4\mathbf{2}^+]$	4.52 ± 0.06
$[H_4\mathbf{2}^+][H^+]/[H_5\mathbf{2}^{2+}]$	Low
$[H_5\mathbf{2}^{2+}][H^+]/[H_6\mathbf{2}^{3+}]$	Low
$[\mathbf{3}][H^+]/[H\mathbf{3}^+]^c$	8.79 ± 0.02
$[H\mathbf{3}^+][H^+]/[H_2\mathbf{3}^{2+}]$	3.67 ± 0.03
$[H_2\mathbf{3}^{2+}][H^+]/[H_3\mathbf{3}^{3+}]$	Low
$[\mathbf{4}][H^+]/[H\mathbf{4}^+]^d$	8.50 ± 0.02
$[H\mathbf{4}^+][H^+]/[H_2\mathbf{4}^{2+}]$	5.62 ± 0.04
$[H_2\mathbf{4}^{2+}][H^+]/[H_3\mathbf{4}^{3+}]$	3.77 ± 0.08
$[H_3\mathbf{4}^{3+}][H^+]/[H_4\mathbf{4}^{4+}]$	low
$[\mathbf{5}^{4-}][H^+]/[H\mathbf{5}^{3-}]^e$	9.89 ± 0.03
$[H\mathbf{5}^{3-}][H^+]/[H_2\mathbf{5}^{2-}]$	7.06 ± 0.06
$[H_2\mathbf{5}^{2-}][H^+]/[H_3\mathbf{5}^-]$	5.53 ± 0.06
$[H_3\mathbf{5}^-][H^+]/[H_4\mathbf{5}]$	5.46 ± 0.09
$[H_4\mathbf{5}][H^+]/[H_5\mathbf{5}^+]$	4.44 ± 0.06
$[H_5\mathbf{5}^+][H^+]/[H_6\mathbf{5}^{2+}]$	4.26 ± 0.09
$[H_6\mathbf{5}^{2+}][H^+]/[H_7\mathbf{5}^{3+}]$	Low
$[H_7\mathbf{5}^{3+}][H^+]/[H_8\mathbf{5}^{4+}]$	Low

Titration solutions: ^{a} $[\mathbf{1}]_{total}$ = 9.30 × 10^{-4} mol dm^{-3}, $[HClO_4]_{total}$ = 3.80 × 10^{-3} mol dm^{-3}. ^{b} $[\mathbf{2}]_{total}$ = 8.90 × 10^{-4} mol dm^{-3}, $[HClO_4]_{total}$ = 6.00 × 10^{-3} mol dm^{-3}. ^{c} $[\mathbf{3}]_{total}$ = 7.30 × 10^{-4} mol dm^{-3}, $[HClO_4]_{total}$ = 3.10 × 10^{-3} mol dm^{-3}. ^{d} $[\mathbf{4}]_{total}$ = 8.80 × 10^{-4} mol dm^{-3}, $[HClO_4]_{total}$ = 4.20 × 10^{-3} mol dm^{-3}. ^{e} $[\mathbf{5}]$ = 1.10 × 10^{-3} mol dm^{-3}, $[HClO_4]_{total}$ = 9.20 × 10^{-3} mol dm^{-3}. pK_w = 14.08.

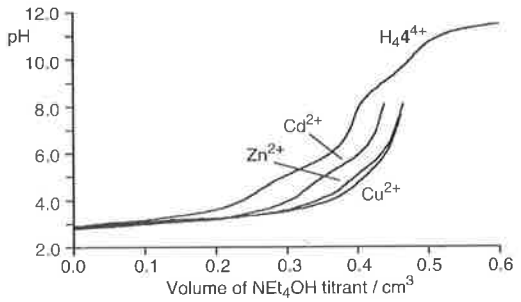

Fig. 3 Titration curve for $H_4\mathbf{4}^{4+}$, formed in a solution, where $[\mathbf{4}]_{total}$ = 1.27 × 10^{-3} mol dm^{-3}, and $[HClO_4]_{total}$ = 5.30 × 10^{-3} mol dm^{-3} at 298.2 K and I = 0.10 mol dm^{-3} (NEt_4ClO_4). Titration curves are also shown for the same solution, except that it was also 7.00 × 10^{-4} mol dm^{-3} in either $[Zn^{2+}]_{total}$, $[Cd^{2+}]_{total}$ or $[Cu^{2+}]_{total}$, up to the pH just below that at which precipitation of the metal complex or hydroxide occurred. Titrant $[NEt_4OH]$ = 0.103 mol dm^{-3}.

course of the titrations are not directly comparable to analogous variations in aqueous solution as the measured pH = 4.98 of the 20 : 80 v/v water–methanol, I = 0.10 mol dm^{-3} (NEt_4ClO_4), mixture reflects the method of electrode calibration. Thus, the ligand pK_as determined here in 20 : 80 v/v water–methanol solution cannot be directly compared with those in aqueous solution as is also the case for pK_as for the coordinated water in $[Cu(\mathbf{1})OH_2]^{2+}$ and the aquated Cu^{2+} ion.

Metal complex formation and speciation

The stoichiometry of the complexes formed and their complexation constants, K, were determined from titrations identical to those employed in the pK_a determinations except that the metal ion of interest was also present in the titration solution. This resulted in titration curves different from those of the protonated ligand alone due to the metal ion competing with the proton for ligand donor group lone electron pairs. In all cases the pH ranges over which these titrations could be carried out were limited by the precipitation of the metal complexes or hydroxides at high pH as indicated in Figs 1–3 and S1 (ESI †). The derived complexation Ks and pK_as for the protonated ligand complexes and coordinated water appear in Table 2. Speciation plots for the $[Zn(\mathbf{1})]^{2+}$, $[Zn(\mathbf{2})]^-$, $[Zn(\mathbf{4})]^{2+}$ and $[Zn(\mathbf{3})]^{2+}$ systems appear in Figs. 4–6 and S2 (ESI †), respectively. Similar speciation plots for the Cu^{2+} and Cd^{2+} systems may be generated from the data in Tables 1 and 2.

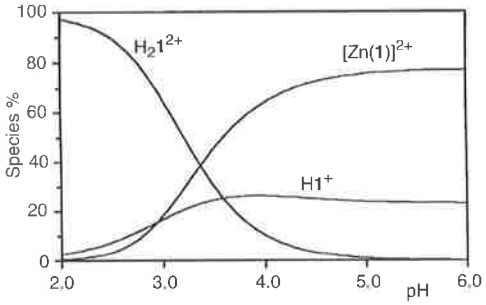

Fig. 4 Distribution variation of **1** containing species with pH, at 298.2 K, for a solution in which $[\mathbf{1}]_{total}$ = 9.10 × 10^{-4} mol dm^{-3}, $[Zn^{2+}]_{total}$ = 7.00 × 10^{-4} mol dm^{-3}, I = 0.10 mol dm^{-3} (NEt_4ClO_4) and for which 100% = $[\mathbf{1}]_{total}$

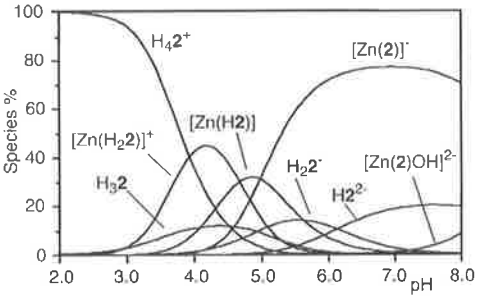

Fig. 5 Distribution variation of H_3**2** and derived species with pH, at 298.2 K, for a solution in which $[H_3\mathbf{2}]_{total}$ = 8.90 × 10^{-4} mol dm^{-3}, $[Zn^{2+}]_{total}$ = 7.00 × 10^{-4} mol dm^{-3}, I = 0.10 mol dm^{-3} (NEt_4ClO_4) and for which 100% = $[\mathbf{2}]_{total}$.

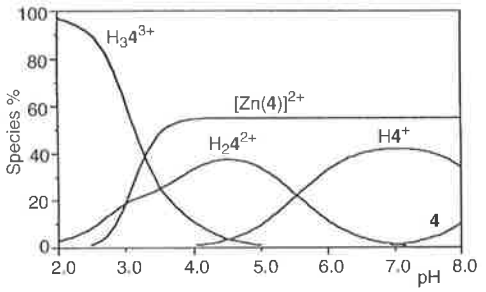

Fig. 6 Distribution variation of **4** containing species with pH, at 298.2 K, for a solution in which $[\mathbf{4}]_{total}$ = 1.27 × 10^{-3} mol dm^{-3}, $[Zn^{2+}]_{total}$ = 7.00 × 10^{-4} mol dm^{-3}, I = 0.10 mol dm^{-3} (NEt_4ClO_4) and for which 100% = $[\mathbf{4}]_{total}$.

The stability variation $[Cu(\mathbf{1})]^{2+}$ > $[Zn(\mathbf{1})]^{2+}$ > $[Cd(\mathbf{1})]^{2+}$ is consistent with the Jahn–Teller effect enhancing the stability of $[Cu(\mathbf{1})]^{2+}$ over that of $[Zn(\mathbf{1})]^{2+}$ within the Irving–Williams series,[10] and $[Cd(\mathbf{1})]^{2+}$ being the least stable complex due to the lower surface charge density of the large Cd^{2+} ion (six-coordinate r_M = 0.73, 0.74 and 0.95 Å, respectively.[9]) The same explanation applies to the analogous complexes of **3** and **4**. The greater stability of $[M(\mathbf{4})]^{2+}$ by comparison with that of $[M(\mathbf{1})]^{2+}$ may arise from a greater flexibility in either donor atom selection or stereochemistry presented by **4** for Cu^{2+} and Zn^{2+} whose coordination numbers do not usually exceed six whereas the larger Cd^{2+} probably becomes eight-coordinate as has been shown for Cd^{2+} complexes of similar pendant arm macrocyclic ligands by X-ray crystallography.[6] The increase in stability of $[M(\mathbf{3})]^{2+}$ over that of $[M(\mathbf{1})]^{2+}$ reflects a change in

Table 2 Complexation constants, $\log(K/dm^3\ mol^{-1})$, and pK_as for the complexes of Zn^{2+}, Cd^{2+} and Cu^{2+} with **1**, H_3**2**, **3** and **4** at 298.2 K and $I = 0.10$ mol dm^{-3} (NEt_4ClO_4)

Equilibrium quotient	$M^{2+} = Zn^{2+}$ $\log(K/dm^3\ mol^{-1})$	$M^{2+} = Cd^{2+}$ $\log(K/dm^3\ mol^{-1})$	$M^{2+} = Cu^{2+}$ $\log(K/dm^3\ mol^{-1})$
$[M(\mathbf{1})^{2+}]/[M^{2+}][\mathbf{1}]$	9.00 ± 0.09[a]	6.49 ± 0.08[a]	10.01 ± 0.05[a]
$[M(H\mathbf{1})^{3+}]/[M^{2+}][H\mathbf{1}^{+}]$		4.54 ± 0.06[a]	
$[M(\mathbf{2})^{-}]/[M^{2+}][\mathbf{2}^{3-}]$	10.68 ± 0.07[b]	4.99 ± 0.08[b]	12.55 ± 0.04[b]
$[M(H\mathbf{2})]/[M^{2+}][H\mathbf{2}^{2-}]$	6.60 ± 0.05[b]	4.64 ± 0.07[b]	7.66 ± 0.03[b]
$[M(H_2\mathbf{2})^{+}]/[M^{2+}][H_2\mathbf{2}^{-}]$	5.15 ± 0.04[b]	3.99 ± 0.05[b]	5.54 ± 0.02[b]
$[M(H_3\mathbf{2})^{2+}]/[M^{2+}][H_3\mathbf{2}]$		3.55 ± 0.05[b]	
$[M(\mathbf{2})_2^{4-}]/[M(\mathbf{2})^{-}][\mathbf{2}^{3-}]$			3.23 ± 0.05[b]
$[M(\mathbf{3})^{2+}]/[M^{2+}][\mathbf{3}]$	10.19 ± 0.05[c]	8.54 ± 0.09[c]	10.77 ± 0.10[c]
$[M(\mathbf{4})^{2+}]/[M^{2+}][\mathbf{4}]$	11.41 ± 0.02[d]	9.16 ± 0.07[d]	11.71 ± 0.02[d]
$[M(H\mathbf{4})^{3+}]/[M^{2+}][H\mathbf{4}^{+}]$		6.16 ± 0.04	
	pK_a	pK_a	pK_a
$[M(\mathbf{1})^{2+}][H^+]/[M(H\mathbf{1})^{3+}]$		6.74 ± 0.06[a]	
$[M(\mathbf{1})OH^+][H^+]/[M(\mathbf{1})^{2+}]$			5.83 ± 0.05[a,e]
$[M(\mathbf{2})^{-}][H^+]/[M(H\mathbf{2})]$	4.98 ± 0.05[b]	8.71 ± 0.07[b]	4.17 ± 0.03[b]
$[M(H\mathbf{2})][H^+]/[M(H_2\mathbf{2})^{+}]$	4.68 ± 0.04[b]	5.48 ± 0.05[b]	4.01 ± 0.02[b]
$[M(H_2\mathbf{2})^{+}][H^+]/[M(H_3\mathbf{2})^{2+}]$		4.49 ± 0.03[b]	
$[M(\mathbf{2})OH^{-}][H^+]/[M(\mathbf{2})^{-}]$	8.91 ± 0.04[b,e]		
$[M(\mathbf{4})^{2+}][H^+]/[M(H\mathbf{4})^{3+}]$		5.50 ± 0.04[d]	
$[M(\mathbf{4})OH^+][H^+]/[M(\mathbf{4})^{2+}]$			5.78 ± 0.06[d,e]
$[MOH^+][H^+]/[M^{2+}]$	4.87 ± 0.04[e]	>7[e,f]	5.14 ± 0.04[e]

Three solutions were titrated for each system in which the total ligand concentration varied in the range shown. The other total concentrations were not varied: [a] $[\mathbf{1}]_{total} = 9.10 \times 10^{-4}$ mol dm^{-3}, $[Zn^{2+}]_{total}$, $[Cd^{2+}]_{total}$ or $[Cu^{2+}]_{total} = 7.00 \times 10^{-4}$–$1.50 \times 10^{-3}$ mol dm^{-3}, $[HClO_4]_{total} = 3.10 \times 10^{-3}$ mol dm^{-3}. [b] $[H_3\mathbf{2}]_{total} = 8.90 \times 10^{-4}$ mol dm^{-3}, $[Zn^{2+}]_{total}$, $[Cd^{2+}]_{total}$ or $[Cu^{2+}]_{total} = 7.00 \times 10^{-4}$–$1.50 \times 10^{-3}$ mol dm^{-3}, $[HClO_4]_{total} = 6.00 \times 10^{-3}$ mol dm^{-3}. [c] $[\mathbf{3}]_{total} = 7.30 \times 10^{-4}$ mol dm^{-3}, $[Zn^{2+}]_{total}$, $[Cd^{2+}]_{total}$ or $[Cu^{2+}]_{total} = 8.00 \times 10^{-4}$–$1.04 \times 10^{-3}$ mol dm^{-3}, $[HClO_4]_{total} = 3.10 \times 10^{-3}$ mol dm^{-3}. [d] $[\mathbf{4}]_{total} = 1.27 \times 10^{-3}$ mol dm^{-3}, $[Zn^{2+}]_{total}$, $[Cd^{2+}]_{total}$ or $[Cu^{2+}]_{total} = 7.00 \times 10^{-4}$–$1.90 \times 10^{-3}$ mol dm^{-3}, $[HClO_4]_{total} = 5.30 \times 10^{-3}$ mol dm^{-3}. [e] pK_a of coordinated water. [f] Precipitation of hydroxide prevented accurate determination. $pK_w = 14.08$.

ligand structure at some distance from the three amine nitrogens and three amide oxygens which are the most probable donor set, judging from the X-ray crystal structure of $[Cu(\mathbf{1})]^{2+}$.[8] A possible explanation is that the substantial increase in ligand bulk on going from **1** to **3** decreases the competitive complexing ability of water for M^{2+} either as a consequence of increased steric hindrance to the approach of water to the complex or a change in water structure around the complex through an increase in hydrophobicity or both. The formation of $[Cd(H\mathbf{1})]^{3+}$ and $[Cd(H\mathbf{4})]^{3+}$, but not $[Cd(H\mathbf{3})]^{3+}$ and none of the analogous Cu^{2+} and Zn^{2+} complexes, may be attributable to the larger size of Cd^{2+} whereby the weaker coordination of $H\mathbf{1}^+$ by Cd^{2+} lowers the pK_a of the protonated ligand from (8.69 to 6.74; Tables 1 and 2) to a lesser extent than do Zn^{2+} and Cu^{2+} so that $[Zn(H\mathbf{1})]^{3+}$ and $[Cu(H\mathbf{1})]^{3+}$ are too acidic to be present in detectable quantities. The decreased stability of $[Cd(H\mathbf{1})]^{3+}$ by comparison with $[Cd(\mathbf{1})]^{2+}$ probably arises from a combination of charge repulsion between $H\mathbf{1}^+$ and Cd^{2+} and the decrease in ligand denticity from six to five. A similar rationale applies to $[Cd(H\mathbf{4})]^{3+}$.

Copper(II) forms two complexes not detectably formed by Zn^{2+} and Cd^{2+} (Table 2). The first is $[Cu(\mathbf{1})OH]^+$ which forms from the conjugate acid $[Cu(\mathbf{1})OH_2]^{2+}$ where the coordinated water has a $pK_a = 5.83$ which compares with a $pK_a = 5.14$ for the aquated Cu^{2+} ion under the conditions of this study. It appears that one of the relatively weak donor amide oxygen atoms may be displaced by water in the first coordination sphere of six-coordinate Cu^{2+}. The second complex is $[Cu(\mathbf{2})_2]^{4-}$ which may involve each of the three amine nitrogens of both $\mathbf{2}^{3-}$ coordinating six-coordinate Cu^{2+} and thereby minimizing charge repulsion between the two $\mathbf{2}^{3-}$. Such a structure requires that the three amide oxygen donor groups of each sexadentate $\mathbf{2}^{3-}$ are not involved in the coordination scheme and reflects the relative donor weakness of amide groups compared with the donor strength of the amine groups. (The bis coordination of **6**, the precursor to $\mathbf{2}^{3-}$, is well known.[11]) The occurrence of these complexes for Cu^{2+} only may reflect its d^9 electronic configuration and the stereochemical preferences that it engenders, whereas d^{10} Zn^{2+} has more flexible stereochemical requirements.

Metal complex NMR spectra and solution structure

Two possible diastereomers of $[Zn(\mathbf{1})]^{2+}$, Δ-(*S*,*S*,*S*) and Λ-(*S*,*S*,*S*) are shown schematically in Scheme 1 where Zn^{2+} is shown at the centre of an octahedron delineated by three amine nitrogens and three amide oxygens. A right hand rotation of the three chelate rings defines one diastereomer as Δ and a left hand rotation defines the other diastereomer as Λ, as was found in the $[Cu(\mathbf{1})]^{2+}$ crystal structure.[8] The adjacent macrocyclic ring methylene protons, Ha–Hd, are inequivalent because of the Δ orientation of the chelate rings in Δ-(*S*,*S*,*S*)-$[Zn(\mathbf{1})]^{2+}$ and should generate a ^1H NMR ABCD multiplet. A similar inequivalence exists for the adjacent methylene group protons, Ha′–Hd′ of Λ-(*S*,*S*,*S*)-$[Zn(\mathbf{1})]^{2+}$ which should also generate an ABCD multiplet with a chemical shift different from that of the Δ isomer as a consequence of the different magnetic environments of the protons in the two diastereomers. The He–Hi and He′–Hi′ sets of proton resonances of the pendant arms in the two diastereomers should similarly be distinguished from each other although being more distant from the coordinating atom set this may not be so apparent in the ^1H chemical shift differences. Similar inequivalences prevail in the diastereomeric complexes of $H_3\mathbf{2}$–$\mathbf{2}^{3-}$, **3** and **4** and collectively provide an opportunity to probe the stereochemistry of their complexes. The Δ and Λ diastereomeric complexes should each exhibit two ^{13}C resonances arising from their inequivalent adjacent methyl-

ene macrocyclic ring carbons to afford a further indication of their stereochemistry.

In the Zn^{2+} and Cd^{2+} complexes, $[M(\mathbf{1})]^{2+}$, $[M(\mathbf{3})]^{2+}$ in CD_3OD and $[M(\mathbf{4})]^{2+}$ in CD_3CN single sets of ^1H and ^{13}C resonances are observed in contrast to the duplicate resonance sets expected for the coexistence of both the Δ and Λ diastereomers in slow exchange on the NMR timescale. (The resonances, their chemical shifts and their assignments are listed in the last section of the Experimental section). The complexes of $H_3\mathbf{2}$ and $H_4\mathbf{5}$ were insufficiently soluble for NMR study.) This is exemplified by **3**, the flexible nature of which renders the three macrocylic pairs of methylene groups equivalent on a time average such that they are characterized by an AA′BB′ multiplet. In contrast the adjacent methylene groups of $[Zn(\mathbf{3})]^{2+}$ are inequivalent and the Ha–Hd protons are unique and produce a single well resolved ABCD multiplet as expected for a single diastereomer (Fig. 7). Thus, only a single diastereomer exists for each complex. 1,4,7-Triazacyclononane and 1,4,7,10-tetraazacyclododecane pendant arm systems in which only one diastereomeric alkali metal complex exists and exchange between equivalent forms of a single diastereomer occurs have been reported.[12]

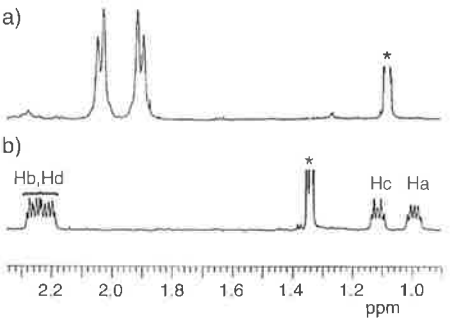

Fig. 7 The ^1H NMR (600 MHz) macrocyclic ring resonances of (a) **3** and (b) of $[Zn\mathbf{3}]^{2+}$ in CD_3OD solution. The proton labelling is as in Scheme 1 and * indicates the solvent proton impurity resonances which appear at differing δ due to the different dielectric constants of the solutions.

Conclusion

The complexation behaviour of ligands **1**, $H_3\mathbf{2}$–$\mathbf{2}^{3-}$, **3** and **4** is similar to that of other pendant arm ligands based on N-substitution of 1,4,7-triazacyclononane and 1,4,7,10-tetraazacyclododecane. The variation in stability of the metal complexes can be rationalized in terms of differing stereochemical influences of the d^9 and d^{10} electronic configurations of $Cu^{2+}$and Zn^{2+}, respectively, the size differences of Zn^{2+} and Cd^{2+}, the differing denticities of the ligands and the differences in bulk of the extremities of the amino acid residues. The chiral centre in each pendant arm makes it possible to form two diastereomers of each metal complex, but the NMR data suggest that only one diastereomer exists. Each diastereomer constitutes a part turn of either a triple or quadruple helix and it is envisaged that the attachment of peptide pendant arms to the macrocycle instead of single amino acid residues may make it possible to study multiple metal complexing by more extended amino acid helices in future studies.

The present study of multiple amino acid coordination may also be significant in the context of tumour specific radionuclide delivery. For example, the integrin $\alpha_v\beta_3$, which is known to be expressed in elevated levels within the cell membrane of several types of tumour cells, will bind to proteins carrying the arginine-glycine-asparagine (RGD) sequence.[13] Accordingly, macrocycles conjugated to a peptide containing the RGD sequence have the potential to carry radionuclides to the site of tumour with some degree of selectivity. The attachment of amino acids to pendant arm macrocycles, as is described here, paves the way for future work in which peptide attachment is undertaken.

Experimental

General

Water was purified with a Waters Milli-Q system to give a specific resistance of >15 MΩ cm and was then boiled for 30 min to remove CO_2 and allowed to cool in flasks fitted with soda lime tubes. AR methanol was redistilled. A 20 : 80 v/v water–methanol mixture was used as the solvent in all titrations. Titration solutions were saturated with nitrogen by passing a fine stream of bubbles (previously passed through aqueous 0.10 mol dm^{-3} NaOH followed by 0.10 mol dm^{-3} NEt_4ClO_4) through them for at least 15 min before the commencement of the titration. During the titrations a fine stream of nitrogen bubbles was passed through the titration solution which was magnetically stirred and held at 298.2 ± 0.1 K in a water-jacketed 20 cm^3 titration vessel that was closed to the atmosphere except for a small vent for the nitrogen stream. The titrations were carried out using a Metrohm Dosimat E665 titrimator, an Orion SA 720 potentiometer and an Orion 8172 Ross Sureflow combination pH electrode. Values of E_o and pK_w were determined by titration of a solution that was 1.00×10^{-4} mol dm^{-3} in $HClO_4$ and $I = 0.10$ mol dm^{-3} (NEt_4ClO_4) against 0.104 mol dm^{-3} NEt_4OH. In the pK_a determinations 0.104 mol dm^{-3} NEt_4OH was titrated against solutions that were 7.30×10^{-4}–1.10×10^{-3} mol dm^{-3} in either **1**, $H_3\mathbf{2}$, **3** or **4**, 3.10–9.20 $\times 10^{-3}$ mol dm^{-3} in $HClO_4$ and $I = 0.10$ mol dm^{-3} (NEt_4ClO_4). Titrations to determine the complexation constants, K, for the Zn^{2+}, Cu^{2+} and Cd^{2+} complexes were carried out at the same concentrations of ligand and $HClO_4$ in the presence of the metal perchlorates at 7.00–8.00 $\times 10^{-4}$ mol dm^{-3}. (The individual concentrations applying to each titration are given in Tables 1 and 2.) At least three runs were carried out for each system and at least two of these runs were averaged; the criterion for selection for this averaging being that χ^2 for each run was < 12.6 at the 95% confidence level. Values for each pK_a and K were determined using the program SUPERQUAD[14] (**CAUTION**: Anhydrous perchlorates are potentially explosive and should be handled with caution.)

^1H (199.953 MHz), ^1H (300.145 MHz) and ^{13}C (75.5 MHz) NMR spectra were run on Varian Gemini 200 and 300 NMR spectrometers. ^1H (599.957 MHz) and ^{13}C (150.8 MHz) NMR spectra were run on an Inova 600 spectrometer. Solutions of either **1**, $(NEt_4)_3\mathbf{2}$, **3**, **4** or $(NEt_4)_4\mathbf{5}$ alone or in the presence of equimolar Zn^{2+} or Cd^{2+} were prepared to give concentrations of 0.013–0.015 mol dm^{-3} in each constituent in either 0.10 mol dm^{-3} ND_3/ND_4Cl buffer at pD 10 or 10^{-3} mol dm^{-3} NaOD and 0.1 mol dm^{-3} in $NaClO_4$ (pD ≤ 11) in D_2O. Chemical shifts were determined against external trimethylsilylpropiosulfonic acid in non-aqueous solvents and against the HOD resonance (assigned $\delta = 4.72$ ppm) in D_2O. ESI mass spectrometric studies were made in positive ion mode with a Finnigan MAT ion trap LCQ mass spectrometer fitted with an electrospray ionization source. Samples were dissolved in water for injection. Elemental analyses were performed by the Microanalytical Service of the Chemistry Department, University of Otago, Dunedin, New Zealand.

Syntheses and characterizations

All reagents used were obtained from Aldrich and were not further purified before use. All solvents used in syntheses were redistilled and dried by standard methods.[15] 1,4,7-Tris(*p*-toluenesulfonyl)diethylenetriamine,[16] 1,4,7-tris(*p*-toluenesulfonyl)diethylenetriamine-1,7-disodium salt,[17] 1,2-di(*p*-toluenesulfonyloxy)ethane,[18] 1,4,7-tris(*p*-toluenesulfonyl)-1,4,7-triazacyclononane,[17,18] 1,4,7-triazacyclononane trihydrobromide,[19] 1,4,7-triazacyclononane,[17] *N*-bromoacetyl-(*S*)-phenylalanine methyl ester,[8] 1,4,7-tris[(2″*S*)-acetamido-2″-(methyl-3″-phenylpropionate)]-1,4,7-triazacyclononane, **1**,[8] {1,4,7-tris[(2″*S*)-acetamido-2″-(methyl-3″-phenylpropionate)]-1,4,7-triazacyclo-

nonane}zinc(II) triflate[8] and *S*-tryptophan methyl ester hydrochloride[20] were prepared by methods similar to those described in the literature. Good elemental analyses, spectroscopic and mp characterizations were obtained.

Tris(tetraethylammonium 1,4,7-tris[(2″*S*)-acetamido-2″-(1″-carboxy-3″-phenylpropane)]-1,4,7-triazacyclononane ((NEt$_4$)$_3$2). An aqueous solution of 0.1 M tetraethylammonium hydroxide (20 cm^3) was added dropwise to a solution of **1** (400 mg, 0.53×10^{-3} mol) in a solvent mixture of water–tetrahydrofuran (10 cm^3, 1 : 1 v/v) and stirred under nitrogen at room temperature for 4 days. The solvent was then removed to yield an oil, subsequent washings with acetone and ether removed excess hydroxide to yield a hygroscopic white crystals in 80% yield, δ_H (600 MHz, D_2O) 1.21 (36H, t, (C*H*$_3$CH$_2$)$_4$N), 2.40–2.70 (12H, AA′BB′, 3 × N(CH$_2$)$_2$N ring), 2.96 (6H, s, CH$_2$C=O), 3.14 (6H, m, ArC*H*$_2$), 3.17 (24H, q, (CH$_3$C*H*$_2$)$_4$N), 4.50 (3H, m, αCH), 7.56–7.97 (15H, m, ArH); δ_C (150.8 MHz) 6.4 ((*C*H$_3$CH$_2$)$_4$N), 37.2 (Ar*C*H$_2$), 51.8 ((CH$_3$*C*H$_2$)$_4$N), 55.2 (αCH), 55.5 (N(CH$_2$)$_2$)N ring), 61.2 (*C*H$_2$C=O), 127.2 (ArH), 129.0 (ArH), 129.4 (ArH), 137.2 (ArH), 173.5 (C=ONH), 178.0 (*C*=OCH); *m/z* (LCQ) 1132 ((NEt$_4$)$_3$**2**$^+$, 20%). The hygroscopic nature of (NEt$_4$)$_3$**2** rendered elemental analysis difficult and accordingly its Zn(II) complex was prepared and gave good elemental analyses as described below.

Tetraethylammonium {1,4,7-tris[(2″*S*) acetamido-2″-(1″-carboxy-3″-phenylpropane)]-1,4,7-triazacyclononane}zinc(II) triflate·4MeOH, NEt$_4$[Zn(H$_2$2)](CF$_3$SO$_3$)$_2$·4MeOH. A solution of Zn(CF$_3$SO$_3$)$_2$ (16 mg, 4.4×10^{-5} mol) in methanol (1 cm^3) was added to a solution of NEt$_4$**2** (50 mg, 4.4×10^{-5} mol) in methanol (2 cm^3). A layer of ether (1 cm^3) was then added and the solution was then left overnight. The resulting precipitate was then collected by filtration under reduced pressure and dried over P_4O_{10} under reduced pressure to yield a yellow solid (55 mg, 84%) (Found: C, 45.83; H, 6.54; N, 7.17. C$_{49}$H$_{67}$N$_7$O$_{15}$F$_6$S$_2$Zn(MeOH)$_4$ (NEt$_4$Zn·H$_2$**2**·4MeOH) requires C, 46.65; H, 6.14; N, 7.19%)

***N*-Bromoacetyl-(*S*)-tryptophan methyl ester.** (*S*)-Tryptophan methyl ester hydrochloride (9 g, 35.4 mmol) was dissolved in a solution of dry tetrahydrofuran (100 cm^3) and triethylamine (18.7 cm^3, 134.5 mmol) under nitrogen and cooled to 0 °C. Bromoacetyl bromide (3.99 cm^3, 46 mmol) in dry tetrahydrofuran (50 cm^3) was then added dropwise to the solution at 0 °C. The reaction was allowed to warm to room temperature over 1 h and was then quenched with a dropwise addition of water (20 cm^3). The solution was extracted with ethyl acetate (40 cm^3) and the organic layer washed with 1 mol dm^{-3} hydrochloric acid (20 cm^3) followed by saturated aqueous sodium bicarbonate (20 cm^3). The organic layer was dried over Na_2SO_4 and the solvent was removed under reduced pressure to give *N*-bromoacetyl-(*S*)-phenylalanine methyl ester as a crystalline solid (9.9 g, 75%) which was used without further purification, mp 56–63 °C, δ_H (200 MHz, $CDCl_3$), 3.33 (2H, d, J = 5.6, ArC*H*$_2$), 3.68 (3H, s, OCH$_3$), 3.82 (2H, s, BrCH$_2$), 4.87 (1H, m, α-CH), 7.00–7.55 (5H, m ArH) 8.34 (1H, br s, NH); δ_C (75 MHz) 27.0 (Ar*C*H$_2$), 28.6 (OCH$_3$), 52.4 (αCH), 53.4 (BrCH$_2$), 109.3, 111.2, 118.3, 118.4, 119.6, 122.2, 127.3, 136.0, (*C*=C), 165.2, 171.6 (C=O); *m/z* (EI) 338 (M$^+$), 258 (20), 201 (19), 170 (9), 130 (98%).

1,4,7-Tris[(2″*S*)-acetamido-2″-(methyl-3″-(1*H*-3-indolyl)propionate)]-1,4,7-triazacyclononane (3). *N*-Bromoacetyl-(*S*)-tryptophan methyl ester (3.43 mg, 9.0 mmol) was dissolved in a solution of diisopropylethylamine (2.72 cm^3, 15.6 mmol) and dry DMF (6 cm^3) under nitrogen and cooled to 0 °C. Solid 1,4,7-triazacyclononane (358 mg, 2.7 mmol) was then added and the solution was left to stir overnight under nitrogen. The solution was then diluted with water (20 cm^3) and extracted with dichloromethane. The dichloromethane was then removed from the extract under reduced pressure and the resulting oil was washed with water, dissolved in dichloromethane–methanol 10 : 0.4 (v/v) and run down a basic alumina column (2.5 × 25 cm). Evaporation of the solvent from the eluent yielded a white fluffy solid (1.19 g, 50%), δ_H (600 MHz, $CDCl_3$) 2.45 (12H, AA′BB′, 3 × N(CH$_2$)$_2$N ring), 3.09 (6H, s, CH$_2$-C=O), 3.16 (6H, m, ArC*H*$_2$), 3.72 (9H, s, OCH$_3$), 4.87 (3H, m, αCH), 7.06–7.25 (15H, m, ArH); δ_C (150.8 MHz) 37.5 (Ar*C*H$_2$), 52.3 (OCH$_3$), 52.6 (αCH), 56.5 (N(CH$_2$)$_2$)N ring), 62.5 (*C*H$_2$-C=O), 109.5 (ArH), 111.4 (ArH), 118.4 (ArH), 119.5 (ArH), 122.1 (ArH), 123.0 (ArH), 127.7 (ArH), 136.0 (ArH), 170.8 (C=ONH), 172.0 (*C*=OCH); *m/z* (LCQ) 904 (**3**$^+$, 95%). Over a period of several weeks **3** underwent a slow hydrolysis of its amide functional groups. Accordingly, its Zn(II) complex, which stabilizes **3** towards hydrolysis, was prepared and gave good elemental analyses as described below.

{1,4,7-Tris[(2″*S*)-acetamido-2″-(methyl-3″-(1*H*-3-indolyl)propionate)]-1,4,7-triazacyclononane}zinc(II) ditriflate–methanol, [Zn(3)](CF$_3$SO$_3$)$_2$·CH$_3$OH. A solution of Zn(CF$_3$SO$_3$)$_2$ (5.8 mg, 1.6×10^{-5} mol) in methanol (1 cm^3) was added to a solution of **3** (20 mg, 2.2×10^{-5} mol) in methanol (2 cm^3). Diethyl ether (1 cm^3) was then added and the resulting solution was left overnight. The resulting precipitate was then collected and dried to yield a yellow solid (12 mg, 60%) (Found: C, 47.27; H, 4.57; N, 9.58. C$_{50}$H$_{57}$O$_{15}$N$_9$F$_6$S$_2$Zn·CH$_3$OH requires C, 47.18; H, 4.74; N, 9.71%).

1,4,7,10-Tetrakis[(2″*S*)-acetamido-2″-(methyl-3″-phenylpropionate)]-1,4,7,10-tetraazacyclododecane (4). *N*-Bromoacetyl-(*S*)-phenylalaninemethylester (500 mg, 1.66 mmol) was dissolved in diisopropylethylamine (0.46 cm^3, 26.5 mmol) and dried dimethylformamide (5 cm^3) under nitrogen. The solution was cooled to 0 °C and 1,4,7,10-tetraazacyclododecane (57 mg, 0.32 mmol) added. The reaction was left to stir overnight at room temperature and was then diluted with water (20 cm^3) and extracted with dichloromethane. The solvent was removed under reduced pressure and the resulting oil was washed with water, dissolved in dichloromethane–methanol 10 : 0.4 (v/v) and run down a basic alumina column (2.5 × 25 cm). The solvent was removed under reduced pressure to give a yellow oil. The oil was dissolved in dichloromethane. Diethyl ether was then added and a milky solution formed which was concentrated under reduced pressure to yield a white fluffy solid which was filtered off (250 mg, 50%), δ_H (600 MHz, $CDCl_3$) 2.36–2.57 (16H, m, AA′BB′, 4 × N(CH$_2$)$_2$N ring), 3.01 (8H, s, CH$_2$C=O), 3.09 (8H, m, ArC*H*$_2$), 3.68 (12H, s, OCH$_3$), 4.87 (4H, m, αCH), 7.08–7.24 (20H, m, ArH); δ_C (150.8 MHz) 37.5 (Ar*C*H$_2$), 52.2 (OCH$_3$), 53.1 (αCH), 56.3 (N(CH$_2$)$_2$)N ring), 62.3 (*C*H$_2$C=O), 127.0 (ArH), 128.4 (ArH), 129.0 (ArH), 136.0 (ArH), 170.7 (C=ONH), 172.0 (*C*=OCH); *m/z* (LCQ) 1071.6 (Na·**4**, 95%) (Found: C, 62.95; H, 6.95; N, 10.51. C$_{56}$H$_{72}$N$_8$O$_{12}$·H$_2$O requires C, 63.01; H, 6.99; N, 10.50%)

Tetrakis(tetraethylammonium) 1,4,7,10-tetrakis[(2″*S*)-acetamido-2″-(1″-carboxy-3″-phenylpropane)]-1,4,7,10-tetraazacyclododecane ((NEt$_4$)$_4$5). An aqueous solution of 0.1 mol dm^{-3} NEt$_4$OH (42 cm^3) was added dropwise to a solution of **4** (600 mg, 5.7×10^{-4} mol) dissolved in water–tetrahydrofuran (20 cm^3, 1 : 1, v/v) and stirred under nitrogen at room temperature for 4 days. The solvent was then removed under reduced pressure to yield an oil, which after washing with acetone and ether to remove excess hydroxide gave a hygroscopic white crystalline product (410 mg, 80%), δ_H (600 MHz, D_2O) 1.21 (48H, t, (C*H*$_3$CH$_2$)$_4$N), 2.10–2.40 (16H, AA′BB′, 4 × N(CH$_2$)$_2$N ring), 2.86–3.14 (12H, m, CH$_2$C=O and ArC*H*$_2$), 3.19 (32H, q, (CH$_3$C*H*$_2$)$_4$N), 4.50 (4H, m, αCH), 7.09–7.48 (20H, m, ArH); δ_C (150 MHz) 8.45 (*C*H$_3$CH$_2$)$_4$N), 37.2 (ArCH$_2$), 53.9 (CH$_3$*C*H$_2$)$_4$N), 55.2 (αCH), 55.5 (N(CH$_2$)$_2$)N ring), 61.2 (*C*H$_2$C=O), 127.2 (ArH), 129.0 (ArH), 129.4 (ArH), 137.2

(ArH), 173.5 (C=ONH), 178.0 (*C*=OCH); *m/z* (LCQ) 993.5 (H_4**5**, 98%). The hygroscopic nature of $(NEt_4)_4$**5** rendered elemental analysis difficult and accordingly its Zn(II) complex was prepared and gave good elemental analyses as described below.

Bis(tetraethylammonium) {1,4,7,10-tetrakis[(2″*S*)-acetamido-2″-(1″-carboxy-3″-phenylpropane)]-1,4,7,10-tetraazacyclododecane}zinc(II) ditriflate–methanol (1/6), $(NEt_4)_2$[Zn($H_2$5)]$(CF_3SO_3)_2$·6MeOH. A solution of $Zn(CF_3SO_3)_2$ (11 mg, 3.0×10^{-5} mol) in methanol (1 cm^3) was added to a solution of $(NEt_4)_4$**5** (50 mg, 3.0×10^{-5} mol) in methanol (2 cm^3). Diethyl ether (1 cm^3) was added and the solution was then left overnight. The resulting yellow precipitate was then collected and dried over P_4O_{10} under reduced pressure (51 mg, 85%) (Found: C, 50.45; H, 7.45; N, 7.60. $C_{70}H_{102}O_{18}N_{10}F_6S_2Zn$·6MeOH requires C, 50.50: H, 7.04; N, 7.76.)

^{1}H (600 MHz) and ^{13}C (150.8 MHz) NMR spectra in CD_3OD and CD_3CN. *1*. δ_H (600 MHz, CD_3OD) 2.45 ([Ha, Hb, Hc, Hd], 12H, AA′BB′, 3 × $N(CH_2)_2N$ ring), 3.05 ([Hf, He], 6H, s, CH_2C=O), 3.18 ([Hg, Hh], 6H, m, ArCH_2), 3.71 (9H, s, OCH_3), 4.74 ([Hi], 3H, m, αCH), 7.06–7.25 (15H, m, ArH); δ_C (150.8 MHz) 38.6 (ArCH_2), 53.3 (OCH_3), 55.0 (αCH), 58.1 ($N(CH_2)_2$)N ring), 63.0 (CH_2C=O), 128.3(ArH), 130.8 (ArH), 133.0 (ArH), 138.4 (ArH), 173.8 (C=ONH), 174.4 (*C*=OCH).

[Zn(1)]$^{2+}$. δ_H (600 MHz, CD_3OD) 1.81 ([Ha], 3H, m, $N(CH_2)_2N$ ring), 2.45 ([Hc], 3H, m, $N(CH_2)_2N$ ring), 2.61 ([Hb], 3H, m, $N(CH_2)_2N$ ring), 2.85 ([Hg], 3H, m, ArCH_2), 2.89 ([Hd], 3H, m, $N(CH_2)_2N$ ring), 3.16 ([Hf], 3H, d, J = 16.5 Hz, CH_2-C=O), 3.33 ([Hh], 3H, m, ArCH_2), 3.55 ([He], 3H, d, J = 16.5 Hz, CH_2C=O), 3.83 (9H, s, OCH_3), 4.98 ([Hi], 3H, m, αCH), 7.17–7.29 (15H, m, ArH); δ_C (150.8 MHz) 39.4 (ArCH_2), 50.4 ($N(CH_2)_2$)N ring), 53.5 ($N(CH_2)_2$)N ring), 53.7 (OCH_3), 56.7 (αCH), 59.5 (CH_2C=O), 128.6 (ArH), 130.1 (ArH), 131.2 (ArH), 138.5 (ArH), 172.2 (*C*=OCH), 174.7 (C=ONH).

[Cd(1)]$^{2+}$. δ_H (600 MHz, CD_3OD) 2.30 ([Ha, Hc], 6H, m, $N(CH_2)_2N$ ring), 2.69 ([Hd], 3H, m, $N(CH_2)_2N$ ring), 2.82 ([Hb], 3H, m, $N(CH_2)_2N$ ring), 2.95 ([Hg], 3H, m, ArCH_2), 3.22 ([Hh], 3H, m, ArCH_2), 3.43 ([He, Hf], 6H, br s, CH_2C=O), 3.71 (9H, s, OCH_3), 4.89 ([Hi], 3H, m, αCH), 7.17–7.28 (15H, m, ArH); δ_C (150.8 MHz) 38.9 (ArCH_2), 53.0 ($N(CH_2)_2$)N ring), 53.5 (OCH_3), 53.8 ($N(CH_2)_2$)N ring), 56.3 (αCH), 61.6 (CH_2-C=O), 128.6 (ArH), 130.0 (ArH), 130.9 (ArH), 138.3 (ArH), 172.8 (*C*=OCH), 173.9 (C=ONH).

3. δ_H (600 MHz, CD_3OD) 1.89 ([Ha, Hb], 6H, d, $N(CH_2)_2N$ ring), 2.02 ([Hc, Hd], 6H, d, $N(CH_2)_2N$ ring), 2.77 ([He, Hf], 6H, s, CH_2C=O), 3.33 ([Hg, Hh], 6H, m, ArCH_2), 3.70 (9H, s, OCH_3), 4.76 ([Hi], 3H, m, αCH), 6.93 (6H, m, ArH), 7.03 (3H, t, ArH), 7.26 (3H, d, ArH), 7.39 (3H, d, ArH); δ_C (150.8 MHz) 28.3 (ArCH_2), 53.4 (OCH_3), 54.6 (αCH), 57.6 ($N(CH_2)_2$)N ring), 63.6 (CH_2C=O), 110.6 (ArH), 112.8 (ArH), 119.5 (ArH), 120.4 (ArH), 123.0 (ArH), 125.4 (ArH), 129.5 (ArH), 138.5 (ArH), 174.2 (C=ONH), 174.4 (*C*=OCH).

[Zn(3)]$^{2+}$. δ_H (600 MHz, CD_3OD) 1.00 ([Ha], 3H, m, $N(CH_2)_2N$ ring), 1.10 ([Hc], 3H, m, $N(CH_2)_2N$ ring), 2.23 ([Hb, Hd], 6H, m, $N(CH_2)_2N$ ring), 2.91 ([Hg] 3H, m, ArCH_2), 3.33 ([He, Hf], 6H, s, CH_2C=O), 3.44 ([Hh], 3H, m, ArCH_2), 3.93 (9H, s, OCH_3), 5.09 ([Hi], 3H, m, αCH), 6.99 (3H, t, ArH), 7.05 (3H, s, ArH), 7.17 (3H, t, ArH), 7.34 (3H, d, ArH), 7.49 (3H, d, ArH); δ_C (150.8 MHz) 29.4 (ArCH_2), 50.3 (OCH_3), 51.9 ($N(CH_2)_2$)N ring), 52.4 ($N(CH_2)_2$)N ring), 53.8 (CH_2C=O), 55.0 (αCH), 111.0 (ArH), 113.3 (ArH), 119.5 (ArH), 120.5 (ArH), 123.0 (ArH), 125.4 (ArH), 128.6 (ArH), 138.2 (ArH), 172.6 (C=OCH), 174.4 (C=ONH).

[Cd(3)]$^{2+}$. δ_H (600 MHz, CD_3OD) 1.20 ([Ha], 3H, m, $N(CH_2)_2N$ ring), 1.61 ([Hc], 3H, m, $N(CH_2)_2N$ ring), 2.12 ([Hb], 3H, m, $N(CH_2)_2N$ ring), 2.31 ([He], 3H, m, CH_2C=O), 2.40 ([Hd], 3H, m, $N(CH_2)_2N$ ring), 2.95 ([Hf], 3H, m, CH_2C=O), 3.01 ([Hg], 3H, m, ArCH_2), 3.37 ([Hh], 3H, m, ArCH_2), 3.77 (9H, s, OCH_3), 5.05 ([Hi], 3H, m, αCH), 6.93 (3H, t, ArH), 7.06 (3H, s, ArH), 7.09 (3H, t, ArH), 7.32 (3H, d, ArH), 7.49 (3H, d, ArH); δ_C (150.8 MHz) 29.5 (ArCH_2), 52.5 ($N(CH_2)_2$)N ring), 53.6 (OCH_3), 53.9 ($N(CH_2)_2$)N ring), 55.0 (αCH), 62.0 (CH_2-C=O), 111.0 (ArH), 113.2 (ArH), 119.8 (ArH), 120.5 (ArH), 123.3 (ArH), 125.8 (ArH), 128.8 (ArH), 138.4 (ArH), 173.1 (*C*=OCH), 173.5 (C=ONH).

4. δ_H (600 MHz, CD_3CN) 2.39 ([Ha, Hc], 8H, AA′BB′, 4 × $N(CH_2)_2N$ ring), 2.48 ([Hb, Hd], 8H, AA′BB′, 4 × $N(CH_2)_2N$ ring), 2.88 ([He, Hf], 8H, m, CH_2C=O), 3.02 ([Hg], 4H, m, ArCH_2), 3.10 ([Hh], 4H, m, ArCH_2), 3.61 (12H, s, OCH_3), 4.62 ([Hi], 4H, m, αCH), 7.14–7.43 (20H, m, ArH); δ_C (150.8 MHz) 37.9 (ArCH_2), 52.7 (OCH_3), 53.6 (αCH), 54.3 ($N(CH_2)_2$)N ring), 59.5 (CH_2C=O), 127.6 (ArH), 129.3 (ArH), 130.4 (ArH), 138.0 (ArH), 171.8 (C=ONH), 173.1 (*C*=OCH).

[Zn(4)]$^{2+}$. δ_H (600 MHz, CD_3CN) 2.03 ([Ha], 4H, m, $N(CH_2)_2N$ ring), 2.35 ([Hc], 4H, m, $N(CH_2)_2N$ ring), 2.54 ([Hb], 4H, m, $N(CH_2)_2N$ ring), 2.73 ([Hd], 4H, m, $N(CH_2)_2N$ ring), 2.82 ([He], 4H, m, CH_2C=O), 2.88 ([Hf], 4H, m, CH_2C=O), 2.92 ([Hg], 4H, m, ArCH_2), 3.14 ([Hh], 4H, m, ArCH_2), 3.65 (12H, s, OCH_3), 4.64 ([Hi], 4H, m, αCH), 7.18–7.40 (20H, m, ArH); δ_C (150.8 MHz) 38.3 (ArCH_2), 50.1 ($N(CH_2)_2$)N ring), 51.6 ($N(CH_2)_2$)N ring), 53.1 (OCH_3), 55.2 (αCH), 56.4 (CH_2C=O), 128.0 (ArH), 129.6 (ArH), 130.4 (ArH), 137.7 (ArH), 171.8 (*C*=OCH), 172.0 (C=ONH).

[Cd(4)]$^{2+}$. δ_H (600 MHz, CD_3CN) 1.28 ([Ha], 4H, m, $N(CH_2)_2N$ ring), 1.96 ([Hc], 4H, m, $N(CH_2)_2N$ ring), 2.03 ([He], 4H, m, CH_2C=O) 2.12 ([Hb], 4H, m, $N(CH_2)_2N$ ring), 2.49 ([Hf], 4H, m, CH_2C=O), 2.65 ([Hd], 4H, m, $N(CH_2)_2N$ ring), 2.88 ([Hg], 4H, m, ArCH_2), 3.27 ([Hh], 4H, m, ArCH_2), 3.84 (12H, s, OCH_3), 4.76 ([Hi], 4H, m, αCH), 7.21–7.40 (20H, m, ArH); δ_C (150.8 MHz) 38.3 (ArCH_2), 47.5 ($N(CH_2)_2$)N ring), 51.1 ($N(CH_2)_2$)N ring), 53.3 (OCH_3), 54.6 (αCH), 55.4 (CH_2-C=O), 128.0 (ArH), 129.7 (ArH), 130.6 (ArH), 138.2 (ArH), 171.6 (*C*=OCH), 172.1 (C=ONH).

Acknowledgements

The Australian Research Council is thanked for supporting this research.

Notes and references

1 S. F. Lincoln, *Coord. Chem. Rev.*, 1997, **166**, 255; K. P. Wainwright, *Adv. Inorg. Chem.*, 2001, **52**, 293.

2 S. L. Whitbread, S. Politis, A. K. W. Stephens, J. B. Lucas, R. S. Dhillon, S. F. Lincoln and K. P. Wainwright, *J. Chem. Soc., Dalton Trans.*, 1996, 1379; A. K. W. Stephens, R. S. Dhillon, S. E. Madbak, S. L. Whitbread and S. F. Lincoln, *J. Chem. Soc., Dalton Trans.*, 1996, 1379; R. Dhillon, S. F. Lincoln, S. Madbak, A. K. W. Stephens, K. P. Wainwright and S. L. Whitbread, *Inorg. Chem.*, 2000, **39**, 1855; K. M. Walters, M. A. Buntine, S. F. Lincoln and K. P. Wainwright, *J. Chem. Soc., Dalton Trans.*, 2002, 3571.

3 L. Fabbrizzi, M. Lichelli, P. Pallavincini and L. Parodi, *Angew, Chem., Int. Ed.*, 1998, **37**, 800; E. Kimura and T. Koike, *Chem. Soc. Rev.*, 1998, **27**, 179; D. Parker, K. Senanayake and J. A. G. Williams, *J. Chem. Soc., Perkin Trans. 2*, 1998, 2129; T. Gunnlaugsson, D. A. MacDónail and D. Parker, *J. Chem. Soc., Chem Commun.*, 2000, 93; S. Aoki, S. Kaido, H. Fujioka and E. Kimura, *Inorg. Chem.*, 2003, **42**, 1023.

4 S. Aime, M. Botta, M. Fasano and E. Terrano, *Chem. Soc. Rev.*, 1998, **27**, 19; P. Caravan, J. J. Ellison, T. J. McMurry and R. B. Lauffer, *Chem. Rev.*, 1999, **99**, 2293; V. Comblin, D. Gilsoul, M. Hermann, V. Humblet, V. Jacques, M. Mesbahi, C. Sauvage and J. F. Desreux, *Coord. Chem. Rev.*, 1999, **185–186**, 451; I. M. Clarkson, A. Beeby, J. I. Bruce, L. J. Govenlock, M. P. Lowe, C. E. Mathieu, D. Parker and K. Senanayake, *New J. Chem.*, 2000, **24**, 377.

5 C. B. Smith, S. F. Lincoln and K. P. Wainwright, *Inorg. Chim. Acta*, 2001, **317**, 21; C. B. Smith, M. A. Buntine, S. F. Lincoln and K. P. Wainwright, *Dalton Trans.*, 2003, 3028.

6 H. Maumela, R. D. Hancock, L. Carlton, J. H. Reibenspies and K. P. Wainwright, *J. Am. Chem. Soc.*, 1995, **117**, 6698; C. B. Smith, K. S. Wallwork, J. M. Weeks, M. A. Buntine, S. F. Lincoln,

M. R. Taylor and K. P. Wainwright, *Inorg. Chem.*, 1999, **38**, 4986; P. J. Davies, S. F. Lincoln, C. B. Smith, M. R. Taylor, K. P. Wainwright and K. S. Wallwork, *Acta Crystallogr., Sect. C*, 2000, **56**, 28; C. B. Smith, A. K. W. Stephens, K. S. Wallwork, S. F. Lincoln, M. R. Taylor and K. P. Wainwright, *Inorg. Chem.*, 2002, **41**, 1093.

7 R. Dhillon, S. F. Lincoln, S. Madbak, A. K. W. Stephens, K. P. Wainwright and S. L. Whitbread, *Inorg. Chem.*, 2000, **39**, 1855; J. M. Weeks, M. A. Buntine, S. F. Lincoln, E. R. Tiekink and K. P. Wainwright, *J. Chem. Soc., Dalton Trans.*, 2001, 2157; J. M. Weeks, M. A. Buntine, S. F. Lincoln and K. P. Wainwright, *Inorg. Chim. Acta*, 2002, **331**, 340.

8 A. A. Watson, A. C. Willis and D. P. Fairlie, *Inorg. Chem.*, 1997, **36**, 752.

9 R. D. Shannon, *Acta Crystallogr., Sect. A*, 1976, **32**, 751.

10 D. F. Shriver and P. W. Atkins, *Inorganic Chemistry*, Oxford University Press, Oxford, UK, 3rd. edn., 1999, p. 244.

11 P. Chaudhuri and K. Wieghardt, *Prog. Inorg. Chem.*, 1987, **35**, 329.

12 R. S. Dhillon, S. E. Madbak, F. G. Ciccone, M. A. Buntine, S. F. Lincoln and K. P. Wainwright, *J. Am. Chem. Soc.*, 1997, **119**, 6126; R. S. Dhillon, S. E. Madbak, F. G. Ciccone, M. A. Buntine, S. F. Lincoln and K. P. Wainwright, *J. Am. Chem. Soc.*, 1998, **120**, 11212.

13 M. L. Janssen, W. J. Oyen, I. Dijkgraaf, L . F. Massuger, C. Frielink, D. S. Edwards, M. Rajopadhye, H. Boonstra, F. H. Corstens and O. C. Boerman, *Cancer Res.*, 2002, **62**, 6146; E. F. Plow, T. A. Haas, L. Zhang, J. Loftus and J. W. Smith, *J. Biol. Chem.*, 2000, **275**, 21785.

14 P. Gans, A. Sabatini and A. Vacca, *J. Chem. Soc., Dalton Trans.*, 1985, 1195.

15 D. D. Perrin and W. L. Armarego, *Purification of Laboratory Chemicals*, Pergamon Press, Oxford, 3rd edn., 1988.

16 G. H. Searle and R. J. Geue, *Aust. J. Chem.*, 1984, **37**, 959.

17 A. McAuley, P. R. Norman and O. Olubuyide, *Inorg. Chem.*, 1984, **23**, 1938.

18 J. E. Richman and T. J. Atkins, *J. Am. Chem. Soc.*, 1974, **96**, 2268.

19 R. Yang and L. J. Zompa, *Inorg. Chem.*, 1976, **15**, 1499.

20 *Beilstein*, Springer-Verlag, Berin, 1980, vol. 22, p. 6771.